SISSA - SCUOLA INTERNAZIONALE SUPERIORE DI STUDI AVANZATI

TRIESTE

Strada Costiera 11

ISAS - INTERNATIONAL SCHOOL FOR ADVANCED STUDIES

International School for Advanced Studies

CONTRIBUTIONS TO THE STUDY OF ACTIVE GALACTIC NUCLEI

by

Annalisa Celotti

A thesis submitted for the degree

of *Magister Philosophiae*

Trieste – October 1991

Supervisor

Prof. A. Treves

TRIESTE

Acknowledgments

I would like to thank Prof. Dennis Sciama, director of the Astrophysics Sector of S.I.S.S.A., who allowed, and always substained, my staying in Cambridge supported by Della Riccia fellowships, and gave me the opportunity to attend stimulating schools and meetings.

I acknowledge the encouragment and invaluable discussions of Prof. Martin Rees, director of the Institute of Astronomy in Cambridge, who accepted me at the I.o.A., so kindly.

My greatest debt is to Prof. Andy Fabian, who accepted to be my supervisor and gave me the opportunity to work in the stimulating 'X–ray group' of I.o.A. He has followed, taught and encouraged me with his enthusiasm (being so patient with my terrible english too!).

Many thanks to Prof. Marek Abramowicz and Prof. Aldo Treves, my tutor and supervisor in S.I.S.S.A. respectively, who, at different stages, supported my staying at I.o.A., and Prof. Aldo Treves for disponibility and discussions (and reading my thesis during his holidays).

I am very grateful to Prof. Laura Maraschi. I benefitted from many scientific discussions with her and from constant encouragement and advice. She has always been a firm reference point well over her duty, particularly in the most difficult periods.

Deep thanks to Dr. Gabriele Ghisellini, for numberless fruitful scientific discussions, for the kind support for my going to work in the 'X–ray group' and for the friendly help and attention, mainly during the first period I was in Cambridge.

Many thanks also to Dr. Ian George, a good scientist and a friend in a strange country, for his patience and attention (and also for the table tennis and snooker matches!).

The list of friends and colleagues of the 'Capannino' (University of Milano), S.I.S.S.A. and 'X–ray group' is long: I thank all of them for being present and available, often just through computer, and in particular Drs. Monica Colpi, Silvano Molendi, Tomaso Belloni, Francesco Haardt, José Acosta–Pulido, Nicola Caon, Mauro e Daniela Orlandini and my friends Corbella.

Deep thanks to my mother, without whom I could never have written this thesis (she knows why).

Table of contents

Introduction

Active Galactic Nuclei (AGN) represent some of the most spectacular events in the Universe. They emit luminosities 10^{39}–10^{48} erg s^{-1} (if emitted isotropically) in regions typically smaller than 1 pc. This energy can be released both as radiation and as kinetic energy of an outflow. In general they show a continuum emission which exceeds the stellar contribution of the host galaxy, but the term 'active' can refer to one or more of very different characteristics, which can not be attributed to stellar evolution: strong continuum, at least partly non-thermal, strong and broad (FHMW > 500 km/s) emission lines of high ionization, strong and fast variability timescales in all frequency bands (in X-rays down to 50 s), polarized radiation, presence of collimated structures sometimes showing relativistic velocities.

All these phenomena range from radio to γ–ray energies, on scales between $\simeq 10^{12}$ to $\simeq 10^{25}$ cm (see Fig. 1), the smaller regions being associated with the hotter phenomena, even if different components seem to coexist with similar powers.

Even if there is not a definitive proof, most astronomers are in favour of the presence of massive (10^6–10^8 $M_\odot$) black holes in the core of AGN, mainly because of their efficiency, inevitability and stability. The described phenomena of 'activity' tend to support this picture: large and compact masses, non–stellar radiation, strong variability, large velocities observed in emission lines, central position in the host galaxy, presence of long scale jets. The release of gravitational energy of the infalling matter in field of the black hole or the extraction of rotational energy of the black hole itself (more efficient than accretion) being the origin of energy (*e.g.* Rees 1984; Blandford 1990). Indeed one of the most striking observation is just that the main properties of AGN seem quite similar over more than eight orders of magnitude in luminosity, suggesting the same fundamental mechanism for all the objects.

Two of the most interesting results becoming evident in the last years should be mentioned. On one hand the fact that the AGN phenomenon is quite common:

for example more than 10 % of E–Sbc galaxies with $M_B < -20$ are Seyfert or radio galaxies (Woltjer 1990), and an unknown percentage, maybe also 100 %, of galaxies showed the quasar phenomenon at some stage; on the other hand there is a sort of continuity in the level of activity between the 'normal' and the active galaxies, and active galaxies themselves (*e.g.* Seyfert 1.5 type galaxies) emphasizing the fact that only quantitative limits on the degree of 'activity' determine the classification of a source.

In this thesis we do not present an exhaustive review of the subject, neither we concentrate on one detailed aspect or physical process, but instead we try to describe some new results in their context.

In Chapter 1 a brief review of taxonomy and observations of AGN, which will be useful in the following and, very schematically, the most common interpretations of the observed spectra are presented.

In Chapter 2 we concentrate on one class of these objects, namely the 'blazar' class, and in particular on the collimated structures of plasma commonly associated to these objects (jets). We examine them under three different aspects. First of all we see how the variability observed at different frequencies can be qualitatively accounted for, in models developed for stationary emission from jets of plasma, involving the presence of perturbations propagating along the jet. Results on cross correlated analysis in two X–ray bands of the BL Lac object PKS 2155-304, which agree with the predictions of the model, are presented. Secondly we examine the possibility that such structures could be constituted predominantly by an electron-positron pair plasma, instead of ordinary electron–proton plasma. And finally the so called 'unification' problem is briefly discussed. It is related to the fact that in the 'jet picture' there is a preferential direction of the line of sight under which objects are observed, and therefore must exist another class of objects ('parent population') with some different observed properties, but intrinsically identical to them. A new alternative physical picture is presented.

Chapter 3 concerns more generally with the AGN phenomena. We present a new method to determine upper limits on the intensity of the magnetic field in the X–ray emitting region of AGN. The results support the idea that the presence of cold

matter in or around the compact region could be responsible for reprocessing most of the primary radiation. This matter can be just in the right physical conditions to free–free absorb part of the emission from the X–ray region.

Finally as projects for the next months two direct developments of these ideas are presented in Chapter 4.

In the appendices, papers containing the discussed models are reported, the aim being to present the context in which they are relevant in the various chapters, but refer directly to them for all the detailed calculations and results.

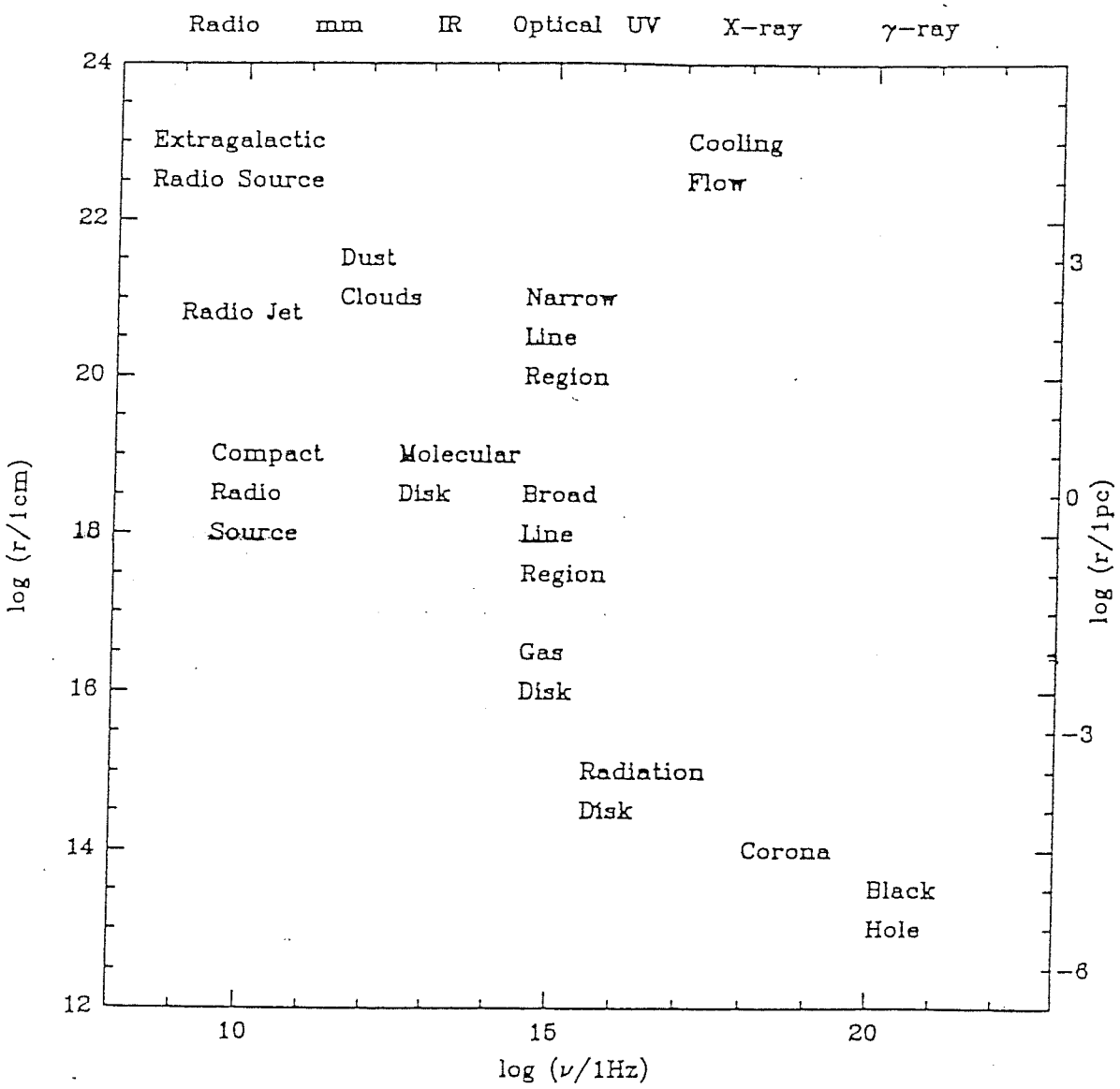

Fig. 1 Illustration of the ranges of activity associated with AGN. The sizes cover 12 orders of magnitude, from the X-ray emitting regions of Seyfert galaxies (less than 10^{12} cm) to extended radio sources. AGN are observed from radio energy band up to energies of about 100 MeV in some Seyfert galaxies and quasars. Some of the described phenomena are observed, while the small scale ones are indirectly inferred. From Blandford (1990).

Chapter 1. Active Galactic Nuclei

The aim of this chapter is to present some relevant observational results about AGN and the basic physical interpretations from the observed radiation of the emission mechanisms, kinematic, spatial distribution of the emitting plasma.

Roughly AGN radiate approximately the same power in equal wavebands: despite of the variety in the spectral distributions, in most of the objects the emission peaks between IR and UV or in the γ–ray band. From 10 to 30 % of the total luminosity is emitted as X–rays (2–20 keV) (*e.g.* Padovani & Rafanelli 1988).

The recent observations of the mm, far and near IR, UV and soft X–ray radiation, fast and multiwavelengths variability and high resolution X–ray spectra help in the effort of understanding the physical conditions and geometrical structures of these objects.

A gross division between AGN can be done on the prevalence of thermal (radio quiet objects) or non-thermal (blazars) emission in the continuum spectra (*e.g.* Bregman 1990; Lawrence 1987), which extend from radio to γ–ray energies, as shown in Fig. 1.1. It is not yet clear if this difference can be attributed to different radiation mechanisms operating in the sources or if just due, for example, to geometrical–orientational effects.

It should be reminded that the taxonomy of AGN is complex, due to at least to three basic reasons. In fact the classification of a specific object depends on the observational selection criteria; furthermore it is often difficult to reconcile classifications based on properties observed in different spectral bands. Finally, if the properties of a source varies with time, it is possible that the more an objects is observed the more it is probable to detect some specific property, which classifies the objects. Nevertheless the attempt in the last few decades is to infer the basic physical structure in the belief that it is substantially the same for all the objects.

1.1 Blazar

The definition 'blazar' includes BL Lac objects, Optically Violent Variable quasars (OVV), Highly Polarized Quasar (HPQ) and at least some, if not all, flat spectrum radio loud objects (Bregman 1990). By definition they present (Miller 1989) a smooth IR-optical-UV continuum, approximated roughly by a power–law $F(\nu) \propto \nu^{-\alpha}$, with $\alpha = 1$, from a point-like nucleus, a linear optical polarization p $> 3\%$, strong and rapid optical variability on timescale of days or less, and strong, polarized and variable radio emission. It has been found a strong correlation between high polarization and optical variability (Moore & Stockman 1984; Impey 1987) presented by OVVs and HPQs, which constitute about 10 % of the radio loud quasars. The main difference between BL Lac objects and HPQs is the absence in the first ones of a thermal component in the UV band and strong emission lines (usually the limit on the equivalent width is set at 5 Å) (see §1.2.e). Some objects has been classified in different classes during different observations (*e.g.* 3C446, Oke 1967; 3C279, Visvanathan 1973; AO 0235+164, Cohen *et al.* 1987), in which an increase of the continuum flux reduced the strength of the lines, when their intensity remained constant. BL Lacs show also a distribution in redshift and an average luminosity lower than HPQs.

1.1.a Radio–UV continuum

The radio spectra are flat (-0.5< α <0.5) and no radio quiet ($F(5\,Ghz) < F(5500\mathring{A})$) blazar has been identified. They present a compact radio morphology and in the plane $\nu F(\nu)$ versus ν (which shows the power emitted per decade in frequency) the spectrum raises toward higher frequencies up to submillimeter-IR region where there is the maximum of emission. For X–ray selected objects the peak can be in the X–ray region (*e.g.* Mkn 421, Makino *et al.* 1987; Ghisellini *et al.* 1986). Average spectral indices in different bands, from a sample of 93 blazars analyzed by Impey & Neugebauer (1988) are listed in Table 1.1.

Table 1.1

	α_R	α_{IR}	α_O	α_{UV}
BL Lac	0.03 ± 0.035	0.84 ± 0.35	1.42 ± 0.89	1.50 ± 0.62
HPQ	0.08 ± 0.52	0.95 ± 0.53	1.41 ± 1.05	1.23 ± 0.69

Spectral indices are evaluated in the $10^{9-10}\,Hz$, $10^{12-13}\,Hz$, $10^{14-15}\,Hz$, $10^{15-16}\,Hz$ bands, respectively.

The most important characteristic of these sources, as far as concern emission processes, is their compactness, *i.e.* a high radiation density (see §1.4.a).

Some characteristics strongly argue for a non-thermal synchrotron origin of the radio-optical radiation: the high degree of linear polarization observed in the radio and optical (up to 45 %) bands, the smoothness of the radio–optical continuum, its variability and the inferred high brightness temperature of about $T_b \simeq 10^{12}$ K in the radio band (*e.g.* Mutel 1990) up to $T_b \simeq 10^{18}$ K (Quirrenbach *et al.* 1989) and $T_b > 10^6$ K in IR and optical bands as inferred from variability timescales (*e.g.* OJ 287, 3C345, Edelson & Malkan 1987, Moore *et al.* 1982), which are well above the blackbody temperatures at these wavelengths (see §1.4.d).

1.1.b BL Lac objects

We now concentrate on BL Lac objects (for a recent review see Maraschi 1991). Some features, like a high frequency turnover, are not at a well defined frequency, but range between IR and UV bands (*e.g.* 1413+134, AO 0235+164, BL Lac, Bregman *et al.* 1990), with a spectral index change $\Delta\alpha \simeq 0.5$ (Impey & Neugebauer 1988); Landau *et al.* (1986) suggested that the spectra from simultaneous observations can be best–fitted even with a parabola in the Log F/Log ν plane.

Some objects show a diffuse emission, an optical excess and absorption lines (from which many redshifts were deduced) probably due to the galaxy of which they constitute the nucleus. Most of the host galaxies have been found to be elliptical, but recently five host disc galaxies have been discovered (Abraham, McHardy & Crawford 1991).

The absence of strong features in their spectra make the identification of a particular emission model difficult. Instruments with a better resolution will be able to observe new features, like the recently confirmed 0.6 keV broad absorption in the soft X–ray spectrum of five BL Lac objects (Madejski *et al.* 1991); high resolution spectra from BBXRT confirmed the presence of this absorption feature in the spectrum of PKS 2155–304.

It has been also noted that the linear polarization in HPQs tends to decrease with increasing frequency near the 'blue bump' component, suggesting that the percentage of nonthermal emission is decreasing (Smith *et al.* 1988). An attempt to reproduce the spectrum of PKS 2155–304 with thermal disc emission has been recently suggested (Wandel & Urry 1989). X–ray polarimetry will be able to discriminate between thermal and nonthermal models.

Most BL Lacs were discovered in radio surveys, but X–rays satellites (HEAO–1, *Einstein*, EXOSAT) have discovered new objects (Schwartz *et al.* 1989; Maccacaro *et al.* 1989; Giommi *et al.* 1989). The X–ray selected objects show a different spectral distribution (see Fig. 1.2), different peak emission frequency (Bregman, Maraschi & Urry 1987), lower polarization and variability. They emit the same average X–ray, but less radio luminosity with respect to the radio selected ones (Maraschi *et al.* 1986). Furthermore the X–ray selected objects have a bigger ratio of UV/X–ray fluxes (Ghisellini *et al.* 1986) and a X–ray spectral index equal or steeper than the UV one (*e.g.* Mkn 421, Makino *et al.* 1987), on the contrary of the radio selected sources, suggesting that probably a different component or emission process produces X–rays (see §2.2.a).

BL Lacs are strong X–ray emitters. They do not show a soft excess at low X–ray energies (*e.g.* Madejski & Schwartz 1989) and, in the blazar class, they present a steeper X–ray spectral index (Maraschi 1991). However the spectral shape is not yet uniquely determined. Urry (1986) suggests the presence, for five bright objects, of a steep ($\alpha > 2$) component in the soft band and a flatter one at higher energies (> 10 keV). Barr *et al.* (1989) fit EXOSAT data, below 8 keV, with two power laws with increasing spectral indices ($\Delta\alpha \simeq 0.5$) and intersecting at 2–4 keV (see also Giommi *et al.* 1990). For three objects (PKS 2155–304, Mkn 421, H0323+022) a single power–law (with $\alpha \simeq 1$) between 2–35 keV best–fit GINGA data (Ohashi

1989). A possible explanation of these different results is that the hard component is strongly variable.

An interesting question concerns the puzzle of the absence in BL Lac spectra of broad emission lines. As demonstrated by Urry (1984) in the assumption of isotropic continuum this cannot be attributed to the lack of photoionizing continuum or thermal instability of the emitting clouds (in the two phase model, see §1.2.e) as the steep optical–UV flux suggested (see *e.g.* Worral & Wilkes 1990; Guilbert, Fabian & McCray 1983).

The absence of emitting gas, the possibility that it is hot, or pair dominated or that anisotropic radiation intercepts only a small fraction of it are other alternative explanations. Madau, Ghisellini & Persic (1987), showing that the average Doppler factor (in the radio band) is lower for BL Lacs than HPQs, disproved the hypothesis that a stronger Doppler amplification could make the BL Lac continuum to overcome thermal and line emission (see §1.4.d). The difference between BL Lac objects and HPQs has been interpreted by Courvoisier (1990) not as due to orientational effects, but to the strength of the magnetic field, which produces different synchrotron components and collimation of the jet (see §2.1.a). An alternative interpretation of this difference has been suggested by Ostriker & Vietri (1985). The idea is that BL Lac objects are OVVs with an optical continuum enhanced by microlensing by a star in an intervening galaxy. This interpretation (which we do not examine further) predicts both the swamping of the lines and a low redshift distribution (which corresponds to the 'lensing' galaxies). This hypothesis do not explain rapid variability and polarization, and predicts multiple images and the source not centered in the galaxy.

1.1.c Beaming

The discovery of rapid radio variability (3C273, Dent 1965), and later the measure of VLBI dimensions, imply a high radiation density (or brightness temperature) and consequently, in the assumption that radio flux is produced as synchrotron in a spherical homogeneous source, a radiation flux by inverse Compton at high frequencies exceeding the observed one. The hypothesis that

the emitting plasma is moving at relativistic velocities (Rees 1966) predicts that the observed luminosities are overestimated and the dimensions (from variability measures) underestimated, solving the Compton problem for appropriate values of the Doppler factor δ, which quantifies the effect (see §1.4.d and §2.2). In 1978 Blandford & Rees proposed that in BL Lac objects the emitting plasma is collimated in beams and that for these objects the line of sight is close to the velocity direction, introducing the idea of anisotropic emission. Consequently the angle under which a source is observed became a fundamental parameter, in the sense that the same object can show different properties when observed at different angles (see §2.4).

Nowadays several observations (see §2.1 and §2.4) argue in favour of the presence of relativistic beaming effects in blazars. X–ray variability could also support evidence of relativistic motion (see §1.4.c).

Nowadays the absence of features suggesting thermal emission in BL Lac objects has often be used as an indication that they show the inner 'naked' emission region. However it is also possible that BL Lac luminosity, being beamed, is not intrinsically intense, and instead most of the power is emitted in the form of kinetic energy of relativistic outflows, as also suggested by the observation of the width of the feature at 0.6 keV (Madejski *et al.* 1991; Krolik *et al.* 1985).

1.2 Radio–quiet objects

This class includes quasars, Seyfert 1 galaxies, which are probably the low luminosity counterparts of radio quiet quasars, Seyfert 2 galaxies, LINERS (see *e.g.* Woltjer 1990).

1.2.a Radio-UV continuum

Their continuum is more complex than the blazars one, but the presence of features at the same rest frame frequency imply that some thermal or atomic process is important.

Most of the objects present a steep ($-1.1 < \alpha < -0.5$) radio spectrum, the emission of which, even if greater than the radio emission from an ordinary spiral

galaxy, is not relevant in term of contribution to the total luminosity, even in radio loud objects.

The peak of the emission is concentrated between 10μm and 100μm. The widely accepted interpretation for the near IR emission, which is about 30% of the total luminosity, is thermal emission from dust (accretion disc models tend to produce too small emission), which must intercept and reprocess from 10 to 50 % of the UV radiation, consistently with what is deduced from observations of warped discs in spiral galaxies (Sanders *et al.* 1989). Furthermore radio loud objects, which show less IR emission, seem to be in elliptical galaxies which contain less dust. This interpretation is supported by the anticorrelation between the intensity of the UV emission and the IR one in a sample of 34 Seyfert 1 galaxies analyzed by Carleton *et al.* (1987). The dust temperature should lie in the range 2000-45 K in regions from 1 pc to 1 kpc. These predicted distances pose constraints on the variability timescales and lags which are consistent with observations (Bregman 1990). Furthermore Clavel, Wamstaker & Glass (1989) found a 400 days delay between the 3.5 and 1–2.2μm fluxes in Fairall 9, compatible with emission from dust at $\sim$ 1 pc.

For all radio quiet AGN there is a turnover in the submillimeter region approximately at the same frequency for all objects with slopes sometimes steeper than $\alpha = -2.5$, excluding that it is due to the self-absorbed part of synchrotron emission (Chini, Kreysa & Biermann 1989). Moreover Sanders *et al.* (1989) revealed in broad band spectra of nearly all of 109 optically selected quasars a minimum around 1 μm consistent with a cutoff in the dust emission because it is destroyed at temperature greater than 2000 K. Finally with narrow band photometry in near IR a bump has been identified in the 3–5 μm range (Edelson & Malkan 1986) which can be due to bremsstrahlung from clouds of the Broad Line Region (see below) or from hot dust at T$\sim$1500 K (Barvainis 1987).

On the other hand the lack in some radio loud objects of dust features, the continuity in their radio-IR continua, the variability of 3C273 in the far IR band with timescales of days-week while the near IR flux varied $< 5\%$ (Marscher & Gear 1985, Courvoisier 1990) argue against a thermal origin of the IR flux. Maybe that different structures lie over a common component, which extend over some decades.

It has been made the hypothesis of the presence of an IR-optical power–law, with spectral index $\alpha \simeq 1$ (Edelson & Malkan 1986), probably of nonthermal origin, which can emerge when thermal emission is weak. The original belief that it extends up to X–rays is now disproved (McAlary & Rieke 1988), because of lack of correlation and different slopes of the IR and X–ray bands.

At higher frequencies the contribution from the Balmer continuum (2700–3800 Å) and the forest of Fe II lines (1800–3500 Å) (Wills, Netzer & Wills 1985) which create a pseudo–continuum, make the spectrum to rise (the '3000 Å' bump) up to the 'big bump', visible to 1200 Å (with the *IUE* satellite). Some objects show a turn down near the high frequency UV point, suggesting that perhaps the peak has been observed (Sun & Malkan 1989), while in most objects the spectrum continues to rise, providing the dominant contribution to the total power between 1200 Å and 100 eV (Elvis, Wilkes & McDowell 1990). An indirect evidence of emission between 10 and 100 Å is the observation of emission lines of high ionization (*e.g.* Fe X), which require a ionizing continuum at these wavelengths (*e.g.* Collin–Souffrin 1991).

The UV–soft X–ray emission is commonly attributed to the thermal emission from material accreting onto a central black hole, probably, if matter has significant angular momentum, in a disc geometry (Schield 1978).

Spherical accretion has low efficiency because the cooling timescales are probably longer than the free fall timescales (*e.g.* Rees 1984). In fact the inflow timescale $t_{in} \sim t_{ff} v_{in}/v_{ff}$, which depends on viscosity, must be compared to the cooling timescale controlling the temperature, and, for radial infall, $t_{cool} \propto \dot{M}$, while t_{in} is independent on $\dot{M}$. t_{ff}, v_{ff} indicate the free–fall time and velocity, v_{in} is the infall velocity, t_{cool} the cooling timescale and $\dot{M}$ the accretion rate. If $t_{in} < t_{cool}$ the thermal cooling is not efficient and plasma can emit only through synchrotron and Compton emission. There is a general trend (Rees 1984) for the emission to be non–thermal for low values of $\dot{m} = \dot{M}/\dot{M}_E$ (where $\dot{M}_E$ is the accretion rate corresponding to the Eddington luminosity, which measures the importance of radiation pressure on dynamics).

If material with angular momentum is able to cool, it forms a thin, centrifugally supported disc, the structure of which is relatively simple. The simplest optically

thick and geometrically thin 'α'–disc model proposed by Shakura & Sunyaev (1973) (see also Pringle 1981), in which the disc radiates locally as a blackbody, leads to simple analytical solutions and gives maximum temperatures of the order of 10^5-10^6 K from the innermost stable orbit and predicts $\nu^{1/3}$ spectra. Despite a qualitative global agreement with observations (*e.g.* Malkan 1983) a more detailed comparison requires a more sophisticated model (Courvoisier & Clavel 1991). In fact it predicts a slope at 1 keV too steep to reproduce the soft X–ray spectrum and the expected anticorrelation between the temperature of the bump and the mass (*i.e.* luminosity, *e.g.* Koratan & Gaskell 1991) of the objects is not observed. Furthermore the simultaneous optical-UV variations observed in NGC 4151 (delays less than 2 days, Ulrich 1990), NGC 5548 (Molendi, Maraschi & Stella 1991) and other AGN is not consistent with this simple picture (Ulrich 1990), which predicts delays of months, corresponding to the sound travel time through different regions of the disc. Some improvements include electron scattering effect, inclination of the disc, relativistic corrections, rotating black holes, radiation or ion supported thick discs (*e.g.* Sun & Malkan 1989; Laor, Netzer & Piran 1990; Treves, Maraschi & Abramowicz 1989). The final aim of the work is to infer, through comparison with observations, physical quantities like the mass of the black hole and the accretion rate.

Alternative models to produce the bump include the possibility of a non-thermal emission for the whole spectrum (Jones & Stein 1990) or bremsstrahlung emission through reprocessing of non-thermal X–rays from dense gas clouds with temperature $\sim 10^4 - 10^5$ K. The last picture is also compatible with the presence of an accretion disc (Rees 1987; Lightman & White 1988; Guilbert & Rees 1988; Barvainis 1990; Ferland, Korista & Peterson 1990).

1.2.b X–ray spectrum

In the soft X–ray range extinction intrinsic to the AGN, probably due to cold matter, can be relevant: in the 0.5–1 keV band absorption with $N_H \simeq 10^{22} - 10^{23}$ cm^{-2} is observed in low luminosity AGN ($L_x < 10^{43}$ erg s^{-1}) (Reichert, Mushotzky & Holt 1986). The absorption can vary with timescales of the order of months (*e.g.* NGC 4051, Yaqoob & Warwick 1989), implying dimensions for the absorbing region

of the order of the Broad Line Region size. Furthermore the observed spectrum shape is not consistent (*e.g.* NGC 4151) with an uniform absorber model (Holt *et al.* 1980, Perola *et al.* 1986), but the covering factor must be <1.

After correction for absorption many AGN show instead a 'soft excess' (at energies < 1–2 keV) with respect to the power–law extrapolated from higher energies (Arnaud *et al.* 1985; Turner & Pounds 1989; Masnou *et al.* 1991 found an excess in 8 of 14 observed QSO) (see Figs. 1.3), implying intrinsic column densities $N_H < 10^{20-21}$ cm^{-2}, inconsistent with a covering of the central source with a 'shell', as proposed *e.g.* for the highly obscured source NGC 4151 (Warwick *et al.* 1989).

The soft X–ray excess can be the high energy tail of the 'big bump' or can constitute a different (maybe thermal) component. An important indication about the origin of this 'excess' is the fact that it is observed to vary rapidly (minute-hours), indicating that it is produced close to the central region (Mkn 841, Arnaud *et al.* 1985; NGC 5548, Kaastra & Barr 1989). See also §3.2 and Appendix D.

At energies above 1-2 keV, or at all X–ray energies if the soft excess is not present, the spectrum can be best–fitted by a power–law (2-20 keV) of 'universal' slope $\alpha \sim 0.6 - 0.8$, *i.e.* with a small scattering (Mushotzky *et al.* 1980) and for the few objects observed up to 120 keV the spectrum is also consistent with such slope (Rothschild *et al.* 1983). Turner & Pounds (1989) found $\alpha = 0.7 \pm 0.17$ in the 2–10 keV band for 42 Seyfert galaxies. The low dispersion has been confirmed at least for Seyfert 1 galaxies, and even if more spread (α =0.5 for the radio loud objects and α =1 for the radio quit ones, Wilkes & Elvis 1987, Brunner *et al.* 1990) has been found for QSO between 0.3–3 keV, their 2–10 keV spectrum follows the standard behaviour (Makino 1988). The presence of a 'universal' slope should be connected with a physical mechanism. A fundamental limit to the interpretation is the fact that it is not yet clear if the characteristics of the observed spectra should be attributed mainly to the radiation processes or to the acceleration mechanisms of the emitting particles. Only recently new features appeared in the X–ray spectrum and an acceptable explanation to this 'universal' behaviour has been suggested (see §1.2.c).

As far as the origin of the X–ray emission is concerned, several models can reproduce an X–ray power law. Both non-thermal emission (*e.g.* synchrotron

self–Compton, SSC), and Comptonization of the soft X–ray or 'blue bump' photons from relativistic or non relativistic, thermal or non thermal distribution of electrons (*e.g.* in a corona above an accretion disc) can reproduce a power–law spectrum. Indeed one of the hardest thing to estimate is the what fraction of the dissipated power can go into ultrarelativistic particles rather than shared among all particles (non–thermal and thermal distributions). However most of the energy of a thermal plasma is in the ions, and the electron–ion coupling timescales (or the timescale to establish a thermal distribution) is $\propto T_e^{3/2}$. Consequently the timescale is longer when T_e is high, as required by the fast varying X–ray hard spectrum (Guilbert, Fabian & Stepney 1982). Moreover it should be noted that a fine tuning seems necessary in order to maintain, during strong and fast variability, a slope which is function of the temperature of the electrons and their optical depth (Shapiro, Lightman & Eardley 1976; Fabian 1989). It requires that the heating and escape rates are in a fixed ratio in order to produce the 'universal slope' observed in Seyfert galaxies. In fact the spectral index α, in the case of hot electrons which modifies a monochromatic photon spectrum at ν_0 (neglecting Compton recoil and induced scattering) is deduced from the Kompaneets equation to be $\alpha(\alpha+3) = 4/y$ between ν_0 and ν_{rec}. $y = 4kT\tau_T(1+\tau_T)/m_ec^2$ is the Compton parameter and $\nu_{rec} = (3+\alpha)kT/h$ is the frequency at which recoil becomes important. However feedback mechanisms can operate, as suggested by Haardt & Maraschi (1991), to link temperature and optical depth also during variations.

The hypothesis of Comptonization of soft photons predicts that variations in the soft X–ray precede those in the hard X–ray band, as observed in NGC 5548 with a delay of 1–2 hours (Kaastra & Barr 1989), but see §3.1 and Appendix D.

As far as bremsstrahlung (or Comptonized bremsstrahlung) emission is concerned it would require such high matter density to generate $L \sim L_E$ that the scattering optical depth is so large that reprocesses the spectrum shape (see *e.g.* 1.4.b).

Thermal and non–thermal models involving pair production tried to reproduce the observed spectral shape (see §1.4.a). Recently it has been suggested that X–ray variability can also be attributed to variations in pair cascade models (*e.g.* Fabian, 1988; Zdziarski & Coppi 1991).

The observations of spectral breaks and measures of polarization in the X–ray band can be critical tests in order to determine the origin of the X–ray spectrum.

1.2.c Iron line and cold matter

The observations of the GINGA spectra of most AGN show the presence of a line at $\sim$ 6.4 keV (*e.g.* Matsuoka *et al.* 1990 for the Seyfert 1 galaxy MGC–6–30–15) and a hump in the 10–30 keV band (*e.g.* Pounds *et al.* (1990) who added the spectra of 12 objects observed by GINGA, see Fig. 1.4). Two models have been proposed as explanation.

The first one involves a partial covering of the central source with a very thick medium and $N_H \sim 10^{24}$ cm^{-2}. The material can be comprised in many clouds covering the central source similarly to the BLR. The covered component turns up at about 10 keV, producing the hump, and emits an iron line with typical EW$\sim 50-100$ eV, for solar abundances (for a detailed discussion of this model see *e.g.* Inoue 1989).

Another possibility (Guilbert & Rees 1988, Lightman & White 1988) is that the hump is produced by the reflection of hard X–ray photons on a cold ($T < 10^6$ K) and thick surface. Hard X–rays ($>$ 40 keV) are Comptonized and decrease their energy for Compton recoil, while soft photons ($<$ 10 keV) are photoelectrically absorbed by high Z ions with a cross section greater than the Thomson one. Consequently the reflected component peaks around 30 keV and adds to the direct spectrum (with spectral index $\alpha \simeq 0.9$), hardening it to α =0.7. This in turn implies that the soft excess can be reduced up to 30% (Piro, Yamauchi & Matsuoka 1990).

The iron inside this matter is not totally ionized ($<$ Fe XVII) and has K and L shell electrons. Therefore matter must be cold. Standard accretion disc model predicts densities in the range $10^{10} < n < 10^{17}$ cm^{-3} (Laor & Netzer 1989) and, in order to keep it cold, relatively neutral and not Compton heated, matter must have $n > 10^{12} L_{43}\, R_{14}^{-2}$ cm^{-3}, with $L = L_{43} 10^{43}$ erg s^{-1}, $R = R_{14}$ cm (George & Fabian 1991).

The observed line, with a typical equivalent width of 100–300 eV is thought to be due to its fluorescence, *i.e.* by 2p–1s transitions after ionization. Kα energy varies between 6.1-6.5 keV, depending on the ionization state. Being the EW$\simeq$

$300\,(\Delta\Omega/4\pi)(Z/Z_o)\tau_T\,eV$, where $Z/Z_\odot$ is the metallicity abundances in solar units, $\Delta\Omega$ the solid angle subtended by the cold plasma, $\tau_T = \sigma_T\,n\,R$ the Thomson optical depth, the observed width of the lines require an optically thick medium ($N_H \simeq 10^{23-25}$ cm^{-2}) and the cold matter must subtend a large angle ($\simeq 2\pi$ sr). This can be satisfied in a disk geometry.

The hard X–ray source must be outside the disk in order to avoid photoelectric absorbtion features, not seen. Energy maybe stored in a strong magnetic field and rapidly released (*e.g.* Begelman 1990, but see also Appendix D). Monte Carlo simulations (*e.g.* George & Fabian 1991) are able to reproduce the observed features and the ratio of direct and reflected continuum in a, maybe clumped, disc geometry (see Fig. 1.5).

A confirmation of this picture comes from the almost simultaneous (delay less than 250 s) variability of the line and continuum in NGC 6814 (Kunieda *et al.* 1990), which also suggest an upper limit of 10^{13} cm for the iron reprocessing region. In NGC 4151 variations imply a limit of light months to the line emitting region also consistent with column density variations (Perola *et al.* 1986).

Reflection also implies that the 2–10 keV spectrum has less contribution from the reflected component than flux at higher energies (by about 50 %, Fabian 1989), and therefore the flux at 10–30 keV and the line should lag and be smeared with respect to variability in the 2–10 keV range.

Again an alternative to the disc geometry is given by cold clouds or filaments (Guilbert & Rees 1988). They probably can be supported, analogously to the BLR clouds by a magnetic field (Rees 1987) more or less in equipartition with the radiation energy density.

Another predicted feature from cold iron is the presence of a K Fe edge at about 7.1-8.8 keV, depending on the ionization state. The observed energy is consistent with neutral matter (*e.g.* Makishima 1986) and the optical depth is within a factor of two of that required by low energy absorption (Perola *et al.* 1986). The possible presence of an absorbtion feature at 8 keV and of a warm absorber is discussed by Nandra *et al.* (1989). For example for NGC 5548 (Nandra *et al.* 1991) the edge energy is more consistent with 'warm' iron. The width of the line instead is not consistent with the observed absorbtion column density in NGC 5548, unless the medium is

highly ionized. Covering greater than 25 % is required to produce line intensity but less 90 % not to be inconsistent with data. The thermal luminosity from this matter would be negligible.

Furthermore the line profiles (functions of the inclination angle and distance from the black hole) can give information about the geometry of the inner region and the mass of the compact object, as shown by Fabian *et al.* (1988), including effects of general relativity. Line broadening (FWHM $\sim$ 1 keV) in MGC–6–30–15 (Matsuoka *et al.* 1990) and NGC 7469 (Piro, Yamauchi & Matsuoka 1990) interpreted as Doppler and gravitational broadening, indicates that the emitting matter is orbiting at 10–50 Schwarzschild radii (Fabian *et al.* 1988).

An interesting consequence of this picture is that the 'universal' X–ray slope (of the primary component) is now $\alpha \simeq 0.9$, and this value is naturally explained in pair plasma models for compact sources in the case of saturated pair cascade (Zdziarski *et al.* 1990) (see §1.4.a).

Therefore, together with the soft excess and the UV bump these features are strong indication of the presence of cold (T$\simeq 10^5$ K) matter close to the central source.

For a recent review of the subject see Treves, Perola & Stella (1991).

1.2.d γ–ray spectrum

As far as concerns γ–rays only few sources has been observed so far, due to the decreasing number of photons and cross section for detection at high energies. Only five AGN has been detected above 100 keV, before the launch of GRO and Sigma. A strong limit is imposed by the γ–ray background: if the AGN spectrum would continue with a spectral index of $\alpha = 0.7$, it would exceed the diffuse background at about 3 MeV (Bignami *et al.* 1979, Rothschild *et al.* 1983), and therefore their spectrum must break below 2–3 MeV.

One of the most interesting feature between 100 keV and 2–3 MeV could be the presence of the electron–positron annihilation line (at 511 keV). In NGC 4151 and Cen A limits are set on its equivalent width of EW$\sim$400 and 300 keV, respectively (Baity *et al.* 1984). It is difficult to observe an annihilation line, because the more

is the annihilation optical depth, the more is the effect of Compton downscattering, which dilutes the line. Also Doppler shift in accreting material contribute to broaden it. One possible situation in which the line could be seen is in a wind of pair (carrying less than 10% of the luminosity of the injected power in a steady situation, Svensson 1990), for example if the outflow encounters matter outside the source.

The spectrum of NGC 4151 has been observed to extend up to 1 MeV in two occasion, while in another observation showed a break at $\sim$ 50 keV (Baity *et al.* 1984, see also Bassani *et al.* 1986). NGC 1275, Cen A and MGC 8–11–11 were observed up to few MeV and then their spectra steepen. The fifth AGN is 3C273: COS B flux is below the extrapolation of the X–ray spectrum, suggesting a γ–ray break (Bignami *et al.* 1979), probably at few MeV (Bassani *et al.* 1985), but the position of the break is not well determined.

1.2.e Line emission

Finally we briefly say something on the line emission (the main reason is that the usual interpretation of their origin can have connection with the model developed in §3.2). We note that as far as concern the understanding of the basic processes in AGN the line emission can be considered, in a sense, of second order, being probably associated with reprocessing of the primary radiation (for a recent review see Netzer 1990).

Generally there are two system of emission lines: a broad (FWHM $\simeq$ 1000–5000 km/s) and a narrow (FWHM $\simeq$ 500 km/s) component. Type 1 Seyfert galaxies spectra show permitted lines (*e.g.* CIV) with width larger than the forbidden ones (*e.g.* [OIII], [NII]). In Seyfert 2 they are both narrow. The most common interpretation assumes that they are produced by clouds or filaments in two different regions (*e.g.* Netzer 1991), with typical parameters:
Broad Line Region : $R \simeq 0.1$ pc, $T \simeq 10^4$ K, $n_e \simeq 10^{8-10}$ cm^{-3} (in order not to have forbidden transitions), $C \simeq 10^{-1}$, $f \simeq 10^{-12}$, $M \simeq 10^2\, M_\odot$, $v \simeq 10^{3-4}$ km s^{-1}
Narrow Line Region : $R \simeq$ kpc, $T \simeq 10^4$ K, $n_e \simeq 10^{8-10}$ cm^{-3} $f \simeq 10^{-8}$, $M \simeq 10^{4-5}\, M_\odot$, $v \simeq 10^{2-3}$ km s^{-1}
where R is a typical dimension of the region deduced by line variability of BLR; only

the NLR has been optically resolved in near Seyfert galaxies (*e.g.* Pogge 1988). T is the temperature, n_e is the electron density, C is the covering factor, f the filling factor, M the involved mass and v the typical velocity.

The fact that the filling factor $f << 1$ suggests that in both regions the emitting gas is clumped in clouds, filaments or shell. Standard photoionization models predict $N_H \sim 10^{22} - 10^{23}$ cm^{-2} for the BLR clouds. It has been also suggested that the BLR region is filled with relativistic pair plasma (*e.g.* Kundt 1987).

The estimated temperatures derive from the relative intensity of lines, the absence of lines emitted if the temperature would be greater and to avoid too high ionization through collisional ionization the temperature must be below 10^6 K. Photoionization by the continuum emitted by the central source can produce low ionization atoms at low temperatures and the amount of UV–X ray photons from extrapolated optical power–laws also suggest that photoionization is able to reproduce quite well the ratios of high ionization lines, quite independently of the slope of the ionizing continuum (Davidson & Netzer 1979, see however Mathews & Ferland 1987 and Netzer 1990). The model is also supported by the correlation between continuum and intensity of broad lines in Seyfert galaxies.

The self–gravity in the cloud is negligible and therefore a confining mechanism is required so that they do not dissolve in the sound travel time.

In the BLR clouds are thought to be in pressure equilibrium with a hot, low density external medium ('two phase model', Maraschi, Perola & Treves 1980; Krolik, McKee & Tarter 1981; Ferland & Rees 1988). The Compton temperature is defined from the average energy of the radiation as $T_C = h < \nu > /4k = (h/4k) \int F(\nu)\nu d\nu / \int F(\nu) d\nu$, when up and downscattering energy transfers balance. Note that it does not depend on density but just on the shape of the continuum. If the radiation energy density U exceeds the electron energy density, the particles reach this temperature, typically in a time $t_c \sim m_e c/\sigma_T U$ The Coulomb scattering exchange time between thermal electrons to reach a Maxwellian distribution is given, for non relativistic particles ($\Theta < 1$) by $t_{e^-e^-} = (4\sqrt{\pi}/\ln\Lambda)\Theta^{3/2}/(n\sigma_T c)$ and for relativistic ones ($\Theta > 1$) by $t_{e^-e^-} = (8/\ln\Lambda)\Theta^2/(n\sigma_T c)$ (Stepney 1983) (see also Chapter 4), typically longer than the Compton timescale, where $\Theta = kT/m_e c^2$ and $\ln\Lambda \sim 20$ is the Coulomb logarithm.

At low densities Compton equilibrium is reached (with typical $T_C \simeq 10^{7-8}$ K), while at high densities bremsstrahlung and lines cooling give another equilibrium phase ($T_C \simeq 10^{4-5}$ K): optically thick gas tends to reprocess radiation to reach equilibrium at the blackbody temperature (see Figs. 1.6). The density required to keep the gas cold is $n > 10^{16}(T_b/10^5)^3$ cm^{-3}. In between thermal instability operates, but for appropriate densities (or ionization parameter) both branches can coexist in pressure equilibrium (and this was in agreement with the fact that similar ionization parameters were found for objects with very different luminosity).

Problems with the model however exist. More realistic continua showed that the unstable branch and the two phases could not exist, because the introduction of a strong UV bump increases the cooling. Moreover for some range of parameters the optical depth in the hot medium may be large, but no effects on the spectrum have been observed, like broad wings in the emission lines and absorbtion edges. Moreover the velocity of the BLR clouds is greater than the sound velocity in the hot medium and they should break into filaments during their motion (see Netzer 1990).

Another possible confining mechanism is through the magnetic field (about 1 G) transported *e.g.* in a relativistic wind or accretion flow (Rees 1987), in which case the emitting matter tends to be in filamentary structures.

Otherwise the lines could be produced directly in the accretion disc, without confinement, and even if the emitted flux is too low, it is possible that some high energy flux is backscattered on the disk.

The width of the broad lines is due to the high, probably supersonic, velocity dispersion of the clouds in-outflowing motion. In fact, defining the ionization parameter $\xi = (L_{UV}/4\pi cR^2)(1/nkT)$ where L_{UV} is the ionizing continuum, and using the values of $\xi = 0.1 - 10$ inferred from lines ratios, it results that the BLR cloud distance is $R_{BLR} \sim 1.4 \times 10^{18}(L_{UV,46}/n_{10}\xi)$ cm, and the Keplerian velocity at that distance is $v_K \sim 10^8(L_E/L_{UV})^{1/2}(L_{UV,46}n_{10}/\xi)^{1/4}$ cm s^{-1}. Thus it results that, being the line width $>> 10^8$ cm s^{-1}, the clouds can not be gravitationally bounded unless $L_E >> L_{UV}$, *i.e.* for very large central masses (*e.g.* $M >> 10^8\, M_\odot$ for a quasar) (Rees 1984).

Recent long monitoring by *IUE* of Seyfert galaxies (Clavel *et al.* 1990) shows

that line emission lags variations in the continuum intensity from few days to months depending on the element and ionization state. This kind of studies ('reverberation') therefore show that the 'standard' picture of BLR size is inadequate and that the region is probably extended, with clouds close to the central source, with $N_H > 10^{24}$ cm^{-2} (Ferland & Persson 1989; Rees, Netzer & Ferland 1989).

Finally the shape of the line profiles can give information on the structure of the emitting matter. For example a double line profile can be the signature of the presence of a disc, but *e.g.* in NGC 5548 variations in its shape are not symmetrical, suggesting that part of the Balmer lines are produced outside the disk (Ulrich 1990).

Note that information on the medium around the object and surrounding the jet at smallest scales (see §2.1), come from the broad emission lines.

1.3 Variability

One of the most interesting test in order to understand the emission mechanism and the spatial distribution of the material in AGN are measures of variability. AGN appear to vary on all timescales, the shortest ones usually in the X–ray band. For this reason it is not yet clear if we really observe an 'equilibrium' spectrum from a single source which varies or if many small regions are heated and cooled and we observe only the averaged spectral flux from all of them (Guilbert, Fabian & Ross 1982).

On one side variability can constrain the upper dimensions of the emitting region through the causal connection argument $R < 2\,c\,t_{var}\,(1+z)^{-1}\,\delta$ cm, where t_{var} is the variability timescale, c the speed of light and R the dimension of the region, z the redshift and δ the Doppler factor (see below). This in turn implies that we are dealing with compact objects, with typical dimensions less than 0.1 pc. Note that in the case of optically thick source ($\tau_T > 1$) the light crossing time is reduced by a factor $\sim (1 + \tau_T)$ and in the case of strange geometries the above limit can be misleading.

Secondly simultaneous studies at different frequencies can identify if the same mechanism is responsible for the emission in different spectral band and/or if the emitting regions are coincident or possibly correlated.

We note that the large and rapid X–ray variability (and hard X–ray continuum) are the strongest evidence against models which try to reproduce the observed activity events through bursts of star formation or supernovae (*e.g.* Heckman 1991). It is also difficult to account for compact radio jets (see §2.1); energy efficiency through nuclear reaction is too low to account for the observed radiation and furthermore a cluster of massive stars can not avoid dynamical instability (Shapiro & Teukolsky 1983). Small increase in the central velocity dispersion of stars, have been reported for nearby galaxies. The central masses inferred range from 3×10^6 to $5 \times 10^8\ M_\odot$.

More generally strong variability (*i.e.* involving a large fraction of the observed flux) require an unique source or a coherent mechanism able to induce simultaneous variations in different spatial regions, even if in principle short variability timescales could not refer to the 'central source'.

In order to quantify both timescales and amplitudes of variations, which are both strongly dependent on frequency, some parameters are usually considered, even if their values generally depend on the number of observations.

Amplitude variability indicators can be defined as $\Phi(\nu) = F_{max}/F_{min}$ or $v(\nu) = \sigma / < F >$, where F_{max}, F_{min}, $< F >$ and σ are the maximum, the minimum and the average fluxes and σ is the standard deviation respectively. The parameter $v(\nu)$ can be independent from the number of observations (if many) and is independent of the average flux (see Celotti, Maraschi & Treves 1991). Supposing, for simplicity, that the source can be observed only in two states (a low and high one) with an amplification factor A and calling p the fraction of times it is observed in the high state, $v(\nu)$ can be rewritten as $v(\nu) = (A-1)\sqrt{p(1-p)}/(1-p+pA)$. This function of p has a maximum at a value of $v(\nu)$ which increases for increasing A. Therefore the same value of v can be obtained for two values of p, for fixed A. (Fig. 1.7).

As far as timescales are concerned it should be noted that different timescales can be present. The shortest timescale, defined *e.g.* as $t_{var} = F/(dF/dt)$, which corresponds to the time required for the sources to double its flux, can be used as an upper limit to the emitting region dimension , even if it does not refer to the true amplitude of variations. If observations are undersampled t_{var} decreases with

the interval between observations (Maraschi 1991). Slower variations can be instead caused by long term changes in the structure of the source. Timescales for increasing and decreasing flux or 'long' timescales with constant flux ('states') can be present. It should be also noted that the probability to observe a minimum timescale is low (Done & Fabian 1989).

1.3.a Variability timescales

As far as concerns radio quiet objects one of the most striking result is that X–ray variability timescales down to 100 s has been detected for few objects (Mkn 335, NGC 4051, NGC 5506, NGC 5548, MGC 6-30-15, Lawrence *et al.* 1987; Pounds & McHardy 1988, Nandra *et al.* 1989; Done *et al.* 1990; Kaastra & Barr 1989) and for the Seyfert 1 galaxy NGC 6814, observed with GINGA satellite, the limit is < 50 s (Kunieda *et al.* 1990), implying extreme small values for the dimensions of the X–ray emitting region ($\sim 10^{12}$ cm, which can be compared to the Schwarzschild radius of a 10^6 $M_\odot$ black hole, $R_s = 2\,GM/c^2 \simeq 3 \times 10^{11}$ cm).

Regarding BL Lac objects the general trend (see Urry 1986; Giommi *et al.* 1990; Treves *et al.* 1989; George, Warwick & Bromage 1988) show decreasing timescales with increasing frequency (see *e.g.* Bregman 1990). The timescales vary from months–years in the GHz band, several weeks in the far IR, days in the near IR, hours–day in the optical and similarly (despite the few data) in the UV bands. Recently Edelson *et al.* (1991) found variations of 12% in 5 hours for PKS 2155–304 in the UV band. Variations on timescales 30 s has been found in X–rays (H0323-022, Feigelson *et al.* 1986) and more often of hours *e.g.* in PKS 2155-304 (Morini *et al.* 1986; Treves *et al.* 1990). No information exist on variability at γ–rays frequencies.

The dependence on frequency of t_{var} can be roughly described as $t_{var} \propto \nu^{-1/2}$ (Bregman 1990).

An interesting point regards the possibility that emission can be interpreted as due to a constant component and a variable contribution (flare). In the X–ray band Maraschi & Maccagni (1988) showed that 35 BL Lac vary less that 50 % for more than 70% of the time.

1.3.b Amplitude

Results on the dependence of the amplitude of variability on frequency has been reported for a sample of 90 blazars by Impey & Neugebauer (1988). The average (or maximum) amplitude increases with frequency from radio to UV band. Treves & Girardi (1990) confirmed this trend in the UV band.

For BL Lac objects Giommi *et al.* (1990) analyzed the properties of 36 sources observed with EXOSAT: all objects bright enough were observed to vary, and for 4 objects the variations were more than a factor 2 in few hours. The hardness ratio (ME over LE flux) increases with ME flux, showing a hardening of the spectrum with increasing flux; also Maccagni *et al.* (1989) found a correlation between the hardness ratio of EXOSAT X–ray bands and the ME flux, showing again a flattening of the spectrum with increasing flux. Correlations between spectral variability and intensity are observed during flares of PKS 2155–304 (Treves *et al.* 1989). The same results are from quasisimultaneous monitoring in the UV–X–ray bands carried for Mkn 421 (George, Warwick & Bromage 1988) (see also Celotti, Maraschi & Treves 1991, Appendix A). Even if these observations are not definitive they extend to high frequencies the results of Impey & Neugebauer (1988).

This trend is present also in narrow bands, as variations in the spectral index. These variations increase with frequency (Impey & Neugebauer 1988), with a sharp increase at optical–UV band. Single sources however show very different behaviours.

An opposite trend has been observed for variability in Seyfert galaxies, with a correlated softening of the X–ray spectrum when the sources brighten (NGC 4051, Lawrence *et al.* 1985; NGC 4151, Perola *et al.* 1986; NGC 5548 Branduardi–Raymont 1989; MR2251–178, Pan, Stewart & Pounds 1990). For NGC 4151 Yaqoob & Warwick (1991) reported a variation $\Delta\alpha \sim 0.3$ with an increase in flux of a factor of ten in the 2–10 keV flux, which can be interpreted as a real steepening of the spectrum or as a variation in the degree of photoionization of the soft X–ray absorbing gas. The same behaviour is presented by 3C120 (Maraschi *et al.* 1991) but with an anticorrelation with the hard (3.5–6 keV) spectrum and a delay of the ME band with respect to the LE. Treves *et al.* (1990) found again a softening of the 0.5–8 keV spectrum from EXOSAT for the Seyfert 1 galaxy MGC 8–11–11.

Another interesting recent result is the observation (with GINGA satellite) of a X–ray flare from an 'ordinary' quasar (neither OVV, nor HPQ), PKS 0558–504 (Remillard *et al.* 1991). The flux increased of 67% in 3 minutes, implying a variation $dL/dt \simeq 2.9 \times 10^{42}$ erg s^{-2}. The authors suggest that it can be an indication of relativistic beaming (see §1.4.c). A similar dL/dt value was observed for an OVV quasar, with observed superluminal motion, 3C279, with a variation of 20% in 45 min (Makino *et al.* 1989).

1.3.c Correlated variability

An important test for theoretical models for emission in AGN therefore comes from simultaneous observations in different spectral bands, obtained during coordinated campaigns. Unfortunately few and not systematic results are available. For X–ray variability this is particularly critical because simultaneity requires delays less than the minimum variability timescale. An example of the powerfulness of such a test is the results obtained for the Seyfert 1 galaxy NGC 4051 (Done *et al.* 1990). During a variation in X–rays (2.3-8.7 keV, with GINGA) greater than 50 %, the flux varied less than 1% in the optical (B band) and less than 4% in IR. If the variations are induced by changes in the electron distribution emitting X–rays, in order that the same amplitude of variations are not present at lower energies, it is necessary that the X–rays are produced in a region either separated or one order of magnitude smaller than that emitting the IR–optical flux.

For 3C273 no correlations between mm and X–ray flux has been observed (Courvoisier *et al.* 1990) excluding an interpretation of the observed spectrum in term of the simple synchrotron self–Compton flux (see §1.4.d), but see Ghisellini, George & Done (1989).

Optical-UV correlations has been observed in NGC 4151, NGC 5548 (Clavel *et al.* 1990) and also for 3C273, suggesting a common origin of the radiation (see §1.2.e).

Uncorrelated UV–X–ray (2–20 keV) variability has been observed for 3C273 (Courvoisier *et al.* 1990). Strong correlations has been shown for NGC 4151 (except in one observation, Perola *et al.* 1986). This variations are interpreted by Ulrich (1990) as due to instabilities in the inner part of the of the disk or irradiation of it

from a X–ray source.

Kaastra & Barr (1989) reported a delay of 1–2 hours between low (0.2–5 keV) and hard (2–8 keV) band in NGC 5548, as already mentioned.

As far as blazar variability is concerned, BL Lac showed a good correlation between optical and near IR fluxes and optical and UV, while delays of weeks has been observed between optical and far IR fluxes (Marscher & Gear 1985). Bregman & Hufnagel (1980) found correlation of optical and radio variations, with delays of typically a year. A delay shorter than 2 months has been observed in OJ 287 (Valtaoja *et al.* 1989).

Also in the radio bands high frequencies precede low frequencies flux variations by weeks–months at 20–100 GHz and months–years at 5–15 GHz (Balonek 1982, Aller *et al.* 1985) with decreasing amplitude toward lower frequencies, similarly in radio quiet objects and blazars (Valtaoja *et al.* 1985).

Very few observations suggest correlated variability between UV and X–ray bands (Maraschi 1991). X–rays appear to be correlated with optical flux when X–ray are on the extrapolation of the IR–UV spectrum (*e.g.* Mkn 421, Makino *et al.* 1987; 0537-441, Tanzi *et al.* 1986). 1156+285 showed a X–ray outburst between two optical flares, maybe correlated with the X–ray one (McHardy 1989).

Correlated variability was observed in X–rays for PKS 2155–304 (between LE and ME bands of EXOSAT satellite), with no evidence of lags in the 0.1–6 keV band (Tagliaferri *et al.* 1991, see Appendix B).

Uncorrelated X–rays and lower frequency emission is found for objects where the extrapolation of the UV flux underestimates the X–ray one (*e.g.* BL Lac, 3C446, 3C345, Makino 1989).

In BL Lac objects radio and UV fluxes are strongly correlated (OJ 287, Pomphrey *et al.* 1976; 3C345, Balonek 1982) and similarly in 3C273, with the UV variations anticipating the radio ones. It is quite surprising if the emission mechanisms radiating at radio and UV energies are different.

Moreover a new VLBI component (see §2.1.d) appeared in the VLBI map of 3C273 at the epoch of fast IR–optical variability (Krichbaum *et al.* 1990, Baath *et al.* 1991) suggesting that the continuum emission is related with the jet structure.

1.3.d Power spectrum

In general X–ray variability shows an irregular behaviour, with outbursts or flickering on the shorter resolution timescales. Power spectrum analysis has been performed for few objects, due to the lack of long trend observations. It shows a dependence on frequency $f^{-1} - f^{-2}$ in the $10^{-6} - 10^{-2}$ Hz band (NGC 4051, Lawrence *et al.* 1987; MGC-6-30-15, McHardy 1988) for Seyfert galaxies (with a tendency to be steeper than f^{-1} at high frequencies, McHardy 1988) and, recently for the BL Lac object PKS 2155–304 (Tagliaferri *et al.* 1991, see Appendix B) for which a dependence $f^{-1.9}$ has been found. Note that the dependence f^{-1} implies that the same power is emitted at all frequencies, and this suggest that there is no preferred timescale (and therefore dimensions) on which the source varies. Furthermore the lack of a cut–off at high f shows that observations are not yet performed on sufficiently short period in order to find a minimum size of the emitting region.

Up to now only two objects have shown significant features in their power spectra. A strong indication of periodicity has been discovered for NGC 6814 (Mittaz & Branduardi–Raymont 1989, Fiore & Massaro 1989) in EXOSAT data and confirmed 4 years later by GINGA. The fundamental frequency of $\sim$ 12000 sec and five harmonics appeared, lasting at least few years with amplitude $\sim$ 30%. The same kind of result has been found for NGC 4151 (Fiore *et al.* 1989) with period 12600 or 5900 s and amplitude $\sim$ 7%. Morini, Anselmo & Molteni (1989) reported the presence of transient periodicity at periods of hundreds to thousands of seconds for the radio galaxy Cen A, observed with EXOSAT.

These results has been interpreted (*e.g.* Abramowicz *et al.* 1989) as a strong indication of the periodic behaviour of bright spots moving in a rotating accretion disc (see §1.4.c).

In some objects periodic events are reported from light curves. OJ 287 showed possible periodicity with timescale of 20 min. in radio and optical (Visvanathan & Elliot 1976, Valtaoja *et al.* 1985), and Mkn 421 in the X–ray band with period of 4 hours (Brodie, Bowyer & Tennant 1986). Optical periodicity of 1540 days has been reported for 3C446 (Barbieri *et al.* 1990).

1.4 Some theoretical considerations

In this section we want to outline some theoretical limits, and emission mechanisms which will be referred to in the following chapters. For a description of the radiative processes see *e.g.* Rybicki & Lightman (1979), Svensson (1990), Tucker (1975) and references therein.

1.4.a Compactness parameter

In the 'standard' picture of the physics of AGN some relevant quantities are: the size R of the emitting region, greater then $\sim 3\,R_s$, where $R_s = 2\,G\,M\,/c^2$ is the Schwarzschild radius; the luminosity L, which is often compared to the Eddington limit $L_E = 2\pi\,m_p\,c^3\,R_s/\sigma_T$, for gravitational force on protons equal to Thomson radiation force, where m_p, m_e are the proton and electron masses. This expression for L_E assumes that the Thomson cross section is applicable, and that the material is primary hydrogen. Note also that in a pure pair plasma the limit is a factor m_p/m_e smaller (Lightman, Zdziarski & Rees 1987).

From these two quantities a (adimensional) compactness parameter can be defined (Cavaliere & Morrison 1980; Guilbert, Fabian & Rees 1983)

$$\ell = \frac{L}{R}\frac{\sigma_T}{m_e\,c^3} = \frac{2\pi}{3}\frac{m_p}{m_e}\frac{L}{L_E}\frac{3R_s}{R} = 2.7\times 10^{-29}\frac{L}{R} \tag{1.1}$$

The maximum 'Eddington' value corresponds to $\ell \sim 3600$. The pair Eddington limit correspond at about $\ell \simeq 2$. If it is overcome pairs outflow is present.

The virial temperature is $T_v \simeq 0.5(m_p\,c^2/k)(R_s/r)$ K where r is the distance from the black hole, implying that electrons are relativistic for $r \lesssim 1000\,R_s$.

The photon density in a source is roughly proportional to $L/4\pi\,R^2\,c$, and therefore the optical depth for interaction with the photons is proportional to the compactness ℓ. High value of ℓ means that Compton scattering and photon–photon interactions are important.

In particular the value of ℓ determines the inverse cooling timescale for Compton scattering, because $t_{IC} \simeq (R/c)\,(1/\gamma\ell)$, implying that for all values $\ell > 1$ a particle releases its energy before escaping the source. For let say $\ell = 100$ and $\gamma = 100$, the

acceleration timescale, which must obviously be shorter than the cooling timescale, should operate on $t_{acc} < 10^{-4} R/c$, which for $M = 10^8 M_\odot$ is < 1 s. Note also that the short cooling timescales imply that breaks in the observed spectra can not be attributed to radiative losses.

The rapid cooling also implies that electrons cannot propagate in the source and that in turn requires that particles are continuously injected or reaccelerated locally in the source in order not to accumulate (Fabian 1986; Done, Ghisellini & Fabian 1990). Among other suggestions (*e.g.* shock acceleration) there is the possibility (*e.g.* Biermann & Strittmatter 1985) that ultrarelativistic electrons are produced by a chain of reactions: proton–proton which create π, which decay as μ and finally in electrons and positrons. But again fast variability could pose constraint on these hypothesis. In fact the proton–proton cross section is $4mb \sim \sigma_T/20$ and therefore high densities $n_p \sim 3 \times 10^{11} R_{14}^{-1}$ cm^{-3} are required, well above the Faraday depolarization limits (see §1.4.d). Also if the particles are confined by a magnetic field, for $n_p = 10^{10}$ cm^{-3}, timescales for variability are > 1 day. Note that for the model proposed by Giovanoni & Kazanas (1990), in which the transport of energy outside the source is due to neutrons that then decade at distance $\simeq 2 \times 10^{13} \gamma$ cm, requirements from radio variability timescales should be considered.

The compactness also determines the optical depth $\tau_{\gamma\gamma}$ for photon–photon interactions. If γ–rays are produced in the source they can create electron–positron pairs interacting with low energy photons if $\tau_{\gamma\gamma} > 1$. The pair production threshold between photons of energies $\epsilon = h\nu/m_e c^2$ is given by $\epsilon_1 \epsilon_2 > 2/(1 - \cos\theta)$ where θ is the interaction angle. On the other hand the pair production cross section peaks around $\epsilon_1 \epsilon_2 \simeq 2$, where it is about $0.2\sigma_T$, and decreases $\propto \epsilon^{-1}$, so that *e.g.* 100 MeV γ–rays can react mainly with 5 keV X–rays. Therefore for energies at about $\sim m_e c^2$

$$\tau_{\gamma\gamma}(\epsilon_1) \simeq 0.2\sigma_T R \frac{1}{\epsilon_1} n(1/\epsilon_1) \simeq \frac{9}{16} \frac{0.2\sigma_T}{m_e c^2} \frac{L(1/\epsilon_1)}{R} \simeq \frac{\ell(1/\epsilon_1)}{30} \qquad (1.2)$$

where the photon density has been estimated as $n(\epsilon) = L(\epsilon)/(4/3\pi R^3)(t_{esc}/\epsilon\, m_e c^2)$, with the escape timescale $t_{esc} \simeq 3R/4c$ for a spherical optically thin source.

Therefore for $\ell(1) > 30$ the source is opaque to pair production at all γ–ray energies and the spectrum should be calculated self–consistently, because a pair

cascade could start and reprocess the spectrum (see *e.g.* Svensson 1987; Ghisellini 1989; Svensson 1990 and references therein).

The limit $\ell > 30$ can be reexpressed as a variability limit, *i.e.*

$$L_{\ell=30} \gtrsim 3 \times 10^{40} \Delta t \qquad \mathrm{erg\,s^{-1}} \tag{1.3}$$

with $R = \Delta t\, c$.

We want now to remind the production and annihilation rates, which will be used in §2.3 and §4.2.

Pair production rates can be expressed in the form $\dot{n}_+ = (3/8\pi)\sigma_T c\, n_1 n_2 F$, where n_1 and n_2 refer to the interacting particles/photons, n_+ is the positron density, and a factor α_f (fine structure constant) must multiply the rates for each particle involved. F is a factor including the energy dependence. Analogously the pair annihilation rate is given by $\dot{n}_+ = (3/8\pi)\sigma_T c\, 2 n_+ n_- F_a$, roughly independent on temperature, being the descrease in particles speed compensated by the increase of cross section as particles cool. If radiative cooling is efficient annihilation of relativistic pairs is unimportant. Averaging over energy the energy dependent terms (Ghisellini 1987):

Table 1.2

	$\Theta << 1$	$\Theta >> 1$	
$F_{\gamma\gamma}$	$\pi^2 e^{-2/\Theta}/8\Theta^3$	$\pi \ln\Theta/2\Theta^2$	Wien
$F_{\gamma\gamma}$	.....	$(2/3)\,(\Theta/2)^{2\alpha}$	power–law
F_{ee}	.....	$(112/27\pi)\ln^3(2\Theta)$	
F_{ep}	.....	$\ln^3(2\Theta)/\pi$	
F_a	π	$(\pi \ln\Theta)/2\Theta^2$	

where $\Theta = kT/m_e c^2$.

'Standard' pair production models assume a continuous injection of luminosity, and through Compton scattering of UV photons an hard γ–ray spectrum is formed.

γ–rays, interacting with low energy photons, produce pairs. The spectrum therefore tends to steepen, because of the depletion of γ–ray photons and the emission of radiation at lower energies by the new pairs created.

The cooled pair reach the Compton equilibrium temperature before eventually escape or annihilate, downscattering hard X–rays and the line producing a break at $0.511/\tau_T^2$ MeV if $\tau_T > 1$, and upscattering low energy photons of the bump and eventually producing a steep EUV spectrum (Arnauld *et al.* 1985, Zdziarski & Coppi 1991). The pairs must be subrelativistic, because in any case primary emission processes produce soft photons and the 'Comptonization parameter' increases for relativistic pairs to $\tau_{e^\pm}^2 \gamma_{e^\pm}^2 > 1$.

Note that the emitted annihilation line is thermal broadened if pairs are not completely cooled and can result not detectable.

Anyway, until recently (see §1.2.c), this model could not fit the observed spectra because $\ell \sim 30$ is required to produce a 0.7 spectral index, but in this case too many γ–rays are predicted (and not a MeV turnover which is required to be consistent with the γ–ray background). For higher ℓ less γ–rays are produced but the spectrum steepens to $\alpha \simeq 1$ after 3–4 pair generations (Lightman & Zdziarski 1987; Svensson 1987; Done & Fabian 1989).

A minimum compactness can be estimated if the source dimension is deduced from X–ray variability timescales. On the contrary if beaming effects are present the compactness is obviously overestimated, of a factor $\ell_{int} = \ell_{obs}/\delta^5$ (using again the size inferred from variability), where $\delta = 1/\gamma(1 - \beta \cos\theta)$ is the Doppler factor, β, γ the bulk velocity and Lorentz factor, θ is the angle of the velocity with the line of sight and ℓ_{int}, ℓ_{obs} are the intrinsic and the 'observed' compactnesses respectively. Therefore the above limit on pair production can be escaped if the source emission is anisotropic, or beamed toward the observer. Done & Fabian (1989), using the luminosities in the 2–10 keV range, estimate the compactness of a sample of AGN. In Fig. 1.8 the distribution they find is reported. Several values are above the limit of 30, suggesting the importance of pair production in many sources.

Note also that this can be an indication that blazars (*i.e.* very compact objects, see also Fig. 1.9) must be beamed or have a very steep X–ray spectrum, otherwise the high pair production implied produces a pairs photosphere which scatters the

optical continuum, smearing variability and high linear polarization.

We considered just photon-photon interactions as pair producing mechanism, because its rate is at the lower order in the fine structure constant.

1.4.b Estimates of matter density

The lack of the spectral break in the observed spectra, as implied by the pair models, suggests values of $\tau_T < 3 - 10$ (Done, Ghisellini & Fabian 1990).

On the other hand (Blandford & Rees 1978) due to the short cooling timescales power must be continuously injected. If new particles are supplied (without pair production) they pile up or escape and their optical depth is

$$\tau_T \simeq \frac{\ell}{< \gamma > \beta_{esc}} \tag{1.4}$$

where $< \gamma >$ is the average injected Lorentz factor. If $< \gamma >$ is high many pairs are produced and they must annihilate (if rapidly cooled) in order not to accumulate and smooth rapid variations, because of the increasing diffusion timescale $\sim \tau_T R/c$.

The requirement that optical depth τ_T inside the source is less than one implies that the total mass is $< m_p R^2/\sigma_T$.

Note also that accretion model implies high opacity. Let us assume spherical accretion, with the matter falling at free fall velocity (which gives lower opacity). Therefore $\dot{M} = 4\pi R^2 \rho v_{ff}$ and

$$\tau_T = \frac{\sigma_T}{m_p} \int \rho dR = \frac{\dot{M} \sigma_T c}{4\pi\sqrt{6} G M m_p} \sim 4 \frac{L}{L_E} \tag{1.5}$$

if $R = 3R_s$ and using $L = \eta \dot{M} c^2 \simeq 0.1 \dot{M} c^2$. This value must be multiplied by v_{ff}/v_{in} in disc geometry, where viscosity determines v_{in}. The implied density are of the order of $n \simeq 7 \times 10^{10} (L/L_E)(v_{ff}/v_{in}) M_8^{-1}$, with $M = 10^8 \, M_8 \, M_\odot$ gr.

Maybe that other opacities are even more important, in any case the core of a maximally accreting black hole is optically thick and effects of feedback and trapping of radiation are effective. In a disk geometry $\tau_T >> 1$.

Moreover if the optical depth in ordinary matter (not pairs) is $\tau_T > 1$ it implies depolarization of non–thermal emission.

This limit can be avoided in sources where the power comes from electromagnetic extraction of the hole's spin energy (therefore the efficiency can be $\eta >> 1$).

The equilibrium pair density (neglecting dynamics) in a steady source can be obtained balancing pair production with pair annihilation rates, which assuming only photon–photon production and no escape of the pairs, can be expressed as $n_{\pm}^2 \sigma_T c \simeq (\xi f_\gamma L)/(4 m_e c^2 R^3)$, where ξ is the pair yield, the fraction of the injected luminosity which is converted into pair rest mass, and f_γ is the fraction of L with energy $\epsilon > 1$. Thus (Guilbert, Fabian & Rees 1983)

$$\tau_{e^\pm} \simeq (\xi f_\gamma \ell)^{1/2} \tag{1.6}$$

ξ increases with ℓ and saturate at $\simeq 0.1$ for $\ell > 10$ (Svensson 1986). Therefore if a consistent fraction of the luminosity is in γ–rays and $\ell > 1$ the source is optically thick for Thomson scattering, because particles can cool on timescales $< R/c$. The cooled pairs with $\tau_T > 1$ as already mentioned cause trapping of radiation, smoothing of variability and features in the spectrum. The problem of the accumulation of these pairs ('dead' electrons) can solved if a reacceleration mechanism operates. Done, Ghisellini & Fabian (1990) analyzed this possibility and discovered that it cannot resolve the problem, because if many pairs are created the same limit as before applies. On the other hand if the injected luminosity is constant and reacceleration operates the mean particle energy must decrease (because the number of particles increases), reducing the pair production. A typical maximum Lorentz factor for the reaccelerated particles, from this feedback mechanism, corresponds to MeV energies.

In the hypothesis that the radio spectrum in compact sources is due to synchrotron emission and from linear polarization measures, it is possible to deduce limits on the maximum amount of cold or thermal electrons and their energy distribution (Jones & O'Dell 1977; Wardle & Roberts 1988). In fact Faraday rotation implies depolarization, measured from the 'Faraday depth' $\Delta\phi \simeq 81 \lambda^2 \int (n_e/\gamma) B \, dl$ where n_e is the electron density, B the magnetic field component parallel to the line of sight, γ is the low energy cut–off Lorentz factor of the emitting particles, λ(cm) is the wavelength and dl the length element along the line of sight (in pc). However *e.g.* in an inhomogeneous source the λ^2 dependence can be not satisfied (Blandford

& Königl 1979).

The absence of Faraday rotation implies that the number and energy densities of cold electrons must be both less than the relativistic ones [$n(\gamma < 100) \ll n(\gamma > 100)$ and $U(\gamma < 100) \ll U(\gamma > 100)$ where U are the energy densities. Therefore the minimum Lorentz factor of the relativistic electron distribution must be typically greater than $\sim$ 100 (however see Jones & O'Dell 1977), implying an efficient acceleration mechanism.

On the contrary the presence of depolarization should be taken with care, because it can be due to the external medium and not refer to the internal matter content.

For example in the case of the jet of 3C120 the deduced limit on thermal electrons density is $n_e < 10^{-3}$ cm^{-3} (*e.g.* Walker, Benson & Unwin 1987), or alternatively electrons must have a minimum Lorentz factor >> 1.

Note that limits on the amount of thermal particles imposed from the absence of Faraday depolarization can not be applied to pair plasma, which do not depolarize radiation (see §2.3).

Upper limits to the electron density could be given by the requirement that free–free optical depth is less than one and from the absence of induced Compton scattering effects, *i.e.* $\tau_{IC} \simeq (kT/m_e c^2)\tau_T < 1$ (Begelman, Blandford & Rees 1984). In fact for $T_b > 10^{11}$ K (*i.e.* $kT \gtrsim 20\, m_e c^2$) radiation is so intense that σ_T must be increased, due to induced effects. As suggested by the requirement of pressure confinement in BLR and depolarization measures, the external medium has $\tau_T \sim 0.1$. Therefore the induced scattering for these temperatures can be relevant. It is frequency dependent and produces spectral variation near the brightness temperature peak (with slope $\simeq 0.2$) and a variable degree in linear polarization. However up to now no signs of its presence has been observed: for ν=1 GHz, size l, and external temperature T this implies $n_e < min[2\times10^3 T_4^{3/2}/l^{1/2}; 3\times10^3/l]$ (Begelman, Blanford & Rees 1984). In particular for a brightness temperature as high as 10^{18} K, the optical Thomson depth should be $< 10^{-8}$, suggesting, together with the Compton scattering limits discussed above, that relativistic effects are present (Blandford 1990).

Summarizing: high optical depths smear fast variability, change the observed

spectrum producing typical features, and for ordinary matter destroy high linear polarization. The above estimation of high τ_T can be overcomed claiming relativistic effects or a strong reacceleration mechanism and fast annihilation for a pair plasma.

1.4.c Variability limits

A limit on the compactness is derived from the efficiency limit (Fabian 1979). It is due to the maximum rate of change of luminosity, when all the rest mass energy is converted into luminosity in the escape timescale $\Delta L\,\Delta t = \eta M c^2$ where η is the efficiency.

The two basic assumptions are that luminosity is stored in the form of matter for a time Δt (and not as magnetic, *e.g.* flares, or rotational energy) and that electrons are not reaccelerated (*i.e.* the emitting electrons do not spend much time at subrelativistic energies, Guilbert, Fabian & Rees 1983). It is also necessary that the process coupling the radiating electrons and the source of energy is rapid. In the case of electron–ion coupling in a thermal plasma it implies $kT_e < 35$ keV (Guilbert, Fabian & Stepney 1982).

The limit derives from the competition between the increasing diffusion time and luminosity with increasing accreting matter. The escape timescale is $\Delta t = 3R(1+\tau_T)/4c$ for a spherical source, where the term $(1+\tau_T)$ accounts for the effects of diffusion if the source is optically thick to Compton scattering in the Thomson limit ($\tau_T > 1$).

Therefore

$$\Delta L \leq \frac{64\pi}{27}\eta\frac{m_p c^4}{\sigma_T}\frac{\tau_T}{(1+\tau_T)^2}\Delta t \leq \frac{16\pi}{9}\eta\frac{m_p c^4}{\sigma_T}\Delta t \simeq 2\times 10^{41}\eta_{0.1}\Delta t \qquad \mathrm{erg\,s^{-1}} \tag{1.7}$$

where the second inequality is obtained for the maximum value of $\tau_T \simeq 1$. Using the compactness parameter

$$\ell \leq \frac{16\pi}{27}\eta\frac{m_p}{m_e} \tag{1.8}$$

with $\ell = (\Delta L/\Delta t/c)(m_e c^3/\sigma_T)$. For an efficiency of $\eta \simeq 0.1$ the maximum compactness is ~ 350.

As already shown in Guilbert, Fabian & Rees (1983) the limit is increased of a factor δ^5 in case of relativistic motion, equivalent to an efficiency $\eta >> 1$. Moreover

if the geometry is sheet– like, the limit must be increased by a factor $\pi\Delta R/R$, where ΔR is the thickness, and the whole region must be switched in a time $< \tau_T \Delta R/c$.

Pair production tends in general to smear variations because an increased luminosity produces more pairs and therefore more optical depth for photons to escape, and therefore also a broadening of the annihilation line. Note instead that in a thin shell configuration maybe that the annihilation line is a prominent feature.

Fast variability poses constrain on the X–ray emission mechanism. The bremsstrahlung cooling rate is given by $const \times n^2 T^{1/2}$ erg s^{-1} cm^{-3} and the Compton one by $\simeq n(L/4\pi R^2 c\epsilon)(\epsilon 4kT/m_e c^2)\sigma_T c$. Thus deriving n from the bremsstrahlung emissivity $L \simeq const \times n^2 T^{1/2} R^3$, and imposing that the bremstrahlung cooling rate is greater than the Compton one, we get

$$L < 10^{39} T_9^{-3/2} \Delta t \qquad \text{erg s}^{-1} \tag{1.9}$$

using $R = \Delta t\, c$ and $T = 10^9 T_9$. This inequality is not satisfied by many rapid varying AGN.

As far as self–Comptonized bremsstrahlung is concerned, upper limit to $\Delta L/\Delta t$ are given by (Zdziarski 1986)

$$\Delta L < 10^{38} \left(\frac{R_s}{R}\right)^{1/2} \tau_T \left[\ln(2.5/x_{min})\right]^2 \Delta t \qquad \text{erg s}^{-1} \tag{1.10}$$

where x_{min} is the low energy cutoff in units of $m_e c^2$.

We can also express the Eddington limit in term of variability limit, using $\Delta t = 3R_s/c$:

$$L_E \simeq 3 \times 10^{42} \Delta t \qquad \text{erg s}^{-1} \tag{1.11}$$

which means also that if the source is sub–Eddington, its dimension from variability is smaller than the Schwarzschild radius.

In Figs. 1.9 we show in a plot Δt versus L that some objects do not satisfy the limits. In the other figure also the previous limits are reported and compared with the data relative to a sample of Seyfert galaxies. In general, as already mentioned, variations with $\Delta L/\Delta t$ exceeding the above limits are considered an indication of

relativistic beaming (*e.g.* PKS 0558–504, Remillard *et al.* 1991; 3C279, Makino *et al.* 1989), even if that does not implies the presence of a jet.

Note that the limits are deduced for a steady situation; special geometries, as already noted, can also overcome these limits (Guilbert, Fabian & Rees 1983). Moreover they do not apply if variations do not involve the whole source.

Another interesting information from variability comes from the short doubling timescales. In the case of observed periodicity in the light curves (*e.g.* NGC 6814, NGC 4151) if one assumes that the variability is due to an enhanced luminosity region orbiting around an accretion disc, a limit on the mass of the black hole can be inferred.

In the simplest approximation, neglecting general relativistic effects, suppose that the variability is due to the orbital rotation of a bright blob in a thin disk at a distance R from the centre of the system. The blob emits isotropically, the system is axially symmetric the emissivity depends just on frequency (and not on position and direction). Let us call βc its tangential velocity, ψ the azimuthal angle measured from the line of sight (corresponding to $\psi = 0$), θ the angle of the line of sight with respect to the normal to the disc and Ω the orbital frequency. The observed variability timescale t_{var} is affected by special relativistic corrections and time delay due to the orbital motion.

If assume that the total luminosity is the sum of the disc luminosity $L_d = L_o/f$ plus an amplified blob luminosity $L_b = \delta^4 L_o$, the doubling observed timescale is given by

$$t_{var} = \frac{L_b + L_d}{d(L_b + L_d)/dt_{obs}} = \frac{\delta^4 + 1/f}{(d\delta^4/dt)(dt/dt_{obs})} = \frac{(1 + \beta \sin\theta \sin\Omega t)^2}{4\beta\Omega \sin\theta \cos\Omega t} \left(1 + \frac{1}{\delta^4 f}\right) \tag{1.12}$$

where t_{obs} is measured in the observer frame.

For $\theta = 90^o, f\delta^4 \gg 1, \beta = 1$, assuming the shortest timescale of NGC 6814 (which also show a periodic behaviour, as already mentioned) of 50 s., this requires $\Omega = 10^{-3}(R/R_s)^{-3/2}(M/10^8\, M_\odot)^{-1}) = 5\, 10^{-3}$, and for $R \simeq 3\, R_s$, implies $M \simeq 10^{-2}(M/10^8 M_\odot)$ and $\delta \simeq 1.5$.

Obviously these results are strongly approximate and do not take into account general relativistic effect, but it shows simply which kind of limits can be set by the

fast variability observations.

1.4.d SSC radiation mechanism

As already mentioned the high polarization and the power–law spectrum in blazars suggest that radiation is synchrotron emission from relativistic electrons with a nonthermal distribution. If the source is compact enough the inverse Compton emission of the same relativistic electron on the photons that they produce is an efficient cooling mechanism, producing also high energy photons (Synchrotron self–Compton process, SSC).

In the original form the model considers an homogeneous spherical region, with a constant and randomly distributed magnetic field B and a stationary isotropic electron distribution (Jones, O'Dell & Stein 1974a,b). Averaging on the pitch angles and incident angles of photons and neglecting the effects of losses on the electron motion, radiation cooling of a relativistic electron of energy $\gamma m_e c^2$, $\gamma \gg 1$, due to synchrotron and inverse Compton are

$$\begin{aligned} \dot{\gamma}_s &= \frac{4}{3}\frac{\sigma_T c}{m_e c^2} U_B \gamma^2 \\ \dot{\gamma}_c &= \frac{4}{3}\frac{\sigma_T c}{m_e c^2} U_R \gamma^2 \end{aligned} \tag{1.13}$$

U_B and U_R are the magnetic and radiation energy densities, the latter is given (for SSC), by the synchrotron radiation U_{Rs} which is in the Thomson limit (Ghisellini 1987), *i.e.* photons with energy less than the electron mass energy in its rest frame ($\gamma h\nu < m_e c^2$). This allow to use a constant Thomson cross section and neglect momentum transfer. For higher photon energies Klein–Nishina cross section should be used ($\gamma \gtrsim 10^4$), smaller than σ_T and decreasing with energy, reducing the radiated power. This in turn implies a limit on the high energy radiation which can be emitted through multiple Compton scattering, solving the 'Compton catastrophe' problem.

In the following we consider only first order scatterings in the Thomson regime. From (1.13)

$$\frac{\dot{\gamma}_s}{\dot{\gamma}_{c,1}} = \frac{U_B}{U_{Rs}} = \frac{L_s}{L_{c,1}} \tag{1.14}$$

which measure the relative importance of the two processes.

The frequency spectrum for synchrotron emission in the ultrarelativistic limit can be approximated by a continuum spectrum:

$$P(\gamma,\nu) = \frac{2}{\sqrt{3}}\frac{e^3 \sin\theta}{m_e c^2} B \frac{\nu}{\nu_c} \int_{\nu/\nu_c}^{\infty} K_{5/3}\left(\frac{\nu}{\nu_c}\right) d\left(\frac{\nu}{\nu_c}\right) \propto \left(\frac{\nu}{\nu_c}\right)^{1/3} e^{-\frac{\nu}{\nu_c}} \qquad (1.15)$$

with

$$< \nu_c >= \frac{3}{2}\frac{eB}{2\pi m_e c} < \sin\theta > \gamma^2 = \frac{3}{2}\nu_B \gamma^2 \qquad \text{Hz} \qquad (1.16)$$

$\nu_B \simeq 1.22\,10^6\, B\, Hz$ is the cyclotron frequency, $K_{5/3}$ the modified Bessel function of order 5/3, e the electron charge.

Eq.(1.15) shows that the single electron emission peaks at $\nu \simeq 0.29\,\nu_c$, and therefore the synchrotron emissivity from an electron distribution assumed fixed with spectrum

$$N(\gamma)d\gamma = K\gamma^{-p}d\gamma \qquad \text{for} \qquad \gamma_{min} < \gamma < \gamma_{max} \qquad (1.17)$$

and $p > 0$, can be approximately obtained using $P(\gamma,\nu) = P(\gamma)\delta(\nu - 0.29\nu_c)$ and integrating on the electron distribution

$$\epsilon_s(\nu) = \int N(\gamma)P(\gamma,\nu)d\gamma = c_1(\alpha)KB^{1+\alpha}\nu^{-\alpha} \qquad \text{erg cm}^{-3}\,\text{s}^{-1}\,\text{Hz}^{-1}\,\text{rad}^{-1} \qquad (1.18)$$

with $\alpha = (p-1)/2$ and c_1 constant ($c_1(0.5) \simeq 3.58\,10^{-19}$). The reported value is not unique in literature due to different approximations (see Urry 1984).

The pressure and energy density of the relativistic electron distribution (1.17) are dominated by the upper cut–off energy γ_{max} for $p < 2$ ($\alpha < 0.5$). The synchrotron emissivity instead is dominated by the upper limit for $p < 3$ ($\alpha < 1$). Therefore for $0 < \alpha < 1$ if the electron energy is derived from the observed cut–off frequency it can be underestimated by a factor $(\gamma_{min,obs}/\gamma_{min})^{(p-2)}$, while the total power overestimated by $(\gamma_{max}/\gamma_{max,obs})^{(3-p)}$.

Eq. (1.18) is valid in the range $3/2\,\nu_B\gamma_{min} \ll \nu \ll 3/2\,\nu_B\gamma_{max}$, *i.e.* not at the extremes of the emitted spectrum, where it follows the behaviour of the single electron emission.

Low energy radiation can be reabsorbed from the same electrons which produce it. For the assumed electron distribution and $\nu \gg 3/2\,\nu_b\gamma_{min}^2$, the absorbing

coefficient is

$$k(\nu) = \frac{3^{\alpha+1}\sqrt{\pi}}{8} \frac{\Gamma[(3p+22)/12]\,\Gamma[(3p+2)/12]\,\Gamma[(p+6)/4]}{\Gamma[(p+8)/4]} \frac{e^2 K}{m_e c} \nu_B^{(p+2)/2} \nu^{-(2.5+\alpha)} \quad \mathrm{cm}^{-1} \tag{1.19}$$

The source term of the transfer equation is therefore given by $S(\nu) \propto \nu^{5/2} B^{-1/2}$. Defining the self–absorbtion frequency ν_t as the frequency for unit optical depth $k(\nu)R = 1$ (Ghisellini 1987)

$$\nu_t = \left[\frac{3^{p/2}\sqrt{3\pi}}{8} \frac{\Gamma[(3p+22)/12]\Gamma[(3p+2)/12]\Gamma[(p+6)/4]}{\Gamma[(p+8)/4]} \frac{e^2 K R}{m_e c} \nu_B^{(p+2)/2} \right]^{2/(p+4)} \quad \mathrm{Hz} \tag{1.20}$$

The spectrum depends on frequency as $F \propto \nu^{2.5}$ for $\nu < \nu_t$. More precisely the low energy spectrum for a stationary electron distribution assume a quasi–Maxwellian shape (Ghisellini, Guilbert & Svensson 1988) and this is suggested to be both an efficient thermalizing mechanism and a mean to transfer energy to electrons (Ghisellini *et al.* 1990) (see §2.3 and §4.1).

The thin synchrotron flux, neglecting the absorbed radiation effects, is obtained integrating emissivity over volume.

Substituting ν_t in the transfer equation it is possible to determine the magnetic field

$$B \simeq 1.3 \times 10^{-3} f(\alpha)^2 \left(\frac{F_m}{Jy}\right)^{-2} \left(\frac{\theta_d}{m.a.s.}\right)^4 \left(\frac{\nu_t}{Ghz}\right)^5 \quad \mathrm{G} \tag{1.21}$$

given the angular diameter θ_d (if θ_d is measured with VLBI, at the frequency ν_t) $F_m = F(\nu_t)$ and the spectral index α of the thin regime ($f(\alpha)$ is a constant, $f(0.5) \simeq 0.5$).

Therefore also the density of the emitting particles can be deduced

$$\tau_T = \frac{8^3 \pi^{3/2}(p+1)}{3^{1+p/2} c} \frac{\Gamma[(p+7)/4]}{\Gamma[(p+5)/4]\Gamma[(3p-1)/12]\Gamma[(3p+19)/12]} \left(\frac{2\pi m_e c}{e}\right)^{\frac{p-3}{2}} \frac{F_m \nu_t^{\alpha} B^{-(1+\alpha)}}{\theta_d^2} \tag{1.22}$$

The inverse Compton emission can be computed approximately using the fact that the energy distribution of the scattered photons has as an average value

$\nu_c = (4/3)\nu_s\gamma^2$ where ν_s is the frequency of the synchrotron scattered photon. The Compton emissivity is obtained integrating on the incident photon and electron distributions.

For a single scattering and electron distribution given by (1.17), in the Thomson regime

$$\epsilon_{c,1}(\nu) = \frac{(4/3)^\alpha}{8\pi}\frac{m_e c^2 \tau_T}{R/c}\nu^{-\alpha}\int_{\nu_{min}}^{\nu_{max}} n(\nu')\nu'^{1+\alpha}\,d\nu' = \left(\frac{3}{4}\right)^{1-\alpha}\frac{\tau_T}{2}\ln\Lambda\,\epsilon_s(\nu) \quad (1.23)$$

for $4/3\,\nu_{mins}\gamma_{min}^2 < \nu < 4/3\,\nu_{max}\,\gamma_{max}^2$. The extreme of the integration depend on the photons and electrons distributions (see *e.g.* Ghisellini 1987) and, in the spectral region where they are constant, the Compton spectrum has the same power–law dependence on frequency of the synchrotron spectrum. Furthermore self–Compton radiation results to be the product of ϵ_s with the scattering probability $\tau_T = \sigma_T\,R\,K$. Λ is approximately given, not at the extreme of the spectrum, by $\simeq (\gamma_{max}/\gamma_{min})^2$.

For $\tau_T \ll 1$ at fixed frequency the thin synchrotron emission or its extrapolation is a factor $(3/4)^{1-\alpha}\ \tau_T/2\ \log\Lambda$ above ϵ_c. τ_T determines therefore the ratio of the two monochromatic fluxes, and similarly for the higher Compton orders: the assumption of considering only first Compton order is satisfied if $\tau_T \ll 1$.

The condition for electrons to cool mainly through synchrotron than first Compton order emission can be expressed as $U_B > U_R$. $U_R/U_B \propto T_b\nu_t^3/B^2 \propto T_b^5\nu_t$, using the brightness temperature T_b at ν_t. The limit can be written, calculating the constants as $T_b \lesssim 6\times10^{13}(1-\alpha)^{4/5}\nu_{max}^{(\alpha-1)/5}/\nu_t^{\alpha/5}$ K (*e.g.* Blandford 1990). If $\alpha > 1$ a spectral correction must be applied. For the relativistic corrections see below; in a non relativistic source, the inequality is satisfied for $T_b \leq 10^{12}\,K$ and this limit on the brightness temperature is weakly dependent on the spectral index.

In fact T_b is the temperature of a blackbody emitting the same flux in the Rayleigh–Jeans part of the spectrum, and thermodynamically it is expected it does not exceed the kinetic temperature $\gamma_t m_e c^2/3$ of the emitting electron, otherwise radiation is self–absorbed. Theoretically the brightness temperature is predicted to be weakly dependent on the parameters of the sources, being directly related to the energy of the electrons emitting at the self–absorbtion frequency (see eq. (1.20), with $\nu_t = (4/3)\nu_B\gamma_t^2$). The hypothesis that the radio emission is due to synchrotron

process requires $kT_b > m_e c^2$ and $T_b \lesssim\!< \times 10^6 (\nu/B)^{1/2} g(\alpha)$ K, where $g(\alpha)$ is a slowly varying function increasing from 0.5 to 2.0 as α increases from 0 to 1. If $\alpha = 0.75$, $T_b \propto (KR/B)^{1/6.5}$.

Therefore the brigthness temperature is reasonably the same for all the objects $T_b \sim 10^{12}$ K, corresponding to $\gamma_t \sim 100$.

T_b bigger than the limit value are supposed to be an indication of relativistic effects. In the case of relativistic beaming the brightness temperature transforms as $T_{obs}(\nu) = \delta T_b'(\nu')$. From the observed quantities and the derived Doppler factor, it is possible to calculate the comoving brightness temperature $T_b' = 1.72 \times 10^{12} (F_m/\theta_d^2 \nu_m^2)(1+z)/\delta$ K. Note that the incorporation of cosmological corrections is analogous to the Doppler corrections, with the substitution $\delta \rightarrow (1+z)^{-1}$.

Let us include relativistic corrections for the brightness temperature in the case the dimensions are estimated from variability timescales *i.e.* $T_{var} = F d_L^2 / 2k\nu^2 c^2 t_{var}^2$, where d_L is the luminosity distance. The observed flux can be written $F = (2k\nu^2 \delta T' R^2)/d_L^2$, and therefore $T_{var} = \delta^3 T_b'$.

SSC standard model allows to determine the expected Compton flux given the synchrotron spectral index, the redshift, the self–absorbtion frequency and flux, the maximum frequency emitted by the more energetic electrons ν_b and the angular diameter. The flux is given (integrating the (1.23)) (Urry 1984)

$$F_c(\nu) = f'(\alpha)^{2(2+\alpha)} \left(\frac{F_m}{Jy}\right)^{2(2+\alpha)} \left(\frac{\nu_t}{Ghz}\right)^{-(5+3\alpha)} \left(\frac{\theta}{m.a.s}\right)^{-2(3+2\alpha)} \left(\frac{\nu}{2.42\,10^8\,Ghz}\right)^{-\alpha} \ln\left(\frac{\nu_b}{\nu_t}\right) (1+z)^{2(2+\alpha)} \simeq \tau_T \; F_s(\nu) \; Jy \qquad (1.24)$$

where $f'(\alpha)$ is a constant (for $\alpha = 0.75$, $f' \simeq 0.2$). The dimension must be deduced from VLBI measures, and when it is estimated from variability timescale it must correspond to the frequency ν_t, not to impose that emission at different frequencies is produced in regions of the same dimensions. Note the strong dependence of the predicted flux on the observable quantities, especially θ_d and F_m, ν_t which are in reality obtained extrapolating of the observed spectrum. For a detailed discussion on the observational aspect see Marscher (1987).

A more consistent approach to the SSC emission model has been developed by Ghisellini (1987). In the assumption of a compact source, such that cooling

timescales are the shorter ones, the emitting particles distribution is not assumed a priori but it is deduced as a solution of a kinetic equation in which the source term is given, with an arbitrary distribution but with a kinetic luminosity equal to the observed luminosity. Assuming a continuous injection term $Q(\gamma) = Q_o\gamma^{-s}$ cm^{-3} s^{-1} the stationary solution is $N(\gamma) = \int Q(\gamma)d\gamma/(\dot{\gamma}_s + \dot{\gamma}_c) \propto \gamma^{-2}$, where the last proportionality is satisfied *e.g.* for monoenergetic injection and Thomson scattering. It implies $\alpha = 0.5$. In the case of many electrons generations, like in pair plasma, the flow of particles in energy space is conserved and $N(\gamma) \propto \gamma^{-3}$, which gives $\alpha = 1$.

The interesting result is that not all the spectral indices p result to be self–consistent, and in particular only flat ($\alpha < 1$) indices can be produced.

1.4.e Doppler amplification of the flux

In the previous sections effects due to relativistic motion of the emitting plasma were quoted. The beaming toward the observer produces an increase in the observed flux, due to aberration, a shift in the observed frequency and a contraction in the observed timescales. All these effects can be quantified by the Doppler factor, defined as $\delta = 1/\gamma(1 - \beta\cos\theta)$ (see Fig. 1.10), where βc and γ are the velocity and the corresponding Lorentz factor of the plasma and θ the angle between the velocity vector and the line of sight

$$(\theta = 90^\circ) \qquad \frac{1}{\gamma} \leq \delta \leq 2\gamma \qquad (\theta = 0^\circ, \gamma \gg 1)$$

and

$$\delta > 1 \text{ for } \theta < \arcsin\left(\frac{2}{1+\gamma}\right)^{1/2} \tag{1.25}$$

We now examine in more detail the dependence of flux on δ assuming that the reference frame comoving with the emitting plasma do not coincide with the frame of the observed volume (Lind & Blandford 1985). The reference frames will be: the frame comoving with the fluid, where emissivity is isotropic (two apices), the emitting region frame (one apex) and the observer frame.

Let be $\epsilon"_{\nu"}(\nu")$ and $k"_{\nu"}(\nu")$ the emissivity and the absorption coefficient in the fluid frame, moving with constant velocity $\beta'(x')c$. If emissivity depends on frequency as a power law $\epsilon(\nu) \propto \nu^{-\alpha}$ ($\epsilon(\nu)/\nu^2$ is an invariant)

$$\epsilon'_{\nu'}(\nu', \vec{n}') = \delta'^2 \, \epsilon"_{\nu"}(\nu") = \delta'^{2+\alpha} \, \epsilon"_{\nu"}(\nu') \tag{1.26}$$

and for synchrotron radiation

$$k'_{\nu'}(\nu', \vec{n}') = \delta'^{-1} \, k"_{\nu"}(\nu") = \delta'^{\alpha+1.5} \, k"(\nu') \tag{1.27}$$

(Rybicki & Lightman 1979).

The intensity along a ray with direction $\vec{n}'$ is

$$I'_{\nu'}(\nu', \vec{n}') = \int_0^{x'} \epsilon'_{\nu'}(\nu', \vec{n}', x') \, e^{-\int dy' \; k'(\nu', \vec{n}', y')} \, dx' \tag{1.28}$$

and transform as $I_\nu(\nu, \vec{n}) = \delta^3 \; I'_{\nu'}(\nu' = \nu/\delta, \vec{n}')$. Let be βc the velocity of the emitting region and Σ' its area. The area projected orthogonally to the line of sight Σ is equivalent to Σ' even if observed in a 'rotated' direction $\vec{n}'$. There is no contraction of the observed area because compensated by the light travel time ($dx^2 - dt^2$ is invariant).

We can get the flux integrating the intensity on the observed area. In the optically thin case $\tau \ll 1$

$$\begin{aligned} F_\nu(\nu) = \int_\Sigma I_\nu \, d\Omega \; = \int_{\Sigma'} I_\nu \, \frac{dA'}{d_L^2} = \frac{1}{d_L^2} \int_{\Sigma'} dA' \int_0^x \epsilon_\nu \, dx = \\ = \frac{1}{d_L^2} \int_{\Sigma'} \delta^3 \int_0^{x'} \epsilon'_{\nu'}(\nu') \, dx' \, dA' = \frac{\delta^{3+\alpha}}{d_L^2} \int_{V'} \delta'^{2+\alpha} \, \epsilon"_{\nu"}(\nu) \, dV' \end{aligned} \tag{1.30}$$

where d_L is the luminosity distance (Weinberg 1972). The result does not depend on the emitting region shape, while in the the optically thick case the optical depth depends on the viewing angle

$$\tau(\nu) = \delta^{\alpha+2.5} \int_0^{x'} \delta'^{\alpha+1.5} \, k"(\nu) \, dx' \tag{1.31}$$

If we observe different components with different optical depths each of them shows a maximum for $\tau \simeq 1$.

If we have only two rest frames the situation is simplified. In the case of a stationary jet, or different components which mimick a continuum, the emitting region frame is the same of the observer, and the Doppler factor exponent will be

$2+\alpha$; if instead the emission region coincides with the observed volume, the exponent will be $3+\alpha$, due to the volume transformation.

In the particular case of a shock wave, three frames must be considered. For a ultrarelativistic fluid (*i.e.* adiabatic index of 4/3 for the up and downstream plasma) the shock conservation equations have a simple solution $u_1 u_2 = 1/3$, where u_1 and u_2 are the pre and post shock velocities measured in the front shock frame. The Doppler corrections reduce to the factor $\delta^{2+\alpha}(\beta_2)\delta(\beta_s)$, where $c\beta_1, c\beta_2, c\beta_s$ are the pre, postshock and front velocities in the observer frame and $\beta_2 = (3\beta_s^2 - 2\beta_s\beta_1 - 1)/(\beta_1\beta_s^2 + 2\beta_s - 3\beta_1)$.

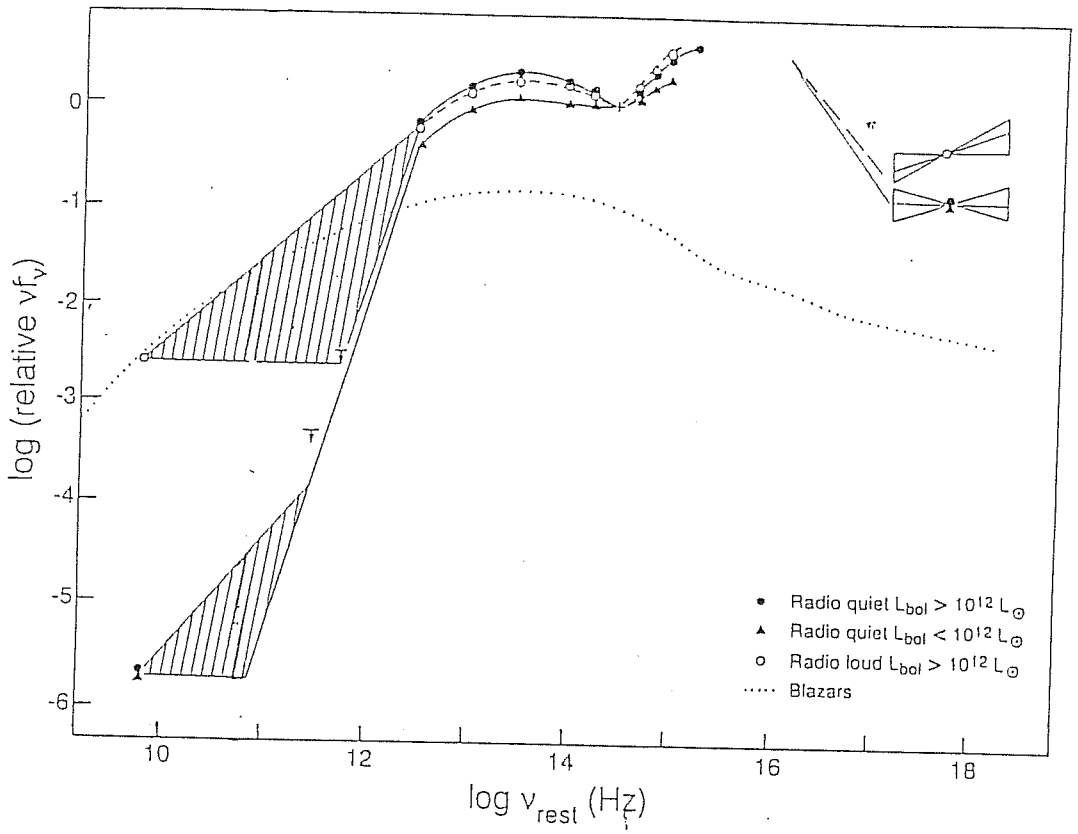

Fig. 1.1 Mean spectral energy distributions of different types of AGN. The labels distinguish the different sources. Note that the spectrum of blazars does not show features. The quantity νf_ν indicates directly where most of the power is emitted. From Sanders *et al.* (1989).

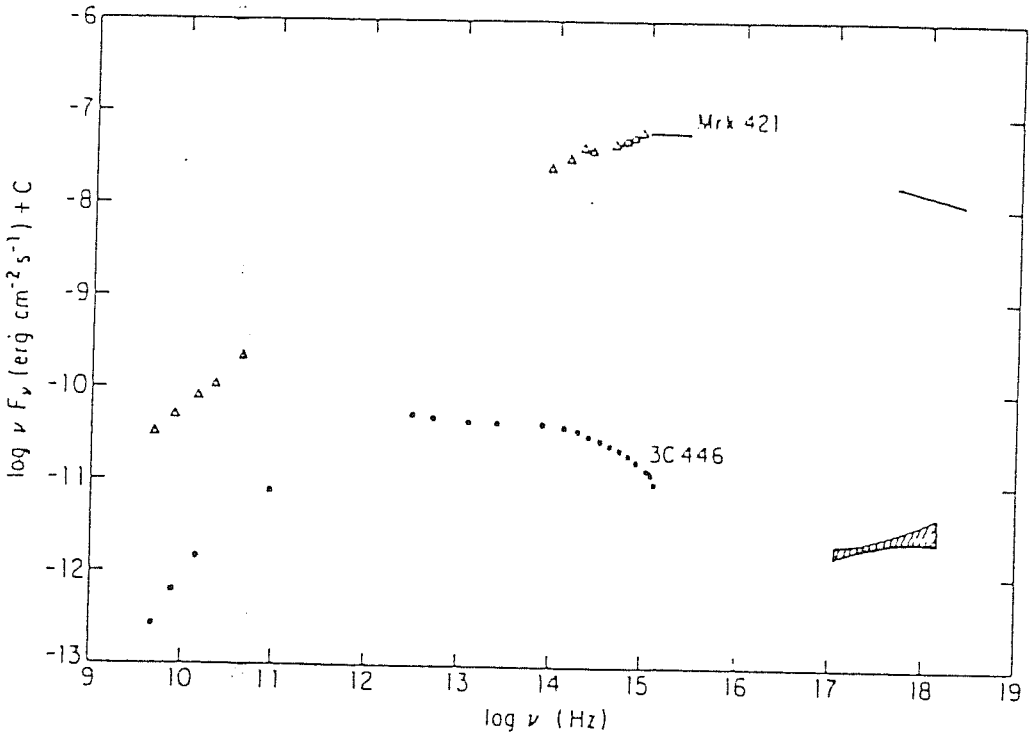

Fig. 1.2 Energy distributions of two BL Lac objects, a X–ray selected (Mkn 421, Makino *et al.* 1989) and a radio selected one (3C446, Bregman *et al.* 1986). It should be noted the different frequency at which the emitted power peaks and the different X–ray slopes. The X–ray power component for radio selected objects tends to be flat, above the extrapolation from the optical–UV band. From Maraschi (1991).

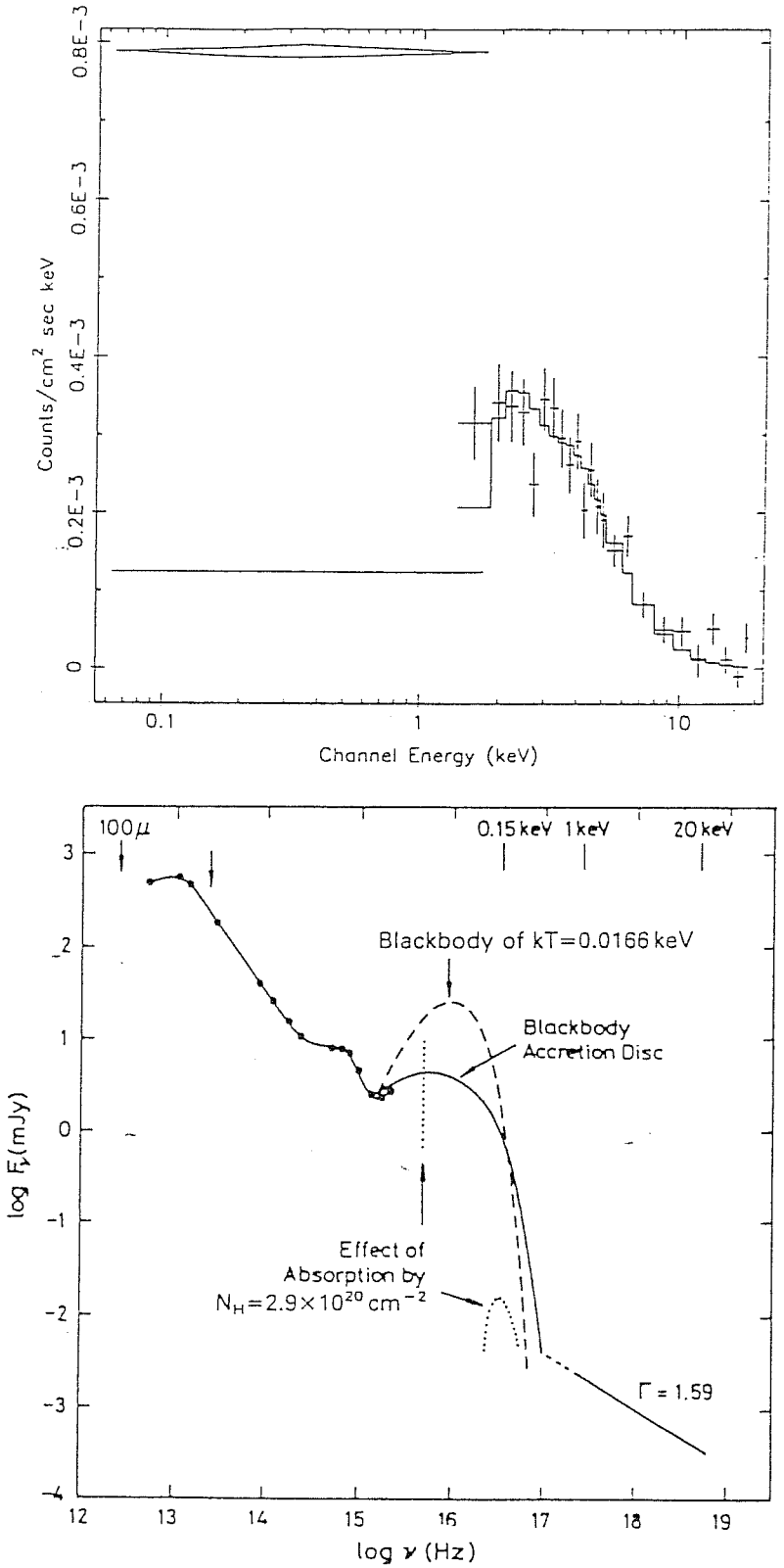

Fig. 1.3 In the upper panel X–ray spectrum of Mkn 841 is reported. The continuous line represents the best–fit model at high energy, which is then extrapolated to the soft X–ray band (horizontal line). The diamond is the low energy measurement, which is well above (soft excess) the model extrapolation.

The bottom figure is the spectral distribution of the same object, where the UV has been connected with the X–ray spectrum with a blackbody (dashed line) and an accretion disc spectra. The blackbody reduces to the dotted line when the effect of galactic absorption is taken into account. From Arnauld *et al.* (1985) and references therein.

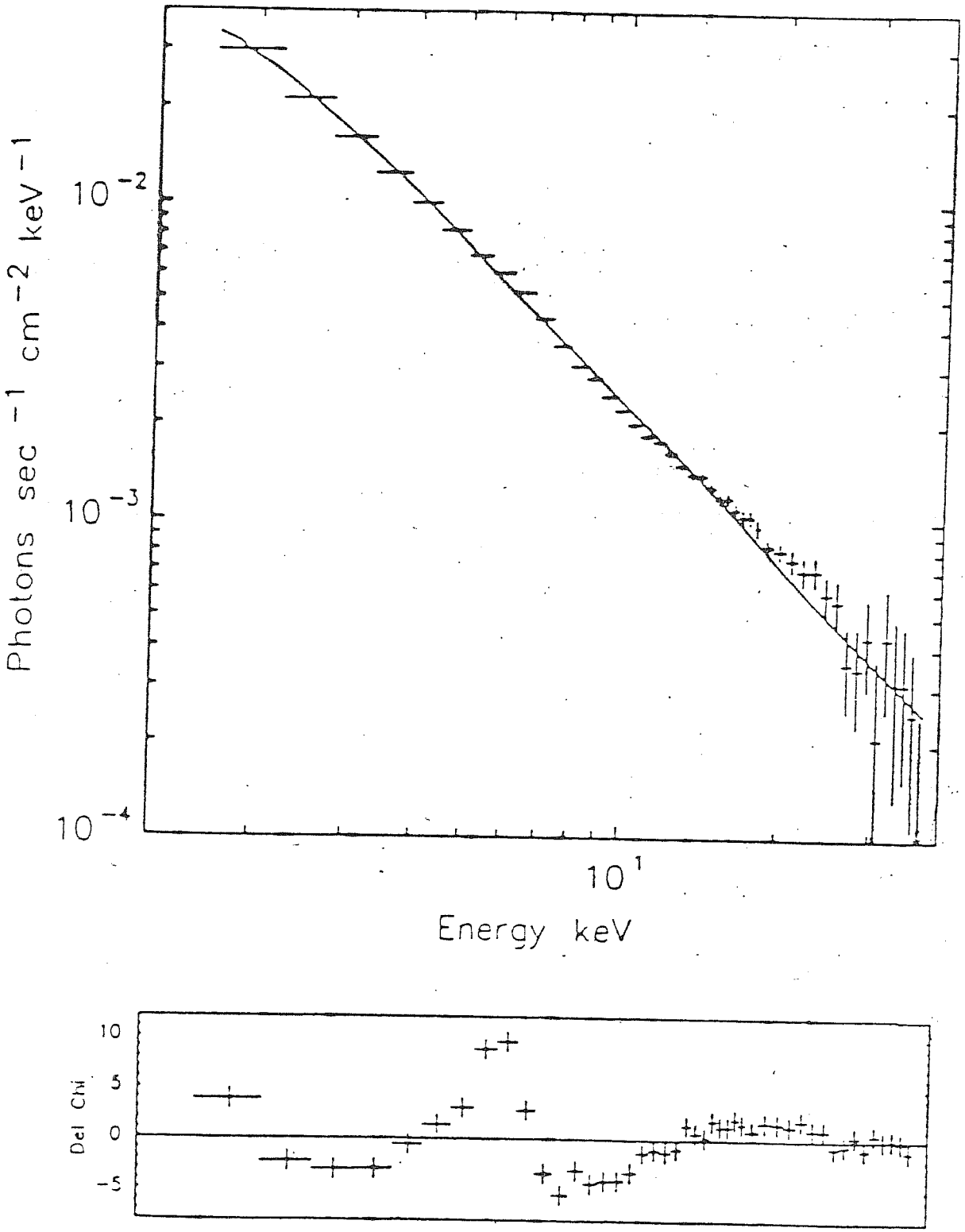

Fig. 1.4 Power–law fit ($\alpha = 0.64$, $N_H = 4 \times 10^{21}$ cm^{-2}) to the average spectrum obtained summing 12 GINGA spectra (see text). The bottom part reports the data minus model residuals. It can be seen the presence of an iron emission line at 6.28± 0.2 keV, with equivalent width of 110 eV, and at about 20–30 keV the presence of a (reflection) bump. From Pounds *et al.* (1990).

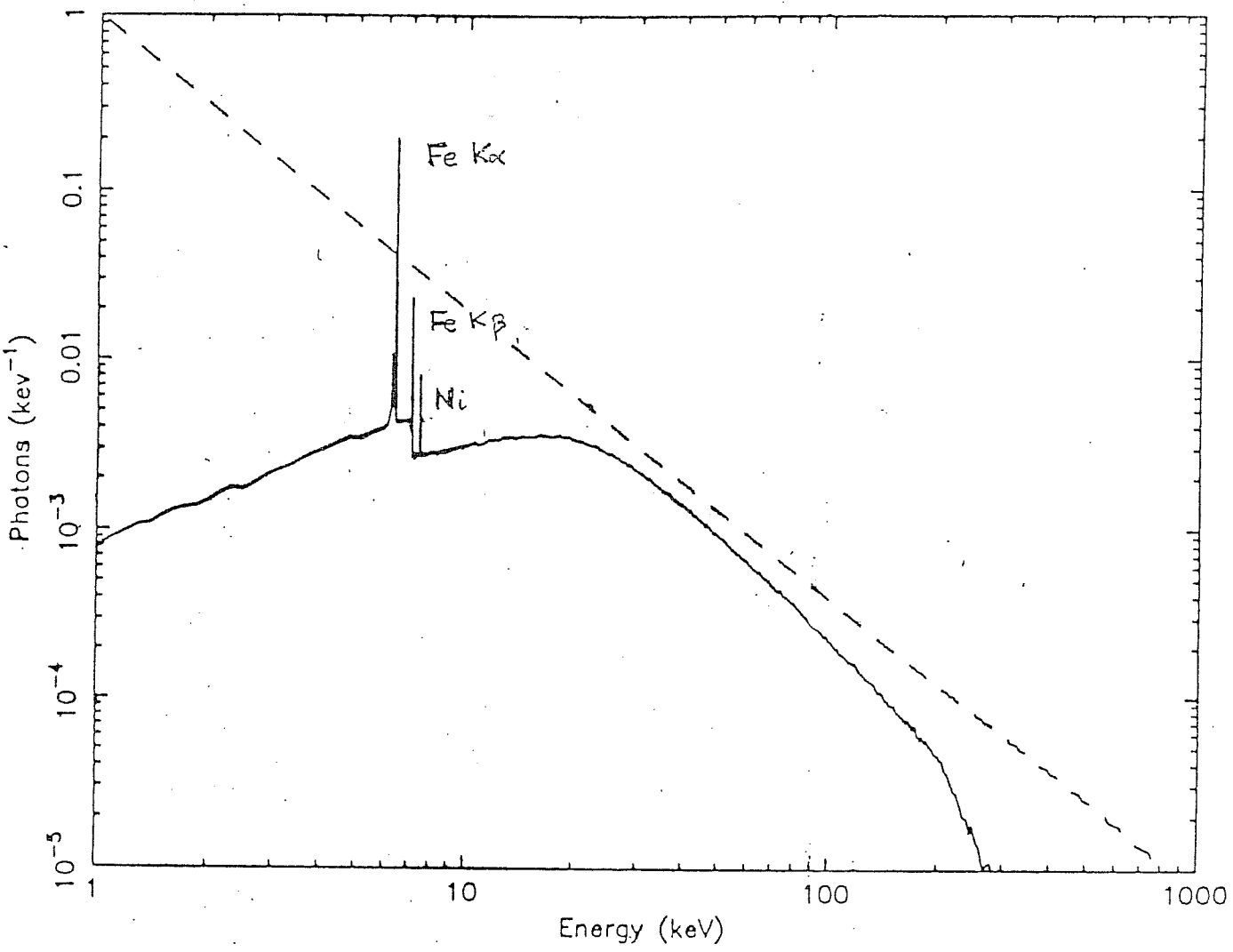

Fig. 1.5 Monte Carlo simulation of the reflected spectrum from a disc illuminated by a direct power-law spectrum with $\alpha = 0.7$ (dashed line). The emitted line are indicated. For the other feature (bump) see the text. The observed spectrum is the sum of the direct and the reflected component. From George & Fabian (1991).

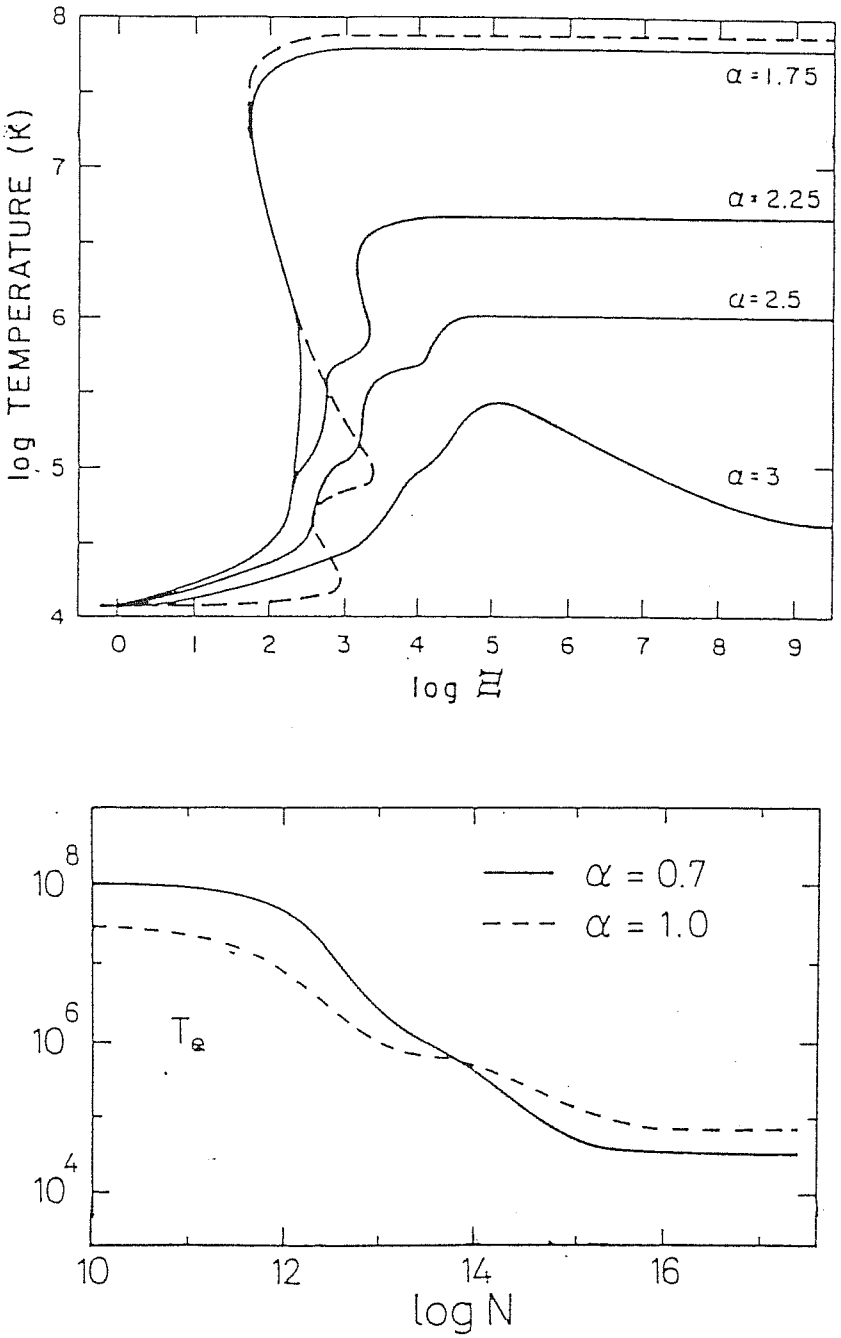

Fig. 1.6 The top figure shows the dependence of temperature of a gas illuminated by a continuum external source with power–law spectrum, as a function of the ionization parameter. The spectral indices has been reported on the figure, and the energy range extends between 13.6 eV and 100 keV (continuous curves) and from 500 eV to 100 keV (dashed line). At low values of the ionization parameter the gas can cool to the bremsstrahlung temperature, while at high values the Compton processes dominate and it reach the Compton temperature of the illuminating photons. For a narrow range of values a two phase medium can be obtained, being the middle temperature phase unstable. From Guilbert, Fabian & McCray (1983).

The bottom figure show the temperature of the gas as function of the gas density for same kind of situation. From Ferland & Rees (1988). The two curves refer to a different power–law radiation spectra, see the paper for further details. The transition between the two phases is for typical densities of $\sim 10^{13} - 10^{15}$ cm^{-3}. At densities greater than $\sim 10^{17}$ cm^{-3} thermodynamical equilibrium is reached.

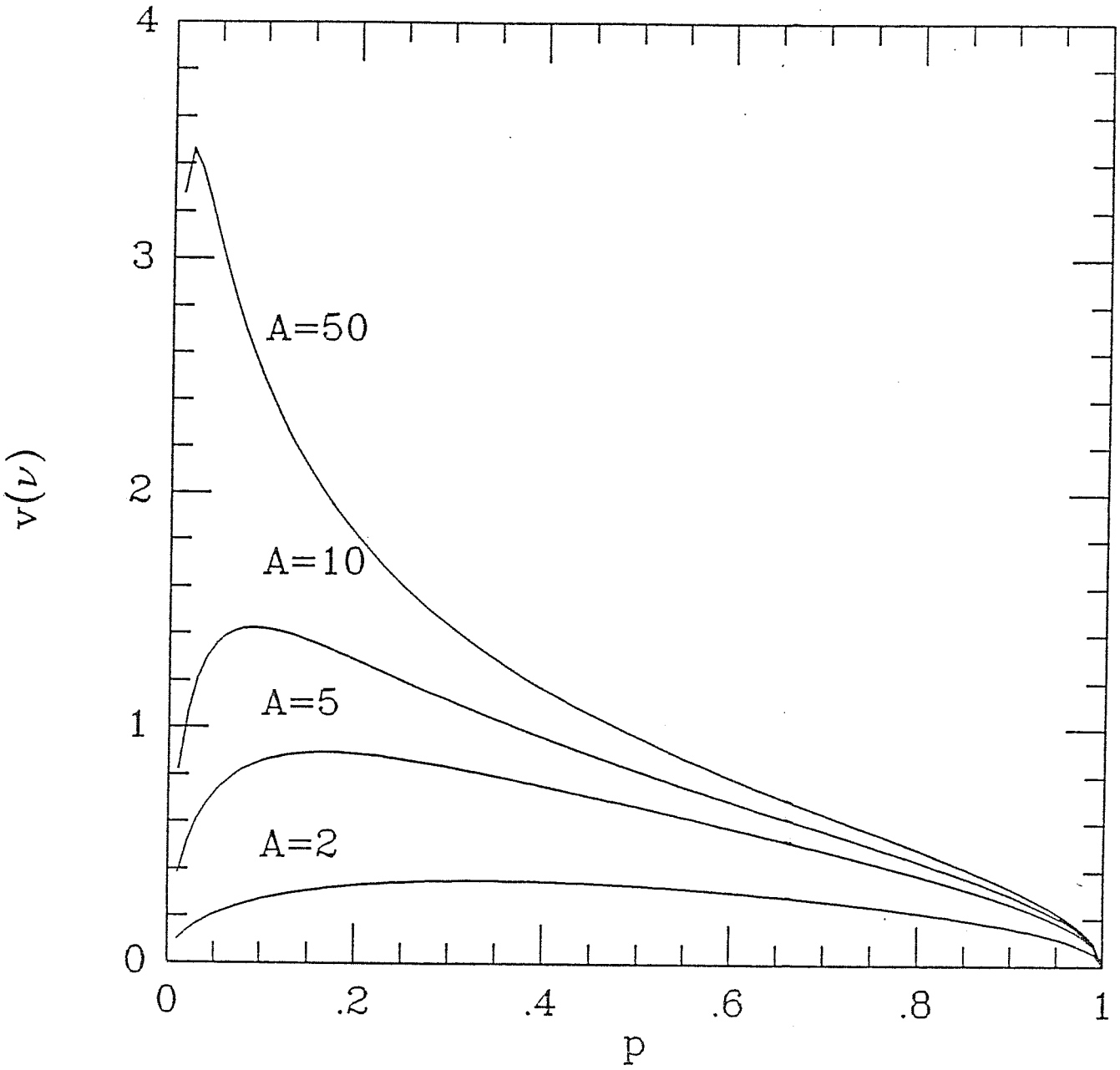

Fig. 1.7 The dependence of the variability indicator $v(\nu)$ defined in the text as a function of the probability p to observe a source with flux varied of a factor A (in the simplest assumption that only a quiescent state and a varied one are possible). The significant point is that for two different values of p the same observational parameter can be estimated. Typically in the Celotti, Maraschi & Treves (1991) model low frequency variability is in the bottom right side of the figure, *i.e.* low values of A and high p, while high frequencies variations correspond to the right upper side of it, for high A and low p.

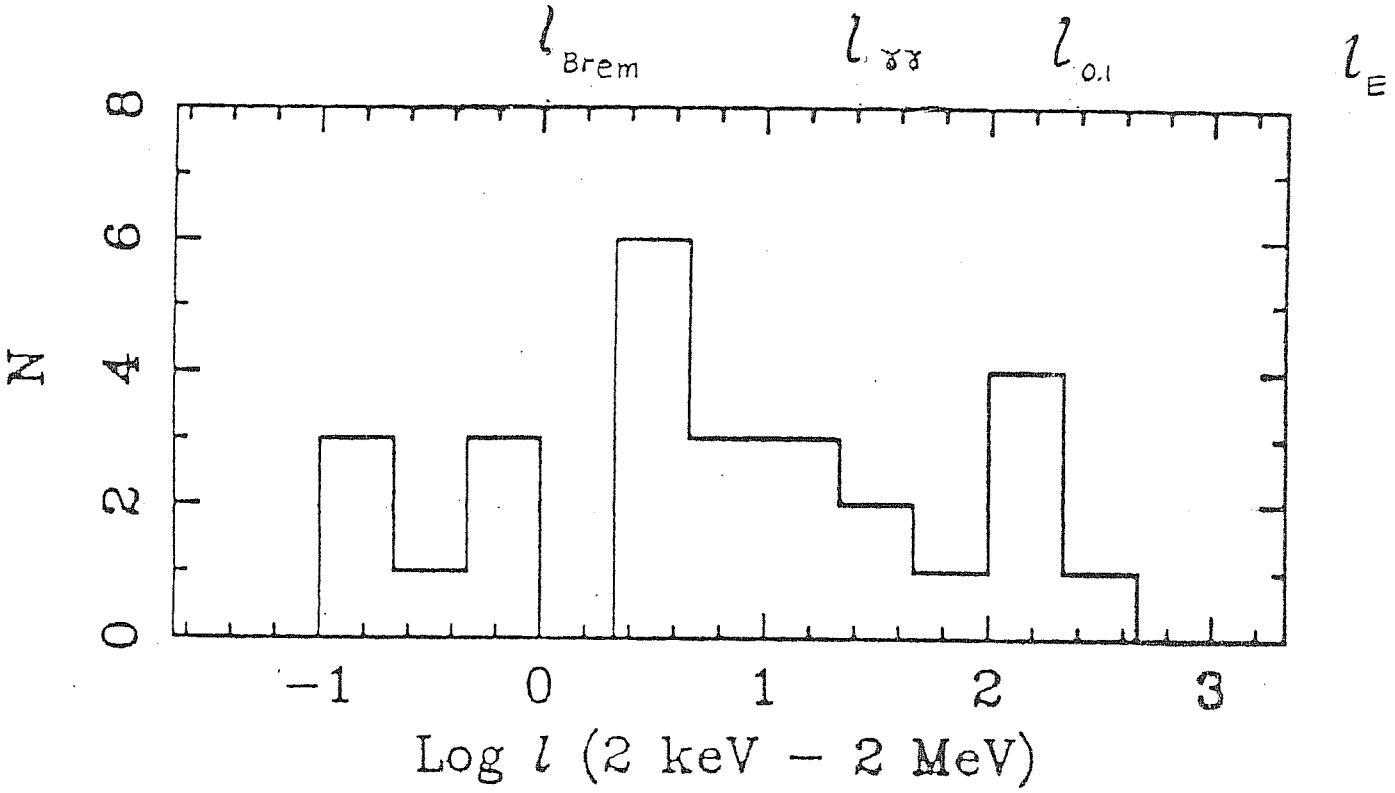

Fig. 1.8 In the figure the number distribution of sources with given compactness is reported (from Done & Fabian 1989). The values of ℓ corresponding to the bremsstrahlung, pair production threshold, efficiency $\eta = 0.1$ and the Eddington variability limits are reported. It corresponds to assume $\Delta t = R/c$, where Δt is the shortest variability timescale, and $R = 3\,R_s$. It can be seen that most of the source have compactness around ℓ~10–100, indicating that pair production is a quite common phenomenon in the compact regions of AGN.

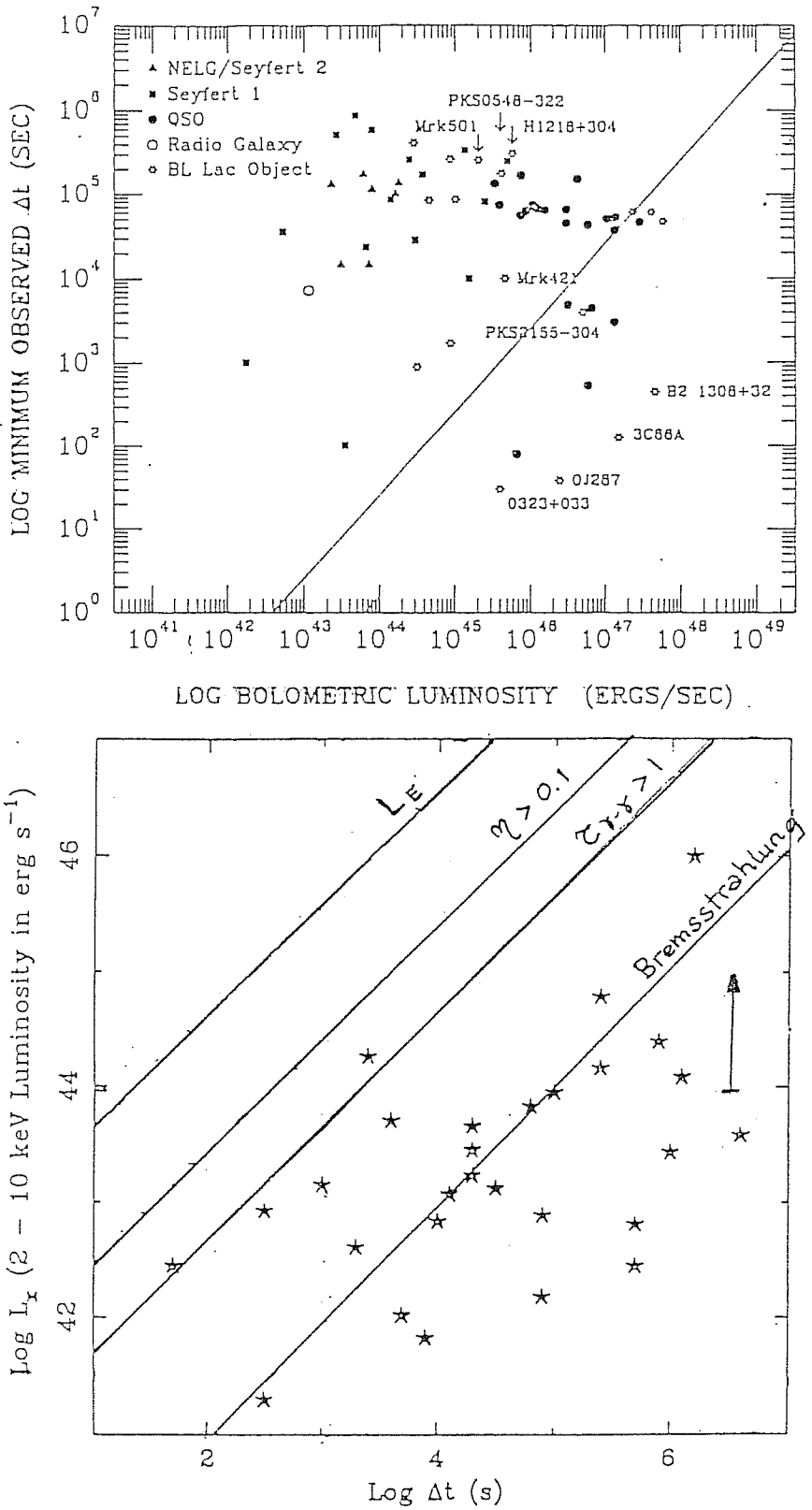

Fig. 1.9 Illustrative diagrams showing the correlation between the luminosity of different source types and the minimum variability timescale observed (for 50% flux variations). The upper one (Bregman 1990, see reference therein) considers bolometric luminosity for the sources indicated. The diagonal line represents the Eddington limit, assuming $R = 3\,R_s = \Delta t\,c$. The bottom one (A. Fabian, private communication), refers only to Seyfert 1 galaxies. The different labelled lines correspond to the same variability limits of Fig. 1.8 (see also the text). Here X–ray luminosity in the 2–10 keV band is considered, and the arrow represents the shift on the diagram corresponding to a X–ray spectra extending up to 1 MeV.

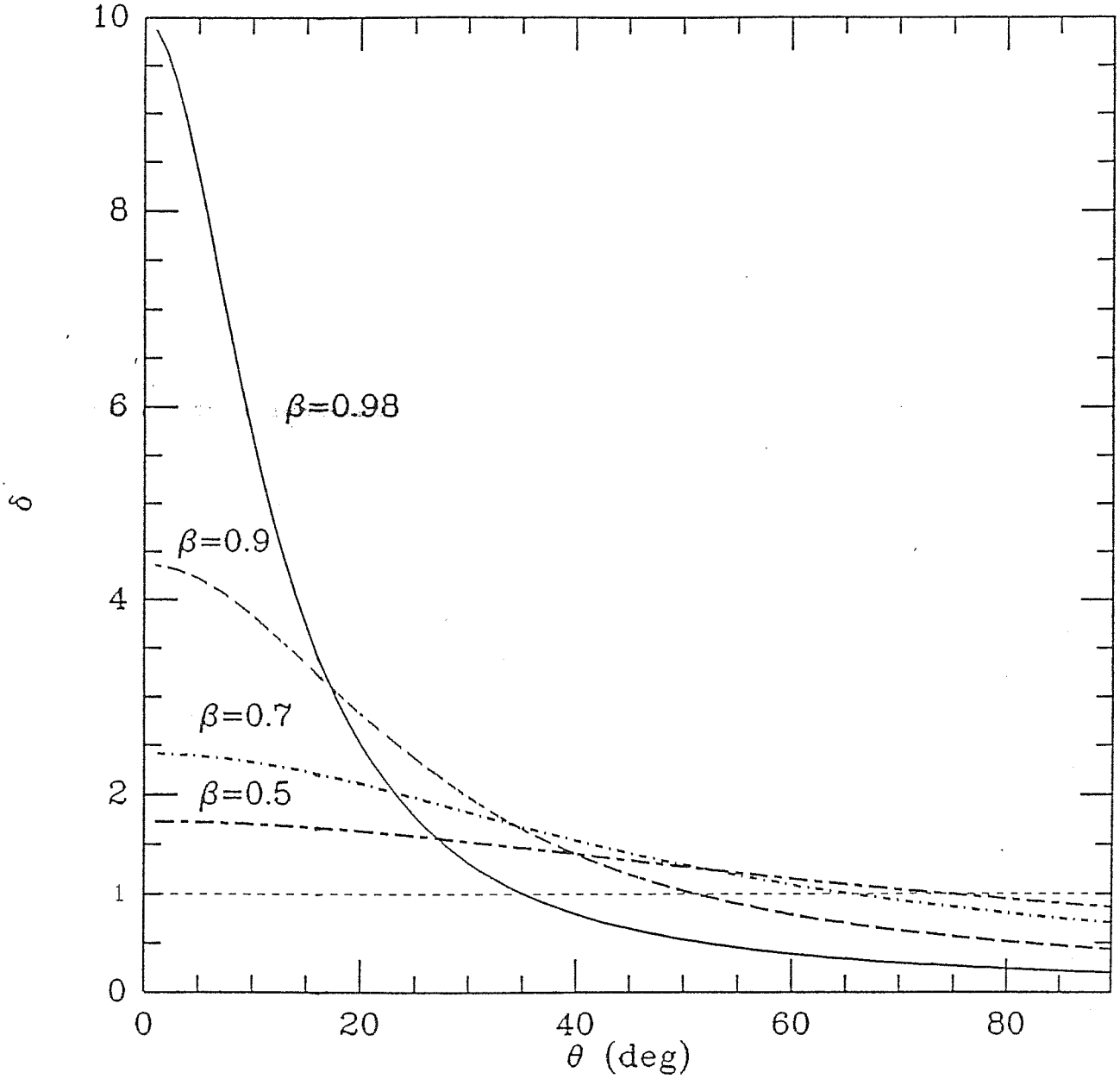

Fig. 1.10 The Doppler factor δ as function of angles of observation with respect to the velocity direction of the emitting fluid, for different velocity βc. The Doppler factor drops at velocity corresponding to $\Theta \sim 1/\gamma$. Sources observed at small angle should present higher flux amplification, shorter variability timescales and stronger variability amplitudes (see text).

Chapter 2. Jets

In this chapter we present the evidences for the presence of collimated beams of plasma in radio sources associated with AGN, and more specifically we would focus on the suggestions that the plasma velocity is relativistic. The beaming hypothesis is able to explain simultaneously different phenomena like superluminal motion, weak X–ray emission, one–sided jets, rapid and strong variability and super–Eddington luminosities observed in blazars.

Consequently we briefly examine models for emission from steady inhomogeneous region (jet) and the possibility that variability in blazars is due to perturbations in the emitting plasma.

It is possible that the flowing plasma in the jets is mainly constituted by electron–positron pair instead of proton–electron plasma. We present an attempt to answer this question.

And, finally, we examine the consequences of assuming anisotropic and beamed emission and the more common interpretations about the 'parent population' of blazars. An new picture, for the unification models for BL Lac objects, is examined.

2.1 Observations

Here we present direct observational evidences for the presence of collimated structures on large and small scales, mainly in the radio band. The discovery of sources moving with apparent velocity greater than the speed of light, the observations of one–sided jets, the optical polarization (up to 45%, Mead *et al.* 1990) variable in both degree and polarization angle and the most common interpretations of the phenomena in connection with blazars are then examined.

2.1.a Large and small scale jets

After the first interpretation that the observed double radio lobes were clouds of magnetized plasma ejected from the central galaxy, Rees (1971), and with more details Blandford & Rees (1974), proposed that the lobes are instead continuously supplied of energy from the central galaxy through jets of plasma, solving the problem of the cloud model to transport the observed energies on such long distances, despite of strong adiabatic losses. The energy would be transported in kinetic form (which does not exert pressure) and dissipated locally at the point where the jet encounters the interstellar matter and a shock wave develops accelerating the emitting particles (hot spots). In fact, due to the short cooling timescales of electrons an in–situ acceleration mechanism is required. Later jets, which loose a negligible fraction of the transported power, were observed. In fact even if acceleration in situ operates probably a small fraction of energy is reconverted in internal particle energy, as the second law of thermodynamics suggests.

With the advent of VLA, with resolution of arcsec (corresponding to linear scale of kpc for typical distance of quasars) and sensibility of 10^{-5} Jy, jets were found to be common in double radio sources, and associated with objects of different luminosity and type. VLBI maps showed the presence of these collimated structures also among compact sources on m.a.s. scale ($\sim$ pc in linear dimension), for wavelengths between the cm and tenths cm and sensibility down to 0.1 Jy. The smallest dimension on which jets are observed is comparable to the BLR size. It is possible (Rees 1984) that all AGN produce beams but only rarely they penetrates into the external medium to generate extended radio sources, or encountering BLR clouds shocks can form.

The same kind of beam structures is observed on scales of more than six orders of magnitudes in dimensions. The flow can not be simply rescaled over different sizes, because the radiative cooling timescales increase faster than the dynamical ones with increasing size. Smaller jets therefore tend to be more dissipative, probably maintaining high internal pressure.

Note that the smallest observable radio dimensions are about five order of magnitude bigger than the supposed black hole dimensions; the only (indirect) information on this size is therefore given from high energy variability. Note also

that the fact that large scale jets appear 'aligned' implies that the central source, which supplies energy, is stable at least over 10^6 years.

The morphology of radio sources has been divided into two categories: the 'extended radio sources', with dimensions from kpc to Mpc and an optically thin steep ($\alpha \simeq 0.5 - 1$) spectra at low frequencies, and the 'compact radio sources' close to the optical nucleus (sizes of $\sim$pc) with an absorbed flat ($\alpha \simeq 0 - 0.5$) spectra at $\sim$ 5 GHz. Nowadays the common belief is that they are substantially the same type of objects, having discovered the presence of both structures in the many sources. The compact objects are generally associated with quasars or BL Lacs, usually found in elliptical galaxies. The m.a.s. size jets are sometimes aligned with the extended ones, sometimes appear blended (maybe not due to projection effects), and one–sidedness is quite common.

Moreover a further division between extended sources has been introduced by Fanaroff & Riley (1974), who evidenced a connection between morphology and the emitted radio power, suggesting that the transport and dissipation mechanisms depend on the radio luminosity. The edge brightened sources (FRII type) have a radio luminosity $L_{178MHz} > 2 \times 10^{33}$ erg s^{-1}, dimensions of about few hundred kpc, bright ends and the linear polarization implies that the magnetic field is predominantly aligned with the jet, maybe stretched by the plasma flow; they are often associated to quasar, show a low brightness surrounding region, the lobes are often aligned with the nucleus and sometimes only one jet is visible.

The edge darkened sources (FRI type) on the contrary show lower power, bigger dimensions (up to 5 Mpc) and most of the luminosity is emitted along two antiparallel jets. They are often associated with elliptical galaxies and the magnetic field is predominantly perpendicular to the jet axis, which is expected over larger distances, because the parallel component, if magnetic flux is conserved, decreases faster ($\propto R^{-2}$) than the perpendicular one ($\propto R^{-1}$), for constant velocity. This effect can be produced also by shock waves which amplify the perpendicular field component $\propto k$ (where k is the density compression factor) but leave unchanged the parallel component.

The difference in the structure of the magnetic field can lead to different levels

of collimation, quantity of incoming matter and survival of the jet. A jet is directly observable if some energy is radiated and that can be due to different reasons, *e.g.* : internal magnetic field can be dissipated and converted in internal particle energy; incoming matter at the jet boundaries or interaction with obstacles can cause dissipation of some kinetic energy of the flow; the ejection velocity varies, leading to formation of shocks, which accelerates electrons (Rees 1981).

From synchrotron emission, an estimate of typical physical parameters in synchrotron sources can be obtained: the minimum internal pressure of the jet is for equipartition between the relativistic particles energy density and the magnetic one. If a source can be resolved, given the distance, it is possible to determine the volume emissivity. Calling ν_p the cut–off frequency which dominates the electron energy density, $\gamma_p \propto (\nu_p/B)^{1/2}$, from eq. (1.17) of §1.4.d, for $\alpha = 0.5$, $\epsilon_s(\nu_p) \propto p_e\, p_B^{3/4}/\nu_p^{1/2}$, where $p_e = N\gamma_p m_e c^2/3$ and p_B are the electron and magnetic energy densities. The total pressure $p = p_e + p_B$ is minimized for $p_e \simeq p_B$. Therefore $p_{min} \simeq 7.2 \times 10^9 \epsilon_s^{4/7}(\nu_p)\nu_p^{2/7}$ erg cm^{-3} (*e.g.* Blandford 1990). The numerical coefficient is slightly dependent on the spectral index. The total energy in the source is $\sim 3p_{min} \times volume$, and the equipartition magnetic field $\sim (8\pi p_{min})^{1/2}$.

Table 2.1

Location	B	ν	γ	t_{cool}	t_{dyn}	p_{min}	U_{min}
	G	Hz		yr	yr	erg	erg
Extended source	10^{-5}	10^9	10^4	10^7	10^8	10^{-11}	10^{59}
Radio jet	10^{-3}	10^9	10^3	10^4	10^4	10^{-7}	10^{57}
Compact source	10^{-1}	10^9	10^2	10	10	10^{-3}	10^{54}
Outer disc	10	10^{14}	$10^{3.5}$	10^{-4}	1	10	10^{49}
Inner disc	10^3	10^{16}	$10^{3.5}$	10^{-8}	1	10^5	10^{47}
B.H. Magnetosph.	10^4	10^{18}	10^4	10^{-10}	10^{-3}	10^7	10^{47}

Typical values (*e.g.* NGC 6251, Perley, Bridle & Willis 1984) are $p_{min} \sim$

$10^{-3} - 3 \times 10^{-12}$ erg cm^{-3} from the pc (or BLR) scale to the external part of the jet, and therefore $B \sim 0.1 - 3 \times 10^{-7}$ G. Reference values in different context deduced from synchrotron emission are reported in Table 2.1 (from Blandford 1990).

The ram pressure of the jet cannot change the trajectory or destroy if dense fast moving clouds (*e.g.* in BLR) that, therefore, must have a small covering factor, otherwise the jet momentum is isotropized (see §2.4.c).

On the other hand the minimum pressure gives also an estimation of the thrust, which, if protons carry most of the kinetic energy, can greatly exceeds the ram pressure of the intergalactic medium.

Note that in the inner part of the jet ($\sim$ pc) thermal confinement for high luminous sources seems unlikely, because X–ray observations set an upper limit to the density of the confining medium, *i.e.* , for a gas at temperature of $\sim 10^7$ K (at which the gas can be in equilibrium in the potential well at $R \sim 10^{18}$), the internal pressure would imply a X–ray luminosity of $\sim 3 \times 10^{48} L_{45}^2$ erg s^{-1}, not observed ($L = 10^{45} L_{45}$). More precisely if the intercloud medium is in pressure balance with BLR clouds and emits X–rays by bremsstrahlung (at Compton equilibrium temperature), for each R must be $n^2 R_{15}^3 \lesssim 10^{24}$ cm^{-3} ($R = 10^{15} R_{15}$), *i.e.* $n < 10^{12}/R_{15}^{3/2}$. Pressure balance with the jet requires $p_{ext} \simeq nkT \simeq 3 \times 10^4 L_{45}/\theta^2 M^2 R_{15}^2$ or $R_{15}^{1/2} > 2 \times 10^2 L_{45}/(\theta M)^2$, which for a confined jet $\theta M < 1$, (M the Mach number), is satisfied for $R \gtrsim 10^{18}$ cm.

In reality the intercloud medium can not be in equilibrium if the Compton cooling keeps its temperature below $m_e c^2 \simeq 10^9$ K, because it is less than the virial temperature $T_v \simeq 10^{11} M_8/R_{15}$ K. Therefore gas is not in equilibrium for $R_{15} \lesssim 10^4 M_8$ ($M_8 = 10^8 M_\odot$) and it outflows or infalls (Rees 1984). This relation is no more valid at R such that the presence of stars contribute to the total mass, and $T_v \sim 10^{6-7}$ K. At $R > 10^{19} M_8$, coinciding with VLBI dimensions, central mass ceases to dynamically dominate, equilibrium can exist and the free jet encounters static gas, with possible formation of shocks or bending.

One way to resolve the problem of the thermal confinement when the external pressure seems to be lower than the minimum internal one, is to regard ('small') high pressure regions (like in edge brightened sources) as transient, perhaps formed by shocks. They would then freely expand.

The confinement problem can be overcome if energy is mainly transported as Poynting flux.

In Fig. 2.1 the jet of 3C120 on many orders of magnitude in resolution is shown (Walker, Benson & Unwin 1987). It should be noted that on the smaller scales the jet appear more like several unresolved bright blobs (core–jet structure) than a continuous flow. The blobs probably indicate regions of high acceleration efficiency or stronger magnetic field (as produced by a shock wave). These core–jet sources are quite common and show a very flat ($\alpha \sim 0$) spectral component and a steeper one at lower frequencies. Impey (1987) suggested that core–jet sources identify with radio loud and blazars.

It is very difficult to reveal jets at higher frequencies. The jet of the elliptical galaxy M87 has been observed in optical, UV and X–rays (Biretta, Stern & Harris 1991). Optical observations confirmed the 'similarity' between the radio and optical jet structure, where dissipation occours. Optical flux therefore is also produced outside the central region (say at $< 10^{15}$ cm). High resolution X–ray observations show that the emission from the outer components is comparable to the emission of the core. Optical jets have been observed also in 3C66, 3C31 (Butcher, Van Breugel & Miley 1980). An X–ray jet has been observed in Cen A (Feigelson 1982) and 3C273 on the kpc scale, even if resolution is quite poor.

An interesting result of high resolution observations in the optical band is that the spectrum tends to be steeper in the knots (*e.g.* M87, Peréz–Fournon 1988) with increasing distance from the core, as in the case of decreasing shock stenght with distance.

Polarization

It seems that there is not much Faraday rotation in VLBI jets. A polarization up to 64 % has been observed in radio knots (OJ287, Wardle & Roberts 1988) reaching almost the theoretical limits for synchrotron emission from a power–law distribution of emitting electrons, implying a very ordered magnetic field and ruling out internal Faraday rotation (excluding the VLBI core). This maximum theoretical limit for thin emission is given by $(\alpha + 1)/(\alpha + 5/3)$ (*e.g.* Rybicki & Lightman 1979). An ordered

magnetic field is also suggested from the correlation between jet axis and magnetic field directions.

When rotation is observed in order to produce the required Faraday depth, if magnetic field is not far from equipartition, electron densities $n_e \sim 10^7$ cm^{-3} are required, similar to the NLR densities (*e.g.* Krolik & Vrtilek 1984).

Furthermore the linear polarization generally increases with the distance from the core (*e.g.* 3C273 Wardle *et al.* 1990; Roberts *et al.* 1990). This is probably due to the presence of disorganized magnetic field in the core region, because internal Faraday depolarization seems not to be efficient in inhomogeneous unresolved jets, always 'thin' in the outer regions (Cobb, Wardle & Roberts 1988). On the other hand external depolarization does not show the expected frequency dependence (Aller *et al.* 1985).

BL Lac objects show polarized radiation with magnetic field mostly perpendicular to the jet axis, but parallel to it in quiescent states, suggesting once more that shocks, which amplify variations and comprise the perpendicular component of the magnetic field, generate in the flow. In a jet, polarization is maximum at an observing angle $\sim 1/\gamma$, similar to the critical angle for superluminal motion (*e.g.* Wardle & Roberts 1988, see §2.1.b). Instead quasars show a magnetic field generally parallel to the axis. Furthermore the polarization in the core of BL Lacs ($\sim$ 1–5 %) is greater than for quasars (where is sometimes $<$ 1 %) (Roberts *et al.* 1990). Both these facts and the lower apparent superluminal velocities of BL Lacs (see §2.1b) strongly argue against the lensing model of Ostriker & Vietri (1985) (see §1.1.b), because radio emission, which is not lensed, should show the same characteristics in BL Lacs and OVVs.

Sometimes radio and optical polarization are correlated (*e.g.* 3C345, Sitko, Schmidt & Stein 1985). Moreover optical polarization implies the presence of ordered magnetic fields on scales much smaller than VLBI radio core.

We also mention that BL Lac showed flux and polarization variations simultaneously to the appearance of a new blob in VLBI map (Phillips & Mutel 1988) and as mentioned in §1.3.c the same has happened in 3C273 with IR–optical flux variations, in agreement with the idea of a connection between flux variability and variations in the jet structure. Note that because the optical emitting region is

not resolved, variability can not attributed just to moving blobs, but should be due to coherent beaming or variations.

Some theoretical notes

We do not examine in detail the hard problems of the generation and collimation of jets along a preferred direction.

Fluid models (*e.g.* Blandford & Rees 1974, Reynolds 1982, see also Begelman, Blandford & Rees 1984) can work, leading to the formation of de Laval nozzles, if an external collimating cloud is present. The collimation involve a preferential direction with lower resistance, probably coincident with a rotation axis. The cloud must be gravitationally bounded, but its pressure should be sufficient to prevent it from collapse into the core or in a thin disc if it has angular momentum. The cloud can be supported by ion pressure if $T_i \simeq T_v$ (and for low density, such that protons cannot transfer all their energy to elcectrons which dissipate it too rapidly, *i.e.* $t_{e,p} < t_{in}$), or by radiation, whose energy must correspond therefore to the Eddington luminosity for the central mass.

The shape of the jet $r(R)$ (with r and R the transverse and axial coordinates) can be estimated in the case of an adiabatic ultrarelativistic flow and a dynamically negligible magnetic field, given the radial dependence of external pressure $p(R)$. The conservation equations of the fluid $(T^{\alpha,\beta})_{;\beta} = 0$, where $T_{\alpha,\beta} = (e+p)u_\alpha u_\beta + p g_{\alpha\beta}$ is the energy–momentum tensor, e the total energy density, p the pressure, give the equations of motion for the fluid. Together with the conservation of the particle number ($r^2 n\beta\gamma = const$), they imply the Bernoulli and Euler equations (Landau & Lifshitz 1959; Blandford & McKee 1976)

$$\frac{(e+p)\gamma}{n} = \gamma_\infty \qquad\qquad \gamma\beta\frac{d\beta}{dr} = -\frac{1}{(e+p)}\frac{dp}{dr} \tag{2.1}$$

where γ_∞/mc^2 is the maximum Lorentz factor which can be reached, if internal energy is zero. Using the adiabatic expansion law $p \propto n^\Gamma$, the adiabatic index $\Gamma = 4/3$, and integrating the Euler equation

$$p = p_0\gamma^{-4} \qquad\qquad r^2 \propto \frac{(p_0/p)^{3/4}}{\left[(p_0/p)^{1/2}-1\right]^{1/2}} \tag{2.2}$$

Collimation increases with an harder equation of state. Some well studied jets show that equipartition pressure falls much slowly than the dependence found for a supersonic, adiabatic flow, suggesting that there is internal dissipation and the entropy increases along the flow.

If $p \propto R^{-a}$, and $\gamma >> 1$, then $r \propto R^{a/4}$ and

$$\gamma\beta \left[\frac{\gamma_\infty}{\gamma} - 1\right]^{1/(\Gamma-1)} = \gamma_0\beta_0 \left[\frac{\gamma_{\infty,0}}{\gamma_0} - 1\right]^{1/(\Gamma-1)} \left(\frac{R_0}{R}\right)^{a/2} \tag{2.3}$$

The last equation, if the mass energy is negligible, $\gamma_\infty >> \gamma$, implies $\beta/\gamma^2 \propto R^{-a/2} \rightarrow \gamma \propto R^{a/4}$ for $\beta \sim 1$.

The jet is therefore confined (for $a < 4$) with parabolic shape, and the cross section has a minimum, *i.e.* maximum momentum flux, when the pressure $p = 4/9p_0$ and $\gamma = \sqrt{3/2}$, *i.e.* the flow becomes supersonic (de Laval nozzle). If it happens at distance $R >> R_s$ gravitational force from the central source can be neglected. After this point internal energy is converted in bulk one.

Note that an elongated structure (like jet) suggests supersonic motion in order that sideways expansion is less than the longitudinal one.

Subsequently the jet can become free (*e.g.* ballistic outflow) if the external pressure decreases fast enough, *i.e.* if the jet walls separate at supersonical velocity from a fluid element, $M > \tan^{-1}\theta$, where M is the Mach number and θ the collimation angle of the jet. It happens if $dp/dR \gtrsim -1.78(p_s/r_s)(p/p_s)^{3/2}$, where the subscript '$s$' refers to quantities at the supersonic point.

All the treatment should be obviously self–consistent including the dependence of the equation of state on R (and the presence of radiation), because during the adiabatic expansion the internal energy is converted into bulk energy (*e.g.* Daly & Marscher 1988).

Magnetic models (*e.g.* with a toroidal magnetic field in a current carrying jet, *e.g.* Bendford 1979) have been also proposed to confine jets. However the polarization due to the presence of a toroidal field is not observed (Blandford 1990) and fueurthermore magnetically collimated plasma are highly unstable. Presently these problems are studied mainly through numerical simulations, accounting for formation of quasi–periodic shocks in subsequent recollimations of the flow maybe on galactic scale, and dynamical instabilities (*e.g.* Normann *et al.* 1981).

In the above descriptions we implicitly assumed that the plasma could be treated as a fluid, even if the energy exchange timescale among electrons is $\sim (8/\ln\Lambda)(\Theta^2/n\sigma_T c) \sim 2 \times 10^{13}/n$ s, for $\Theta = kT/m_e c^2 \simeq 1$ (see §1.4.a). Therefore the collisional mean free path can exceed the region size. However, a weak homogeneous magnetic field is able to make the plasma fluid like, being the Larmor radius of a proton $m_p c^2 \gamma\beta/eB \sim 3 \times 10^6(\gamma/B)$ and the Debye length of electrons $(kT/4\pi n e^2)^{1/2} \sim 5 \times 10^5(\gamma/n)^{1/2}$ smaller than the typical dimension of the region. Furthermore a small magnetic field is also sufficient to isotropize the electron distribution. A strong magnetic field instead can make pressure highly anisotropic and potentially can confine jets, as already mentioned; however it is generally assumed that magnetic field is sufficiently disordered that it is possible to define a mean magnetic pressure.

2.1.b Superluminal sources

One of the first discovery about compact radio sources is their rapid variability, on timescales of $\sim$ months. The inferred upper limit on the angular dimension of the source, in the assumption of synchrotron emission, gives a lower limit to the brightness temperature, which exceeds the Compton limit $T_b \sim 10^{12}$. The hypothesis suggested by Rees (1966) that the sources were expanding at relativistic velocities, reduced the Compton problem and predicted that they would be observed to move with superluminal velocities. The observations of rapid variability in the dimensions of 3C279, implying velocities of $2c$, were interpreted by Moffet *et al.* (1972) as the first observational evidence of the Rees's model.

In order to reveal superluminal motion a source must emits more than ~ 1 Jy to be observed with VLBI, and its distance must be known. Zensus (1989) shows a list of superluminal sources, reported in Table 2.2 (for $h = 1$, $h = H_0/100$, which tends to underestimate the observed velocities).

An example of a superluminal source is shown in Fig. 2.2, in which a compact component of 3C179 is assumed to be stationary and the other moves with apparent linear velocity $\beta_{app} \sim 4.8h^{-1}$. Even if the two components are both moving in

Table 2.2

Source		z	Identification	μ [mas yr^{-1}]	$\beta_{\rm app} h$
0212+735		2.367	Bl	0.09	3.9
0333+321	NRAO 140	1.258	Q	0.15	4.8
0430+052	3C 120	0.033	G	1.35	2.1
				2.53	3.9
				2.47	3.8
				2.66	4.1
				2.54	3.9
0723+679	3C 179	0.846	Q	0.19	4.8
0735+178		0.424	Bl	0.18	2.8
0836+710		2.16	Q	0.13–0.25	5.2–10.4
0850+581		1.322	Q	0.12	3.9
0851+202	OJ 287	0.306	Bl	0.28	3.3
0906+430	3C 216	0.669	Q	0.11	2.4
0923+392	4C 39.25	0.699	Q	<0.006	<0.1
				0.16	3.5
1040+123	3C 245	1.029	Q	0.11	3.1
1137+660	3C 263	0.652	Q	0.06	1.3
1150+812		1.25	Q	0.13	4.1
1226+023	3C 273	0.158	Q	0.79	5.3
				0.99	6.6
				1.20	8.1
				0.76	5.1
1253−055	3C 279	0.538	Q	0.5	9.2
				0.11	2.0
1641+399	3C 345	0.595	Q	0.48	9.5
				0.30	5.9
				0.07,0.3	1.4,5.9
1642+690		0.751	Q	0.34	7.9
1721+343	4C 34.47	0.206	Q	0.36	3.1
1901+319	3C 395	0.635	Q	<0.06	<1.2
				0.64	13.2
1928+738		0.302	Q	0.6	7.0
1951+498		0.466	Q	∼0.07	∼1.2
2200+420	BL Lac	0.0695	Bl	∼0.76	∼2.4
2230+114	CTA 102	1.037	Q	∼0.65	∼18.5
2251+158	3C 454.3	0.859	Q	<0.05	<1.3
				0.35	8.9

List of superluminal sources from Zensus (1989). G: Galaxy; Q: Quasar; Bl: BL Lac object.

opposite directions the inferred velocity is greater than c. The emitting knots appear to be separated by about 1 pc.

Different behaviours of these knots are observed: linear or curved trajectories (CTA 102, Wehrle & Cohen 1989), sometimes accelerating (*e.g.* 3C345, Biretta & Cohen 1987) or decelerating, but contracting components have never been observed. For a review of observations of superluminal sources see *e.g.* Zensus & Pearson (1987). It is even possible that sometimes strong variations in the flux do not correspond to real motion (*e.g.* 3C446, Pauliny–Toth 1987).

All the superluminal sources show also an extended radio component (> arcsec, Browne 1987): the superluminal components, like the 'subluminal', often are not aligned with the larger scale jet (Mutel 1990). The compact objects associated with luminous extended radio lobes, which are probably less beamed, show lower superluminal velocities.

The simplest model suggested in order to explain the velocities greater than c is the 'ballistic' model (Blandford & Rees 1978, Blandford & Königl 1979). It assumes that the emitting components are blobs of magnetized plasma which propagates along a jet at relativistic velocities (even if the various behaviours described require a more sophisticated model). The quantity observed is the proper motion μ , *i.e.* the apparent angular separation velocity. If the redshift is known, transforming the time intervals (between the observer and source frames) it can be converted into the projected linear velocity $\beta_{app}c$ (in a Robertson–Walker metric)

$$\beta_{app} = \mu \frac{d_\theta (1+z)}{c} = 47.4 \mu \frac{q_0 z + (q_0 - 1)(\sqrt{1+2q_0 z} - 1)}{h q_0^2 (1+z)} \quad \text{(m.a.s. yr}^{-1}\text{)} \qquad (2.4)$$

where $d_\theta = d_L/(1+z)^2$ is the angular distance and q_0 the cosmological deceleration parameters.

Suppose that one component is at rest, while another moves toward the observer with an angle θ with the line of sight (see Fig. 2.3). If the observer time t is measured when the component starts to separate from the other it would move a transverse distance $\beta c\, t \sin\theta$ after t. If the observer receives a photon from the moving blob, the time spent to move from the stationary source is $t_{obs} = (1 - \beta\cos\theta)\, t$ because the component moved toward the observer. The measured apparent transverse speed

would be

$$\beta_{app} = \frac{\beta \sin\theta}{1 - \beta \cos\theta} \tag{2.5}$$

which has a maximum $\gamma\beta$ for $\beta = \cos\theta$, and $\beta_{app} > 1$ for $\gamma > \sqrt{3/2}$ (see Fig. 2.4).

Note that the same argument applies in a jet, where for example the radio photosphere is fixed and the moving component can be a shock wave. In the latter case the relativistic motion is not connected directly with the plasma motion, but with the velocity of the perturbation. Alternative explanations involve in fact the motion of perturbations or radiation flux which make bright the region in which are passing through (*e.g.* accelerating locally the emitting particles). For a review of the possible interpretations see Blandford, McKee & Rees (1977), Zensus & Pearson (1987). It is an interesting problem to determine if really the matter is moving or not: the important difference is that in the case of real motion of the plasma also the emitted radiation is amplified (as described in §1.4.e).

2.1.c One–sidedness

Another possible evidence suggesting that relativistic motion is involved is the observations of one–sided jets. It is not clear why some sources present two oppositely directed jets and in some others just one of them is seen. If beaming effects are present, the jet emission directed toward the observer would have an observed flux amplified while the jet oppositely directed would be fainter. Therefore the ratio between the two fluxes would be

$$\left(\frac{1 + \beta\cos\theta}{1 - \beta\cos\theta}\right)^{c} \sim \left(\frac{2}{\theta}\right)^{2c} \qquad \text{for } \gamma > \frac{1}{\theta} > 1 \tag{2.6}$$

where c depends on the considered structure of the emitting plasma (as described in §1.4.e). In Fig. 2.5 this ratio is shown as a function of θ and β. It can be seen that extreme values of the parameters are not required in order to account for a ratio in the fluxes greater than the dynamical range of VLBI (with at least a ratio 100:1).

Other explanations include the possibility of intrinsic one–sidedness due to an alternation of ejection side, at angle of about 2π ('flip flop' behaviour, Rudnick & Edgar 1984), but the dead side must have been recent to generate electrons still

radiating when two beams are observed. But when jets are very long, the beam must keep a direction for $> 10^6$ yr. Only a restricted range of time interval between the change of side is therefore consistent with this picture. Asymmetric dissipation, *e.g.* due to different ambient conditions and/or luminosity is also possible. Another alternative is that a central disc or cloud is along the line of sight obscuring one of the jets. Measures of polarization tend to show that even when the oppositely directed beam is observable, it is less polarized. It should be a signature of the fact that radiation from that jet should pass through more material (Laing 1988). Free–free absorption could work at < 5 GHz if $n^2 l \gtrsim 10^{27}$, for $T = 10^4$ K, where l is the thickness. Density $n > 10^4$ cm^{-3} can be present on pc scale, but it does not work at bigger scales (10–100 kpc), where density is too low.

2.1.d Blazars

There is increasing evidence that most compact radio sources show features characteristic of blazars: most, if not all, flat spectrum radio quasars are blazars (Fugmann 1988; Impey & Tapia 1990). At least 70% of superluminal sources have IR, optical or X–ray properties typical of blazars; viceversa Cohen (1986) found that the 80 % of bright sources at 10 GHz showed superluminal motion and for blazars (which by definition show a flat radio component) there is a correlation between flat spectrum and optical polarization (Moore & Stockman 1981).

More specifically Bl Lac objects always show core–jet radio structure. They present weak extended radio emission, with a 'core–halo' morphology, and deprojected linear dimensions consistent with double sources observed at small angles (Antunucci & Ulvestad 1985); the ratio R = core/extended fluxes (usually used as a beaming indicator, in the hypothesis that extended emission is not beamed) correlates with polarization, variability and one–sidedness.

Most of superluminal sources are identified with quasars, however more and more superluminal BL Lacs have been found (Stickel *et al.* 1991). The first four BL Lacs observed more that once with VLBI showed apparent velocities smaller than the average of quasars (Mutel 1990) and this fact suggested (Roberts, Gabuzda & Wardle 1987) that they were observed at very small angles, which implies lower β_{app}

but stronger Doppler amplification. If the ballistic model is correct, observations suggest bulk Lorentz factors $\gamma \sim 5 - 10$ (apparent velocities $< \beta_{app} >= 5.5 \pm 3.2$) and γ ~2–6 ($< \beta_{app} >= 3.3 \pm 1.2$) for BL Lac objects (Mutel 1990), consistent with the values requested by brightness temperature considerations. It is not yet clear if the distribution in apparent velocities for BL Lacs is really different from the other sources.

Very fast jets have also the advantage to minimize the mass flux required to produce the observed energy input, which otherwise can be greater than that believed to be in a whole elliptical galaxy.

Moreover relativistic speeds are not unexpected, if relativistic potential wells are present.

If densities are deduced from internal Faraday depolarization (see §1.4.b) the plasma velocity can be inferred in two ways: assuming a power carried by the beam or assuming that the jet is free, so v must exceed the sound speed by at least θ^{-1}.

Furthermore if the bending often observed is due to external ram pressure, the curvature results proportional to the beam velocity (Begelman, Rees & Blandford 1979). Non–relativistic flows therefore would imply implausible high values for the external pressure.

Another indication of fast speed comes from the fact that plasma must flow faster than the separation velocity of lobes, which can be $\sim 0.1c$ (Longair & Ryle 1979).

Beaming effects are also suggested in order to explain the observed conical patterns of ionized gas close to radio galaxies (Tadhunter & Tsvetanov 1989).

There are also arguments against this picture. The redshift distribution (independent of orientation) of BL Lacs is different from the other superluminal sources (Cohen 1990); models for VLBI radio jets are consistent with large viewing angle (Mutel *et al.* 1990; Hughes, Aller & Aller 1989b). However it should be reminded that the opening angle of the beamed radiation ($\sim 1/\gamma$) can be greater or smaller than the angle of the bulk motion (see §2.4). Finally, there is not the expected correlation between core dominance and apparent superluminal speed (Gabuzda, Wardle & Roberts 1990).

In many sources a lower bound to the momentum flowing can be calculated multiplying the minimum pressure in the hot spots by their area, with typical values $\sim 10^{34-35}$ dyne. If multiplied also by $v/2$ the jet power can be obtained, which for high velocities is much greater than the power that appear dissipated in the lobes.

It should be noted that observations of iron line emission, with large equivalent width, in the X–ray band strongly argue against beaming effects. In fact, if the X–ray emitting region is beamed perpendicularly and in the opposite direction of the iron line emitting disc, the observed X–ray luminosity is proportional to $\delta^{3+\alpha}$, while the luminosity observed by the disc is proportional to $\gamma^{-3-\alpha}$. The equivalent width of the line is therefore proportional to $(\gamma\delta)^{-3-\alpha}$ (see Appendix D).

Systematic differences in the two lobes of extended radio sources could be another proof against Doppler favoritism.

Summarizing, the basic idea for the unification of radio sources is that the angle of sight is a basic parameter. The powerful sources should be fed by the core with relativistic particles, whose emission can be beamed. Therefore compact sources can be relatively weak, but because beamed in our direction, its core emission tends to overcome the extended one. The edge–brightened sources can move with mildly relativistic speeds, with the approaching jet brighter than the opposite one; the edge–darkened sources instead can have a sub-relativistic velocity and both jets can be observed.

2.2 Emission from jets

2.2.a Inhomogeneous SSC emission

The earlier and simpler interpretation of the observed spectra assumed that the spectrum from blazars was due to SSC emission from a spherical homogeneous region (see §1.4.d, Jones, O'Dell & Stein 1974a,b). However, as already mentioned, the predicted X–ray flux greatly exceeds the observed one ('Compton catastrophe'), as much as 14 orders of magnitude. Following the suggestion of Blandford & Rees

(1978) of relativistic effects (which imply an overestimation of synchrotron photon density) the Doppler 'correction' to the Compton flux as estimated in §1.4.d (Urry 1984) gives

$$F_c(\nu, \delta) = F_c(\nu, \delta = 1)\delta^{-2(2+\alpha)} \tag{2.7}$$

Therefore a minimum Doppler factor can be evaluated in order to produce the observed flux. A greater value of δ could just imply that another X–ray emitting component is present. Values of $25 < \delta < 40$ for PKS 2155–304 were estimated by Urry & Mushotsky (1982), $\delta > 25$ for PKS 0537–441 (Maraschi *et al.* 1983) and $10^{-2} < \delta < 15$ have been found for a sample of 30 BL Lacs from Madau, Ghisellini & Persic (1987) (see also Ghisellini *et al.* 1991, Appendix C).

It should be noted that the argument can be applied at all frequencies, in particular at the optical one, and not only at the X–ray fluxes, as usually done (see Appendix C).

Such high values of δ, implying extreme values for velocity and line of sight, and the VLBI observations which showed the presence of different components with flat spectra at different frequencies, suggested that an inhomogeneous model for emission is more probable. The flat radio spectra are therefore interpreted as the superposition of synchrotron spectra from different regions self–absorbed at different frequencies. Because the more compact source absorbs at higher frequencies, the requested Doppler amplification is significantly reduced (typical values of $\delta \simeq 2$–5). The smoothness of the spectrum and the variability correlations suggest that these components are strongly connected and, together with the direct observations of collimated structures, lead to develop emission models from inhomogeneous jets (Marscher 1977).

A physical description of the dynamic and emission properties of jets is still lacking, therefore the simpler assumption is that physical quantities (magnetic field, emitting particle density and their maximum energies, bulk velocity) are functions of the distance along the jet and constant on its sections. These dependences are parameterized as power–laws, characterized by their exponents. This in turn implies power–law dependences for the maximum and minimum emitted frequencies, emissivities and observed fluxes. A power–law dependence of physical quantities

on five orders of magnitude in dimensions (from 1 pc to 100 kpc) describes the observations of the jet of 3C120 (Walker, Benson & Unwin 1987).

Different models have been developed on the basis of different shapes of the jet (parabolic or conical, *i.e.* hydrostatic confined or free expanding beam, see §1.2.a) and the above dependences, *e.g.* increasing or decreasing maximum energy of electrons with distance (Marscher 1977, 1980; Königl 1981; Reynolds 1982; Ghisellini, Maraschi & Treves 1985; Ghisellini & Maraschi 1989).

All the models are able to describe the observed spectra, from radio to X–rays, as a superposition of locally emitted SSC spectra in an unresolved, relativistic and stationary jet (for a comparison of the different models see also Königl 1989). However the different models predict different behaviour of variability. We do not enter in details, describing the models. We just want to mention their predictions on variability, which are at the base of the choice of one stationary emission model to include time dependence (see §2.2.b).

The competition of the external or internal emitting regions, dominating the emission at a given frequency, is the important feature of the models, and this depends on the gradients of physical quantities. Typical values of the exponents correspond to the conservation of flux of particles or the parallel or perpendicular magnetic field components.

The model developed by Ghisellini *et al.*(1985), which assumes an internal confined parabolic jet and an external conical part, implies naturally that high frequencies are produced in the inner (and smaller) part of the paraboloid, as synchrotron radiation, and lower frequencies are emitted at increasing distance (and dimensions) of the jet. The X–ray predicted spectrum is steeper than the intrinsic one due to the superposition of components, and show continuity with the UV one. The conical part produces the flat radio spectrum and possibly a hard flat (with the 'intrinsic' spectral index) X–ray component through self–Compton on from 'local' photons (see Fig. 2.6), which can be connected to the hard energy tail observed in some BL Lacs (see §1.1.b). By the way, an hard X–ray component is also predicted in the model of Melia & Königl (1989), which explains also the superluminal velocities observed as due to Compton drag against the jet bulk motion.

An opposite behaviour (increasing dimensions for increasing frequency) is

predicted by the model of Marscher (1980). The model of Königl (1981) predicts that very low and high frequencies are emitted in the same large region, while intermediate frequencies can be produced in the smaller part of the jet (see the schematic Fig. 2.6), implying correlated variability between low and high frequencies. Reynolds' (1982) approach substantially includes all the models, trying to justify physically the assumed gradients, the dynamical acceleration of the emitting fluid and adds the possibility of different equations of state (even if this increases the number of free parameters).

Therefore the Ghisellini *et al.* model can naturally reproduce the variability trend described in §1.3.b, of decreasing variability timescales with increasing frequencies. The precise shape of the spectrum depends obviously on the assumed value of the exponents (substantially the competition between the increase of volume and the decrease of emissivity) and the normalizations of the various quantities.

Also the energy densities involved are functions of the distance along the jet, and depending on the assumed parameters they can increase or decrease: in particular while the emitting particle energy density is always a small fraction of the total energy involved, radiation energy density dominates in the inner regions, but can decrease faster than the magnetic one, suggesting that often Compton emission is dominant also in the inner regions. The distance dependence of luminosity indicates moreover where the dissipation process is more efficient (*e.g.* accelerating particles): its dependence is monotonic, generally decreasing with distance. As far as concerns the relevant timescales, it should be noted that for typical parameters, escape and adiabatic losses of the electrons can be relevant (for low energy particles) only in the external conical region (Celotti 1989).

The resultant spectrum presents two steepening, at the self–absorbtion and at the maximum frequencies emitted in the region between paraboloid and cone, producing naturally the observed spectral break and three spectral indeces: a flat one in the optically thick radio band from the conical part, the 'intrinsic' one in the intermediate region, and a steep one produced by the superposition of spectra emitted in the parabolic region. Another interesting aspect of the model is that it does not require high values of the Doppler factor in order to reproduce the observed spectra: for example the spectrum of PKS 2155–304 can be fitted with no beaming

effects ($\delta = 1$, Ghisellini *et al.* 1985).

For a detailed description of the model we refer directly to Ghisellini, Maraschi & Treves (1985) and to Celotti, Maraschi & Treves (1991) (Appendix A).

2.2.b Variability

Variability observations can impose strong constraints and help to discriminate among various emission models. Consequently it has become necessary to include and examine with more details predictions of theoretical models on time dependent behaviours.

Even if the idea of shock waves adiabatically expanding and propagating along the jet and responsible for variations in the emitted flux, had been already suggested by Blandford & Rees (1978), detailed models has been developed quite recently (usually the shock front is also identified with the superluminal features, Blandford & Königl 1979). They all examine variability of the flux (and sometimes of polarization) in the radio–mm band.

Hughes *et al.* (1985) reproduced BL Lac radio variability with a time dependent model with three components moving in an adiabatic inhomogeneous jet, showing that a pure adiabatic expanding region (van der Laan 1966) cannot explain the observed variations. They reproduce a light curve assuming a general functional form for the three components, and best–fit with the observed behaviour; the interesting aspect is that they can constrain parameters also with the polarized flux measures.

A shock moving at constant velocity along a conical jet has been considered by Marscher & Gear (1985) in order to explain a 'flare' in the mm–IR region of 3C273, assuming a stationary and a varying components: the different dependence of the self–absorbing frequency and flux from distance, is taken as an indication that the variations are due to the expansion of the source. The shock is assumed to accelerate adiabatically the emitting particles and the shocked region dimension is a function of frequency (deduced from cooling timescales): the emission is dominated by Compton, synchrotron and adiabatic losses, subsequently during propagation. Limits on the strength of the shock are imposed in order that the shocked region does not emit too much flux with respect to the stationary component.

A similar approach is also considered by O'Dell *et al.* (1988) and O'Dell (1988) for the radio variability of AO 0235+164, for a perturbation propagating along a jet. Including delay effects due to the transverse dimension of the jet and different time profiles for injection, the dependence of luminosity on frequency and time is derived. The model reproduces quite well the observed light curve.

More recently Hughes, Aller & Aller (1989a) considering again variability of BL Lac deduce the Lorentz factor required to reproduce the variations ($\gamma \simeq 2.5$ and a compression factor $k \simeq 2$) and compare it to the value derived from VLBI observations, assuming a 'reverse' shock wave (see also Jones 1988), so that the Lorentz factor of the superluminal component is lower than that derived from the amplification of the flux.

We note that part or all the time dependent evolution of the flux at low frequencies in the models examined is due to the fact that the optical depth of a 'perturbed' region changes during expansion, from optically thick to optically thin.

The models described so far are able to reproduce with surprising details the observations of low frequency variability, assuming adiabatic perturbations (call it shock or not is unimportant indeed). They can be considered as perturbations propagating in the conical low–frequencies emitting region of the Ghisellini *et al.* (1985) model.

Other kind of studies suggested the presence of shock waves. Cawthorne & Wardle (1988) derive two different velocities from the intense variable polarization of OJ 287 and the observed VLBI motion. Shock are required in order to create the distributions of particles emitting in the jet of M87 (Perèz–Fournon *et al.* 1988) and 3C273 (Meiseneimer & Heavens 1986).

We have on the contrary explored the effect of a perturbation moving in the inner parabolic region, which produces variability at high frequencies (typically optical–X–ray band). Until recently the observational informations about variability in these energy bands were quite loose, and also nowadays X–ray light curves show such a rapid variability that a detailed comparison with observations is not possible. Furthermore it should be noted that at high frequencies radiative losses are faster than adiabatic ones, and therefore an accelerating mechanism (like shock wave

acceleration, see Blanford & Eichler 1987 for a review) is required to accelerate locally the electrons.

However, as described in §1.3 some general trends are appearing: variability timescales decrease and amplitude of variations increases with frequency; different kind of correlations are observed between different bands.

We therefore consider (Celotti, Maraschi & Treves 1989; Maraschi, Celotti & Treves 1989; Celotti Maraschi & Treves 1991, see Appendix A for details and calculations) a perturbation of fixed amplitude moving in the parabolic region of the model of Ghisellini *et al.*(1985), with constant velocity, in two different geometrical structures. It produces an increase in the electron density and in the intensity of the magnetic field with respect to the stationary values when crosses the different regions. Consequently the emitted flux increases starting from high (inner region) energies and propagating to lower ones. The details of the resulting spectrum and time evolution depend obviously on the assumed parameters of the stationary jet and of the perturbation (*i.e.* its intensity). The model is able to reproduce different behaviours, like simultaneous or delayed variations at different frequencies, correlated or uncorrelated variations in the X–ray and low frequencies. If X–rays are produced as self–Compton flux they can be in an 'high state' until the perturbation weakens in the external regions: in the case of objects with flat X–ray spectra correlated variability should be observed between X–rays and the synchrotron photons which are Compton scattered, with a long X–ray variability timescale. It has been in fact observed for 0735+178, BL Lac and 3C345 (Bregman *et al.*1984, 1986, 1990; Maraschi 1991). When X–ray flux is supposed to be synchrotron emission the X–rays can precede optical–UV variations (OJ 287, Pollock *et al.*1985; 1156+295, McHardy, 1989).

The analysis of Tagliaferri *et al.*(1991) for PKS 2155–304, (Appendix B), is consistent with the computed cross correlation function from theoretical light curves of the model, in the X–ray band.

However the more significant general results are that timescales decrease (except for Compton flux), amplitudes increase with increasing frequency and the spectrum hardens with increasing flux (see eqs.(4.10) and (4.5b) of Appendix A): delays due to opacity or propagation effects appear to be consistent with the observed timescales. At low frequencies variations due to decreasing optical depth occurs.

In order to compare the results of the model with observations we simulated, at randomly chosen times, the observations at different frequencies and evaluated the parameter $v(\nu)$ defined in §1.3. However the comparison should also involve a 'recurrence' time between perturbations, and assume the presence of an underlying continuous jet. Celotti (1989) studied also the evolution of a series of perturbations, without a stationary component, the effects of a weakening of the perturbation and of acceleration of the emitting plasma along the jet.

The second important result is related to the dependence of the amplitude of variability on the line of sight. We assumed that the perturbation is a planar relativistic shock wave, in a ultrarelativistic fluid. This assumption gives a simple solution to the conservation equations which relates the fluid velocities in the shock front reference frame (see *e.g.* Blandford & McKee 1976): requiring that the energy flux $4pu_1\gamma^2$ and the momentum flux $(3u^2+1)p\gamma^2$ are conserved across the shock, it follows that $u_1u_2 = c_s^2 = 1/3$, where u_1 and u_2 are the up and downstream speeds measured in the shock front frame and c_s is the sound speed in an ultrarelativistic plasma. The upstream fluid is supersonic. The limit of strong shock can be expressed as $\gamma_1 u_1/(9u_1^2-1)^{1/2} >> 21/8$, for $u_1 \rightarrow 1$ gives $u_2 = 1/3$ and $p_2 = 8\gamma_1^2 p_1/3$. Transforming the velocities in the observer frame, it easily shown that the front velocity is greater than the shocked fluid speed. The amount of Doppler boosting of the emitted radiation is therefore smaller than that predicted from direct observations of superluminal velocities.

The results are presented in Figs. 7a,b and 8a,b of the Appendix A, also for a reverse shock wave, in which case relativistic corrections tend to decrease the variability amplitude. We note that the predicted amplitudes can be easily compared to the observed ones; sources observed at small angles should also show large amplitude variations, even for moderate values of bulk velocity. The case of mildly relativistic fluid is considered in Celotti (1989).

The energetic, even if reduced due to Doppler effects, should be substantial in order for the perturbation to last on such long distances: the perturbation 'life time', defined as the ratio of (injected kinetic energy $\times$ injection time)/(emitted luminosity), depends on the jet parameters. In order to be greater than the light crossing time for the length of the jet, the density in protons should be greater or comparable of that in

the relativistic (emitting) electrons, their kinetic energy and the bulk Lorentz factor should be great, and the magnetic field not too intense. If the energy is initially in a kinetic form and is transported by protons, the ratio between the energy in the perturbation relative to the energy of the 'stationary' jet is about $\sim \gamma_s/(R_{max}/R_o)$ (in the assumptions of our model), where γ_s, R_{max} and R_o are the Lorentz factor of the shock, the length of the jet, and its 'starting' point.

An important test for the model would obtained from correlations between UV and X–ray light curves: more precisely it predicts different correlation behaviours in BL Lac objects with steep or flat X–ray spectra.

2.3 Pair plasma jets

It is generally believed that jets are charge neutral: electrons and protons, and/or positrons, which neutralize them, have the same density and move with the same velocity.

The possibility that jets are 'light' (*i.e.* made mainly by an electron–positron plasma, *e.g.* Guilbert, Fabian & Rees, 1983) has some advantages. In fact if the estimated bulk Lorentz factor has to be greater than, let say, 5–10 (as implied from superluminal sources). Therefore in the case of an electron–proton plasma, each proton must have an energy of 5-10 GeV, which is at least an order of magnitude greater than the energy it can get from accretion, while for an electron-positron plasma an energy of $\sim$ 5 MeV per particle is sufficient. In term of the intensity of the radiation field the energy from accretion can be estimated by the ratio $(U_R/nm_pc^2) \simeq 0.1(v_{in}/v_{ff})$, implying that the radiation energy density U_R corresponds to $\sim$ 100 MeV for each particle.

Another advantage comes from the fact that in order to accelerate an 'heavy' fluid by radiation pressure an Eddington luminosity is required (but *e.g.* Cen A presumably contains a massive black hole, but radiates far below the Eddington limit), while for a pair plasma the effective Eddington limit is about 2000 times smaller, and the jet can be accelerated also in a thin disc structure (*i.e.* it is not requred beamed radiation): the radiation pressure acceleration (but also the Compton drag) is more efficient for a 'light' jet with lower inertia.

Furthermore the estimated thrusts can become consistent with the external ram pressure. An efficient mechanism to transfer energy from mildly relativistic protons to ultrarelativistic electron is not necessary; indeed one of the hardest thing to be estimated is which fraction of the dissipated power can go to into few ultrarelativistic or rather shared among all thermal particles.

Moreover, as we mentioned in §1.4.a, pair production in compact objects should occur. Therefore it is an interesting question to determine the matter content of jets. Unfortunately it is not possible to discriminate between the two alternatives on the basis of energy or momentum estimations. In fact the last two quantities could be transported from the central region to the outer ones in electromagnetic form, which can subsequently *e.g.* accelerate the emitting particles (*e.g.* Rees 1981), or by 'invisible' protons.

In fact let us estimate which fraction of energy carried by a pair plasma can be trasported to the outer regions. If fL_{45} is the fraction of luminosity carried in the $e^{\pm}$ beam, the comoving number density is given by $\sim (10^{15}/m_e c^3)(fL_{45}/\gamma_r \gamma_b^3 \theta^2 R_{15}^2)$, where γ_r and γ_b are the random and bulk Lorentz factors, θ is the aperture angle of the jet and $R = R_{15}10^{15}$ cm a typical distance. Suppose (Rees 1984) that σ is a cross section for one interaction in the dynamical timescale, then $\sigma/\sigma_T \simeq 0.02\gamma_b^3\gamma_r R_{15}\theta^2/fL_{45}$ and the number of scattering in the same timescale is therefore $N_{sc} = \sigma_T/\sigma = max[1; 50fL_{45}/\gamma_b^3\gamma_r R_{15}\theta^2]$, where 1 include *e.g.* the case in which σ is an absorption cross section. Therefore N_{sc} is high, implying a fast cooling of the pairs, unless γ_r or γ_b are high. But γ_r can not be large because the meaninful quantity to estimate Compton cooling is $N_{sc}\gamma_r^2$, which in the last hypothesis would be greater than 1. Furthermore if an equipartition magnetic field is present also synchrotron losses reduce γ_r to one, in the outflow timescale. And, however, Compton losses are effective even if re–absorption could lead $\gamma_r \sim 10$.

If γ_r is low, annihilation (with cross section $\sim 0.2\sigma_T$) is effective. Therefore γ_b should be high enough to allow γ_r not to be low, and to keep N_{sc} small. A lower limit is set $\gamma_b \gtrsim 3.5(fL_{45})^{1/3}/(R_{15}^{1/3}\theta^{2/3})$. Rees (1984) therefore concluded that the energy flow should be in ordered motion or Poyinting flux: only $\gamma_b mc^2$ (γ_r^{-1} of the initial energy) survives as kinetic energy.

Furthermore particles can exchange momentum with a photon flux produced

near the central engine through Compton interaction on timescale $t_C/t_{dyn} \simeq 0.02 L_{45} R_{15}/\gamma$. If $L_{45} > 1$ the Compton interactions are important, and if radiation is initially collimated, the jet can be accelerated; if instead it is isotropic the jet can be decelerated (see §4.1). Here we just report the result that, in quasars environment even if $\gamma_b >> 1$ initially, a small isotropic radiation component, *e.g.* at NLR distance ($L(R = 10^{18}) > 0.1 L_{45}$) or in BLR region, implies $(\gamma_b - 1) < 0.02 R_{15}/f L_{45}$, which is a strong upper limit, overall when $f \simeq 1$ as in a pair plasma beam. Phinney (1987) deduces for an $e^{\pm}$ plasma, a final bulk Lorentz factor $\gamma_b \simeq \ell^{1/7}$, where ℓ is the compactness parameter (§1.4.a).

An alternative test, to determine if pair flows can power the outer regions, that we explored (Ghisellini *et al.* 1991, see Appendix C) is to compare number densities of particles. More precisely, quite independently of pair production models, it is possible to estimate the density of surviving pairs in an outflow, *i.e.* the number density of pairs able to escape the source despite of annihilation and expansion, adopting a very simple dynamical model for the escaping flow. Furthermore using the SSC model (see §1.4.d) we were able to estimate a minimum number of emitting particles in the radio emitting regions.

The comparison of these two quantities has been done for two samples of blazars (see Appandix C), and implies that, in our simple assumptions, the predicted pair density is not enough to account for the observed radiation. (see Figs. 3,4 of Appendix C). The jets should be therefore 'heavy'.

Our results are in agreement with the above discussion on energetics (strong annihilation is present and not enough energy can be transported by a 'light' jet), however we explored the possibility that the number density of surviving particles can be (or not) compatible with an $e^{\pm}$ jet, if the energy can be transported in electromagnetic form.

It should be mentioned however that some escapes to the above conclusion are possible, but in order to be consistent for all the sources, only three alternatives seem plausible: *i)* pairs do not annihilate and therefore are able to survive because their initial velocity is only into bulk motion, and not random, *i.e.* the flow of particles is parallel (Rees 1981). The pairs could be reheated on SSC radio scale. This

assumption however requires a very high initial densities in the compact source in order to account for the simple volume espansion, which implies extreme values for the compact source optical depth; *ii)* γ–rays can transport energy outside a magnetized source and convert it into pairs locally, when interact *e.g.* with X–ray photons (Rees 1981); *iii)* emitting particles are not cold, *i.e.* the minimum Lorentz factor of the pairs is $\gamma \simeq 50 - 100$. In this case comparatively fewer particles are required from the SSC emission model (for a steep energy spectrum) and their number can be reconciled with the predicted one. This alternative, which requires few relatively cold particles with $\gamma \sim 100$, which are reaccelerated outside to $\gamma_r \sim 1000$ to emit the observed radiation has been already proposed (Rees 1984). In fact, we think that this is the most interesting result. Faraday depolarization arguments (see §1.4.b) in the case of electron–proton plasma require a low energy cut–off in the particle energy distribution at about $\gamma \simeq 50-100$. Similar values are thus required, in order to be compatible with the hypothesis of a pair jet plasma. This interesting 'coincidence' strongly argues for a heating mechanism which does not allow the particles to completely cool.

The presence of pair jets has been already suggested (*e.g.* Kundt & Gopal–Krishna 1980), for extended radio jets. In fact if the velocity of the beam is estimated from the kinetic energy density with a density evaluated from the Faraday rotation data, non–relativistic velocities are implied. We have already mentioned many reasons to believe that the flow are instead relativistic, and consequently the above constraint can be overcome if there is no more limit on the particle density from polarization observations, as is the case of pair plasma jets.

Another site where probably jets are constituted of pairs, is the Galactic Centre (*e.g.* Burns 1983), where a narrow, variable annihilation line is observed. The width of the line gives an upper limit of $10^3\ R_s$ for the emitting region (for $M \sim 10^6 M_\odot$) in order not to be gravitationally redshifted and broadened. Relativistic jets can transform kinetic energy in mass of pairs if high energy photons encounter soft ones, at the appropriate distance.

2.4 Unification models

Recently many attempts have been tried in order to include different classes of AGN in a unified picture (*e.g.* Lawrence 1987; Urry, Maraschi & Phinney 1990), based mainly on two important parameters: directionality and relativistic beaming. The first one can be *e.g.* associated with the presence of a certain amount of obscuring dust in a torus shape or to the presence of an accretion disc or thick gas clouds. A large and geometrically thick torus or a warped disc (with different prediction on the IR emission) have been suggested to unify Seyfert 1 and Seyfert 2 galaxies, the emission of the latter being reflected by electrons and dust (*e.g.* Bregman 1990; Krolik & Begelman 1988; Phinney 1989).

Large consensus exists on the idea that high luminosity quasars are the high redshifts counterpart of low luminosity local Seyfert 1 galaxies.

Note that particularly in the case of beaming effects a larger unbeamed population should exist. For a given randomly observed sample, with intrinsic velocity β the fraction of objects with $\beta_{app} > \beta$ is $2\sqrt{1-(\beta_{app}/\beta\gamma)^2}/(1+\beta_{app}^2) < 2/(1+\beta_{app}^2)$ (Cawthorne *et al.* 1986). Not enough sources has been observed: a way to improve this difficulty is suppose that the source can beam radio emission in a cone with opening angle much larger than $\sim \beta_{obs}^{-1}$. One way to get this is to invoke the presence of relativistic shock waves.

Moreover for each object with an opening angle of the jet $\sim 1/\gamma$ there should be $\sim 4/\gamma^2$ misaligned sources ('parent population').

The identification of the 'parent population' is strongly affected by the intrinsic dispersion of physical quantities, selection effects and evolution.

Scheuer & Readhead (1979) tried to unify radio quiet (more numerous) and radio loud quasars, but their model encounters some difficulties, like differences in the strength of the large–scale, diffuse, unbeamed emission of the two classes. Unification model for flat and steep spectrum radio quasars (suggested by Orr & Browne 1983) is not easy to be tested due to the strong evolution of the sources. It seems that the correlations between the core dominance parameter R and δ, β_{app} (Browne 1987), linear projected dimensions (which sometimes seem extreme) are not very strong.

Statistic counts require $\gamma \sim 5$ in order that the model works.

Unification of powerful radio galaxies (FRII type) and radio loud quasars (OVV and HPQ) has been explored by Barthel (1989). The former present narrow lines and weaker radio core and jets (Miley 1980), requiring an obscuring torus as well as beaming effects (suggested by one–sidedness) FRII should been observed at an averaged angle of 69^o, while quasars at about 31^o. At intermediate angles, between the torus and the beaming angle, broad line radio galaxies could be observed.

Similarly, at lower luminosity, it has been suggested that the 'parent population' of BL Lac objects is instead constituted by FRI galaxies (Wardle, Moore & Angel 1984; Browne 1989; Woltjer 1989; Ulrich 1989), on the basis of similar unbeamed characteristics like the large scale radio structure, extended radio power and emission line properties.

Ulrich (1989) found that both the extended radio flux and the absolute magnitude of the host galaxies of BL Lacs agrees with FRI radio galaxies of the B2 catalogue. The underline galaxies seem for both classes of objects to be elliptical (even if some BL Lacs in disc galaxies have been recently observed, Abraham, McHardy & Crawford 1991).

Another evidence comes from the observation of the FRI galaxy Cen A, in which narrow emission lines imply that the emitting gas 'sees' a continuum about 200 times the observed one (Morganti *et al.* 1991).

Whether the number of FRI galaxies is consistent with this picture has not been explored so carefully. An estimated ratio of the beamed and unbeamed objects (80 Gpc^{-3} BL Lacs and 3000 Gpc^{-3} FRI, Woltjer 1989) gives the opening angle of the beam ($\sim 30^o$), which measures or the opening angle of the flow if it is greater than the beaming angle, or alternatively the beaming factor (about $\gamma \simeq 4$). A similar value of γ is required in order that the observed core of FRI galaxies have the same radio luminosity of BL Lacs. This aspect will be examined in detail in §2.4.b,c.

Finally note that, even if the spectral distribution and other properties of HPQ and BL Lacs are quite similar (§1.1), their redshift distribution is quite different, suggesting distinct 'parent populations' (Browne 1989).

2.4.a BL Lac objects and beaming

Recently some indications that relativistic bulk motion could be frequency dependent have been found (Stocke *et al.* 1985; Maraschi *et al.* 1986; Impey & Tapia 1990), and models with a jet opening angle determined by the bulk Lorentz factor has been considered (Blandford & Königl, 1979; Ghisellini, Maraschi & Treves 1985).

Even if X-ray selection of BL Lac objects should be unbiased with respect to the radio properties, yet produces only (or mostly) radio weak objects (see §1.1.b). Therefore, for a given X-ray luminosity, radio weak X–ray selected objects represent the majority of the population, *i.e.* their space density is larger than that of radio strong objects (Maraschi *et al.* 1986). The result has been confirmed by the *Einstein* EMSS observations (containing $\sim$ 30 BL Lacs, more than half with redshift) and by the 11 X–ray detected BL Lacs discovered by EXOSAT.

This lead to the conclusion that X–rays are more isotropic than radio flux, also in agreement with the two different spectral distributions. In fact we remind (see §1.1.b) that the radio to X-ray flux ratio, as measured by the spectral index α_{RX} for X–ray selected BL Lacs is substantially smaller than for radio selected (see Fig. 1.3), while the X-ray luminosity of the two groups is comparable, even if for radio selected objects it extends to larger values (see Fig. 2.7).

Furthermore Impey & Tapia (1990), assuming that the Lorentz factor and the intrinsic ratio of core and extended radio luminosity are the same for all objects, using the observed parameter R determined the angle of sight. Because R correlates with the optical polarization this implies that also the optical emission is beamed, but appear to be less than the radio one.

The frequency dependence of anisotropy can be reproduced or with increasing Lorentz factor (acceleration) or decreasing opening angle (*i.e.* collimation) for increasing distance along a jet, (*i.e.* for decreasing frequency). The two different models are examined in the next sections.

2.4.b Acceleration

The relativistic beaming affects the form of the luminosity function of the beamed objects. Urry & Shafer (1984) and Urry & Padovani (1991) develop the formalism

to infer the luminosity function of the beamed objects as a function of the parent population luminosity function and the Doppler factor (assumed constant for all the objects), for a random orientation of the jets in the sky. In fact because the beamed objects appear brighter due to Doppler amplification, they will be more numerous in a flux limited sample and consequently their luminosity function can not be obtained simply multiplying by δ^p the luminosities of the parent one.

If the parent luminosity function is assumed to be a power–law $\Phi_u(\ell) = \Phi_0 \ell^{-B}$, between ℓ_{min} and ℓ_{max}, the beamed one, $\Phi(L)$, is a broken power–law, with the same slope B above $L = \delta^p \ell_{min}$ and flatter, with slope $(1 + 1/p)$ below this value (for the possible values of p see §1.4.e). In fact at each ℓ corresponds a range of values of L, angularly distributed like δ, with probability $P(L,\ell)dL = P(\delta)d\delta = d(\cos\theta)$. Substituting $d\cos\theta/d\delta = \delta^{-2}(\gamma^2 - 1)^{-1/2}$ and $d\delta/dL = L^{(1/p-1)}/p/\ell^{1/p}$, then $P(L,\ell) \propto L^{(-1-1/p)}$ (see Fig. 2.8).

As a further hypothesis it is assumed that only a part of the intrinsic luminosity is enhanced by beaming, and this effect is included adding a parameter f which is the fraction of ℓ which is beamed: the ranges in luminosity change, but the shape of the derived luminosity function is the same as before. Note however that f (and γ) could both be functions of ℓ (*e.g.* if Compton drag limits the maximum reachable γ).

The flat part of the beamed luminosity function, which depends on the spectral index, can generate a $\log N - \log S$ flatter than the euclidean value 1.5, without involving evolution (Cavaliere, Giallongo & Vagnetti 1986).

Ghisellini & Maraschi (1989) discuss in detail the effect of accelerating the plasma flowing in the Ghisellini, Maraschi & Treves (1985) jet model, with velocity increasing with distance from the core. The spectral differences between X-ray and radio selected BL Lacs is explained by differences in viewing angles (see Fig. 2.9), assuming a smooth acceleration of the plasma in the jet, corresponding to bulk Lorentz factor $\gamma \sim 1$ in the inner (X-ray emitting) regions, $\gamma \sim 2 - 3$ in the intermediate (optical emitting) zones, and $\gamma \sim 4 - 5$ in the outer (radio emitting) parts. The ratio of the radio to the X–ray flux changes according to the viewing angle Θ: for $\Theta \sim 0°$ the radio emission is strongly enhanced in the observer direction, while it is dimmed for $\Theta \sim 90°$. Radio selected BL Lacs are the ones with small viewing angles, while X–ray

selected ones correspond to sources observed at larger angles.

Moreover, if radio selected objects are seen at $\Theta < 1/\gamma$, their percentage in an X-ray selected sample should be roughly the ratio of solid angles $\cos(1/\gamma)/[1 - \cos(1/\gamma)]$, which yields 1/50 for $\gamma = 5$, consistently with the absence of radio selected BL Lacs in the EMSS survey sample.

Recently, complete radio and X-ray selected samples of BL Lacs have become available and allow to compute the respective luminosity functions (Stickel *et al.* 1991; Morris *et al.* 1991), giving constrains on beaming models.

In a recent series of papers, Padovani and Urry (1991a) and Stickel *et al.* (1991), test the hypothesis that *all* BL Lacs are FRI beamed at us. They consider the X-ray and radio luminosity functions of the parent population and derive the X-ray and radio luminosity functions of BL Lac objects, applying substantially the Urry & Shafer's formalism. Due to the lack of redshift informations for a large part of the BL Lac samples, the theoretical luminosity functions obtained cannot be directly compared with data and therefore they calculate the counts (Log N–Log S), and compare them with data in the X–ray band.

They find that the scheme is successful if the X-ray emitting plasma has $\gamma \simeq 3-4$ and the radio emitting plasma has $< \gamma >= 7.5$ (with a power law distribution extending up to 35), implying that BL Lacs are observed at angles less than 10^{o}.

They applied the same kind of formalism for the unification of flat spectrum, steep spectrum and FRII radio type galaxies in the radio band, for decreasing angles of observation, as already suggested by Peacock (1987) and Barthel (1991). Linear radio size distributions are consistent with this picture. For details see Padovani & Urry (1991b).

2.4.c Recollimation

The model of Padovani & Urry does not however address the question of which physical acceleration mechanism could work on the appropriate scale, a factor $10^2 - 10^3$ at least in distance from the core, and requires Lorentz factors as great as ~ 40. This value implies a 'Doppler angle' $1/\gamma \sim 1.5^0$, smaller than any reasonable

opening angle of jets and it does not agree with the smaller superluminal velocities observed in BL Lacs. Furthermore it may be difficult to account for large and fast luminosity variations observed in the X-ray band (*e.g.* Treves *et al.*1989) without invoking relativistic beaming. Other assumptions can be critical in their derivation of the Lorentz factors.

For these reasons we (Maraschi, Celotti & Ghisellini 1991) quantitatively examine the alternative to the above model, in which keeping a constant Lorentz factor γ of the flow along the jet, the solid angle subtended by the streamlines is allowed to be much larger than $1/\gamma$ near the core and to decrease with distance. Therefore we consider a jet with increasing collimation rather than with increasing velocity. A more detailed analysis will be the subject of a paper in preparation.

Note that as far as the spectral distributions are concerned, an observer at intermediate angles would observe a steep, synchrotron X–ray spectrum, because observes mainly radiation from the inner regions. At small angle instead the flat X–rays inverse Compton spectrum is dominating and should show connection with the low frequencies spectrum (see Maraschi 1991).

We discuss joint constraints from the radio and X-ray luminosity functions assuming that γ is the same in both bands but the opening angle of the jet is wider for the X-ray emitting plasma.

Let us consider a relativistic flow with fixed bulk Lorentz factor γ but with velocity directions uniformly spread in a cone of semiaperture Θ_j, larger than the critical semiaperture angle for relativistic beaming $\Theta_c \simeq 1/\gamma$. Further out the collimation of the jet increases so that Θ_j decreases possibly reaching $1/\gamma$.

An estimate of the effect of a spread in the velocity directions can be derived on the basis of a very simple argument, whose validity is shown by the exact formulae given below.

Since the radiation emitted by particles with Lorentz factor γ is practically entirely concentrated in a cone of angle $\Theta_c \simeq 1/\gamma$, we can estimate the observed flux assuming that at an angle Θ to the jet axis ($0 < \Theta < \pi/2$) the contributing particles are those within the small aperture Θ_c cone close to the observer line of sight. For $\Theta < \Theta_j$ there will be always one such cone on the line of sight while for $\Theta > \Theta_j$

the nearest of such cones will be on the border of the jet cone.

The number of Θ_c small cones within the Θ_j cone is simply the ratio of the subtended solid angles

$$N = \frac{1 - \cos\Theta_j}{1 - \cos\Theta_c} \tag{2.8}$$

We can then write the luminosity observed at an angle Θ in terms of the total rest frame luminosity of the jet as

$$L(\Theta, \Theta < \Theta_j) \simeq \frac{\ell}{N}\delta^p(0) \sim \frac{2\pi}{\Delta\Omega_j}\,\ell\,(1+\beta)^p\,\gamma^p[1 - \cos(1/\gamma)] \tag{2.9}$$

ℓ/N being the rest frame luminosity fraction emitted by particles with velocity direction within Θ_c and $\delta^p(0)$ being the relativistic correction of the flux observed at zero angle with respect to the small cone. $\Delta\Omega_j = 2\pi\,(1 - \cos\Theta_j)$ is the solid angle subtended by the jet. The exponent p is assumed hereafter to be $p = 3 + \alpha$, appropriate for amplification of monochromatic luminosity from *e.g.* blobs of plasma (see §1.4.e).

This luminosity can be compared with the value obtained in the case of parallel velocities, for which $L(0) = \ell\delta^p(0) \sim (2\gamma)^p\ell$, for $\gamma \gg 1$: the observed luminosity in the case of large jet angle is smaller than that because only the fraction $(1/N) \sim [1/\gamma^2(1 - \cos\Theta_j)]$ of the jet is beamed exactly towards the observer, and therefore $L(0) \propto \gamma^{p-2}$.

By the same approximate arguments, we can derive the observed luminosity at $\Theta > \Theta_j$. In this case the plasma contributing the most is in the '$1/\gamma$' little cone at an angle between $\Theta - \Theta_j$ and $\Theta - \Theta_j - 1/\gamma$, on the border of the jet. Taking $\Theta - \Theta_j$ as the relevant angle we have

$$L(\Theta, \Theta > \Theta_j) \sim \frac{\ell}{N}\delta^p(\Theta - \Theta_j) = \frac{2\pi}{\Delta\Omega_j}\,\ell\,\frac{[1 - \cos(1/\gamma)]}{\gamma^p[1 - \beta\cos(\Theta - \Theta_j)]^p} \tag{2.10}$$

The minimum luminosity corresponds to $\Theta = \pi/2$. At this value of Θ, eq. (2.10) has to be compared with $L(\pi/2) = \ell/\gamma^p$ obtained in the case of parallel velocities. Depending on Θ_j and γ, eq. (2.10) can yield smaller or greater values than those obtained for parallel velocities.

In Fig. 2.10 we show the intensity profiles computed with exact formulae for the case of $\gamma = 10$, $p = 4$ and for different apertures of the velocity cone. From this figure

it can be seen that, approximately, the the wide angle cone profiles can be matched by assuming a lower γ in the parallel velocities scheme.

We now derive the exact expressions relating intrinsic and observed luminosities and the resulting luminosity function for the beamed population.

Calling ℓ the intrinsic luminosity of the jet, the observed luminosity at an angle Θ with the jet axis, $L(\Theta)$, is given by

$$L(\Theta) = \ell R(\Theta) \equiv \frac{\ell}{\Delta\Omega_j} \int_0^{\Theta_j} \sin\theta d\theta \int_0^{2\pi} \delta^p(\Theta,\theta,\phi) d\phi \tag{2.11}$$

where δ is

$$\delta(\Theta,\theta,\phi) = \frac{1}{\gamma\left[1-\beta(\sin\Theta\sin\theta\cos\phi+\cos\Theta\cos\theta)\right]} \tag{2.12}$$

The function $R(\Theta)$ is defined by eq. (2.11). It involves the integration of the contribution from each part of the jet flow: the integrand therefore depends on the angle, call it χ, between the line of sight and the velocity direction of each volume of the jet, the position of which is identified by the two angular coordinates ϕ and θ. ϕ is the azimuthal coordinate and θ is measured from the jet axis (see Fig. 2.11). The combination of sinusoidal functions multiplying β in eq. (2.12) is just the cosine of χ.

The integral in ϕ in eq. (2.11) can be done analytically for integer values of p (see below). $R(\Theta)$ is a monotonic (decreasing) function of Θ, shown in Fig. 2.10. For $\Theta < \Theta_j$, the emission is mostly due to the plasma moving exactly towards the observer; therefore we expect $L(\Theta)$ to be almost constant with a value approaching $L(0)$. For $\Theta = 0$, the integral in eq. (2.11) simplifies, and can be done analytically. The result is

$$L(0) = \ell\frac{2\pi}{\Delta\Omega_j}\frac{(1+\beta)^{p-1}}{\beta(p-1)}\gamma^{p-2}\left[1-[\gamma^2(1+\beta)(1-\beta\cos\Theta_j)]^{1-p}\right] \tag{2.13}$$

Eq. (2.13) differs from the approximate value given by eq. (2.9) by the factor $(p-1)$, in the limit of large γ.

Given the relation between the intrinsic and the observed luminosity, we can compute the luminosity function for the beamed population of objects $\Phi(L)$, depending on the intrinsic luminosity function of the parent population $\Phi_u(\ell)$.

Sources with the same intrinsic luminosity ℓ will have different observed luminosities $L(\Theta)$, according to eq. (2.11). For a random distribution of jet directions in the sky, the probability $P(L,\, \ell)$ to observe a source with a given L is distributed as the solid angle corresponding to that L

$$P(L,\, \ell)dL \,=\, \frac{P(\Theta)}{2\pi}d\Theta \tag{2.14}$$

If the intrinsic luminosities have a distribution $\Phi_u(\ell)$, the observed luminosity function is

$$\Phi(L) \,=\, \int_{\ell_1}^{\ell_2} \Phi_u(\ell)P(L,\, \ell)d\ell \tag{2.15}$$

where the limits of integration are functions of L and the extremes ℓ_{min} and ℓ_{max} of the intrinsic luminosity function. Changing variable, from ℓ to Θ, and noting that

$$d\ell \,=\, -\frac{L}{R^2(\Theta)}\,\frac{dR(\Theta)}{d\Theta}d\Theta \tag{2.16}$$

we obtain

$$\Phi(L) \,=\, -\int_{\Theta_1}^{\Theta_2} \Phi_u\left(\frac{L}{R(\Theta)}\right)\frac{\sin\Theta}{R(\Theta)}d\Theta \tag{2.17}$$

The limits of integration, functions of L, ℓ_{min} and ℓ_{max}, must be found by solving the equations

$$\begin{aligned} L - \ell_{max}R(\bar{\Theta}_2) \,&=\, 0 \qquad \Theta_2 = \min(\bar{\Theta}_2,\, \pi/2) \\ L - \ell_{min}R(\bar{\Theta}_1) \,&=\, 0 \qquad \Theta_1 = \max(\bar{\Theta}_1,\, 0) \end{aligned} \tag{2.18}$$

This is equivalent to find the range of observing angles for which there are objects, with intrinsic luminosity $\ell_{min} < \ell < \ell_{max}$ which are observed to have a luminosity L. The range of these angles must be between 0 and $\pi/2$.

Note that eq. (2.11) is very general, and can be used in all cases in which the emitted luminosity is anisotropic. For instance, it can be used in the case of thin disks, where $L(\Theta) = L(0)\cos\Theta$, (also spiral galaxies are thin disks), or in the case of thick disks, where the presence of the funnel makes the emitted luminosity very anisotropic.

In the case discussed here the observed luminosity function has to be found numerically, due to the complexity of the integral in eq. (2.11). Nevertheless, some crude approximations allows us to have some analytical insights. In fact, the

approximate information about the behaviour of $L(\Theta)$ derived in the previous section can be used to qualitatively construct the observed luminosity function.

In the luminosity range $L(\Theta > \Theta_j)$ we have, from eq. (2.11)

$$\frac{dL}{d(\Theta - \Theta_j)} = p\beta\gamma\delta^{p+1}(\Theta - \Theta_j)\frac{\ell}{N}\sin(\Theta - \Theta_j) \tag{2.19}$$

Then, using eq. (2.14), we obtain

$$P(L, \ell) = \frac{1}{p\gamma\beta}\left(\frac{\ell}{N}\right)^{1/p} L^{-(1+1/p)} \tag{2.20}$$

Once substituting ℓ with ℓ/N, eq. (2.20) is the same as the eq. (2) of Urry and Shafer (1984), although it is applicable in a restricted luminosity range. Substituting eq. (2.20) into eq. (2.15) we can derive the observed luminosity function.

When $\Theta < \Theta_j$, the observed luminosity is almost constant, and the derivative $dL/d\Theta$ (which is almost zero) cannot be found analytically.

We can nevertheless obtain a value for the observed luminosity function at the particular luminosity $L_3 \equiv \ell_{min}R(0)$, if the luminosity function of the parent sources $\Phi_u(\ell)$ is a power law of slope B, $\Phi_u(\ell) = \Phi_0\ell^{-B}$.

At L_3 eq. (2.15) can be approximated by setting $R(\Theta) = R(0)$, and integrating in the range $(0, \Theta_j)$:

$$\Phi(L_3) \sim \Phi_0 L_3^{-B}[R(0)]^{B-1}\int_0^{\Theta_j}\sin\Theta d\Theta = \Phi_0\frac{\ell_{min}^{-B}}{R(0)}(1 - \cos\Theta_j) \tag{2.21}$$

Note that eq. (2.21) is independent of B and of Θ_j [because $R(0) \propto 1/(1 - \cos\Theta_j)$].

In the previous calculations we assumed that the luminosity L of the beamed object is obtained by beaming all the intrinsic luminosity of the parent object. We now include the possibility that the observed luminosity L is the sum of two components: an unbeamed part, ℓ_u, and a beamed one, L_b.

Similarly to the Urry and Shafer's formalism all the above can be generalized in the simple assumption that only a fraction f of the unbeamed luminosity is enhanced by beaming, $L_b = f\ell_u R(\Theta)$. Therefore we have:

$$L = \ell_u[1 + fR(\Theta)] \tag{2.22}$$

Assuming also that f is constant for all sources, we can define

$$\tilde{R}(\Theta) = 1 + fR(\Theta) \tag{2.23}$$

The luminosity function in this case can be obtained by replacing $R(\Theta)$ with $\tilde{R}(\Theta)$ in the above expressions. Note however that this fraction f can be different for the radio and X–ray domains.

The parent population and the beamed one are distinguished by the value of $\tilde{R}$. We define *beamed* an object with $\tilde{R} \geq 2$, i.e. an object with $L_b \geq \ell_u$.

We can now apply the above formalism to the unification model between radio selected, X–ray selected BL Lac objects and FRI galaxies.

Suppose that the X-ray jet has a greater opening angle ($= \Theta_X$) than the opening angle of the radio jet ($= \Theta_R$), but that the bulk Lorentz factor is the same.

For $\Theta_R < \Theta < \Theta_X$, the X-ray luminosity is enhanced and approximately constant, but the radio luminosity is dimmed. These sources could be X–ray selected BL Lacs.

For $\Theta < \Theta_R$, both the X-ray and the radio luminosity are enhanced, appearing as radio selected objects.

Finally, for $\Theta_X < \Theta < 90^0$, both the X-ray and the radio luminosity are dimmed. These could be FRI sources.

The ratio of number density of X–ray selected BL Lacs and FRI sources is simply $(1 - \cos\Theta_X)/\cos\Theta_X$, which is 0.015, 0.155, 0.414 and 1 for $\Theta_X = 10^0$, 30^0, 45^0, and 60^0, respectively.

In the above picture we can constraint parameters on the basis of observed quantities, from X–rays and radio data.

1) The relative number of X-ray and radio selected BL Lacs.

If the radio jet has an opening angle Θ_R narrower than $1/\gamma$, the ratio between X–ray and radio selected BL Lacs is approximately given

$$\frac{\mathrm{XBL}}{\mathrm{RBL}} \equiv R_N = \frac{1 - \cos(\Theta_X)}{1 - \cos(1/\gamma)} - 1 \sim 10 - 50 \tag{2.24}$$

which is 8, 24, and 48 and 99 for $\Theta_X = 60^0$ and $\gamma = 3,\ 5,\ 7$, and 10, respectively.

This ratio has to be greater than ~ 50, according to the results of the EMSS and of the EXOSAT survey (Giommi *et al.* 1990).

2) The ratio between maximum luminosities

Introducing the parameter f the maximum beamed luminosity is

$$L_{max} = \ell_{max}[1 + fR(0)] \tag{2.25}$$

where $R(0)$ is (see eq.(2.11))

$$R(0) = \frac{1}{1-\cos\Theta}\frac{(1+\beta)^{p-1}}{\beta(p-1)}\gamma^{p-2}\left[1-[\gamma^2(1+\beta)(1-\beta\cos\Theta)]^{1-p}\right]$$

In the limit of $\gamma \gg 1$ we have

$$\frac{L_{max}}{\ell_{max}} \equiv R_L = 1 + \frac{f}{1-\cos\Theta}\frac{2^{p-1}}{(p-1)}\gamma^{p-2} \tag{2.26}$$

This ratio in the X–ray band has to be greater than 100–300, according to Padovani & Urry (1991a). The parameter R_L is critical and less extreme parameter values are implied for lower R_L. It can be smaller than the above estimates if some high luminosity X–ray selected BL Lac is actually HPQ whose continuum is so beamed to swamp the lines, *i.e.* is a beamed FRII, instead of FRI. Also the luminosity function of Morris *et al.*(1991) extends up to $L_X = 5 \times 10^{45}$ (small de-evolution), *i.e.* 10 times less than the value used by Padovani & Urry (1991a).

3) The ratio between luminosity functions

Considering cases in which $\Phi_u(\ell) = \Phi_0 \ell^{-B}$ is a power law, we can estimate analytically the luminosity function of the beamed objects, at the luminosity L_3 corresponding to the break, *i.e.* $L_3 = \ell_{min}[1 + fR(0)]$ as described above.

$$\frac{\Phi(L_3)}{\Phi_u(L_3)} \equiv R_\Phi \sim [1 + fR(0)]^{B-1}(1-\cos\Theta_j) \tag{2.27}$$

This ratio is of the order of 10 in X–rays (Morris *et al.* 1991, luminosity function with de–evolution) or slightly more if not all the FRI radio galaxies contain a BL Lac object.

In the radio band it should be of the order or greater than $R_{\Phi,R} \sim 0.2$.

Three unknowns, three equations, therefore:

$$\gamma \simeq \left[\frac{R_N R_L^{B-1}}{2R_\Phi}\right]^{1/2}, \qquad 1-\cos\Theta_X = \frac{R_\Phi}{R_L^{B-1}}, \qquad f = \frac{3R_\Phi^2}{4R_N R_L^{2B-3}} \tag{2.28}$$

Some cases are reported in Table 2.3, for different values of the above ratios for the radio and X–ray parameters, $p_X = 4$ and $p_R = 3$, $B_X = 2.1$ and $B_R = 2.5$ (from Padovani & Urry 1991a; Stickel *et al.* 1991), and $R_{\Phi,R} \simeq 0.2$. Other obvious constraints are $f_R, f_X < 1$, $1/\gamma < \Theta_X < 90°$, $\gamma > 1$. In Fig. 2.12 the limits on Θ_X are plotted. The two dashed curves refer to values of $R_N = 10, 50$, implying that Θ_X must be comparable or above the corresponding values (see above).

Table 2.3

$R_{\Phi,X}$	$R_{L,X}$	R_N	γ	Θ_R	$R_{L,R}$	Θ_X	f_R	f_X
10	250	50	25	2.3°	40	16.2°	$6\,10^{-4}$	$6\ 10^{-4}$
		10	11.2	5.1°	26	16.2°	$2.3\,10^{-3}$	$3\,10^{-2}$
	30	50	8.7	6.5°	9.7	48°	$3.3\,10^{-3}$	$5\,10^{-2}$
		10	3.9	14.6°	3.9	48°	$1.2\,10^{-2}$	$2.5\,10^{-1}$

In Figs. 2.13, as an example, we report the luminosity functions determined with our model, for one choice of the above parameters (second set of Table 3), for the X–ray and radio band. the dashed lines are the FRI luminosity functions.

It can be seen that the model is able to reproduce the 'observed' luminosity functions, as well as the Padovani & Urry model. The peak in the X–ray luminosity function is due to the increased number of sources (X–ray selected ones) with substantially the same luminosity in the large cone. However this feature is smoothed when the Log N–Log S is derived. Therefore the only difference with respect to the acceleration model is that in our case X–rays are beamed a lot and consequently a small variation of the intrinsic luminosity can result in a large and rapid variation of the observed one.

Even if there is not a precise physical model, some possible recollimation mechanisms are given by: external confinement, *e.g.* in a parabolic jet, where the jet angle is $\tan\theta = \epsilon x^{1-1/\epsilon}$, where $x = r/r_o$ (r transverse dimension); the plasma moving at large angles could suffer more Compton drag than plasma at small angles; the geometry of the magnetic field, *e.g.* dipole-like. Note that the presence of clumped

material in the jet could operate against collimation (*e.g.* Kundt 1987), changing the velocity directions.

Finally we explicitly show the analytical solution of the integral in the variable ϕ of eq. (2.11), for integer values of p. We have

$$I_p \equiv \int_0^{2\pi} \frac{d\phi}{[1-\beta(\sin\Theta\sin\theta\cos\phi+\cos\Theta\cos\theta)]^p} = \frac{2}{b^p}\int_0^{\pi}\frac{d\phi}{[a-\cos\phi]^p} \qquad (2.29)$$

where

$$b \equiv \beta\sin\Theta\sin\theta, \qquad c \equiv 1-\beta\cos\Theta\cos\theta, \qquad a \equiv c/b \qquad (2.30)$$

The calculation of the integral I can be reduced to the calculation of I_1:

$$I_p = \frac{2}{b^p}\frac{1}{(1-p)(2-p)...(-1)}\frac{d^{p-1}I_1}{da^{p-1}} \qquad \text{where} \qquad \mathrm{I_1} = \int_0^{\pi}\frac{\mathrm{d}\phi}{(\mathrm{a}-\cos\phi)} \qquad (2.31)$$

With the two changes of variable

$$\cos\phi = \frac{1-t^2}{1+t^2}, \qquad x = t\left(\frac{a+1}{a-1}\right)^{1/2} \qquad (2.32)$$

we obtain

$$I_1 = \frac{4}{\sqrt{a^2-1}}\left[\mathrm{artg}\left(\sqrt{\frac{a+1}{a-1}}\sqrt{\frac{1-\cos\phi}{1+\cos\phi}}\right)\right]_0^{\pi} = \frac{2\pi}{\sqrt{a^2-1}} \qquad (2.33)$$

Substituting in eq. (2.29) we obtain

$$I_3 = \frac{1}{2}\frac{1}{b^3}\frac{d^2}{da^2}I_1 = \frac{\pi}{b^3}\frac{2a^2+1}{(a^2-1)^{5/2}} = \pi\frac{(b^2+2c^2)}{(c^2-b^2)^{5/2}}, \qquad p=3 \qquad (2.34)$$

and

$$I_4 = -\frac{1}{6}\frac{1}{b^4}\frac{d^3}{da^3}I_1 = \frac{\pi}{b^4}\frac{a(2a^2+3)}{(a^2-1)^{7/2}} = \pi c\frac{(3b^2+2c^2)}{(c^2-b^2)^{7/2}}, \qquad p=4 \qquad (2.35)$$

The last two equalities in eqs. (2.34) and (2.35) avoid the vanishing of the denominator at $\Theta = 0$.

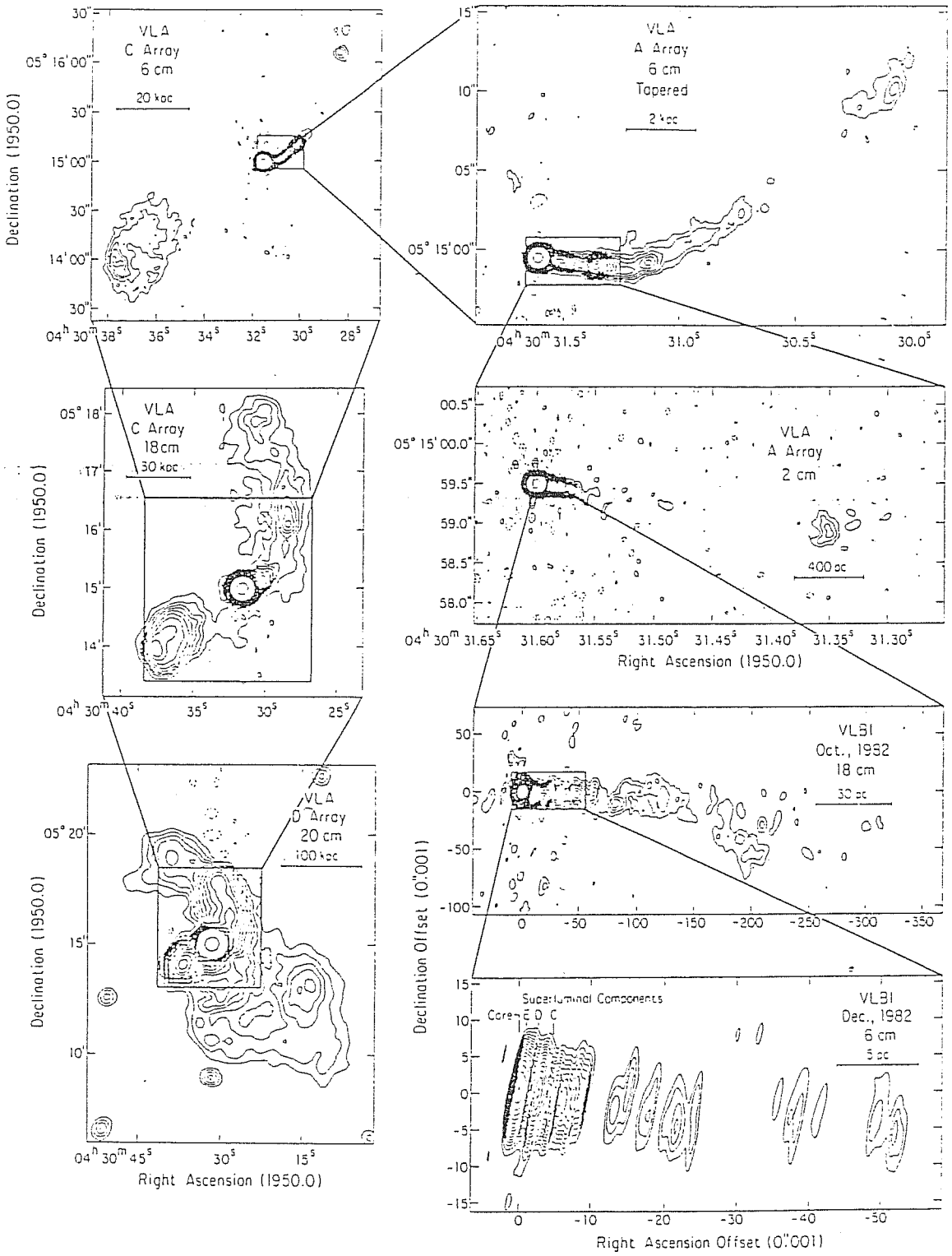

Fig. 2.1 Radio jet of 3C120. The observations at different radio frequencies illustrate the jet structure at different resolution and therefore linear sizes, which ranges from $\sim$ pc to $\sim$ 100 kpc scale. From Walker *et al.*(1987). At higher resolution the blob structure is evident. With increasing size the jet show before a net asymmetry in the emission and then bending up to 90° with respect to the pc scale jet.

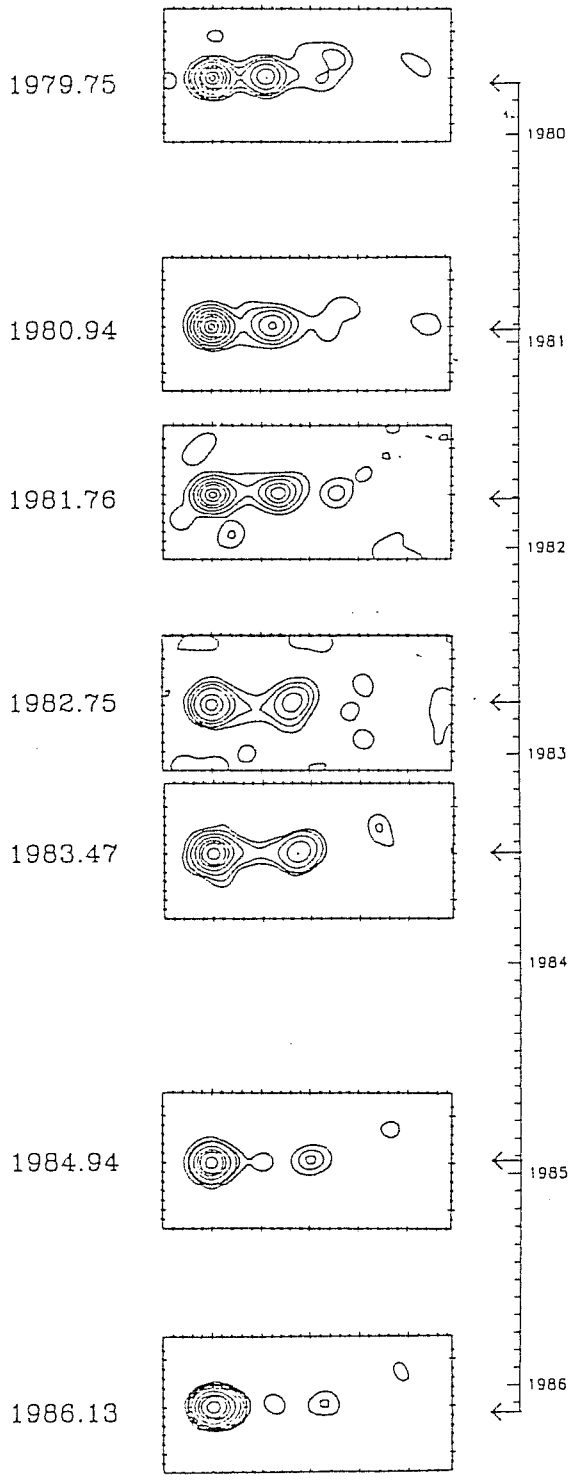

Fig. 2.2 Superluminal components of the source 3C179. On the scale observational dates are reported. The left component is assumed to be stationary, while the ejection of others can be seen. Thick marks correspond to 0.2 m.a.s. From Porcas (1987).

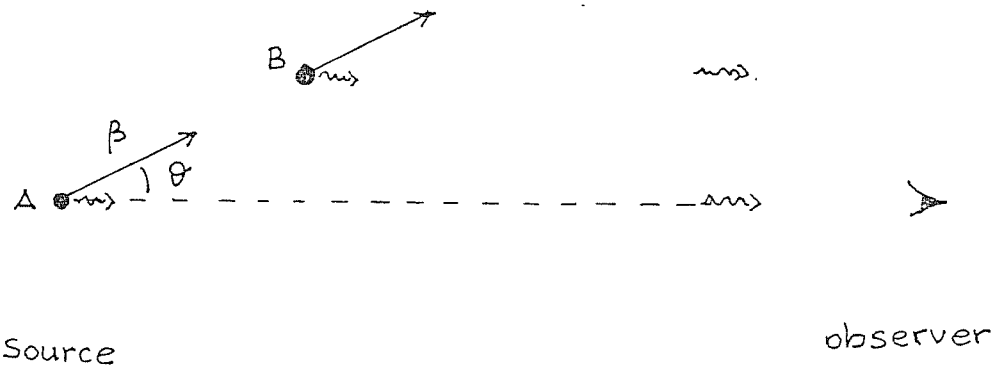

Fig. 2.3 Schematic picture to represent the more widely accepted interpretation about superluminal motion. The photon emitted at later time has a shorter way to reach the observer, who consequently measure a delay between the arrival of the two photons smaller than the real emission delay, and therefore an higher projected velocity, maybe greater than c.

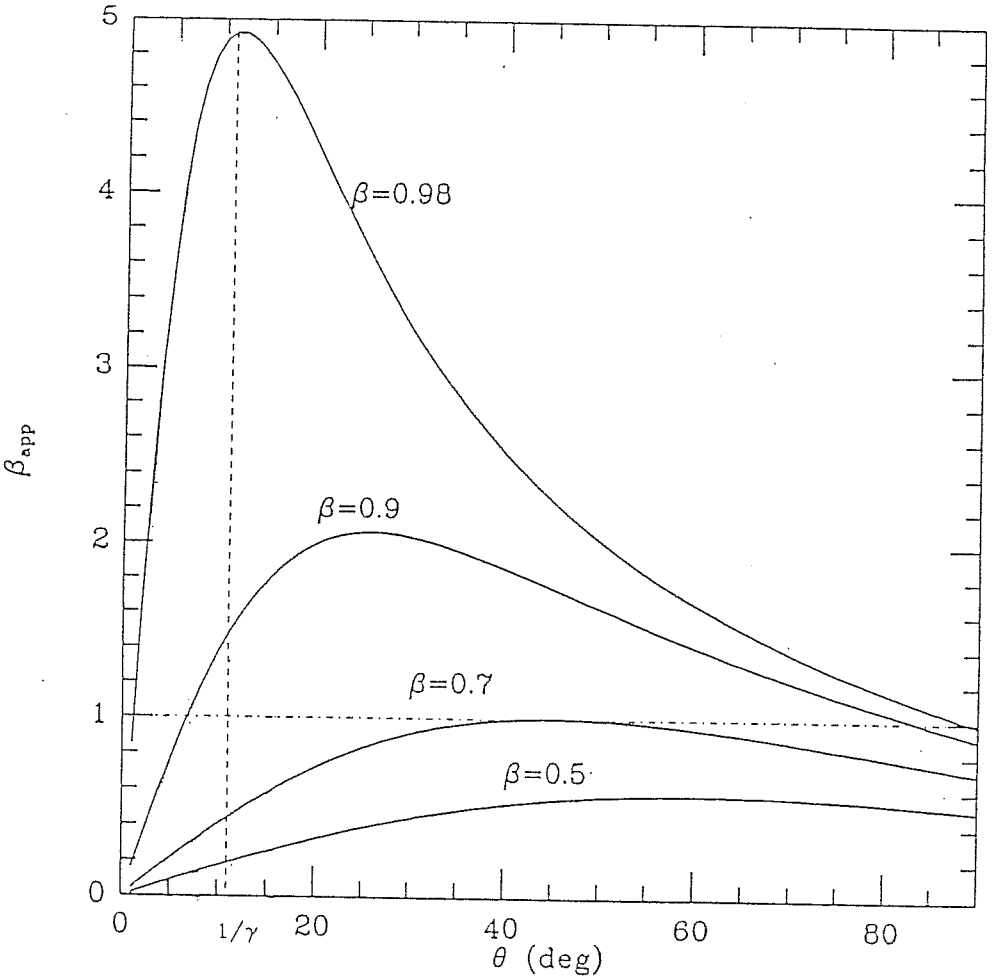

Fig. 2.4 The apparent projected velocity $\beta_{app}c$ as function of angles of observation θ with respect to the velocity direction of the emitting component, for different real velocities βc. β_{app} is maximum for $\theta \simeq 1/\gamma$. Sources observed at very small angles ($< 10^o - 20^o$) can show a high Doppler factor (see Fig. 1.10), but a low apparent superluminal velocity. For $\beta \lesssim 0.7$ no superluminal motion can be observed.

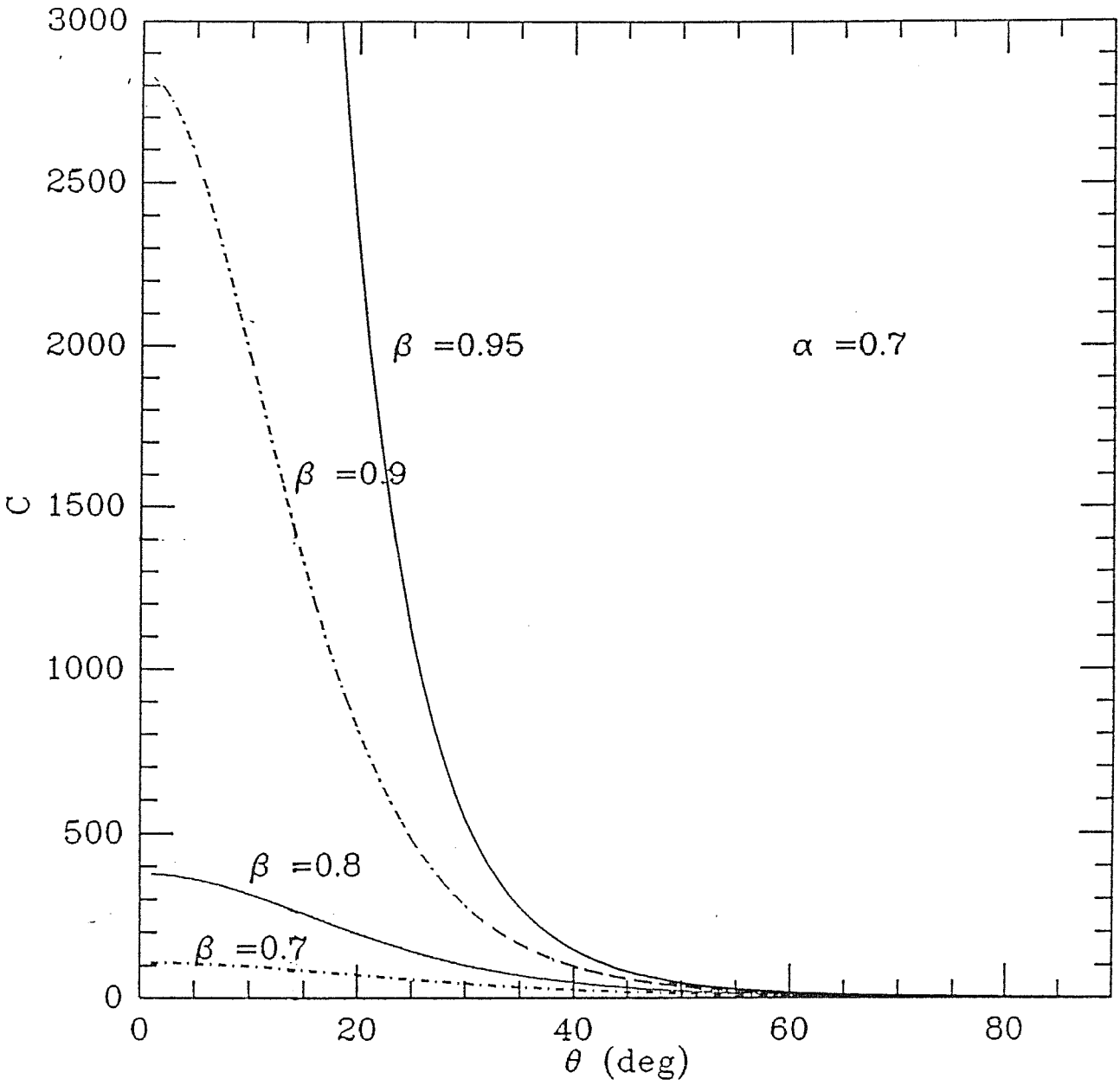

Fig. 2.5 The apparent contrast C (fluxes ratio) of the Doppler shifted component moving toward the observer and the component moving in the opposite direction in a double–sided jet . It is shown as function of angles of observation θ with respect to the velocity direction of the emitting components, for different velocities βc. The spectral index is assumed to be $\alpha = 0.7$. Also for not extreme values of β and θ enormous ratios are possible, well above the observational detection limits, possibly explaining the observations of one–sided sources.

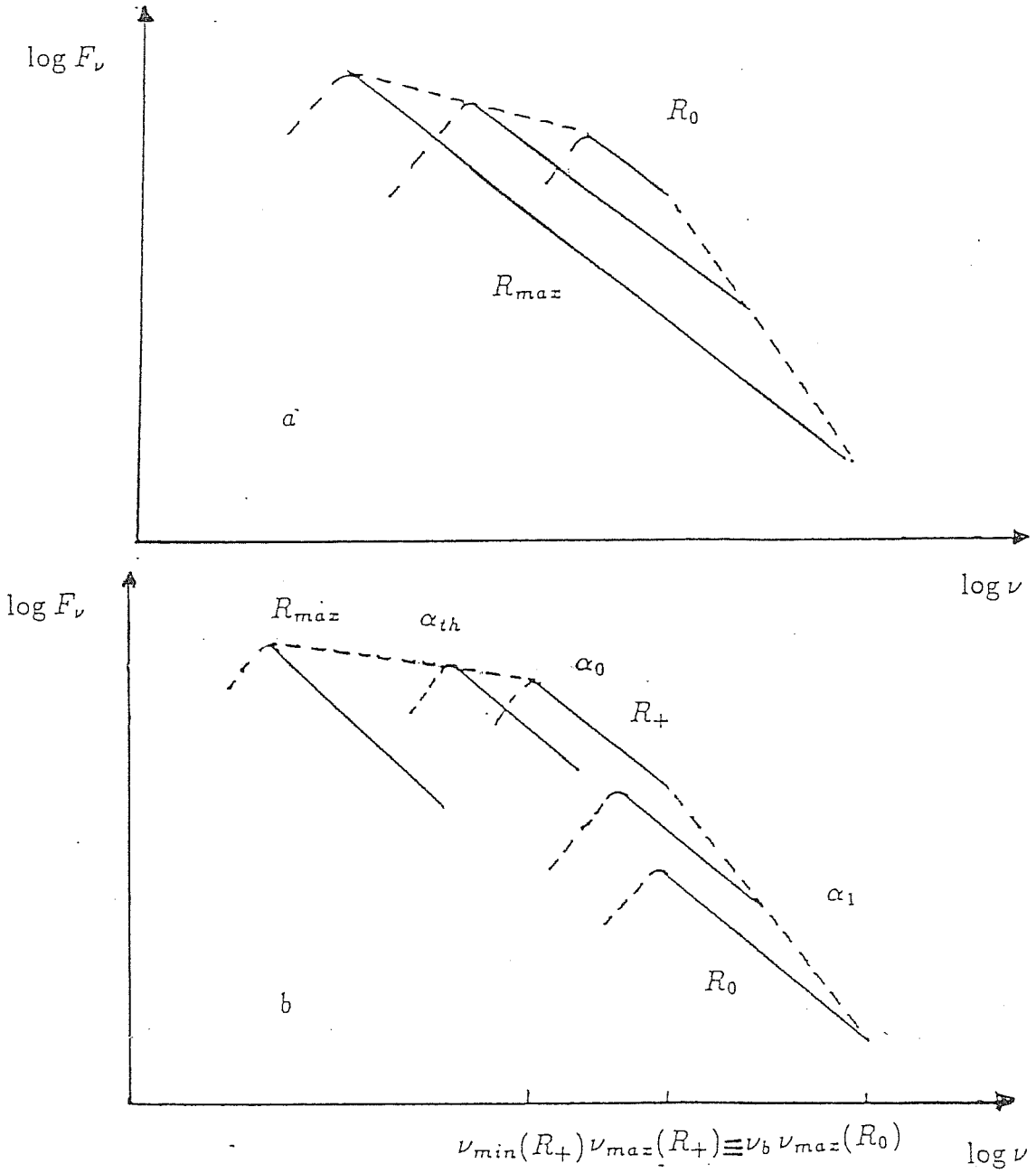

Fig. 2.6 Schematic representation of the superposition of SSC spectra emitted locally in an inhomogeneous jet, according to the models of Königl (1981) (a) and Ghisellini *et al.* (1985) (b). R_0 is the smallest dimension, R_{max} the biggest one, R_+ the distance of connection between the parabolic inner zone and the conical one. α_{th} is the flat spectral index in the radio band produced in the conical jet, while α is the intrinsic (local) spectral index and α_1 the steeper index produced in the parabolic part. ν_m, ν_b and ν_{max} are the minimum self–absorption, the 'break' and the maximum emitted frequencies respectively. Note that in the Ghisellini *et al.* model with increasing frequency the dimensions of the dominant emitting region decrease, while the opposite is true for the high energy emission in the Königl model.

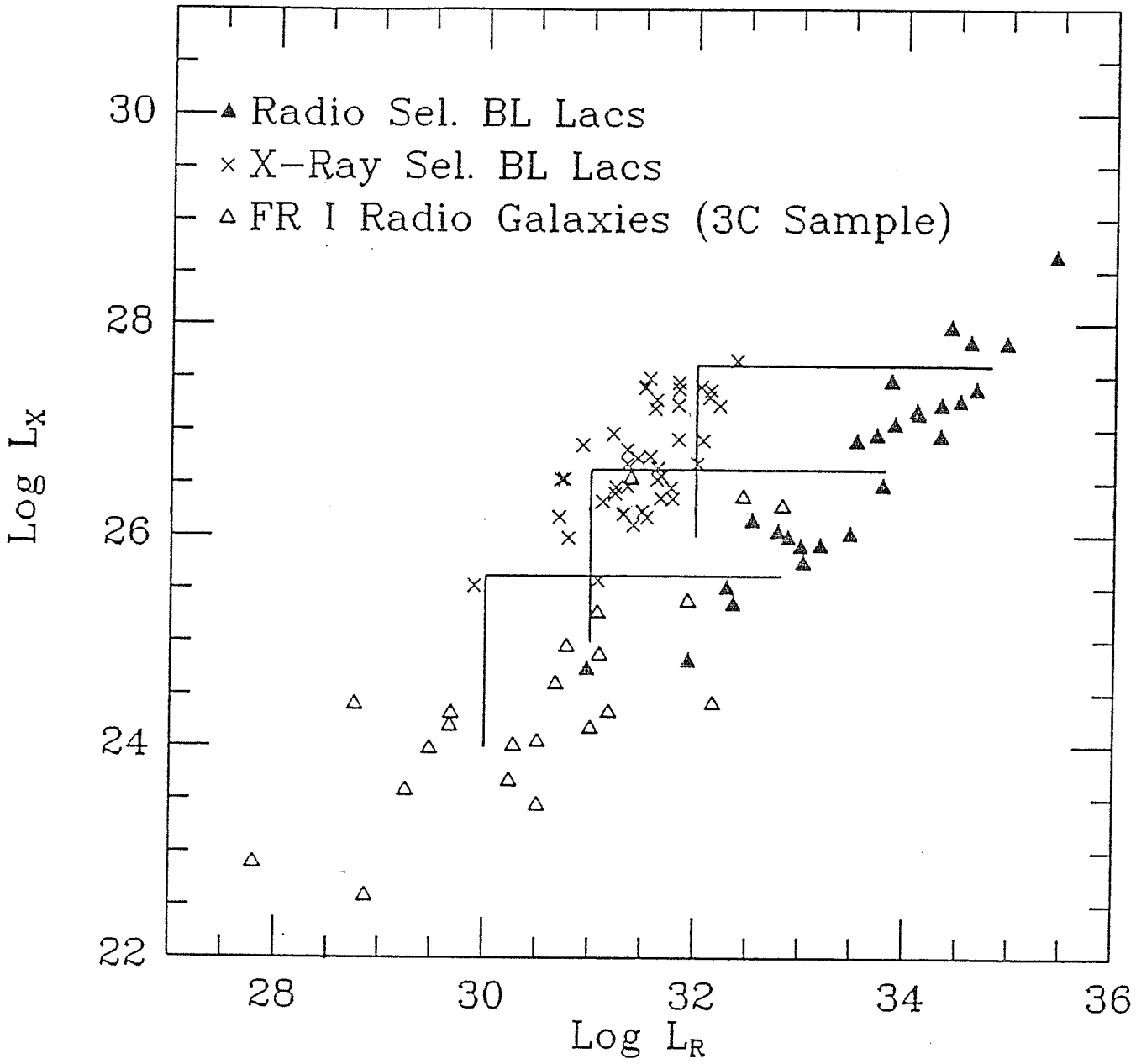

Fig. 2.7 X–ray luminosity at 2 keV versus (core) radio luminosity at 5 Ghz for FRI galaxies (Fabbiano *et al.* 1984), X–ray selected BL Lac objects and radio selected ones (Ghisellini *et al.* 1986; Maraschi *et al.* 1986; Morris *et al.* 1991; Giommi *et al.* 1991). The mean X–ray luminosity of X–ray selected and radio selected BL Lac is approximately the same, while the radio one is greater for the radio selected objects. The 'L' shape lines correspond to the variations of L_X and L_R changing the line of sight direction according to the model described in §4.2.c. Starting from the right end, for small angle the radio luminosity has a fast decrease with constant X–ray luminosity (inside the X–ray cone), thenthe radio luminosity becomes constant (and equal to the unbeamed component) and the X–ray luminosity decreases. Along this path radio selected BL Lac, X–ray selected BL Lac and FRI galaxies are observed, as shown on the diagram.

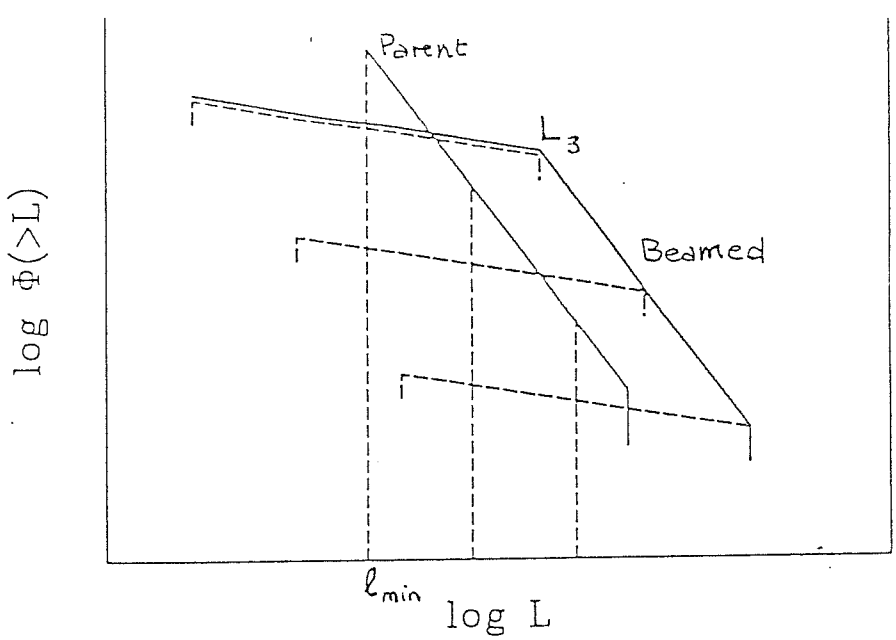

Fig. 2.8 Schematic diagram showing the effect of beaming on the observed integral luminosity function. The steeper line represents the parent population luminosity function and the 'broken' one the beamed luminosity function according to the formalism of Urry & Shafer (1984). The beamed one presents two spectral indices. The luminosity of the break is $L_3 = \ell_{min}\delta^p(0)$, where ℓ_{min} is the minimum luminosity of the parent. The dashed lines represent the effect of beaming on an intrinsic δ function luminosity. From Urry & Padovani (1990).

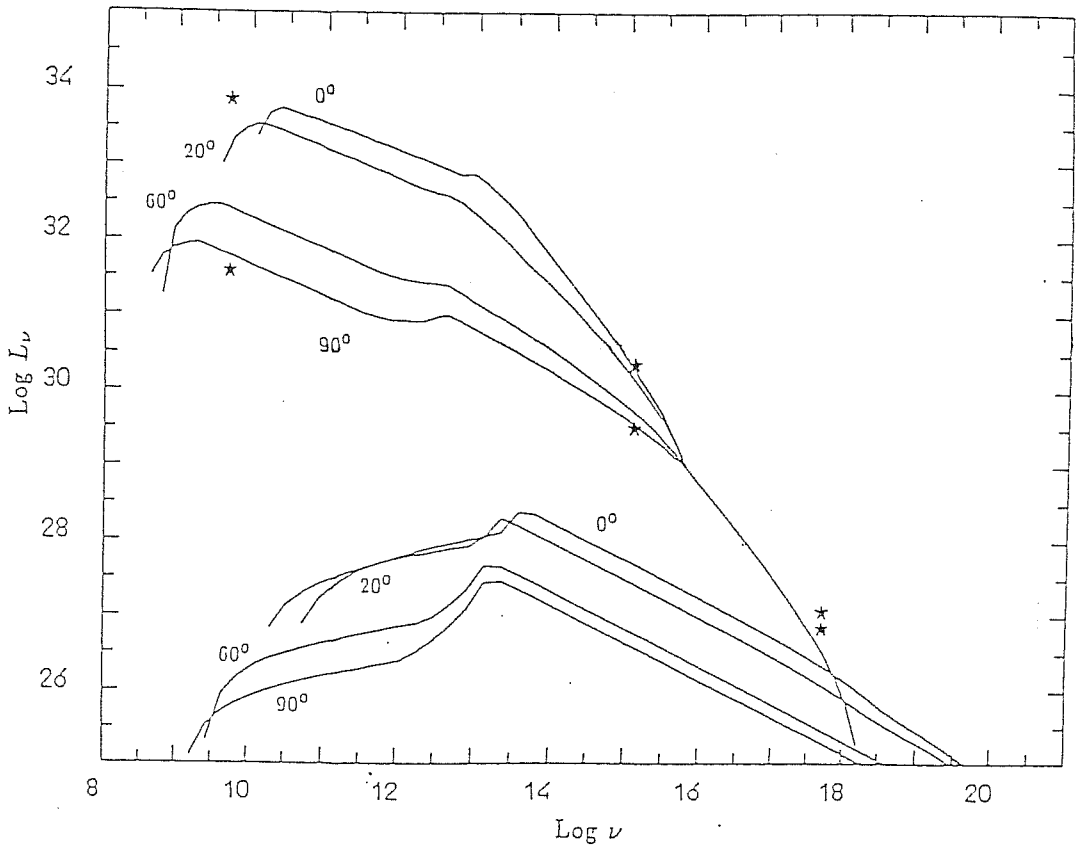

Fig. 2.9 Spectral energy distribution of SSC emission from a jet, in which the Doppler factor of the emitted radiation increases with increasing distance from the core (acceleration), at different observational angles. We do not enter in details. Note only that the model is able to reproduce the same (almost unbeamed) X–ray luminosities and different spectral indices and radio (beamed) luminosities for different observational angles. The two distribution correspond to the averaged luminosities in the two bands of X–ray selected BL Lac and radio selected ones, whose values are reported as stars in the figure. From Ghisellini & Maraschi (1989).

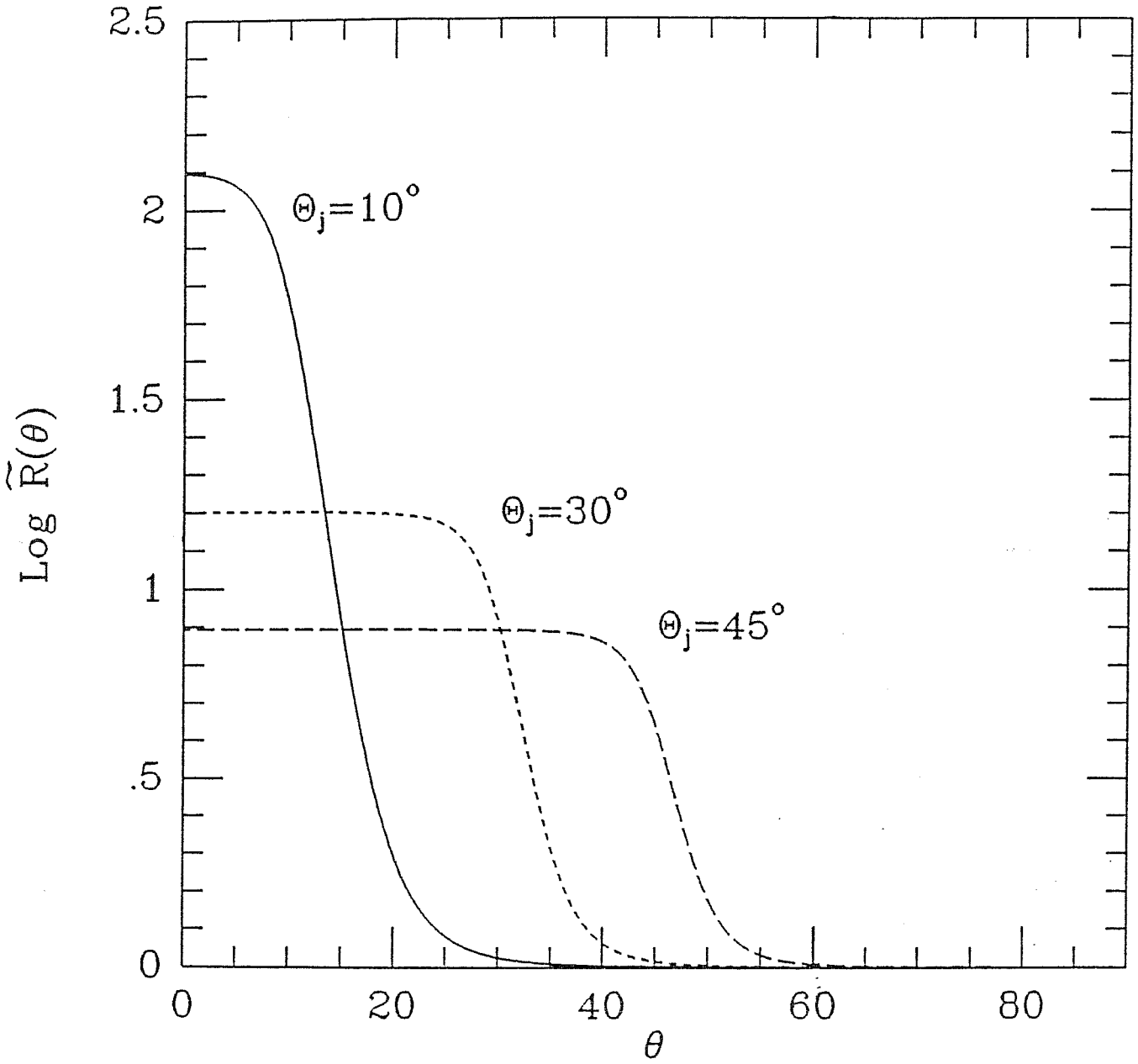

Fig. 2.10 Intensity distribution as a function of the angle between the line of sight and the jet axis, represented by the function $\tilde{R}(\theta)$ defined as $L = \tilde{R}(\theta)\ell$ where L is the beamed and ℓ the parent luminosities, respectively. The intensity is almost constant for angle smaller than the angle of the conical jet, and decreases outside, because the dominant emission is from the cone along the line of sight with aperture angle $\simeq 1/\gamma$, for $1/\gamma$ smaller than the jet angle. Comparing it with Fig. 1.10, it can be seen that for the same Lorentz factor, the sources observed at very small angles would have both X–ray and radio emission enhanced, while at greater angle, only the X–ray luminosity is amplified (see text), according to the model of Maraschi, Celotti & Ghisellini (1991). The curves reported are for $f = 0.1$ and $p = 4$.

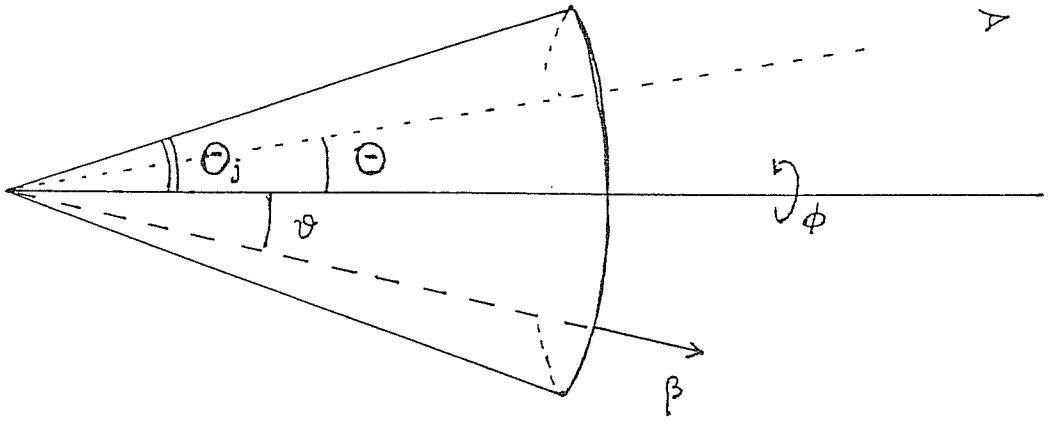

Fig. 2.11 Schematic representation of the coordinate system for the model described in §2.4.c. Θ, Θ_j, θ, ϕ are the angles between the jet axis and the line of sight, the aperture angle of the jet, the angular coordinate from the axis which determines each element of fluid and the azimuthal coordinate around the axis.

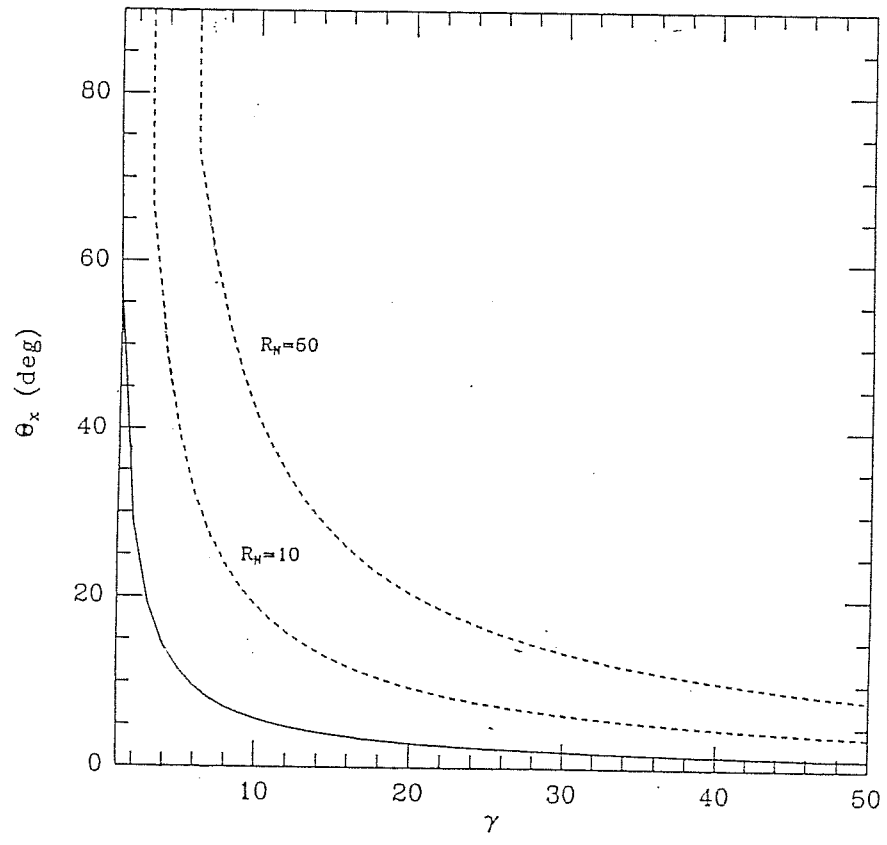

Fig. 2.12 The figure illustrates the limits imposed on the parameter Θ_X of the model described in §2.4.c., *i.e.* the angle of the jet emitting the high frequency radiation. It must be greater than $1/\gamma$ (continuous line), and as reference values the two dashed curves, which correspond to $R_N = 10, 50$ (the number ratio of X–ray selected and radio selected BL Lacs) are reported. The value of R_N is suggested to be > 10 and possibly > 50 (see text).

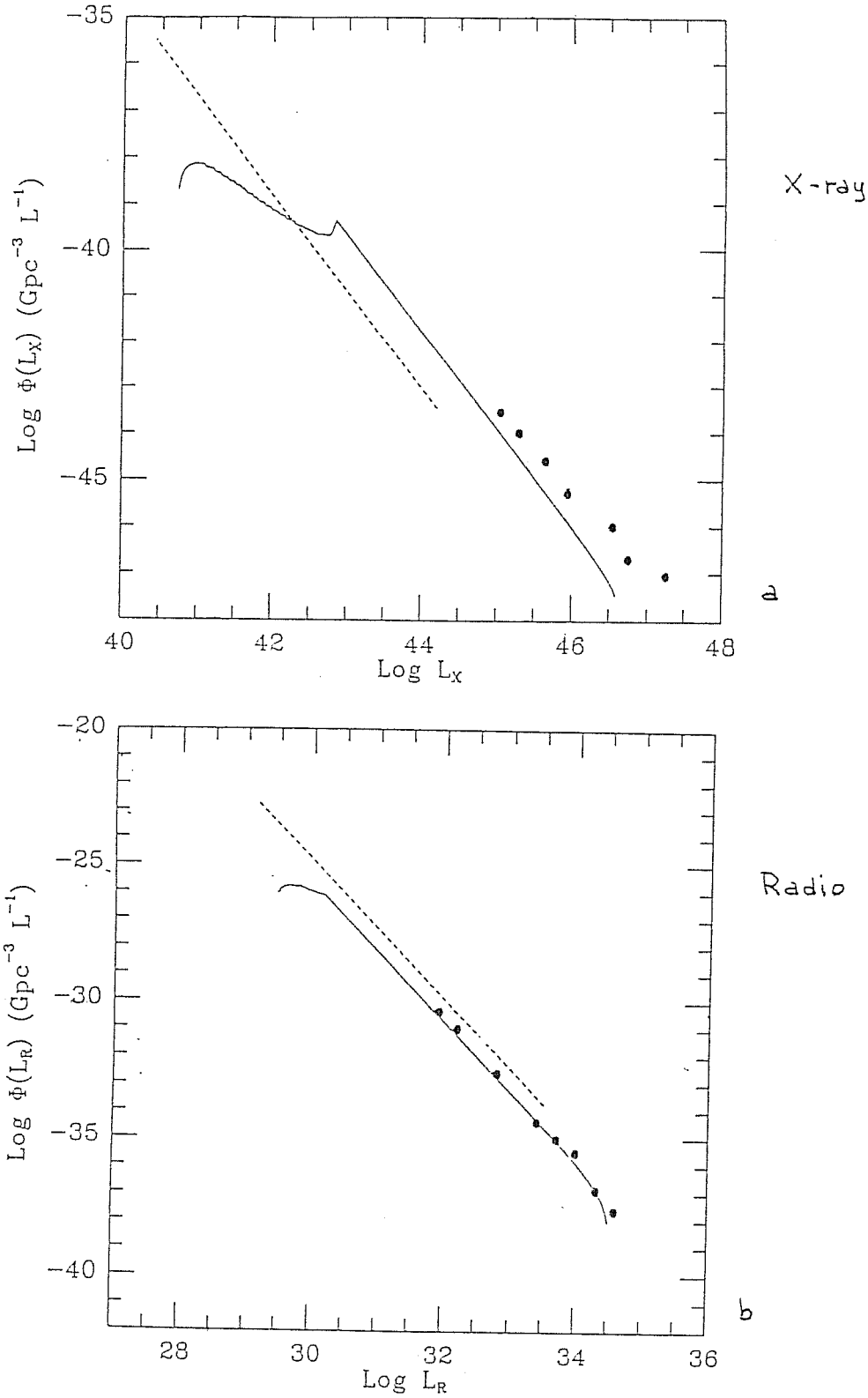

Fig. 2.13a,b The two figures reproduce the X–ray and radio differential luminosity functions according to the model described in §2.4.c. The dashed lines represent the parent population (FRI) luminosity functions, from Padovani & Urry (1990) and Urry, Padovani & Stickel (1991).

The BL Lac luminosity functions are represented by the continuous lines. The peak appearing in the X–ray one is due to the fact that many objects are observed in the large cone of the X–ray emitting region, and they have substantially the same luminosity. The points are from the luminosity function of BL Lac objects computed by Morris *et al.* (1991) (X–ray band) and Stickel *et al.* (1991) (radio band). The Morris *et al.* points are however calculated assuming luminosity deevolution for th objects, with a law $L(z) = L(z = 0)(1 + z)^{-7}$. If it is calculated with no evolution (as from the model) the points must shift toward lower luminosities of the same factor. The parameters correspond to the second set of table 2.3 (see §2.4.c).

Chapter 3. Primary or reprocessed radiation?

The attempt of this chapter is to present suggestions that a considerable fraction of the observed radiation in AGN (excluding at most BL Lac objects) can be due to reprocessing of radiation produced in the inner compact region, the emission of which is directly observed in the X–ray band as synchrotron or SSC radiation.

3.1 Primary X–ray radiation

With the adjective 'primary', we simply refer to the radiative process which mainly operates in the 'central', compact region of AGN and possibly transforms accretion or rotational energy into radiation.

At first we show that the assumption that X–ray radiation is produced as Compton scattering from relativistic electrons imply that the X–ray emitting region is strongly dominated by radiation energy, while magnetic energy is well below the equipartition value.

As already described in §1.4.d the standard SSC model from a homogeneous source allows the determination of the magnetic field and electron density, when radio self–absorption frequency, flux and dimension are known. This method has been applied up to now to determine the above physical parameters in the radio emitting regions.

We instead (Celotti, Ghisellini & Fabian, 1991a, Appendix D; Celotti, Ghisellini & Fabian 1991b) apply substantially the same model to infer upper limits to the magnetic field intensity in the compact X–ray emitting region, which however does not necessary coincide with the 'central region'. One possibility is in fact that emission is produced in localized rapid events due to impulsive release of energy,

maybe stored as magnetic energy, *e.g.* during reconnection of field lines. It is suggested by the fact that increasing time resolution shorter variability timescales have been observed.

We assume that X–rays are due to Comptonization from a non–thermal distribution of electrons of soft 'blue bump' photons, the maximum intensity of which is inferred from a maximum temperature blackbody, consistent with the UV and soft X–ray data and produced in the same volume. This allows to determine a minimum density of electrons required in order to emit the observed X–ray flux. Their distribution has a slope p determined from observations of the X–ray spectrum ($p = 2\alpha_x + 1$).

Upper limits on the X–ray region dimensions are estimated from X–ray variability timescales.

Consequently, having determined dimension and electron density, for a given magnetic field and maximum Lorentz factor γ_{max} of the electron distribution, the whole SSC spectrum is determined.

For each pair ($B - \gamma_{max}$) we compare the predicted spectrum with the spectra of five sources, belonging to different classes of AGN (see Figs. 1 of Appendix D): two Seyfert galaxies, NGC 4051 and NGC 6814, the OVV 3C279, the radio quiet quasars H1821+643 and the radio loud quasar 3C273. Requiring that the predicted SSC spectra do not exceed their flux at any observed frequency, upper limits on B for each source are deduced from the optically thin part of the spectra. The γ_{max} dependence enters because it determines which radiation mechanism mainly emits at the considered frequency.

Complications due to self–absorbed flux, inversely proportional to B, and higher Compton orders are considered. We also examine the dependence of our results on various parameters, like the source dimensions, the effects of varying the assumed unobserved blackbody spectrum (*e.g.* through a dilution factor), the observed X–ray states for non–simultaneous observations, the slope of the intrinsic particle distribution as would be the case in presence of a X–ray reflection component, the presence of beaming and the possibility that the induced Compton modifies the observed spectra allowing an escape to our conclusions (for details see Appendix D).

Results are presented in Figs. 2 of this Appendix: they show the 'allowed' region

of the $B - \gamma_{max}$ two parameters plane, for which the SSC radiation flux does not exceed the observed one, together with the magnetic field values in equipartition with the radiation energy density. It can be seen that the allowed magnetic field intensity is well below the equipartition value in the relevant range of γ_{max} (a minimum value is set from the requirement that the blue bump photons can be scattered up to the maximum observed frequency), unless implausible values of dimensions are assumed.

The application of this model seems to imply three alternative conclusions: *i)* the assumed emission model is too simplified, in the intrinsic assumptions (homogeneity, particle distribution or geometry); *ii)* the X–ray radiation mechanism is not non–thermal Comptonization of blue bump photons, as instead often assumed; *iii)* the magnetic field in the X–ray emitting region is below the equipartition value.

In the last hypothesis two considerations therefore follow.

First, a low magnetic field (less than equipartition) poses problems both to magnetic confinement of jets and to acceleration particles models. In fact the latter imply that if acceleration is 'linear', *e.g.* due to electric fields, produced by a variation in the magnetic field, $dB/dt = c\,rot E$, then being R/c the minimum timescale in which B can vary on the source size, then $\Delta B/R \simeq E/R$ and thus to strongly accelerate particles a high magnetic field is required $\Delta B \sim B \sim E$.

Because the energy gain term does not depend on the particle energy, while the cooling term does, a maximum energy is obteinable. It is given by $c\,t_{cool} \simeq r_L$ (Cavaliere & Morrison 1980), where r_L is the Larmor radius, *i.e.* when $eBc \simeq (4/3)(\sigma_T c/mc^2)U\gamma^2$, where U is the magnetic or radiation energy density, depending which one dominates. This condition can be written also equating the radiative cooling timescale and the accelerating one. The more efficient acceleration is along the magnetic field lines (*i.e.* with $\vec{E} \cdot \vec{B} \neq 0$), because synchrotron losses are not effective; however Compton losses if important can give a comparable maximum energy. In the case of shock acceleration a maximum energy correspond to γ such that the synchrotron lifetime ($\propto \gamma^{-1}B^{-2}$) is comparable with the gyroperiod (γB^{-1}), and a high synchrotron frequency cutoff, which does not depend on B, at wavelength equal to the classical electron radius $e^2/m_e c^2$, *i.e.* $\simeq$ 70 MeV. However Compton scattering then can lead to energies up to $\gamma m_e c^2$. Note that proton can easily reach higher energies.

The alternative hypothesis is that X–rays are produced as synchrotron or SSC emission. However recent simultaneous variability observations of the Seyfert galaxy NGC 4051 (Done *et al.* 1990), as already mentioned in §1.3.c, showed variations of 50 % in X–rays while optical and IR fluxes varied less than 1% and 4% respectively, implying that the same electron population of electrons can not produce X–rays and lower frequencies in the same region.

We propose an alternative explanation: we find that an equipartition field would lead to a synchrotron self-Compton flux that exceeds the IR–X-ray spectrum at some point, or the variability limits in the optical/IR band, but IR/UV limits can then be overcome if there are small clouds or filaments at very high density along our line of sight, around or in the X–ray emitting region. In fact these can absorb at UV and lower frequencies, by the free-free process, the primary SSC radiation and allow an equipartition magnetic field to exist. Possibly they reemit the power at UV–EUV energies, contributing partly or totally to the blue bump radiation.

The density of these clouds must exceed $n \approx 2.6 \times 10^{18} T_5^{1/2} \nu_{15}^3 / N_{21} (1 - \exp(-h\nu_{15}/kT_5))\,\mathrm{cm}^{-3}$, where their temperature is $10^5 T_5$ K, column density $N_H = 10^{21} N_{21}\,\mathrm{cm}^{-2}$ and the absorption is up to frequency $\nu = 10^{15}\nu_{15}$ Hz. The observational column density constraints mean that the clouds must be small. The thermal pressure is high (see §3.2.b) and consistent with the pressure of the equipartition magnetic field: it means that they can be confined by the field itself.

3.2 Reprocessing

In this section, we show how such small dense clouds can arise and why they are a likely constituent of the 'central' emission region of AGN. Much of the primary radiation produced in AGN could be reprocessed and re-emitted at other wavelengths.

3.2.a Cold matter

At first we therefore summarize the observational evidences or suggestions for the presence of cold matter in AGN (for further details and references see §1.2.c and

§1.4.b), while in §3.2.b we examine with more details how this matter could be in the right conditions to absorb by free–free just up to UV frequencies (Celotti, Rees & Fabian, 1991).

Recent detailed studies of the X-ray spectra of many AGN have revealed the presence of much cold gas in the central engine. In the context of the X-ray emission region of AGN, cold means at temperatures of about 10^6 K or less, so that the matter is not fully ionized. The strong soft X-ray excess in the spectra are best interpreted as quasi-blackbody emission from gas at a few hundred thousand K, and the strong fluorescent iron emission line show that at least 2π sr of the sky viewed from the emission region is covered by gas with iron more neutral than about FeXVII. This gas is also revealed by the presence of a strong reflection component in the hard X-ray spectrum (above 15 keV). That the cold gas does occur in the central engine is shown by variability of all the above spectral components.

The density of this gas, n, is not known, although photoionization arguments suggest that it must have $n > 10^{15}\,\mathrm{cm}^{-3}$ (Ferland & Rees 1988). Its geometry is also uncertain, although a disk-like structure, with the X-rays emitted from above and below the disk is plausible. The lack of any obvious soft X-ray absorption shows that our line of sight is obscured by a column density of less than about $10^{21}\,\mathrm{cm}^{-2}$ at solar abundances. It is possible (and in some cases inferred) that a warm absorber, consisting of gas which is almost fully photoionized and of column density $10^{23}\,\mathrm{cm}^{-2}$, does occur along our line of sight.

The idea that there could be clouds hotter, denser and closer to the central engine than the clouds of the BLR, has been already suggested by Rees (1984) at least for two reasons: the first (not well confirmed at the epoch) is the presence of a broad absorbtion feature in the X–ray spectrum of PKS 2155–304 (see §1.1.b) (Canizares & Kruper 1984; Krolik *et al.* 1985), which could be due to O VIII with outflow velocity up to $2.5 - 5 \times 10^9$ cm s^{-1}, maybe in a clumpy wind at $R < 10^{16}$ cm. Furthermore he suggests that blue bump could be emitted by small clouds with $n > 10^{13}$ cm^{-3} at similar distances.

The thermal and ionization equilibrium of clouds in a non–thermal radiation flux of a compact object, have been carefully studied in order to understand the

physical conditions of clouds of the BLR. From the first suggestion (see mainly Krolik, McKee & Tarter 1981) that these clouds could be in pressure equilibrium with a hotter medium at $T \simeq 10^7$ K, in a two phase equilibrium (the change of phase corresponding to comparable radiation and gas energy densities), many studies developed. The equilibrium exists for a narrow range of ionization parameter values, and for a continuum from the central source with spectral index $\alpha \lesssim 2$ (Guilbert, Fabian & McCray 1983). The main processes involved are Compton and photoelectric heating and Compton and bremsstrahlung cooling.

A basic paper on the subject is due to Ferland & Rees (1988). As a consequence of the inferred presence of thermal matter in the inner region ($< 10^{15}$ cm) of AGN, they discuss the equilibrium for clouds in very intense radiation fields, closer than the BLR clouds. The important aspect of this detailed study of the thermal and ionization mechanism involved (including collisional and stimulated processes), is that it deals with unexplored physical conditions (densities up to 10^{17} cm^{-3}). These clouds could attenuate and harden the soft–medium X–ray continuum (mainly due to carbon and oxygen K shells opacities) and produce a thermal emission in the IR–optical band and possibly broad lines. The high densities $n > 10^{14}$ cm^{-3} are required in order to keep the clouds cold despite of the strong radiation flux.

The important result we are interested in is that the clouds can reach practically a thermodynamical equilibrium with a source function almost identical to the Planck spectrum (not exactly because the continuum radiation is non-thermal), for densities greater than 10^{17-18} cm^{-3} (see their Figs. 4a and 7, and Fig. 1.6). At low densities $n \simeq 10^5$ cm^{-3} the plasma is totally ionized and the equilibrium temperature is the Compton one; at intermediate densities $n \simeq 10^{10}$ cm^{-3} three-fourth of the heating and cooling is due to Compton scattering and the remaining is due to free–free and free-bound processes. At $n \simeq 10^{15}$ cm^{-3} the temperature balance is between free–free (one–third) and free–bound processes. The lines (*e.g.* Lyα) are broadened by a strong Doppler effect and by Compton scattering, maybe producing large wings.

The densities we require are above $n \simeq 10^{18}$ cm^{-3} and this would allow us to neglect all the line emission and free-bound processes and simply consider our clouds in thermodynamical equilibrium, with a blackbody emission at the 'equivalent' temperature of the non–thermal radiation.

Then they consider the equilibrium of clouds or filaments embedded in the central region, with a non–thermal continuum with equivalent blackbody temperature of $\simeq 5 \times 10^4$ K. The confining material must have a pressure $> 2 \times 10^6$ erg cm^{-3}.

The observational suggestions that the BLR is extended (see §1.2.e), or closer than that predicted by the 'standard model', has been analyzed by many authors. Kazanas (1989) suggested the hypothesis that the clouds are in reality stratified, *i.e.* not homogeneous, maybe winds from evolved stars. Rees, Netzer & Ferland (1989) explored the effect of a clouds distribution in density and distance, parametrizing the radial dependence of pressure, and integrating to find the relative contributions of matter at different distances. They found that the covering factor and emission are predominantly due to clouds at large distances. The high density ($n \simeq 10^{13}$ cm^{-3}) of the inner clouds, however implies that the free–free is an important heating mechanism. The idea that clouds are indeed a wind or a corona has been considered also by Ferland & Persson (1989) who deduced, from the study of CaII emission, a large column density for clouds close to the 'core', the pressure of which is dominated by radiation. They also have to include the free–free heating process at low frequencies ($n \simeq 10^{9-10}$ cm^{-3}) in their computations, important mainly for high ionization parameter, *i.e.* when photoelectrical heating is less relevant. By the way with their computations thermodynamical equilibrium is reached at densities comparable to that deduced in Ferland & Rees (1988).

The relevant points we wanted to stress with the previous short review is that the presence of relatively cold matter close or in the central region of AGN has been suggested also by line studies. However ranges of density well below the values we require have been considered. Anyway at our extreme conditions thermodynamical equilibrium is reached.

From an 'observational' point of view the importance of free–free emission has been envisaged in some recent papers. We mention only two of them. Barvainis (1990) analizes the IR-optical spectrum of 36 radio quiet quasars, and claims that in order to fit the spectra three components are sufficient: one due to warm dust in the inner kpc, emitting in the IR; the stellar and cold dust emission of the host galaxy, important in

low luminosity objects; a flat $\alpha \simeq 0.2$ component in the optical, extending from UV to 1 μm. This spectral index has been already found from Neugebauer *et al.* (1987) for high luminous objects where the galaxy component does not contribute. Barvainis (1990) attributes this last component to free–free emission. The spectral fits of *e.g.* Malkan (1983) gave a flat optical spectrum just as a right sum of a non–thermal IR power–law and the blue bump disc emission. Barvainis (1990) also attributes the soft excess to the free–free component.

Suggestion of the presence of optically thin matter very close to the central region has been suggested by Ferland, Korista & Peterson (1990), on the basis of the observation of a variable continuum and core line emission in the Seyfert galaxy Mkn 590, while the broad wings of the hydrogen lines manteined constant luminosity. They propose that the wings are produced in a Very Broad Line Region, whose luminosity can account for the UV continuum, reprocessing 50–500 eV photons into the blue bump. They also identify this matter with the warm absorber (with $T \simeq 10^5$ K) suggested from X–ray observations (see §1.2.c) and with the plasma also responsible for radio free–free emission observed in the radio quiet quasar PG 1634+706 (Antonucci & Barvainis 1988). It should be partially ionized gas, as suggested by low extinction at $\simeq 1230$ Å in NGC 4151 and the fact that it does not respond to the central source variations. The matter should have a very low filling factor but high $\simeq 1$ covering factor.

From a 'theoretical' point of view some articles should be quoted, which mention or sustain the presence of cold matter.

The first suggestions can be attributed to Guilbert, Fabian & Rees (1983), who strongly claim the importance of pair reprocessing for the observed spectrum of rapidly varying sources (compact objects), and the consequent presence of large optical depth of the pairs cooled at the Compton equilibrium temperature. This matter also contributes to modify the spectrum, Comptonizing the radiation and also trapping it inside the source.

A more detailed analysis of the effects of cold matter in AGN is developed in Guilbert & Rees (1988). We report the suggestions and results contained in this paper, because it is a fundamental article on the importance of cold matter. The

gas should be present unless the source is well below the Eddington limit and very efficient. In fact, as seen in §1.4.b, an optical depth greater than one is due to accreting matter, in a maximally efficient source, with $v_{ff} = v_{in}$ and $L \gtrsim 0.1 L_E$. Furthermore there is the contribution to the Thomson optical depth from cooled pairs in compact sources.

In order to avoid cold matter a very efficient accelerator must operate, and only recently heated particles would be relativistic as implied by the very short cooling timescales (see §1.4.a). The minimum temperature of this matter would be given by the equivalent blackbody temperature of the radiation energy which the plasma absorbs. If gas is sufficiently dense and optically thick the emergent spectrum is thermal, but in order to stay cold at T_{bb} an efficient cooling mechanism must exist. Bremsstrahlung emission could do the job only if matter is dense enough (due to its low efficiency): more precisely the matter should have a density n greater than the mean density $< n >$ of the accreting material up to a factor $n/ < n > \lesssim m_p c^2 (R_s/R)(1/kT_{bb})$ and be confined by hot external gas (or magnetic field with a pressure equivalent to an hot medium at temperature T_v and density $< n >$).

The amount of reprocessing depends obviously on the covering and filling factors of this matter, which can be clumped in small clouds. The optical depth is then $\simeq C\tau_T$ where C is the covering factor and τ_T the optical depth of the single cloud.

Photoelectric absorption affects soft–medium X–ray band, and Comptonization produces features in the 100 keV–1 Mev region. In particular Compton scattering produce a spectral break at energy $\simeq m_e c^2/\tau_T^2$, where the downscattering is effective $(4kT/m_e c^2)\tau_T^2 = 1$ (see §1.4.a) and the spectrum steepens at higher frequencies. When Klein–Nishina cross section is effective, the spectrum is not significantly affected. Furthermore if the gas is cold the K shells of elements are filled and significant photoelectric absorption is expected.

Scattering depths greater than 4 are required in order to convert more than 50% of non–thermal radiation into heat, reradiated at kT_{bb}.

At lower frequencies Compton recoil is negligible, but at energies lower than 10 keV, the effective cross section due to free–free and photoelectric processes, is greater than σ_T. If the brightness temperature of radiation in IR exceeds T_{bb} the radiation

heats the cold matter. This material can also provide the soft X–ray excess.

Variability is predicted to be simultaneous at all frequencies (if thermal response is fast) except at the energies which are Compton downscattered (10 keV–1 Mev), which lag the primary source variations on timescale determined by the mean free path $1/n\sigma_T$.

The cold matter could be either more distant from us than the central source, so that we see the primary and reflected radiation, or between the source and us, and their covering factor determines the percentage of reprocessing. If it is substantial an X–ray hump is predicted (see §1.2.c). The geometry could be in principle inferred from the amount of non–thermal radiation observed in the IR–optical and absorbed soft X–ray bands. Brightness temperatures greater than T_{bb} in the optical would exclude thermal reprocessing.

Guilbert & Rees (1988) underline the fact that the presence of a primary thermal radiation is not required in order to produce the blue bump component, which can be due to reprocessing, like the dust features, line emission etc. The intrinsic spectrum itself can however contain various features. The sources whose spectrum does not show thermal features require that: or the power is rotational energy extracted from the hole, without accreting matter; or the observed luminosity is relativistically amplified in a beamed outflow; or non–thermal heating prevent the thermal component to cool.

The alternative of non–thermal reprocessing or/and thermal gravitational energy responsible for the blue bump emission is also analyzed by Lightman & White (1988). In both cases a covering factor about 0.5 and an optical depth $\tau_T \gtrsim 10$ are inferred: in the first case in order to reprocess about the same luminosity observed in X–rays, and in the second one because the optically thick medium must be close and probably has an area comparable to the non–thermal source. The fact that non–thermal emission above $\sim$ 10 keV is observed, implies that the non–thermal emission and the reprocessing matter should lie close but not mixed together, maybe again in a cold clouds geometry. They compute the detailed X–ray emergent spectrum with the predicted hump.

Collin–Souffrin (1991) strongly argue against the cold clouds reprocessing model, which degrades high primary energy. Her arguments are based on recent observations

of no time lag between the UV continuum and the line emission (see §1.2.e). An interesting observation is the fact that the correlation between the UV continuum and lines like C^{+3}, which is ionized by photons at 100 Å, together with the observation of one simultaneous variation in UV and X–rays for NGC 4151, reported by Perola *et al.* (1986), indicate that X–ray and UV varies simultaneously. However the argument against the clouds model is based on the fact that in order to reprocess the UV radiation, the clouds must be very thick, implying an absorbtion feature in X–rays up to 10 keV and a Lyman edge in absorbtion or emission, and neither of the two features has been observed. Her calculations are however in the hypothesis of column densities as large as $N_H \simeq 10^{21-25}$ cm^{-2}. But, as we show below, if the density is sufficiently high, the clouds can reach the thermal equilibrium and emit like a blackbody, as calculated by Ferland & Rees (1988), but with a column density $N_H < 10^{21}$ cm^{-2}, such that the X–ray spectrum is not affected by crossing them.

As already mentioned the idea of a strong magnetic field confining cold matter has been proposed by Rees (1987) in relation with the BLR clouds. In fact detailed observations of the shape of the continuum spectra showed that the radiation can not keep the hot medium temperature above $T \simeq 10^7$ K, but this value is not enough to confine clouds. It would be necessary to require another heating process or unlikely high densities (*i.e.* opacities). Moreover the internal sound speed of the clouds is less than the velocity deduced from the width of the lines, implying stability problems.

3.2.b Small clouds

Gas at still higher density than that described in §3.2.a and required by the soft X-rays absorbtion may also exist in the X-ray emission region. Indeed it seems required if the region contains a magnetic field which is in equipartition with the radiation field, as expected if the field is responsible for accelerating the radiating electrons.

We now present a picture and constraints on the physical conditions of cold and dense clouds (or filaments). Part of these considerations are the content of a paper in preparation (Celotti, Rees & Fabian 1991).

Macrophysics

For simplicity in the following we refer to r as the radius of a cross sectional circular area under which the central source sees each cloud, and to Δr as its thickness. If not specified the clouds are supposed to be external to the central region, at a distance R from it.

The clouds are assumed to be in pressure equilibrium with the magnetic field, which confines them. In fact the thermal confinement (in the two phase model) could work at BLR distances, but not surely closer to the compact region, where the virial temperature exceeds also the Compton temperature of the hot medium. The field can be transported outside the central region as Poynting flux.

Therefore a first requirement on the physical parameters of the clouds is the balance between gas and magnetic field pressures, that, if the field is not within the clouds, can be written as

$$3\,n\,k\,T = \frac{B^2}{8\pi} \tag{3.1}$$

Estimations of the magnetic field intensity can be obtained requiring equipartition with radiation energy density, whose intensity can be quantified by an equivalent blackbody temperature $T_{bb} = (L/4\pi R^2 a)^{1/4}$, which can be written as as

$$B_{eq} = 4.5 \times 10^{-7} T_{bb}^2 \qquad \text{G} \tag{3.2}$$

The magnetic field strength in the environment of AGN can be also estimated requiring equipartition with the kinetic energy (*i.e.* $B^2/8\pi \simeq nkT_v$) in an accretion flow, or in a corona above an accretion disc. This gives (Rees 1987)

$$B_{eq} \simeq 7 \times 10^5 \eta^{-1} \left(\frac{L}{L_E}\right)^{1/2} \left(\frac{R_s}{R}\right)^{5/4} \frac{1}{M_6^{1/2}} \left(\frac{v_{ff}}{v_{in}}\right)^{1/2} \qquad \text{G} \tag{3.3}$$

$$\simeq 2.4 \times 10^4 \frac{1}{\eta_{0.1}} \left(\frac{L_{43}}{L_E}\right)^{1/2} \left(\frac{R_s}{R_{13}}\right)^{5/4} \frac{1}{M_6^{1/2}} \left(\frac{v_{ff}}{v_{in}}\right)^{1/2} \qquad \text{G}$$

A reasonable approximation can be $v_{ff} > v_{in}$, because a strong magnetic field can itself provide viscosity. $M = 10^6 M_6\, M_\odot$ gr, $R = 10^{13} R_{13}$ cm, $L = 10^{43} L_{43}$ erg s^{-1}.

In the case of a outflowing wind, carrying a luminosity L_w powered by extraction of spin energy of the black hole together with Poynting flux, the equipartition field is

$$B_{eq} \simeq 7 \times 10^5 \left(\frac{L}{L_E}\frac{L_w}{L}\right)^{1/2} \left(\frac{R_s}{R}\right) \frac{1}{M_6^{1/2}} \left(\frac{c}{v_w}\right)^{1/2} \quad \text{G} \qquad (3.4)$$

$$\simeq 2 \times 10^4 \left(\frac{L}{L_E}\frac{L_w}{L}\right)^{1/2} \left(\frac{R_s}{R_{13}}\right) \frac{1}{M_6^{1/2}} \left(\frac{c}{v_w}\right)^{1/2} \quad \text{G}$$

A solid angle factor must be added in the case of non isotropic emission, *e.g.* in a jet.

The matter could be in a corona (pervaded by loops of magnetic field anchored in a disc) or a wind or jet outflow with a mainly toroidal field. The clouds can be anchored in the magnetic field and this implies that they do not orbit at the Keplerian velocity $v_k \simeq \sqrt{GM/R} \simeq 0.12\, c(M_6/R_{13})^{1/2}$.

A minimum dynamical timescale is obviously given by $\Delta r/c$. The sound and Alfven timescales, assumed equal, are given by

$$t_s = t_A \simeq \frac{\Delta r}{\sqrt{p/\rho}} \simeq \frac{\Delta r}{c}\frac{1}{\sqrt{\Theta}} \simeq 1.9 \times 10^6 \frac{\Delta r}{c}\frac{1}{\sqrt{T}} \quad \text{s} \qquad (3.5)$$

As far as radiative timescales are concerned, we consider bremsstrahlung, synchrotron and Compton cooling timescales.

$$t_{br} \simeq 1.8 \times 10^{11} \frac{T^{1/2}}{n} \quad \text{s} \qquad (3.6)$$

$$t_C \simeq \frac{3nkT}{(4kTc\sigma_T n U_R/m_e c^2)} \simeq \frac{3 \times 10^7}{U_R} \simeq \frac{4 \times 10^{21}}{T_{bb}^4} \quad \text{s} \qquad (3.7)$$

where the last equality is true in the assumption of blackbody emission, $U_R = aT^4$ erg cm^{-3}. We estimated the cyclotron thermal emission as $m_e c^2 \dot{\gamma}\, n = (4/3)\sigma_T c \beta^2 \gamma^2 n U_B \sim (4/3)\sigma_T v^2 n U_B/c$ and therefore

$$t_{cyc} \simeq \frac{3nkTc^2}{(4/3)\sigma_T c v^2 n U_B} \simeq \frac{3.7 \times 10^{22}}{nT} \quad \text{s} \qquad (3.8)$$

The requirements that should be satisfied are that $t_C, t_{cyc} < t_{br}$, such that the thermal equilibrium of the clouds is due to bremsstrahlung absorption and emission.

In order to estimate the equilibrium temperature we consider the thermal behaviour (already described in §1.2.c, for a two phase medium) of a gas irradiated

by a non–thermal photon source. It can reach two stable conditions, one at the Compton temperature, typically for densities less than $n \lesssim 10^{14}$ cm^{-3} (or ionization parameters less than 10^3) and the other, for high densities, given by the equivalent blackbody temperature $U_R = aT_{bb}^4$ erg cm^{-3} .

A rough estimation of these two temperature can be done:

$$T_C = \frac{h < \nu >}{4k} \simeq \frac{h\nu_{max}}{k \ln(\nu_{max}/\nu_{min})} \simeq 1.3 \times 10^7 \qquad \text{K} \tag{3.9}$$

where we assumed a typical spectrum $\alpha = 1$, extending between 0.2 keV and 20 keV (and having ignored the cooling effects of soft blue bump photons, and other cooling processes). And

$$T_{bb} = \left(\frac{L}{4R^2 ca}\right)^{1/4} \simeq 9 \times 10^4 \left(\frac{L_{43}}{R_{13}^2}\right)^{1/4} \qquad \text{K} \tag{3.10}$$

where we used as reference values L_{43}, R_{13}, M_6. Magnetic field in equipartition with radiation energy density is therefore $B \simeq 3.6 \times 10^3 L_{43}^{1/2}/R_{13}$ G. In general (without magnetic fields) gas cooled at $T = T_{bb}$ can be supported against gravity only if radiation pressure exceeds gas pressure by a factor T_v/T_{bb}.

Therefore if our matter can be compressed at sufficiently high densities, it cools down to the blackbody temperature and can reach the pressure equilibrium with the magnetic field.

If matter reach the $T_{bb} \simeq 10^5$ K temperature, determined by the radiation field and its own emission properties, it is only partially ionized and, consequently, radiation with energy $> 13.6\, eV$ can be photoelectrically absorbed by hydrogen. More precisely, for cosmic abundances, the maximum equivalent hydrogen column density allowed by the spectra observed from typical variable AGN, is $N_{21} \sim 1$, with values of about 3 and 0.1 being measured by Turner & Pounds (1989) for NGC 6814 and NGC 4051, respectively.

We can now examine the requirement that the blobs are able to absorb through bremsstrahlung the radiation up to UV frequency. The absorption coefficient is given by

$$k_{br}(\nu) = 3.7 \times 10^8 \frac{n_e n_i}{T^{1/2}\nu^3}(1 - \mathrm{e}^{-h\nu/kT}) Z^2 g_{ff} \tag{3.11}$$

where $g_{ff}(\nu,T) \sim 1$ is the Gaunt factor (*e.g.* Rybicki & Lightman 1979), $Z \simeq 1$, and we assume $n_e \simeq n_i = n$. Therefore the optical depth $\tau_{br} = k_{br}\Delta r = 1$ at $\nu_{15} \simeq 1$, with $(1 - \mathrm{e}^{-h\nu/kT}) \simeq 1 - 0.4$ for $T = 10^{4-5}$ K and $N_H = n\,\Delta r$ cm^{-2}, requires

$$n > 2.3 \times 10^{18} \frac{T_5^{1/2}\nu_{15}^3}{N_{21}(1 - \mathrm{e}^{-h\nu_{15}/kT_5})} \tag{3.12}$$

This implies a gas pressure of about

$$p_{gas} \gtrsim 9.5 \times 10^7 \frac{T_5^{3/2}\nu_{15}}{N_{21}(1 - \mathrm{e}^{-h\nu_{15}/kT_5})} \quad \text{and} \quad B \gtrsim 4.9 \times 10^4 \frac{T_5^{3/4}\nu_{15}^{3/2}}{N_{21}^{1/2}(1 - \mathrm{e}^{-h\nu_{15}/kT_5})^{1/2}} \tag{3.13}$$

where the last inequality follows from pressure equilibrium of eq. (3.1).

The limit on the column density in turn implies that

$$\Delta r < \frac{10^{21}N_{21}}{n} = 4.3 \times 10^2 \frac{N_{21}}{T_5^{1/2}\nu_{15}^3} \tag{3.14}$$

i.e. the thickness Δr of the cold clouds must be such that its Thomson optical depth is lower than $\tau_T < 6.6 \times 10^{-4}$. Note that this limit does not applies to totally ionized or pair plasma.

The most plausible reason that the cloud size should be small is that this is the pressure scale height of such cold gas. If the gas is confined and supported above the X-ray source, but not penetrated by the magnetic field, then its thickness will be similar to that scale height. Much thicker (or thinner) regions require much lower (or higher) densities, which are not compatible with the pressure of the magnetic field.

The simplest maximum scale height is the gravitational one Δr_{grav} , *i.e.*

$$\nabla p_B = \rho g = n m_p \frac{GM}{R^2} \tag{3.15}$$

and consequently Δr_{grav} is of order $(T/T_v)R$, where T_v is the virial temperature at a distance R from the central mass, which has a Schwarzschild radius R_s and mass M_6

$$\Delta r_{grav} < 5.5 \times 10^{-13}(R/R_s)RT \simeq 10^7 T_5 M_6^{-1} R_{13}^2 \text{ cm} \tag{3.16}$$

in a static magnetosphere, where we assumed equilibrium pressure. This is about 4 orders of magnitude too large.

The argument breaks if the blob is in free fall. In fact if the clouds are unmagnetized they can drop almost in free–fall pushing aside the field ('melon seed', *e.g.* Rees 1987). The field between clouds tends toward a force free configuration, and the clouds would acquire a filamentary structure, along the field. The interface between clouds and the intercloud medium are sites for particles acceleration, which can irradiate the clouds. On the other hand if they are magnetized , the field intensity increases with compression, and the clouds in a wind tend to lag behind the flow, distorte the lines and are accelerated by the stretched field. Even if the field does not penetrate the plasma initially due to diffusion, it can do through instabilities, probably at speed lower than the sound one (Rees 1987). When this situation is reached, we self–consistently require that the short synchrotron cooling timescales are long enough that the plasma does not become field dominated (low β plasma).

Another possibility is that Alfven waves 'catapult' the clouds around in the case that magnetic field permeates the plasma, subjecting them to a high force and therefore reducing their scale height, which can not be however calculated.

The gas is more likely to be held above the source being expelled by radiation pressure than supported against falling under gravity. Note that instead self–gravity is completely negligible: in fact it is much less than the internal energy $GM_{cl}^2/\Delta r << 3nkT(4/3)\pi\Delta r^3$. This implies that a external confining mechanism is required in order that the clouds do not to disperse in a sound travel time (see above).

We can estimate the effect of radiation simply by noting that the free-free opacity of the clouds must be at least 1000 times higher than electron scattering opacity in order that a column density of $N_{21} \lesssim 1$ is sufficient to absorb most of the optical radiation. If the source is then operating near the Eddington limit, the radiation pressure due to free-free absorption then causes the effective gravity (now acting outward) on the clouds to be higher than the true gravity by a factor $\gtrsim 1000$, and the scale height to be smaller by the same factor. The absorption property of the clouds, which is what is required to account for the presence of an equipartition field, means that they are squeezed by the radiation and must be thin.

Quantitatively it can be seen writing the 'radiation' acceleration as

$$g_{rad} \simeq \int_{\nu_{min}}^{\nu_{br}} \frac{L(\nu)}{h\nu}\frac{h\nu}{c}d\nu \frac{2\pi r^2}{(4\pi R^2)(2\pi r^2 \Delta r m_p n)} \qquad (3.17)$$

and therefore

$$\frac{g_{rad}}{g} \simeq \frac{L(<\nu_{br})}{L_E}\frac{1}{\tau_T} \tag{3.18}$$

where ν_{br} is the absorption frequency for bremsstrahlung and, for simplicity, we assumed a step function for the dependence of the absorbtion coefficient on frequency. The effective gravity (directed outward) is therefore given by $g_{eff} = g_{rad} - g \simeq g_{rad}$.

Consequently the maximum thickness Δr is given by $\nabla p_B = \rho g_{eff}$, which gives $\Delta r \sim 6.6 \times 10^3$, about an order of magnitude greater than the upper dimension estimated in eq. (3.14).

Another possibility is that the formation and propagation of a shock wave can lead to the formation of thin shells of gas.

Our picture requires a covering factor of these small clouds of about one. Radiation pressure also explains why the covering fraction of the source provided by the clouds is about unity and why there are not many clouds along each line of sight. Cold gas from below the source (for which there is strong evidence, as reviewed) will be blown upwards by radiation pressure along tube of force and trapped at the points in the field where it is perpendicular to the radiation pressure. (There would be one such point on all closed field lines). If the field geometry is complicated (as expected if the magnetic field is attached to an accretion disk) then the entire solid angle may be covered by a surface. For an ordered field geometry, like in a dipole, these argument does not work.

Most of the radiation that supplies the pressure is absorbed in the first cloud along the line of sight (and reradiated as a quasi-blackbody in the UV), so clouds above the first one cannot exist.

Note that on the contrary the volume filling factor is very small. It is in fact of the order of $f \simeq 3\Delta r/R \simeq T/T_v \simeq 10^{-9}$.

Therefore the dense cold gas has a high covering fraction and a low filling factor. The situation may resemble that of solar prominence where small filaments of cool gas are supported above the surface by magnetic fields, except in this case the magnetic field is holding the clouds back against the radiation pressure.

If the clouds are *in* the X–ray emitting region, let us estimate the minimum values of the magnetic field and gas density in energy equipartition with the radiation density, $U_R = L/4\pi R^2 c$. L is the luminosity and $R = c\Delta t$ is now the size of the X-ray region, where Δt is the shortest timescale, $\sim 100 - 1000$ s, on which the luminosity changed by a factor of 2. Rewriting the luminosity in terms of the compactness parameter $\ell = (L/R)(\sigma_T/m_e c^3)$, which is typically about 100 in X-ray variable AGN (see Table 1 in Done & Fabian 1989, Fig. 1.8), we obtain

$$U_R = \frac{\ell}{\Delta t}\frac{m_e c}{4\pi\sigma_T} \approx 3.2\times 10^6 \frac{\ell}{\Delta t}\,\mathrm{erg\,cm^{-3}}\,. \tag{3.19}$$

Then $B \approx 9\times 10^3(\ell/\Delta t)^{1/2}$ G and $n \approx 7.7\times 10^{16}(\ell/\Delta t)^{1/2}T_5^{-1}$ cm^{-3} . Consequently, we derive again a small cloud size, $\Delta r < 1.3\times 10^4 N_{21}(\Delta t/\ell)^{1/2}T_5$ cm.

We note that in this situation also relativistic particles pressure could contribute, mainly through Coulomb collisions. For a spectrum $\alpha \simeq 1$ the relativistic pressure can be estimated $p_{rel} \simeq n_{rel} m_e c^2 < \gamma > \simeq n_{rel} m_e c^2 \gamma_{min} < 10^5\, n_{rel,10}\, \gamma_{min,10}$ erg cm^{-3}, where we assumed that only electrons have a non–thermal distribution, $\gamma_{min} \lesssim 10$, and $n_{rel} \lesssim 10^{10}$ cm^{-3}. In a strong magnetic field it is easy that such particles can interact with other particles crossing the cloud; however in order to be an important contribution their energy density should exceed the thermal one by an order of magnitude (Ferland & Rees 1988). This contribution therefore is unimportant with respect to the total pressure involved.

The advantage of this 'mixed' situation (*i.e.* the clouds inside the emitting region) is that a fraction of the low energy spectrum (less than optical–UV frequencies) of the primary radiation can be directly observed, and it is not required outer low density regions emitting non–thermal radiation.

We note however that outer regions at lower particle density and magnetic field can reproduce the observed low frequency non–thermal continuum. In particular the dependence of f^{-1} of the power spectrum suggests that it is possible that emitting regions are present on all scales.

We already mentioned that in the regime of densities considered the matter and radiation reach practically thermal equilibrium and the radiation absorbed from the clouds is therefore expected to be re–emitted as blackbody radiation at $T \simeq 10^5$ K.

Obviously the amount of radiation emitted depends on the absorbed one, *i.e.* on the flux of the primary, not observed, radiation. Consequently, if the X–ray emission is due to synchrotron extending to high energy, the peak of the blackbody should be on the extrapolation of this power law (with $\alpha \simeq 1$ from the reflection model), but if Compton emission contributes mainly to X–rays, the amount of absorbed radiation depends on the 'relativistic' optical depth (*i.e.* involving the density of relativistic electrons), as already seen in §1.4.d.

Microphysics

We now consider microphysical constraints on the plasma parameters. First of all the plasma below which the clouds can not emit is given by

$$\nu_p = \frac{1}{2\pi}\left(\frac{4\pi n e^2}{m_e}\right)^{1/2} \simeq 9 \times 10^3 n^{1/2} \qquad \text{Hz} \tag{3.20}$$

and the Razin frequency, below which synchrotron radiation can not be absorbed and emitted, because of the suppression of beaming in the presence of plasma is ν_p^2/ν_B

$$\nu_R \simeq 20\,\frac{n}{B} \qquad \text{Hz} \tag{3.21}$$

This constraint could be therefore relevant if cloud contains magnetic field too.

The Larmor radii, $r_L = mvc/eB$, for electron and protons are given respectively by

$$r_L^e \simeq 3.7 \times 10^{-2} T^{1/2} B^{-1} \simeq 3.7 \times 10^5 n^{-1/2} \qquad \text{cm}$$

$$r_L^p \simeq 1.6\, T^{1/2} B^{-1} \simeq 1.6 \times 10^7\, n^{-1/2} \qquad \text{cm} \tag{3.22}$$

where it is assumed that protons and electrons have the same temperature, and pressure equilibrium holds.

The Debye length is given by

$$\lambda_D = \left(\frac{kT}{4\pi n e^2}\right)^{1/2} \simeq 6.9\,\frac{T^{1/2}}{n^{1/2}} \qquad \text{cm} \tag{3.23}$$

while the interparticle distance is about

$$l \sim \frac{1}{n^{1/3}} \qquad \text{cm} \tag{3.24}$$

All these lengthscales are typically smaller than the smaller dimensions of the cold reprocessing matter structures, for the considered conditions and therefore, as long as $\lambda_D > l$, $\Delta r > r_L, l, \lambda_D$, the gas can be treated as a plasma.

Typical timescales are the energy exchange timescale between the same species and between electron and protons

$$t_{e,p} = \frac{6.3 \times 10^{-3} \sqrt{2} \pi^{3/2} m_e m_p}{e^4 n \ln \Lambda} \left(\frac{kT_e}{m_e} + \frac{kT_p}{m_p} \right)^{3/2} \simeq 4.2 \frac{T^{3/2}}{n}$$

$$\simeq \left(\frac{m_p}{m_e} \right)^{1/2} t_{p,p} \simeq \left(\frac{m_p}{m_e} \right) t_{e,e} \quad \text{s} \tag{3.25}$$

for $T_e = T_p$, and therefore the longer mean free path is approximately given by $\lambda_{e,p} \simeq v_e \, t_{e,p}$

$$\lambda_{e,p} \simeq 2.8 \times 10^6 \frac{T^2}{n} \quad \text{cm} \tag{3.26}$$

If $\Delta r > \lambda_{e,p}$ and $t_{cool} > t_{e,p}$ the assumption of one temperature thermal plasma is consistent.

A general argument in order to estimate a lower limit on the dimension Δr, is imposed by the requirement that the diffusion timescale of the magnetic field in the plasma is smaller than radiative timescales, such that the cloud can be confined by the magnetic field for a time sufficient to absorb and reemit. The argument is relevant if the mean free path due to collision is less or comparable to the Larmor radius and smaller than the size of the region, *i.e.* for a collision plasma. The plasma diffusion time is defined from the equation $\partial B/\partial t = (c/4\pi\sigma)\nabla^2 B + \nabla \times (u \times B)$, where σ is the plasma conductivity. The ratio of the two terms gives the relative importance of diffusion, and the corresponding timescale is given by

$$t_{diff} \simeq \Delta r^2 \frac{4\pi\sigma}{c} \simeq 1.6 \times 10^{-3} T^{3/2} \Delta r^2 \simeq 1.6 \times 10^{39} \frac{N_{21}^2 T^{3/2}}{n^2} \quad \text{s} \tag{3.27}$$

where we estimate $\sigma \simeq ne^2/m_e t_{coll} \simeq 3.6 \times 10^6 T^{3/2}$ (Boyd & Sanderson 1969).

The requirement therefore becomes that $t_{diff} > t_{br}$. A rough estimation of the particles which can 'accumulate' before diffusion can be done assuming that an Eddington kinetic luminosity escapes the source, and consequently, $n\Delta r \sim v \, n \, t_{diff} \sim 2 \times 10^{19} N_{21}^4 T_5 M_6 / \nu_{15} R_{13}^2$ cm^{-2}.

The micro and macrophysical limits described, are reported in Fig. 3.1. It can be seen that the 'allowed' region of the $n - T$ parameter space is relatively constrained and corresponds to the required values for the primary radiation reprocessing.

The limits corresponding to each line are labelled on the figure and explained in the caption. The limits which are not shown, and examined in the chapter, are satisfied in all the parameter space we are considering. It can be seen that the allowed region is rather delimited, around $T \simeq 10^5$ K and $n \simeq 10^{18}$ cm^{-3}. The line labelled $\nu = 0.1$ keV determines an indicative 'maximum' frequency which can be absorbed through bremsstrahlung without contradicting the observations.

We summarize the described picture: a central compact SSC emitting region is surrounded by a blanket of dense cold matter which reprocesses most of the radiation, and reemits it in the UV band, and possible by low density matter on larger scale which radiates as synchrotron the observed radio–optical continuum, required by the strong polarization observed at least in HPQs.

Further observations and analysis of existing data are required to determine stronger limits on measurements of the column density intrinsic to the quasi-power-law X-ray emission region. The free-free absorbing clouds do not necessarily have to cover all of the soft X-ray excess emitting region as well and so that must be separated in the spectrum, presumably by variability analysis. Further optical and UV studies of rapidly X-ray varying AGN will also help to determine the maximum free-free absorption frequency.

Slightly thicker regions of partially-ionized gas, the so-called warm absorber (see *e.g.* Nandra *et al.* 1991) in which $N_{21} \sim 100$ and $T_5 \sim 10 - 100$ are also a possible source of free-free absorption. The required density is then yet higher than that considered above by about an order of magnitude. It is then difficult to see why the gas has not cooled to an equilibrium temperature.

We have shown that the plausible scale height and column density of cold gas trapped by the equipartition magnetic field in the X-ray emission region of an AGN are consistent with both X-ray observations and the requirement that the optical/IR flux produced by the synchrotron self-Compton process is absorbed. Small quantities of cold gas thereby have an important influence on the observed spectrum.

Variability predictions are not well determined. Low energy (less than UV) can presumably vary when clouds along the line of sight are destroyed and primary radiation is observed. In this case a decrease in the variability amplitude with decreasing frequency is possible, because the free–free optical depth increases with decreasing frequency. It also implies that high energy variability is more frequent than low energy one. If the absorbing clouds are in the X–ray region timescales are presumably the same at all frequency. However if only part of the primary radiation is absorbed (presumably a larger fraction at lower frequencies) an energy dependent timescale indicator (as the doubling timescale) could be smaller at low frequency, where for the same global variation in the primary source, a smaller fraction of it is directly observable. Timescales also could increase with decreasing frequency if the absorbing medium is not homogeneous: low frequency radiation could be absorbed and emitted in a bigger region.

An interesting possibility concerning variability is that, other than cold clouds, an accretion disc is effectively present. In this hypothesis part of the re–emitted reprocessed radiation from the clouds can re–heat the disc and induce simultaneous variations in the radiation emitted in different regions of the accretion disc. Therefore also very short time lags between optical and UV radiation can be observed, solving the problem of delays required to transmit a perturbation through different parts of the disc (see §1.2.a).

If jets of plasma are ejected from a central source a possible effect is that in the region which they pass through cold blobs cannot form because a stronger radiation flux hits them and a completely non–thermal source is observed (BL Lacs?). With increasing angle of sight some clouds can be present the beaming decreases and a thermal component starts to appear. On the other hand in the galactic source SS433 there are some evidences of the presence of very dense cold matter inside the jets (see §4.1.a), with $T \simeq 10^4$ K.

Another possibility which would escape the column density (and therefore the dimension) constraints is that clouds are constituted by pair plasma. Pair plasma wind are not unlikely in surrounding region of AGN (see §1.4.a). If the requested conditions in order to free–free absorb can be reached (the main problem being the

reheating by annihilation photons), is the subject of a present study, the lines of which are described in §4.2.

Finally it should be noted that the presence of cold dense clouds close or in the primary emitting region, and the clouds of BLR and NLR are probably a continuum distribution on different scales and physical parameters like temperature and density, which surround the core region. The gas is presumably continuously supplied by outflows from it.

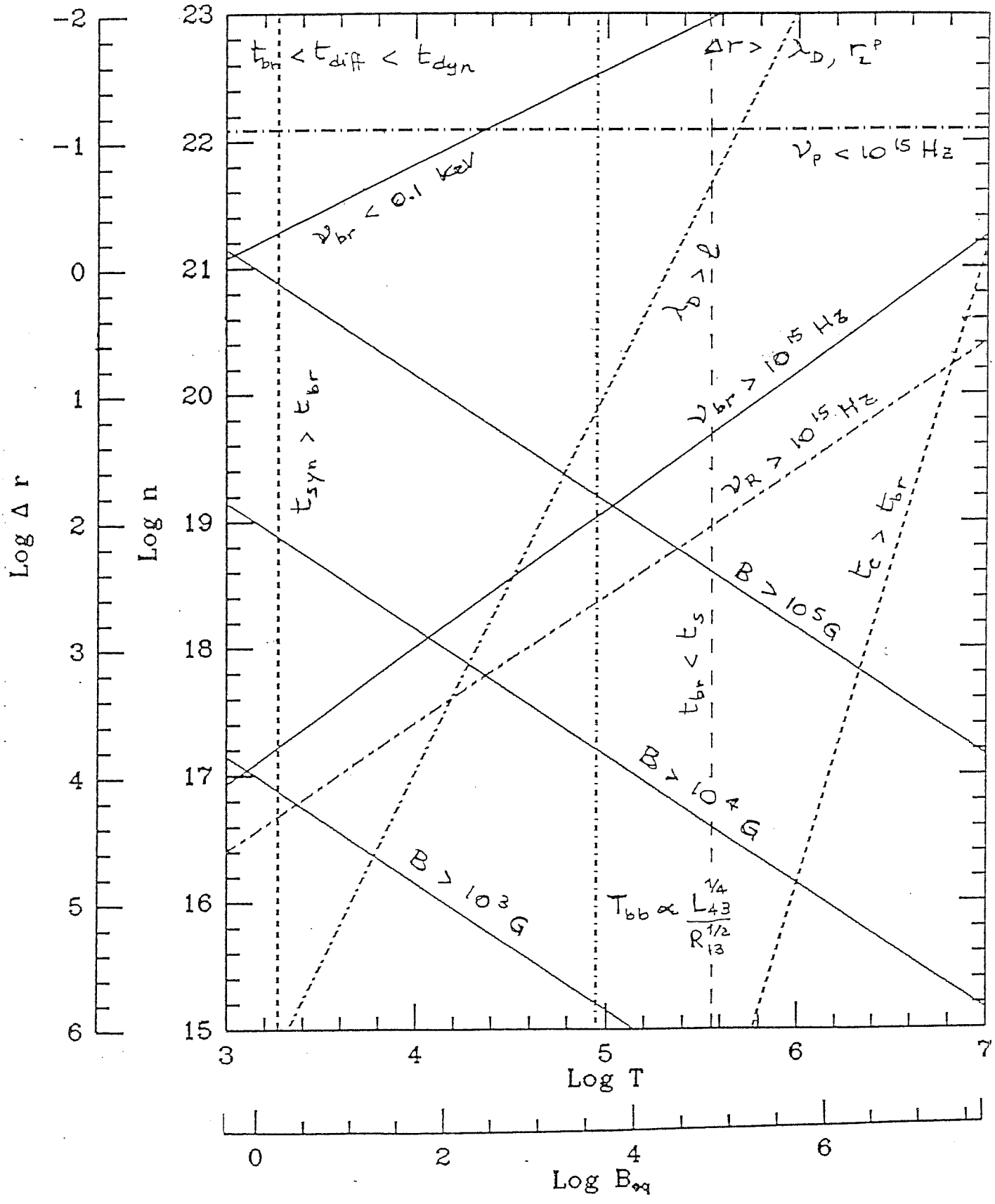
$t_{br} < t_{diff} < t_{dyn}$
$\Delta r > \lambda_D, r_L^p$
$\nu_p < 10^{15}$ Hz
$\nu_{br} < 0.1$ keV
$\lambda_D > \ell$
$t_{syn} > t_{br}$
$\nu_{br} > 10^{15}$ Hz
$\nu_R > 10^{15}$ Hz
$t_c > t_{br}$
$B > 10^5$ G
$t_{br} < t_s$
$B > 10^4$ G
$B > 10^3$ G
$T_{bb} \propto \frac{L_{43}^{1/4}}{R_{13}^{1/2}}$
Log Δ r
Log n
Log T
Log B_{eq}

Fig. 3.1 The (quite complicate) figure illustrates all the macro and microphysical limits, described in §3.2.b., on the temperature and density of the plasma which constitutes the small cold clouds, which absorb the primary radiation. The to assumed conditions are $N_{21} \simeq 1$ and the pressure equilibrium $p_{gas} = p_B$.

The axis B_{eq} (G) refers to value of the magnetic field in equipartition with the radiation energy density aT^4. The vertical axis Δr indicates the maximum dimension (in cm) of the cloud thickness allowed for each n (cm^{-3}), in order to satisfy the condition $N_{21} \simeq 1$ cm^{-2}. All the lines are labelled: the inequalities refer to the region of the parameter space on the side of the line where the label is located. $t_{br}, t_C, t_{syn}, t_{diff}, t_{dyn}$ indicate the bremsstrahlung, Compton and synchrotron cooling timescales, the diffusion time for the magnetic field to penetrate in the plasma, the dynamical timescale $\Delta r/c$. $\Delta r, \lambda_D, l, r_L^p$ are the cloud thickness, the Debye length, the interparticle mean distance and the proton Larmor radius. ν_p, ν_R, ν_{br} are the plasma, Razin frequencies and the bremsstrahlung self–absorption one (the last one must be less than 0.1 keV, because no effects of absorption are seen at X-ray frequencies. B is the magnetic field, T_{bb} the equivalent blackbody temperature of the central source radiation, L_{43} its luminosity and R_{13} its distance.

The allowed region of the parameter space is quite small, around $T \simeq 10^5$ K, $n \simeq 10^{18-19}$ cm^{-3}. Conditions at the top of the diagram or not shown are satisfied in the range of parameter considered in the figure.

Chapter 4. Some future perspectives

In this chapter we present some of the 'work in progress', or better to say the new projects that we want to explore in the next months. We present two ideas. The first one concerns the detailed study of the effects of bremsstrahlung absorbtion, while the second one the examination of the possibility that cold clouds are constituted by pair plasma, and more generally, the study of the time evolution of a contracting (or expanding) blob of pairs. In the two sections we present the reasons for such studies and their possible 'application' to the physics of AGN.

4.1 Bremsstrahlung radiation force

The first idea is to examine the effects of bremsstrahlung absorbtion. We saw in Chapter 3 that at high density and low temperature, matter can absorb a substantial fraction of the emitted luminosity of a source. The main effects are the transfer of energy to the absorbing plasma (heating), but also the transfer of linear momentum. In other words, we want to explore the acceleration effects of bremsstrahlung absorbtion. Radiation pressure acceleration has been already suggested as an effective mechanism in order to accelerate jets (optically thick radiation driven jets), but, as far as we know, nobody explored this particular radiation process.

Compton process (the first mechanism considered) can lead to acceleration, the limit of which is imposed by Compton drag, *i.e.* even if the radiation is beamed in the reference frame of the accelerated plasma, the aberration effect implies that photons can be seen as coming from the forward direction. Furthermore such photons are also blueshifted and therefore the more energetic photons tend to oppose the acceleration of the flow. Even if the matter has already reached a high velocity the drag reduces

it to a final Lorentz factor $\gamma \simeq 5$ (Phinney 1987). This saturation limit is reached when the power coming forward equals that from backward.

Synchrotron self–absorbed radiation pressure (Ghisellini *et al.* 1990) reduces these two effects, and results more effective in accelerating a magnetized blob. In fact, on one side the synchrotron cross section is frequency dependent and at low energies is much greater than σ_T (for $\nu < \nu_B(e/B\sigma_T)^{3/5}/\gamma$), Ghisellini *et al.* 1990), and on the other hand the blueshifted photons can be above the self–absorption frequency in the moving frame and consequently do not decelerate the plasma. There is no dependence on density and consequently the mechanism works for lower Thomson opacities (and less mass) than in the case of Compton acceleration, and luminosity of the central source $< L_E$.

Bremsstrahlung has two advantages on that, *i.e.* a larger cross section at low frequencies (obviously dependent on the physical consitions) and it does not require the presence of a magnetic field, which in the previous case was assumed to be frozen in the accelerating blob. On the contrary a high density is required, in order to get very efficient acceleration, which enhances the total inertia of the blob.

The bremsstrahlung acceleration deals with thermal distribution of particles, while Ghisellini *et al.* (1990) consider relativistic electrons. Synchrotron radiation acceleration can work for superluminal components. On the contrary for this situation strong limits on the thermal density from Faraday rotation arguments, suggest that bremsstrahlung can not be very effective.

Also $Ly\alpha$ absorbtion could produce acceleration. It however requires $T \lesssim 10^4$ K such that hydrogen is almost neutral (Shapiro, Milgrom & Rees 1986). In this last case the force can be written as $f = (dL/d\lambda)\sigma n_H/(4\pi R^2 c N_H^{tot})$ per unit volume, *i.e.* $F = (dL'/d\lambda')\int \sigma(\lambda')d\lambda' n_H/n_H^{tot}[\gamma(1-\beta)^2/(1+\beta)4\pi R^2 c]$, with $N_H^{tot} = volume \times n_H^{tot}$ the total number of hydrogen atoms and n_H the density of hydrogen atoms in the ground state.

The equation of motion for the accelerating blob is given, as for the previous processes by (Ghisellini *et al.* 1990; Abramowicz, Ellis & Lanza 1990):

$$\frac{dp_{\|}}{dt} = m_b c^2 \frac{d\gamma}{dR} = F'_{\|} - \frac{GMm_b}{R^2}\gamma \qquad (4.1)$$

where $F'_{\parallel}$ is the radiative force, measured in a frame comoving with the blob and parallel to the velocity. According to the Ghisellini *et al.* formalism, the primed quantities are measured in the the blob's frame. The mass of the blob is m_b and its volume is fixed, with radius r.

In order to determine $F'_{\parallel}$ the same procedure of the synchrotron case applies. Photons with frequency $\gamma\nu(1-\beta\cos\theta) < \nu'_{br}$ are absorbed, where θ is the angle between the photon direction and β. The radiation intensity from the central source is assumed to be $I(\nu) \propto \nu^{-\alpha}$ for $\nu_{min} < \nu < \nu_{max}$ and

$$F'_{\parallel} = \frac{\pi r^2}{c} 2\pi \int_0^{\theta'_1} \cos\theta' \sin\theta' d\theta' \int_{\nu'_{min}}^{min(\nu'_{max},\nu'_{br})} I(\nu')d\nu'$$
$$= \frac{\pi r^2}{c} 2\pi \int_0^{\theta_1} (\cos\theta - \beta)(1-\beta\cos\theta)\sin\theta d\theta \int_{\nu_{min}}^{min(\nu_{max},\nu'_{br}/\gamma(1-\beta\cos\theta))} I(\nu)d\nu \tag{4.2}$$

The simplest assumption is that the cross section is given by a step function, *i.e.* that the accelerating material absorbs completely radiation at frequencies smaller than the self–absorbtion one, and is transparent for higher energy photons.

For an extended source with radius R_s, θ_1 is the minimum between $\theta_1 = \arccos\sqrt{1-\sin^2\theta_1} = \arccos\sqrt{1-(R_s/R)^2}$ and the condition that only photons with frequency less than ν'_{br} are absorbed, *i.e.* $\theta = (\gamma - \nu'_{br}/\nu_{min})/\gamma\beta$. This in turn reduces the decelerating effect of blueshifted photons.

The eq. (4.1) can be written as

$$\frac{d\gamma}{dx} = \gamma \frac{R_s/R_o}{2x^2}\left[x^2\gamma\frac{(3/2)(L/L_E)}{(R_s/R_o)^2\tau_T}\int_0^{\theta_1}(\cos\theta-\beta)(1-\beta\cos\theta)\sin\theta d\theta \right.$$
$$\left.\left(\frac{[(\nu'_{br}/\gamma(1-\beta\cos\theta))/\nu_{min}]^{1-\alpha}-1}{[\nu_{max}/\nu_{min}]^{1-\alpha}-1}\right)-1\right] \tag{4.3}$$

with $x = R/R_o$, and R_0 the starting point of acceleration. For

$$\frac{L}{L_E} \gtrsim \frac{[(\nu'_{br}/\gamma(1-\beta\cos\theta))/\nu_{min}]^{1-\alpha}-1}{[\nu_{max}/\nu_{min}]^{1-\alpha}-1}\tau_T \tag{4.4}$$

the initial acceleration is positive, *i.e.* acceleration can be relevant also for $L < L_E$. The more important factor is the ratio of L/L_E and the right hand side of eq. (4.4). The results would be similar to the Ghisellini *et al.* (1990) ones (see Figs. 4.1, *i.e.*

their Figs. 1) where the results of integration of eq. (4.3) is reported for different values of $(L/L_E)/\tau_T$ and the spectral index α.

All the relative discussion and analytical estimations are similar to our case, but it seems not useful to report their discussion here. In our case however higher maximum bulk Lorentz factors are expected. In fact, for similar τ_T (in our case obtained with high density and small dimension), in the case $\alpha < 1$ the denominator is a factor $[(\nu'_s/\nu_{min})^{1-\alpha} - 1]/[(\nu'_{br}/\nu_{min})^{1-\alpha} - 1]$ larger than their: the low energy cutoff of the central source is the same (probably due to self–absorption frequency), while the ratio with absorbtion frequency of the blob can reach 10^3 (see below). In the figure shown they assume a factor 2.

In order to estimate under which conditions bremsstrahlung acceleration is more effective than Compton and synchrotron one, we can compare the relative cross sections.

The bremsstrahlung cross section, averaged on a Maxwellian distribution of particles is given by (*e.g.* Rybicki & Lightman 1979):

$$\sigma_{br} \simeq \frac{k_{br}}{n} = \frac{4\,e^6}{3m_e hc}\left(\frac{2\pi}{3km_e}\right)^{1/2}\frac{n_e}{T^{1/2}\nu^3}(1-\mathrm{e}^{h\nu/kT})Z^2 g_{ff}$$
$$\simeq 3.7\times 10^8 \frac{n_e}{T^{1/2}\nu^3}(1-\mathrm{e}^{h\nu/kT})Z^2 g_{ff} \qquad (4.5)$$

The synchrotron cross section (Ghisellini & Svensson 1991):

$$\sigma_{syn} = \frac{3\pi^2}{8}\frac{\sigma_T}{\alpha}\frac{B_{cr}}{B}\left(\frac{\nu_B}{\nu}\right)^2\left(\frac{2\nu}{\nu_B}+1\right)\left(\frac{e}{2}\right)^{2\nu/\nu_B}(m_e c\gamma\beta)^{2(\nu/\nu_B-1)} \qquad (4.6)$$

for $\gamma\beta << 1$, $\nu >> \nu_B$, $B_{cr} = \alpha(m_e c^2/r_e^3)^{1/2} \simeq 4.4\times 10^{13}$ G and $\alpha = 1/137$ is the fine structure constant.

As a first, very crude approximation (just to estimate order of magnitudes) we simply consider the synchrotron cross section as representing the cross section for a particle of energy $(1/2)m_e v^2 = (3/2)kT$ multiplying by a normalization factor 0.92, where this numerical factor gives the density of particles at the peak of a Maxwellian distribution, and compare it with the cross section averaged on a Maxwellian distribution of particles of eq. (4.5). A detailed comparison must be done or estimating the bremsstrahlung cross section for a single particle of momentum p,

or averaging the expression eq. (4.6) on a Maxwellian distribution. More precisely we compare the two cross sections with respect to the Thomson one.

Therefore (for $Z = 1$ and $g_{ff} = 1$)

$$\frac{\sigma_{br}}{\sigma_T} \simeq 6 \times 10^{32} \frac{n}{T^{1/2}\nu^3}(1 - \mathrm{e}^{h\nu/kT}) \rightarrow 2.8 \times 10^{22} \frac{n}{\nu^2 T^{3/2}} \qquad h\nu < kT \qquad (4.7)$$

The ratio σ_{syn}/σ_T is reported directly from the Ghisellini *et al.* paper (Fig. 4.2). The ratio σ_{br}/σ_T is shown in Fig. 4.3 for some values of T, n, B, as function of frequency (normalized at the Larmor frequency, for $B = 1$ G, in order to compare the results with Fig. 4.2). It can be seen that the bremsstrahlung cross section can be much bigger than the other ones even for not extreme values of n and T.

Consequently the radiation pressure accelerates matter outwards for $L < L_E$, being greater that gravitational acceleration.

Another interesting consequence that we want to explore is the possible effects on an accreting flow. Standard disc theory predicts very high density in the inner regions of the accretion disc, as high as (Lightman & White 1988)

$$n \simeq 2 \times 10^{13} \frac{\eta_{0.1}^2}{\alpha_{0.1}} \left(\frac{L_E}{L}\right)^2 \left(\frac{R}{3R_s}\right)^{3/2} \frac{1}{M_6} \qquad \mathrm{cm}^{-3} \qquad (4.8)$$

and for $L \simeq 0.1 - 0.01\, L_E$ (Wandel & Mushotzky 1986) at $R \simeq 3R_s$, and temperatures $T \sim 10^5$ K, $\nu_{br} \simeq 10^{15-16}$ Hz. α is the viscosity parameter and η the accretion efficiency. Consequently bremsstrahlung could possibly oppose to the accretion flow, at least in the 'standard' disc (Shakura & Sunyaev 1973). This limit can be partially overcome if matter is clumped, maybe in a two phase structure.

Another, similar, effect which can slow accretion is Compton heated winds, *i.e.* if $T_C > T_v$: in this case there is not a steady inflow and multiphase structures are possible, with evaporation of dense clouds or disc (Rees 1984). Winds of pairs can furthermore reprocess primary radiation and smear fast variability.

A possible application of the above results is the galactic source SS433. The two main reasons we are interested in this object are that it is the object with the better estimation of the flow velocity and secondly, but perhaps more important, it is

inferred from the spectral observations that cold material with low filling factor and high density is in the jet. It is therefore the ideal candidate for bremsstrahlung acceleration. Furthermore, in the observed physical conditions bremmstrahlung acceleration must operate and we are interested to determine its effects. Therefore in the next section we briefly outline observations (only concerning the jet and this cold material) in SS433.

In general a beam filled mainly by relativistic plasma may contain cool material owing to: injection in the nucleus, entrainment from the surrounding medium, obstacles along the jet, cooling of material leading to thermal instabilities, if $t_{cool} < t_{outflow}$. So dense cold clouds may be expected in pressure balance with an outer medium and eventually self-gravitating. The magnetic confinement has been suggested also for cloud structures observed in some large double sources (kpc scale) which emit narrow lines (Whittle *et al.* 1987, Rees 1987).

4.1.a SS433

The most interesting aspect of this source is the presence, on galactic scale, of jets. The distance of the object is estimated to be $\simeq$ 5 kpc. It is probably the only source for which the flow velocity has been well determined.

Two systems of Balmer and He I lines are observed one red and the other blueshifted, which move with a fixed periodicity.

These observations are consistent with the presence of material moving away from the central object in opposite directions and preceeding, with period of $\sim$ 164 days. This matter is supposed to be ejected in two jets (Fabian & Rees 1979), the velocity of which is $\beta \simeq 0.26c$ ($\gamma = 1.035$), constant to better than 4% (Margon 1984).

In particular the emitted lines indicate the presence of cold (T$\simeq 10^4$ K) thermal matter inside the channel wall.

Both radio and X-ray imaging provide support for the jet model (with a cone angle of $\simeq 20^o$), even if there are not definitive proofs of correlate variability in these two bands (Margon 1984). In the radio, on scales of $10^{-3} - 10^{-1}$ pc, the relativistic blobs are directly observed with VLBI. In the X-ray band (1-3 keV)

Einstein observations showed that about 90% of the flux is coincident with the optical region, while about 10% is emitted in the jets. The X–ray emitting region has been estimated to have dimensions less than 10^{12} cm. Limits on time dalays between red and blueshifted emission lines systems are < 1 day implying that the radiating regions are separated by less than 100 AU, comparable with the lenght of each optical jet (about 10^{14-15} cm). Two possible lines at about 1 MeV are reported (Lamb *et al.* 1983), but not confirmed.

In order to achieve the observed saturation velocity an interesting model has been suggested (Milgrom 1979). The observed velocity of jets is the value needed to Doppler shift the hydrogen Lyman continuum limit to the wavelenght of Lα, including special relativistic corrections. The acceleration is due to absorption of the sub–Lyman continuum photons from a central source, whose spectrum is blanketed at the Lyman limit, presumably by cool gas. The velocity reached corresponds to the value where the longest continuum photons at 912 Å can no longer 'line lock' with Lα. However a considerable ultraviolet luminosity is required and the jet should be not completely ionized *e.g.* by the X–ray radiation. This requires clumped matter, possibly in the form of cold clouds. They could be produced as a consequence of formations of shocks, which makes the matter to be compressed and cool (Fabian & Rees 1979) or from interactions with the external medium.

It has been also suggested that the acceleration could be due to line radiation pressure from other hydrogen lines, He (Shapiro, Milgrom & Rees 1986) or heavy elements, to avoid the problem of the X–ray photoionization, but it requires an unusually high aboundance of high Z elements, in contrast with the equivalent width of the iron line observed. In fact X–ray spectral observations of EXOSAT (Watson *et al.* 1986) and *Tenma* (Matsuoka Takano & Makishima 1986) are consistent with an iron line emission of FeXXV at 6.7 keV, with the Doppler shift predicted in the kinematical model. The best–fits are consistent with a $N_H \simeq 10^{22}$ cm^{-3}.

Other possible acceleration mechanisms include electromagnetic acceleration, or radiation pressure in a accretion funnel.

The kinetic energy of the jets, which must be at least 10^{36-40} erg s^{-1} (Begelman *et al.* 1980), may well exceed the radiated luminosity, and it is in fact required if the

jet is accelerated by radiation pressure, *i.e.* $(1/2)v^2\dot{M} < \eta L$. Note that the presence of clumped matter reduces the $\dot{M}$ requirement, (for low filling factors and $n > 10^{13}$ cm^{-3}), *i.e.* the kinetic energy estimates and could account for fluctuations observed in the Doppler shifts. The equipartition magnetic field is estimated to be $\simeq 10^{-2}$ G at 10^{-2} pc.

Supercritical accretion has been discussed in connection with this object, and it has been suggested that the object contains a 5–10 $M_\odot$ black hole (Zwitter *et al.* 1989). The system indeed presents other complex structures and the presence of an accretion disc, with dimension $\simeq 10^{12}$ cm (Margon 1984), is also probable.

Around the cold matter the jets must contain hot X–ray emitting gas. If it is produced as thermal (bremsstrahlung) emission its temperature should be about $T \sim 10$ keV. Also non–thermal X–ray emission models have been proposed (Grindlay *et al.* 1984). Thermal Comptonization on the contrary has been escluded.

Bodo *et al.* (1985) suggest that cold regions ($T \simeq 10^4$ K, $n \simeq 10^{16} - 10^{19}$ cm^{-3} and dimensions $\simeq 10^6 - 10^7$ cm) can form in an hot phase ($T \simeq 10^7$ K and $n \simeq 10^{14}$ cm^{-3}) due to thermal instabilities in the inner zone of the jet, at $10^{12} - 10^{15}$ cm. The hot medium does not necessarely ionize the cold matter, due to the fast decrease of hydrogen cross section with frequency. The two phases can be in pressure balance, with $p \simeq 10^3$ erg cm^{-3}. The filling factor should be very small $\simeq 10^{-3}$. In this model the clouds could move at the same velocity of the jet matter from which they form, consistently with observations of narrow lines and the jet does not transfer momentum to the clouds. They can subsequently expand, when the sound speed is low high enough and evaporate at larger distances.

Consequently the direct evidence in the jet structure of SS443 of cold matter, probably clumped, and the inferred physical conditions imply that radiation pressure due to bremsstrahlung absorption is present.

4.2 Pair clouds

As already mentioned at the end of the previous chapter, an interesting possibility about the cold material absorbing the primary radiation, is that the clouds

are constituted by an electron–positron pair plasma.

Two reasons are in favour of this possibility. First of all the presence of pair plasma winds or outflows can be quite common in the environment of AGN. In fact, as mentioned more than once, pair formation is almost inescapable in compact sources and an Eddington source is optically thick to radiation, which therefore is trapped and can accelerate an outflow, transferring its internal energy to it. If the source is pair dominated the acceleration is very efficient, being the Eddington limit for a pair plasma ~ 2000 smaller than L_E (Lightman, Zdziarski & Rees 1987) and winds naturally form.

Secondly, if the absorbing matter is constituted by pairs, the limits on the equivalent hydrogen column density does not apply at all. This means that there are no more strong constraints on the clouds thickness.

For these reasons we want to explore with more detail this possibility. The major point, with respect to the production of ordinary proton–electron clouds examined in §3.2, involves the possibility that pairs annihilate. This produces two effects: one is the obvious reduction of the particles density, which could, however, be continuously supplied; the other one is that the γ–rays produced by annihilation, maybe after formation of positronium, can heat the cloud. If it happens maybe it is not possible to reach the required density and temperature in order to free–free absorb the primary radiation up to UV frequency.

In order for our mechanism to work it is enough for the clouds to survive just the time required to absorb and reemit radiation, then they can evaporate and other clouds form.

It is quite simple calculate the annihilation timescale, but the problem is to compare it with the bremsstrahlung timescales. If, as assumed for the ordinary plasma, we require an optical depth $\tau_{br} = 1$ for the higher energy photons, the timescale required in order to absorb them is given approximately by $\Delta r/c$, *i.e.* the crossing time. We therefore requires that the annihilation timescale is longer than that one.

However both the annihilation timescale and the bremsstrahlung optical depth depend on the temperature of the particles, with opposite dependence, and the temperature itself depends on the annihilation timescale (which determines how many

γ–ray photons are produced inside the cloud and could heat it).

In order to study the problem we are developing a simple program, the aim of which is to calculate the density and the temperature of a pair plasma blob which contracts, as functions of time.

We want to determine if it can reach conditions in order to absorb through free-free, frequencies as high as $\nu = 10^{15}$ Hz, before annihilating. Note that bremsstrahlung cooling rate for electron–electron and electron–positron collisions are given by $(dE/dt)_{e,p} = 1/2(dE/dt)_{e,e} = 1/4(dE/dt)_{e+,e-}$ (Stepney 1983). Consequently within a small factor all the estimations concerning the bremsstrahlung process are similar to the case of an ordinary plasma.

We can also calculate the gas pressure $p_{gas} = 3n\Theta m_e c^2$ and compare it to the magnetic pressure $p_B = B^2/8\pi$, fixed as function of distance from the central region.

The clouds contract either if magnetic pressure exceeds gas pressure (probably at $v \simeq v_A = (p_B/m_e n)^{1/2}$) or if radiation pressure from the central source compresses the plasma against the magnetic field (rather like a sheet than a blob).

The approach is very simple. Our basic assumptions are:

1) the blob is illuminated by an external source, with a power law spectrum $L(\epsilon) = L_0 \epsilon^{-a}$, where ϵ is the energy of photons (erg), between ϵ_1 and ϵ_2.

The normalization is given by

$$L_0 = L_{bol}(1-a)(\epsilon_2^{1-a} - \epsilon_1^{1-a})^{-1} \tag{4.9}$$

We assume $a = 0.9$ and a bolometric luminosity $L_{bol} \simeq 10^{42}$ erg s^{-1}.

2) the source is at a distance R from the blob

3) the blob contracts at the speed of light (not self–consistent dynamical evolution is considered)

4) the magnetic field is assumed scaling with R as $B = 2 \times 10^4/R_{13}$ (*e.g.* eq.(3.4))

5) the only internal radiation is that due to annihilation of pairs, assumed to have photon energy $\simeq m_e c^2$

6) the blob size is small enough to be considered homogeneous

7) the system of particles and radiation in the blob is in thermodynamical equilibrium, and therefore its energy evolution depends on the temperature Θ.

• Physical quantities are:

n density of electrons (or positrons)

$\Theta = k_B T/m_e c^2$ temperature of pairs. Because the Coulomb interactions between electrons and positrons is given by (Stepney 1983)

$$t_{e\pm} = \frac{1}{n\sigma_T c}\frac{2\sqrt{\pi}}{\ln\Lambda}\Theta^{3/2} \qquad \Theta < 1$$

$$= \frac{1}{n\sigma_T c}\frac{4}{\ln\Lambda}\Theta^{2} \qquad \Theta > 1 \tag{4.10}$$

we will assume that a Maxwellian distribution for the particle is maintained during the contraction. The Coulomb logarithm is assumed to be $\ln\Lambda \simeq 20$.

t time

r is the dimension of the blob $r(t) = r_0 - ct$, where the subscript '0' refers to quantities measured at $t = 0$.

The time evolution for the density is determined by:

$$\frac{dn}{dt} = \left(\frac{dn}{dt}\right)_A + \left(\frac{dn}{dt}\right)_p - \left(\frac{dn}{dt}\right)_a \tag{4.11}$$

The first term refers to the compression of the cloud, the second to pair production due both to γ–γ photons and to $e - e$ interactions, the latter to annihilation. We neglect an escape term, assuming that the magnetic field confines the particles inside the blob, as long as $r_L < r$. This in turn defines a minimum size for the cloud.

The contraction term is given by

$$\left(\frac{dn}{dt}\right)_A = -3\beta c\frac{n}{r} \tag{4.12}$$

($\vec{\beta} = -1$), while for the pair production term we have (see Table 1.2)

$$\left(\frac{dn}{dt}\right)_{p,\gamma-\gamma} = \frac{3}{8}\sigma_T c n_\gamma^2\left[\frac{\pi}{8}\frac{\exp(-2/\Theta)}{\Theta^3}\right] \qquad \Theta < 1 \tag{4.13a}$$

$$= \frac{3}{8}\sigma_T c n_\gamma^2\left[\frac{1}{2}\frac{\ln\Theta}{\Theta^2}\right] \qquad \Theta > 1 \tag{4.13b}$$

(for a Wien distribution of photons, which can mimic a thermal distribution). More precise rates will be considered.

$$\left(\frac{dn}{dt}\right)_{p,e-e} = \frac{3}{8}\sigma_T c n^2 \alpha^2 \left[\frac{112}{27\pi^2}(\ln 2\Theta)^3\right] \qquad \Theta > 1 \tag{4.14}$$

where $\gamma - \gamma$ and $e - e$ pair production processes are considered.

The annihilation term is given by

$$\left(\frac{dn}{dt}\right)_a = \frac{3}{8}\sigma_T c n^2\, 2 \qquad \Theta < 1 \tag{4.15a}$$

$$= \frac{3}{8}\sigma_T c n^2 \left[\frac{\log\Theta}{2\Theta^2}\right] \qquad \Theta > 1 \tag{4.15b}$$

The density of γ-ray photons comparing in eq. (4.13b) produced by annihilation can be estimated as

$$n_\gamma \simeq 2\left(\frac{dn}{dt}\right)_a \frac{R}{c}(1+\tau_{KN}) \tag{4.16}$$

where $\tau_{KN} = n r \sigma_{KN}$, where σ_{KN} is the Klein–Nishina cross section, and the $(1+\tau_{KN})$ term accounts for diffusion of the γ–ray photons.

The temperature is assumed to evolve according to:

$$\frac{d\Theta}{dt} = \left(\frac{d\Theta}{dt}\right)_A + \left(\frac{d\Theta}{dt}\right)_H - \left(\frac{d\Theta}{dt}\right)_C \tag{4.17}$$

where the first term refer to the heating due to adiabatic contraction, the second term to the cooling mechanisms, and the third one to the heating processes:

$$\left(\frac{d\Theta}{dt}\right)_C = \left(\frac{d\Theta}{dt}\right)_b + \left(\frac{d\Theta}{dt}\right)_c + \left(\frac{d\Theta}{dt}\right)_s \tag{4.18a}$$

$$\left(\frac{d\Theta}{dt}\right)_H = \left(\frac{d\Theta}{dt}\right)_b + \left(\frac{d\Theta}{dt}\right)_c + \left(\frac{d\Theta}{dt}\right)_s + \left(\frac{d\Theta}{dt}\right)_\gamma \tag{4.18b}$$

The subscripts b, c, s, γ refer respectively to bremsstrahlung, Compton scattering and synchrotron processes and to Compton scattering on γ–ray photons produced by annihilation, assumed to have energy $\simeq m_e c^2$. The latter is the only term which considers radiation produced inside the blob itself. For all the other terms we consider just photons coming from the central source.

• Cooling terms.

Bremsstrahlung cooling term is given by (Svensson 1982)

$$\left(\frac{d\Theta}{dt}\right)_b = \frac{1}{3\pi^{3/2}}\sigma_T\, c\, \alpha\, n \left\{\frac{5}{3}(44-3\pi^2)\Theta^{3/2}(1+1.1\Theta+\Theta^2-1.25\Theta^{2.5}) \right.$$
$$\left. +16\Theta^{1/2}(1+1.7\Theta^{3/2})\right\} - \frac{\Theta}{n}\frac{dn}{dt} \qquad \Theta < 1 \tag{4.19a}$$

$$= \frac{12}{\pi}\sigma_T\, c\, \alpha\, n\Theta[\ln(2\eta\Theta)+5/4] - \frac{\Theta}{n}\frac{dn}{dt} \qquad \Theta > 1 \tag{4.19b}$$

with $\eta = 0.5616$ is the Euler constant.

The synchrotron cooling can be estimated as:

$$\left(\frac{d\Theta}{dt}\right)_s = \frac{4}{3}\frac{\sigma_T c}{m_e c^2} U_B \Theta \qquad \Theta < 1 \tag{4.20a}$$

$$= \frac{16}{3}\frac{\sigma_T c}{m_e c^2} U_B \Theta^2 \qquad \Theta > 1 \tag{4.20b}$$

using $d(\Theta m_e c^2)/dt \simeq m_e c^2 \dot{\gamma} = (4/3)(\sigma_T c/m_e c^2)\beta^2\gamma^2 U_B$, with $\beta^2 = 3\Theta$ and $< \gamma^2 >= 12\Theta^2$ in the two limits.

• Heating terms

The term due to contraction reads

$$\left(\frac{d\Theta}{dt}\right)_A = -3\Gamma\Theta\frac{\beta c}{r} - \frac{\Theta}{n}\frac{dn}{dt} \tag{4.21}$$

where Γ is the adiabatic index and it is fixed at the relativistic value $\Gamma = 4/3$, because we consider that the blob is photon dominated.

Bremsstrahlung heating is assumed to be given by the flux (number s^{-1}) of photons entering the surface of the blob πr^2, and below the free-free absorbtion energy ϵ_{ff}. In the Rayleigh–Jeans domain, with $g_{ff} = 1$ it is given by

$$\epsilon_{ff} = \left[\frac{8}{3}\sqrt{\frac{2\pi}{3}}\frac{h^2 e^6}{m_e^5 c^7}\right]^{1/2} r^{1/2}\frac{n}{\Theta^{3/4}} \qquad \Theta > 1, \epsilon_{ff} < \Theta \tag{4.22a}$$

$$= h\left[\frac{8}{3}\sqrt{\frac{2\pi}{3}}\frac{h^2 e^6}{m_e^5 c^8}\right]^{1/3} r^{1/3}\frac{n^{2/3}}{\Theta^{1/6}} \qquad \epsilon_{ff} > \Theta \tag{4.22b}$$

with $\epsilon = h\nu/m_e c^2$. Therefore, for $\epsilon_{ff} > \epsilon_1$

$$\left(\frac{d\Theta}{dt}\right)_b \simeq \frac{1}{16\pi m_e c^2} L_0 \frac{\epsilon_{ff}^{(1-a)} - \epsilon_1^{(1-a)}}{(1-a)}\frac{1}{nrR^2} \tag{4.23}$$

From the annihilation photons

$$\left(\frac{d\Theta}{dt}\right)_\gamma = \frac{1}{3}\sigma_T c n_\gamma [4\Theta(1+4\Theta) - \sigma_{KN}] - \frac{\Theta}{n}\frac{dn}{dt} \tag{4.24}$$

where σ_{KN} is estimates at $\epsilon = m_e c^2$, *i.e.* $\sigma_{KN} = 0.43\sigma_T$.

For synchrotron absorbtion, we assume the radiation is absorbed up to ϵ_s, determined from the Kirchoff law using eqs. (4.10a), (4.20b).

For $\epsilon_s > \epsilon_1$

$$\left(\frac{d\Theta}{dt}\right)_s = \frac{1}{16\pi m_e c^2} L_0 \frac{\epsilon_s^{(1-a)} - \epsilon_1^{(1.-a)}}{(1-a)} \frac{1}{nrR^2} \tag{4.25}$$

Compton cooling and heating, including relativistic corrections (*e.g.* Guilbert, Fabian & McCray 1983) is given by

$$\left(\frac{d\Theta}{dt}\right)_c = \frac{1}{12\pi} \frac{\sigma_T}{m_e c^2} L_0 \frac{(\epsilon_2^{(1-a)} - \epsilon_1^{(1-a)})}{(1-a)} \frac{(1+\tau_{es})}{R^2}$$
$$\left[4\Theta(1+4\Theta) - \frac{1-\alpha}{2-\alpha} \frac{\epsilon_2^{(2-a)} - \epsilon_1^{(2-a)}}{\epsilon_2^{(1-a)} - \epsilon_1^{(1-a)}}\right] - \frac{\Theta}{n}\frac{dn}{dt} \tag{4.26}$$

$(1+\tau_{es})$ accounts for diffusion of photons into the source.

From a 'technical' point of view, the time steps are assumed to be a function of time and correspond to ~ 0.1 the minimum, density or radiative, timescale, defined as $t_n = n/(dn/dt)$ and $t_\Theta = \Theta/(d\Theta/dt)$, respectively, and the other relevant timescales which are:

$$t_{dyn} = \frac{r}{c} \qquad t_{sound} = \frac{r}{c}\frac{1}{\Theta^{1/2}} \qquad t_{magn} = \frac{r}{c}\frac{\sqrt{n m_e c^2 8\pi}}{B} \tag{4.27}$$

The initial conditions are given as n_0, Θ_0, r_0, for fixed $L(\epsilon)$, R and B.

As far as our problem is concerned a critical point is the choice of the initial conditions. In fact the final aim is to be able to reach, for a reasonable range of initial conditions, a region, in the parameter space (n, Θ). The final point of the evolution, given by the pressure equilibrium with the magnetic field, or the reaching the minimum acceptable size, is obviously dependent on them.

Limits on the range of parameter are imposed, *i.e.* $r > r_L, l$; $r_0 << R$, $n_0 >> r_0^{-1/3}$, $\Theta > \alpha^2$, $n\Theta < B^2/24\pi m_e c^2$.

We realize that, some, maybe relevant, processes are neglected up to now, but we want before detailing more the equations, to check our approach.

As applications of the described program, we can also study both the time evolution of the ordinary plasma blob, described in Chapter 3, in order to determine both how the described conditions can be reached and its stability.

Secondly, reversing the time dependence, we can explore the evolution of an 'exploding' blob of pairs. The aim is to determine if rapid variability in X–ray sources, can be attributed to the fast release of magnetic energy (*e.g.* during reconnection), involving local phenomena. The first effect of the strong magnetic field is probably to accelerate suddenly particles, which emit. Detailed studies of 'fireballs' has already developed, starting with the 'qualitative' description of Cavallo & Rees (1979), but they are mainly devoted to the dynamical effects of radiation in an expanding flow (*e.g.* Becker & Begelman 1990). Furthermore they do not consider the presence of magnetic field. We suspect that if radiation is self–absorbed by synchrotron, very high energy photons can escape the central region, because they cannot interact with low energy photon to produce pairs, and release their energy only outside. This has two effects: the transport of energy outside the source, and the possibility to form an annihilation line of observable intensity.

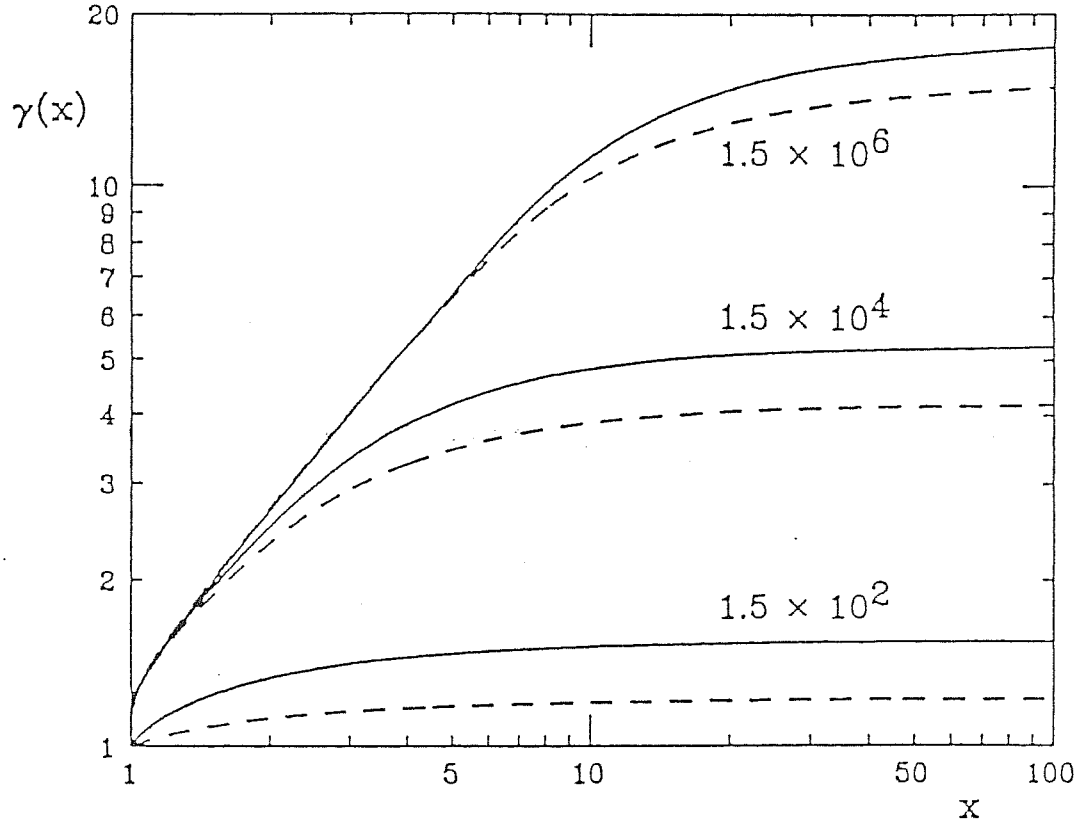

Fig. 4.1 The figure shows the bulk Lorentz factor of a blob as function of the distance x from the central source, for $\gamma = 1$ at $x = 5R_s$. The labels indicate the values of the ratio $(L/L_E)/\tau_T$, and dashed and continuous lines refer to different spectral indices of the incident radiation ($\alpha = 0.8, 1.2$). It refers to calculations for synchrotron acceleration. From Ghisellini *et al.* (1990).

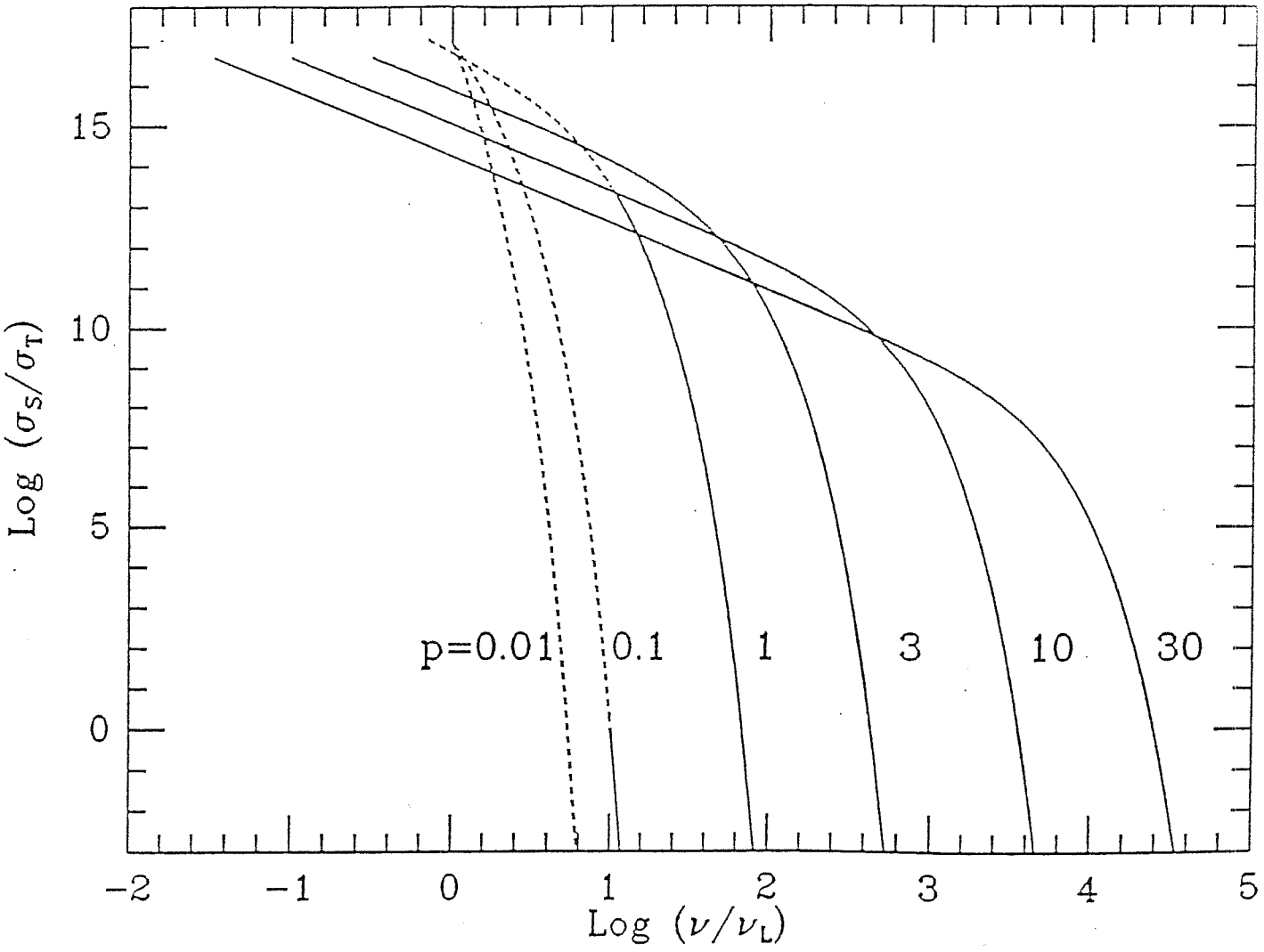

Fig. 4.2 The figure reports the ratio of the synchrotron and Thomson cross sections, as function of frequency (normalized at the Larmor frequency for a magnetic field of $B = 1$ G). Curves refer to different values of the momentum (in units of $m_e c$) $p = \gamma\beta$ of the particle. From Ghisellini & Svensson (1991).

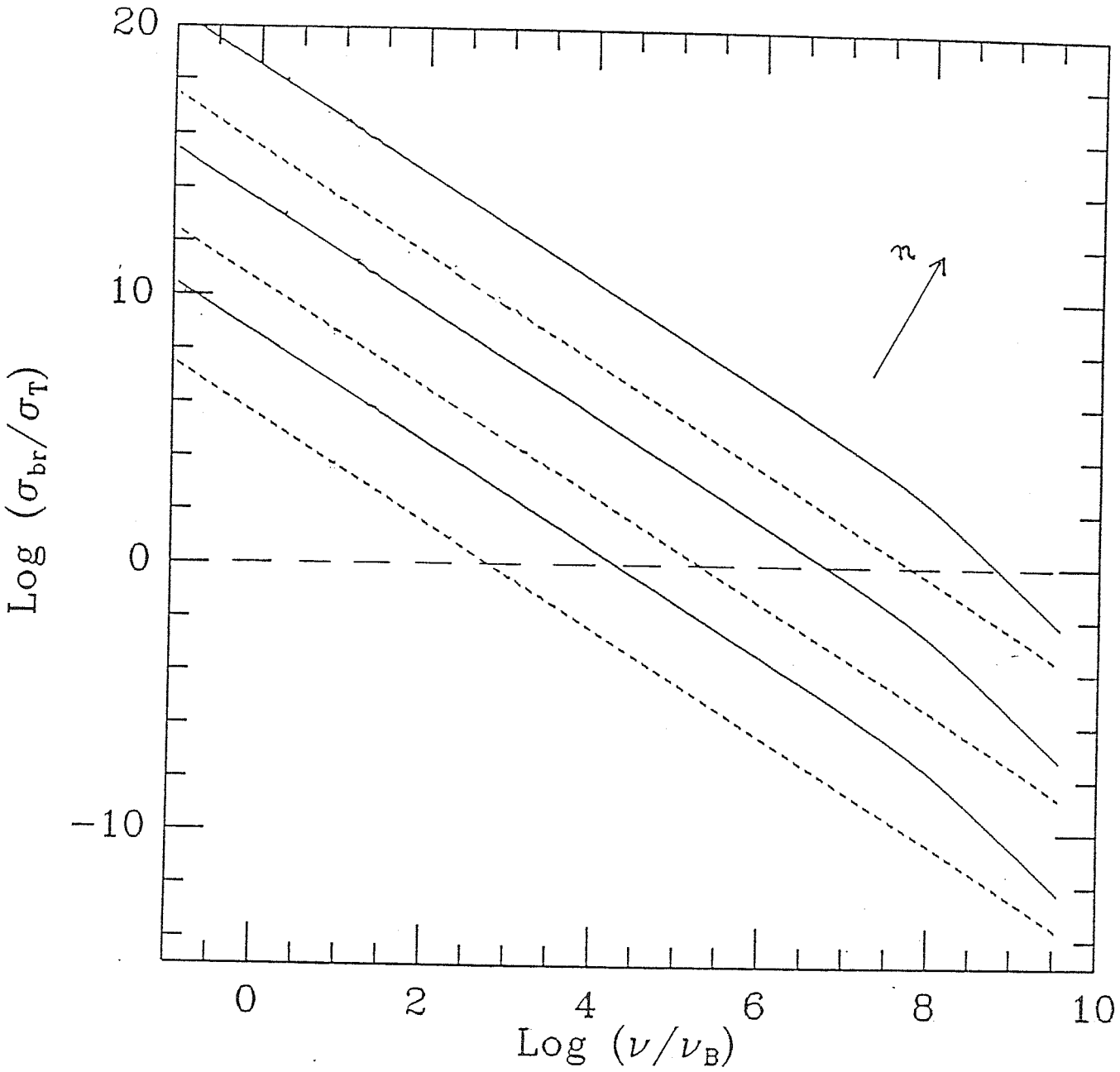

Fig. 4.3 The ratio of the bremsstrahlung and Thomson cross sections as function of frequency (in units of Larmor frequency with $B = 1$ G, in order to be compared with Fig. 4.2). The dashed curves refer to temperature $T = 10^6$ K, while the continuous one to $T = 10^4$ K, and the three different curves are for $n = 10^5, 10^{10}, 10^{15}$ cm^{-3}, from bottom to top. The change of the slope in the continuous curves corresponds to the change of the dependence due to the exponential term, with respect to the Rayleigh–Jeans behaviour. The bremsstrahlung cross section can be therefore much bigger than the Thomson one for not extreme values of parameters in the range $\nu \simeq 10^9 - 10^{14}$ Hz for the parameters considered. These curves could be compared to a curve for $p \simeq 7 \times 10^{-3}$ of Fig. 4.2 (using $p^2 \simeq 3\,k\,T/m_e\,c^2$, with $T = 10^5$ K), showing that bremsstrahlung cross section can be much bigger than the synchrotron one. A more detailed comparison, including the B dependence will be explored.

Appendix A

Variability in blazars

A model for the spectral variability of BL Lac objects at high frequencies

A. Celotti[1], L. Maraschi[2] and A. Treves[2]

[1] International School for Advanced Studies, Trieste, Italy

[2] Dipartimento di Fisica, Università di Milano, Italy

Astrophys. J., in press

Abstract

The average amplitude of variability of BL Lac objects is larger at higher frequencies and the spectra in the X-ray range show a hardening with increasing intensity. This is shown to be a natural consequence of the relativistic jet model proposed by Ghisellini, Maraschi and Treves (1985), where higher frequencies are produced nearer to the jet core. Time dependent properties are computed assuming that a perturbation travels at fixed speed down the jet, producing enhancements of constant amplitude of the relativistic particle density and of the magnetic field, in a slab or self-similar cone geometry. The time dependent spectral intensities due to synchrotron radiation and first order Compton scattering are computed numerically and approximate analytic formulae are given. The evolution of the spectral shape with time and the light curves at fixed frequencies are presented and discussed in detail. The results are compared with observations. Finally we estimate the expected intrinsic amplitude assuming that the perturbation is due to a planar relativistic shock wave. Using the results obtained by Lind and Blandford (1985) the dependence of the observed amplitude on the viewing angle and on the shock and fluid velocities is discussed.

Subject Headings: *BL Lacertae objects – galaxies: jets – galaxies: X-rays – radio sources: variable*

I. Introduction

There is presently a wide consensus that the strong non thermal continuum responsible for the high polarization and rapid variability of BL Lac objects is produced by relativistic plasma within collimated regions, briefly called relativistic jets. This is manifest for the radio domain where VLBI is able to resolve structures and reveals superluminal motions.

Models of emission from relativistic jets can naturally explain the observed overall spectra, but are only weakly constrained by the spectral shape alone (e.g. Königl 1989). However stringent constraints are obtained when the information on the spectral shape is combined with that on the variability time scales at different frequencies. It was thus shown that the short time scales observed for the highest frequency emission (X–rays) can be accounted for, if X–rays originate in the innermost part of the jet, close to its "nozzle", in a region much smaller than that responsible for the radio emission (Ghisellini, Maraschi and Treves 1985, GMT hereafter). The degree of anisotropy of the X–ray emission and of the radio emission may then be different, due to possible differences in the bulk flows within different regions of the jet (Stocke *et al.* 1985, Maraschi *et al.* 1986a, Ghisellini and Maraschi 1989).

A further step in the direction of coupling spectral and time information are multifrequency monitoring programs, which have already yielded a large quantity of data in the radio frequency domain, allowing reconstruction of the spectral evolution of outbursts from mm to cm wavelengths. This information has been used to model the physical evolution of the flaring components in terms of shock waves within the jet (e.g. Marscher and Gear 1985, Hughes, Aller and Aller 1989a,b) as envisaged in the pioneering work of Blandford and Rees (1978).

Multifrequency programs have been performed also in the IR–optical–UV and X–ray ranges, despite the obvious problems associated with using different observatories and techniques and despite the intrinsic difficulty, that a more frequent sampling is required at higher frequencies due to the decreasing variability timescales. A wide, intensive campaign on BL Lac itself has shown that optical and infrared variations are nearly simultaneous and precede radio flares by few years (Bregman *et*

al. 1990).

Interestingly, a group of recent results, referring to the X–ray and UV bands, though much less detailed than those at lower frequencies, seem to indicate a systematic behaviour of the spectral variability, i.e. an average amplitude increasing with frequency and a hardening of the X–ray spectral shape with increasing intensity, at least over sufficiently short time scales (Treves *et al.* 1989, George *et al.* 1989, Giommi *et al.* 1990). This behaviour consistently extends the findings of Impey and Neugebauer (1988) who, from a large collection of data from the radio to the optical–UV band, showed that the variability amplitude averaged over all objects increases regularly in the explored frequency range.

Motivated by this systematic pattern of the multifrequency variability, which will hopefully be confirmed and extended in the near future, we report here the study of the spectral evolution of perturbations propagating in the relativistic jet model developed by GMT in order to account for the energy distribution of BL Lac objects. Some preliminary results were published in Celotti, Maraschi and Treves (1989) and Maraschi, Celotti and Treves (1989).

We first adopt a schematic description of the perturbation showing how some general features naturally follow from this "elementary" model. The perturbation is assumed to produce a fixed enhancement in magnetic field and particle density and to travel with constant velocity along the jet. This simple model allows us to give approximate analytic expressions for the time dependence of the spectral flux, which are sufficient to understand the essential results of the model. Spectra at different times and light curves at different frequencies are computed numerically for some illustrative cases.

Finally we estimate the intrinsic strength of the perturbation for the case of a planar shock wave in an extremely relativistic fluid and introduce appropriate relativistic corrections for the observed amplitude.

The paper is organized as follows. The basic observational results are summarized in §II and the emission model for the stationary jet is briefly reported in §III. In §IV the spectral evolution of model perturbations and the time scales relevant at different frequencies are derived and discussed. The case of a planar shock wave is considered in §V and the results are discussed in §VI.

II. Observations

Several BL Lac objects were repeatedly observed in X-rays with EXOSAT, with typical durations of few hours for each observation and irregular spacings, ranging from days to several months. For some of these sources, namely Mkn 421, Mkn 501, 1218+304 and PKS 2155−304, complete results have been published (George, Warwick and Bromage 1988, George, Warwick and McHardy 1989, Treves *et al.* 1989).

The cases of PKS 2155-304 and Mkn 421 are of particular interest, in that observations in the UV and optical bands, quasi-simultaneous to the X–ray ones, are also available.

A systematic analysis of all the data in the EXOSAT archive, referring to BL Lac objects, is presented by Giommi *et al.* (1990). From the latter authors we derive data on 3 objects 1H 0414+009, Mkn 180 and PKS 2005−489, which show clear evidence of variability in both the Low Energy (LE: 0.2–2 keV) and Medium Energy (ME: 2–10 keV) bands of the EXOSAT instrumentation.

For each source we use the count–rates in different bands, averaged over the entire observation, to compute a variability indicator defined as

$$v = \frac{\sigma_v}{\bar{f}} = \frac{\sqrt{\sum_i (f_i - \bar{f})^2 / N - \sigma_{err}^2}}{\bar{f}} \tag{2.1}$$

where, for each target, f_i are the fluxes measured at different epochs, $\bar{f}$ is their mean, N is the number of observations and σ_{err} is the measurement error. We assume in the following a fixed value of $\sigma_{err}/\bar{f} = 5\%$ for the X–ray measurements and of $\sigma_{err}/\bar{f} = 10\%$ for the ultraviolet ones (see Giommi *et al.* 1987 and Hackney, Hackney and Kondo 1982). The use of a normalized variability parameter allows to compare the average variability in different energy bands and in different sources.

For PKS 2155–304, 9 EXOSAT observations are available. Taking into account the spectral shape, the effective energies of the LE and ME bands are ∼0.2 keV and ∼3 keV respectively. UV fluxes at 1500 and 2500 Å, obtained from quasi simultaneous observations (delay or leads of few hours) with IUE, with integration times of ∼ 1 h are available for 8 of the 9 observations. Data in the optical range derive from the

Fine Error Sensor on IUE and have integration times of minutes.

The resulting variability parameter at the various frequencies is reported in Tab. 1. It is apparent that v increases regularly with frequency. Roughly the dependence is of the type $v \propto \log \nu$.

The variability parameter can also be computed for the collection of all IUE spectra of PKS 2155–304 taken over a larger time span, from 1979 to 1984 (see Maraschi *et al.* 1986). For this large set of observations we obtain $v = 0.17$ and $v = 0.23$ at 2500 and 1500 Å respectively. The dependence of v with frequency is similar to, but the values are significantly smaller than those obtained for the UV observations quasi simultaneous with the EXOSAT ones, indicating that at the latter epoch the object was more active.

For Mkn 421, v could be computed in the two ultraviolet and in the two X–ray bands from the data of George *et al.* (1988) (11 and 14 observations respectively). Again a regular increase with frequency is apparent, which also in this case appears logarithmic.

For all the other objects the available data refer only to the two X–ray bands. Again an increase of specific variability with frequency is present.

The trend, found here, of increasing variability amplitude with increasing frequency in the UV to X–ray range, agrees with the results of Impey and Neugebauer (1988) for a much larger collection of data from the radio to the UV bands. A more quantitative comparison is impossible, since those authors considered the ratio f_{max}/f_{min} for a large number of sources and averaged over the source population.

It is important to recall that the 7 objects listed above are X–ray bright and radio weak. They belong to the so called "X–ray selected" BL Lac objects, that is objects appearing in flux limited X-ray surveys (Maccacaro *et al.* 1989, Giommi *et al.* 1989). It has been shown that the overall energy distribution of such objects differs significantly from that of the "classical" radio selected members of the BL Lac population (e.g. Maraschi *et al.* 1986b) so that conceivably also the X–ray properties may be different. In fact Worral and Wilkes (1990) find that the X-ray spectra of radio selected BL Lacs ($\alpha_X \simeq 1$) are on average flatter than those of X-ray selected BL Lacs ($\alpha_X \simeq 1.5$, Maraschi and Maccagni 1988). This is in agreement with the model of Ghisellini and Maraschi (1989), which attributes the X-ray emission of the

two types of objects to different radiation processes, that is inverse Compton for the radio selected and synchrotron for the X-ray selected BL Lac objects respectively.

III. The stationary model

We will adopt the stationary inhomogeneous jet model described in GMT. This model naturally explains the decrease of variability time scales with increasing frequency because the higher frequency emission is produced in regions of decreasing size.

The overall continuum is obtained as an appropriate superposition of locally produced synchrotron self-Compton (SSC) spectra. The inner portion of the jet, emitting at high frequencies, is confined by external pressure with parabolic shape (e.g. Marscher 1980)

$$r = r_o \left(R/R_o\right)^{\epsilon} \tag{3.1}$$

where r and R are the transverse and axial coordinates and ϵ is a geometrical parameter ($\epsilon < 1$ corresponds to a parabolic jet). r_o and R_o are linear dimension scales and we assume $r_o = R_o$.

In order to explain the observed flat radio spectra, the outer part of the jet should have conical shape, $\epsilon = 1$. Here we shall be concerned only with the high frequency emission; therefore, only the inner, parabolic portion of the jet will be considered.

The distribution of emitting electrons is given by $N(\gamma) = K\gamma^{-p}$, for $\gamma < \gamma_{max}$, with p assumed constant along the jet. The maximum Lorentz factor γ_{max}, the relativistic particle density and the magnetic field intensity are assumed to be decreasing functions of the distance from the central engine, according to the simple parametric laws ($x = R/R_o$):

$$\gamma_{max} = \gamma^o_{max} x^{-\epsilon e} \tag{3.2a}$$

$$K = K_o x^{-\epsilon n} \tag{3.2b}$$

$$B = B_o x^{-\epsilon m} \tag{3.2c}$$

The local synchrotron emissivity as a function of the distance from the "core" is therefore given by

$$\epsilon_s(\nu, x) = \frac{c_1(\alpha_o)}{4\pi} K_o B_o^{1+\alpha_o} \nu^{-\alpha_o} x^{-\epsilon[n+m(1+\alpha_o)]} \quad \nu_{min}(x) < \nu < \nu_{max}(x) \tag{3.3}$$

where $\alpha_o = (p-1)/2$; the self absorption frequency, $\nu_{min}(x)$, and the maximum emission frequency, $\nu_{max}(x)$, are given by

$$\nu_{min}(x) = \nu^o_{min} x^{-k_m} \tag{3.3a}$$

$$\nu_{max}(x) = \nu^o_{max} x^{-\eta} \tag{3.3b}$$

where $\eta = \epsilon(2e+m)$, $k_m = \epsilon[m(1.5+\alpha_o)+n-1]/(2.5+\alpha_o)$. For the numerical values and expressions of $c_1(\alpha_o)$ ($c_1(0.5) \simeq 3.6 \times 10^{-19}$) ν^o_{min} and ν^o_{max} see GMT. The model assumes that $\eta > 0$, so that high frequencies are produced only at small x.

The monochromatic luminosity is obtained integrating $\epsilon_s(\nu, x)$ over the volume emitting at the considered frequency

$$L_s(\nu) = \pi R_o^3 c_1(\alpha_o) K_o B_o^{1+\alpha_o} \nu^{-\alpha_o} \int_{x_1(\nu)}^{x_2(\nu)} x^{\xi-1} dx \tag{3.4}$$

where $\xi = 1 + \epsilon[2 - n - m(1+\alpha_o)]$ and the integration limits derive from inverting eqs.(3.3a), (3.3b).

Note that the sign of ξ determines whether the upper or lower integration limit is important. For $\xi > 0$ the dominant contribution to $L_s(\nu)$ comes from $x_2(\nu)$ (outer regions). It was shown in GMT that the model can reproduce the steepening of the continuum for positive values of ξ and η. The positive values for the two parameters guarantee the essential feature of the model. Therefore we adopt this choice hereafter.

With these assumptions ($\eta > 0$ and $\xi > 0$) the integrated synchrotron spectrum can be described by two power laws. At low frequencies, $\nu_{min}(x_{max}) < \nu < \nu_{max}(x_{max})$ the spectral index is α_o. This represents essentially the thin synchrotron spectrum from the outer region of the jet $x \simeq x_{max}$. Above $\nu_{max}(x_{max}) \equiv \nu_b$, the spectrum steepens to $\alpha_1 = \alpha_o + \xi/\eta$ due to the fact that the volume contributing above ν_b decreases with increasing ν.

If the photon density is high, the inverse Compton emissivity must also be considered. The model assumes that the radiation energy density is due to photons produced locally. The monochromatic inverse Compton luminosity can then be derived analogously to the synchrotron one:

$$L_c(\nu) = \frac{3}{8} b(\alpha_o) \tau_o K_o B_o^{1+\alpha_o} R_o^3 \nu^{-\alpha_o} \int_{x_1(\nu)}^{x_2(\nu)} x^{l-1} \ln \left[\frac{\nu_2(R)}{\nu_1(R)} \right] dx \qquad (3.5)$$

where $\tau_o = \sigma_T K_o R_o$, $l = \xi - (n-1)\epsilon$ and ν_1 and ν_2 are the minimum and maximum synchrotron frequencies which contribute to the Compton emission at frequency ν. $b(\alpha_o)$ is a constant and it is listed in GMT ($b(0.5) \simeq 1.4$). For ν in the X–ray band the limits of integration can be taken to coincide with the minimum and maximum dimensions of the jet in most relevant cases. The parameter l has a role analogous to ξ: for $l > 0$ the largest contribution to the luminosity at fixed frequency is produced in the outer regions.

The inverse Compton emission produces a component with constant spectral index equal to α_o. This component always becomes dominant with increasing frequency, since it is flatter than the synchrotron spectrum above ν_b and extends to very high frequencies.

IV. Time dependent emission in the presence of a perturbation

In the frame just described we introduce a perturbation propagating outwards along the jet. A similar approach was adopted to interpret variability in the radio to infrared frequency domain by Marscher and Gear (1985), O'Dell (1988), Hughes, Aller and Aller (1989a,b).

The perturbation is modelled as an increase in the relativistic electron density and magnetic field strength by constant factors, $(1+k)$ and $(1+b)$ respectively, relative to the stationary values, the shape of the particle distribution being unchanged. The latter assumption is clearly a minimal one. In fact it is possible that the average energy and also the spectral shape will be affected by the perturbation.

The front of the perturbation is assumed to move at constant velocity $\beta_p c$,

starting from R_o. Here we will not introduce Doppler and relativistic corrections, which will be discussed in §V Thus the time used strictly refers to an observer at rest with the nozzle of the jet and with line of sight nearly perpendicular to the jet axis, for which the Doppler factor is 1. The velocity of the stationary fluid is assumed to be subrelativistic.

In the region affected by the perturbation the synchrotron emissivity is given by:

$$\epsilon_s^*(\nu, x^*) = (1+k)(1+b)^{1+\alpha_o} \frac{c_1(\alpha_o)}{4\pi} K(x^*) B(x^*)^{1+\alpha_o} \nu^{-\alpha_o} = (1+a_s)\epsilon_s(\nu, x^*) \quad (4.1)$$

within the frequency range defined by

$$\begin{aligned} \nu_{min}^*(x^*) &= \nu_{min}(x^*)[(1+b)^{1.5+\alpha_o}(1+k)]^{\frac{1}{2.5+\alpha_o}} \\ \nu_{max}^*(x^*) &= \nu_{max}(x^*)(1+b) \end{aligned} \quad (4.1a)$$

where the asterisk denotes quantities referring to the perturbation, whose location is given by $x^* = 1 + \beta_p ct/R_o$ and $(1+a_s) = (1+k)(1+b)^{1+\alpha_o}$.

The inverse Compton emissivity has a stronger dependence on particle density and its perturbed value is

$$\epsilon_c^*(\nu, x^*) = (1+a_c)\epsilon_c(\nu, x^*) \quad (4.2)$$

where $(1+a_c) = (1+k)^2(1+b)^{1+\alpha_o}$.

The perturbation is assumed to extend to the full cross section of the jet. As for the thickness we consider two cases: *i*) constant thickness $\Delta x^* = h \leq 1$, i.e. a slab geometry; *ii*) the perturbed region is self-similar with a conical shape determined by the sound velocity, c_s, in the stationary fluid. Thus the height of the cone is $\Delta x^* = (\beta_p c/c_s)x^{*\epsilon}$ which increases as the jet width, x^ϵ, when the perturbation moves outward. This geometry could represent the emission region after the transit of a planar shock wave as suggested by Lind and Blandford (1985).

The total monochromatic luminosity at frequency ν can be thought of as the sum of contributions from two regions: 1) from the volume V^* affected by the the perturbation, 2) from the unperturbed portion, $V - V^*$, of the stationary jet. In both cases the volumes emitting at the given frequency, $V^*(\nu)$ and $V(\nu)$ may be smaller than V^* and V respectively. Moreover, due to the frequency shift of the

emission from the perturbed region with respect to the unperturbed one, $V^*(\nu)$ is not simply a portion of $V(\nu)$. In Appendix A we give the exact definitions of the two contributions, which are used in the numerical computations.

It is useful to derive analytic expressions: to this end we will neglect the frequency shift due to the perturbation, which is small compared to the frequency range of the emission. With this approximation $V^*(\nu)=V(\nu)\cap V^*$, where the intersection symbol defines the volume emitting at ν within the perturbed region. We can thus write:

$$L(\nu,t) = L^1(\nu,t) + L^2(\nu,t) \tag{4.3}$$

where

$$L^1(\nu,t) = 4\pi \int_{V^*(\nu)} \epsilon^*(\nu,x)\ dV \qquad\qquad L^2(\nu,t) = 4\pi \int_{V(\nu)-V^*(\nu)} \epsilon(\nu,x)\ dV \tag{4.3a}$$

With $V(\nu) - V^*(\nu)$ we indicate the unperturbed part of $V(\nu)$. Recalling (4.1) we have

$$\begin{aligned} L(\nu,t) &\simeq 4\pi \int_{V(\nu)} \epsilon(\nu,t)\ dV + 4\pi \int_{V^*(\nu)} (\epsilon^*(\nu,t) - \epsilon(\nu,t))\ dV = \\ &= L^{st}(\nu) + 4\pi a \int_{V^*(\nu)} \epsilon(\nu,t)\ dV \end{aligned} \tag{4.3b}$$

where L^{st} is given by eqs. (3.4) or (3.5) and a coincides with a_s or a_c defined in eqs. (4.1), (4.2) depending on whether we consider synchrotron or Compton radiation.

We further define a normalized amplification factor $A(\nu,t)$ as the ratio between the monochromatic, time dependent luminosity and the stationary one: $A(\nu,t) \equiv L(\nu,t)/L^{st}(\nu)$.

With the simplifying assumption mentioned above

$$A(\nu,t) = 1 + a\frac{\int_{V^*(\nu)} \epsilon(\nu,x)\ dV}{\int_{V(\nu)} \epsilon(\nu,x)\ dV} \tag{4.4}$$

Using for a and ϵ the values appropriate for synchrotron or Compton emission, the approximate expressions (4.3b) and (4.4) or the corresponding exact eqs. (A.6) and (A.7) in Appendix A allow to derive the two dimensional behaviour of $L(\nu,t)$, which can be represented on one-dimensional plots either as frequency spectra at different times or as light curves at different frequencies. We neglect delays due to

the light travel time across the jet and (to the same accuracy) across the perturbation. The results are presented below. All the figures derive from numerical computations of eqs. (A.6), (A.7).

4.1 Time dependent spectra

Let us first consider the synchrotron flux from a perturbation of fixed size, $\Delta x^* = h$ (case *i*). Since $h \leq 1$ we can approximate the perturbed region as homogeneous: in this case $V^*(\nu)$ is either $\simeq V^*$ or null. Furthermore let us treat V^* as a cylindrical slab. Then

$$A_s(\nu,t) \simeq 1 + a_s\xi\frac{hx^{*(\xi-1)}}{x_2^{\xi}(\nu)} \tag{4.5}$$

This expression is valid for frequencies in the interval $\nu^*_{min}(x^*) \leq \nu \leq \nu^*_{max}(x^*)$. For ν outside this range $A_s(\nu,t) = 1$.

$x_2(\nu)$ is the outer boundary of the region emitting at frequency ν in the stationary jet, and is derived inverting eq.(3.3*b*). For $\nu > \nu_b$, where ν_b is the "break" frequency for the stationary spectrum (see §3), $x_2 = (\nu^o_{max}/\nu)^{1/\eta}$, while, for $\nu < \nu_b$, x_2 is constant $x_2 = x_{max}$. This behaviour of x_2, which is responsible for the occurrence of the break in the stationary spectrum, also determines the spectral evolution of the perturbation. In fact, for $\nu > \nu_b$, $A_s(\nu,t)$ increases with increasing ν, whereas, for $\nu < \nu_b$, it is independent of frequency. We can thus write, introducing the explicit time dependence, for $t_0 \leq t \leq t_{max}$,

$$A_s(t) \simeq 1 + a_s\xi\frac{h(1+t/t_o)^{(\xi-1)}}{x^{\xi}_{max}} \qquad \nu^*_{min}(x_{max}) \leq \nu \leq \nu_b \tag{4.5a}$$

$$A_s(\nu,t) = 1 + a_s\xi\frac{h(1+t/t_o)^{(\xi-1)}}{(\nu^o_{max})^{\xi/\eta}}\nu^{\alpha_1-\alpha_o} \qquad \nu \geq \nu_b \tag{4.5b}$$

where $t_o = R_o/\beta_p c$ and $t_{max} = (R_{max} - R_o)/\beta_p c$.

The perturbed spectrum is obtained multiplying $A_s(\nu,t)$ by the stationary spectrum. For $\nu < \nu_b$ the result is a power law with index α_o , while for $\nu > \nu_b$ the perturbed spectrum is given by the sum of two power laws with index α_1 and α_o. Thus above ν_b the effective spectral index will be intermediate between α_o and α_1, close to α_o when the amplitude of the perturbation is large. Therefore the model predicts no spectral variability below ν_b and a hardening of the spectrum above ν_b when the flux increases, with a limiting value α_o.

The calculation of the amplification factor for the first order Compton follows the same lines, yielding

$$A_c(\nu,t) = 1 + a_c l \frac{h x^{*(l-1)}}{x^l_{1(2)}} \tag{4.6}$$

where a_c is given by (4.2) and x_1 or x_2 appear in the denominator depending on whether $l < 0$, or $l > 0$ respectively. For ν in the X–ray domain, which is relevant here, neither x_1 nor x_2 depend on frequency (see §3). Thus the amplification factor for the Compton spectrum is independent of frequency, implying no spectral change.

Figs. 1a and 1b show the evolution with time of the energy spectrum, due to the passage of a perturbation with constant thickness, for different sets of parameters describing the stationary jet structure (see Tab. 2) which we will refer to as case *a*) ($\xi < 1$) and *b*) ($\xi > 1$). In both cases at high frequencies the spectrum flattens with increasing intensity, while for $\nu < \nu_b$ the change in intensity is not associated with spectral changes. Variations of one order of magnitude in X–rays are reproduced for values of the enhancement parameters b and $k \simeq 3$, for $h = 1$, while, below ν_b, the variation amplitude is much smaller.

The value of the parameter ξ measures the importance of the outer regions in building up the stationary luminosity and plays a similar role in the perturbed luminosity. For larger ξ the effect of the perturbation is comparatively stronger (with respect to smaller ξ) at low frequencies, which are emitted at larger distances. In particular, for $\xi > 1$, the dependence of the amplitude on x^* changes substantially, from decreasing to increasing with increasing x^* (see eq. (4.5)). We will come back to this point in discussing light curves.

Let us now consider the case of a perturbation of increasing thickness (case *ii*). The behaviour of the perturbed flux can be derived, computing again expressions (A.6) and (A.7) of Appendix A.

In order to derive simple analytic results, we assume again in the following that the perturbation region is homogeneous: due to the larger size of the perturbation the approximation is more severe here than in the previous case. We will evaluate the perturbed emissivity at an intermediate position in the interval $[x^* - \Delta x^*, x^*]$, which divides the emitting region in two parts of equal volumes. We indicate this position with $x^{**} \simeq (x^* - 0.2\ \beta c/c_s\ x^{*\epsilon})$. For $x^* \gg 1, x^{**} \to x^*$.

We can thus write

$$L(\nu,t) \simeq L^{st}(\nu) + 4\pi a \int_{V^*} \epsilon(\nu,t)\, dV \simeq L^{st}(\nu) + 4\pi^2 R_o^3 a\, \epsilon(\nu, x^{**}) \frac{x^{*2\epsilon}\Delta x^*}{3} \qquad (4.7)$$

where the fraction represents the volume of the emitting cone. Full expressions are given in Appendix A and are used in the numerical computations.

The amplification factor for synchrotron emission in case *ii*) is thus given by:

$$A_s(\nu,t) \simeq 1 + a_s \xi \frac{\beta c}{c_s} \frac{x^{*\xi-1+\epsilon}}{x_2^{\xi}} \qquad \text{for } x^* \gg 1 \qquad (4.8)$$

The amplification will be greater than 1 for frequencies in the interval $\nu^*_{min}(x^{**}) \leq \nu \leq \nu^*_{max}(x^{**})$.

An analogous procedure is followed to obtain the amplification of the Compton emission A_c.

Eq. (4.8) shows that the dependence of the amplification factor on frequency is qualitatively the same as for a perturbation of constant thickness, but the amplitude of the variation is larger at lower frequencies, because the emitting volume is larger. In this case the critical value of ξ, above which the dependence of the amplitude on x^* changes trend, is $\xi \simeq 1 - \epsilon$.

The time evolution of the energy spectra for case *ii*) is shown in Figs. 2a, 2b adopting for the stationary jet and for the initial perturbation the same parameters as for the perturbation of constant size. Comparing Figs. 1 and 2 one can see that, as argued above, at high frequencies the behaviour is similar but at low frequencies the effect is stronger due to the larger volume of the perturbation.

The Compton emission varies without spectral changes, in a similar way to the low frequency synchrotron emission. In each case the Compton spectra associated with the synchrotron ones are shown in the figures.

4.2 Light curves at different frequencies

Another way of examining the results is to plot the flux at a given frequency vs. time (light curve). This allows a better understanding of the timescales involved. In the following we shall discuss the general properties of the light curves and give formulae for interesting time intervals and time scales, adopting the same approximations introduced above in the description of the spectral evolution.

The light curves for the synchrotron flux are computed at three representative frequencies: in the X-ray ($2\,10^{17} Hz$), UV-optical ($10^{15}\ Hz$) and far-infrared ($10^{13} Hz$) bands, chosen to illustrate different behaviours in observationally relevant spectral regions. They are shown in Figs. 3 for a model *a* jet ($\xi < 1$), and in Figs. 4 for a case *b* jet ($\xi > 1$). Both, amplitude and timescales, are logarithmic in the figures.

The lowest frequency considered, $\nu = 10^{13} Hz$, is below the self–absorption frequency of the perturbation at its start. As the perturbation moves down the jet, the self–absorption frequency decreases, causing the delayed rise in the light curve when it falls below $10^{13} Hz$. At lower frequencies still the model becomes inadequate since it does not include the far regions of the jet which are important at low frequencies.

In all the high frequency light curves one can recognize a first time interval τ_1 corresponding to the time necessary for the perturbation, which has a finite thickness Δx^*, to fully enter the emission region for a given frequency

$$\tau_1 = \Delta x^* t_o = \begin{cases} h t_o & \text{case } i), \text{ fixed thickness} \\ (\beta c/c_s)(1 + t/t_o)^{\epsilon} t_o & \text{case } ii), \text{ growing thickness} \end{cases} \tag{4.9}$$

For case $ii)$ τ_1 is somewhat larger than for case $i)$. In all cases the amplitude grows during τ_1.

A second time interval τ_2 corresponds to the time it takes for the perturbation to cross the region of the jet which emits at the considered frequency. We have

$$\tau_2(\nu) = (x_2^*(\nu) - x_1^*(\nu)) t_o \simeq \begin{cases} x_{max} t_o & \nu < \nu_b \\ (\nu^o_{max}(1+b)/\nu)^{1/\eta}\, t_o & \nu > \nu_b \end{cases} \tag{4.10}$$

where x_1^*, x_2^* are the boundaries of the region emitting at frequency ν with the enhanced value of the magnetic field. The factor $(1 + b)$ accounts for this frequency shift.

From (4.10) one can see that at high frequencies, the crossing time decreases with increasing frequency, with a dependence assigned by the parameter η. This is shown, for example, in Figs. 3, where the duration of the 10^{15} Hz light curves is much longer than that of the $2\ 10^{17}$ Hz light curves.

The value of ξ is critical in determining the shape of the light curves during τ_2. For $\xi < 1$ (or $\xi < 1 - \epsilon$ for case ii, eq. (4.8)) the flux decreases, while for $\xi > 1$ (or $\xi > 1 - \epsilon$) the flux continues to increase. Thus the structure of the jet, characterized

by the parameter ξ, introduces a fundamental difference between the light curves of Figs. 3 and 4. For $\xi < 1(-\epsilon)$ the maximum intensity is reached after the interval τ_1, that is simultaneously for all frequencies above $\nu^*_{min}(1)$ (Fig. 3a). For values of $\xi > 1(-\epsilon)$ (see Fig. 4a) the maximum intensity is reached after the crossing time τ_2.

Since τ_2 depends on frequency, eq. (4.10), there is a time lag between the maxima at different frequencies given by the difference in the two crossing times. For $\nu_1, \nu_2 > \nu^*_b$

$$\tau_{lag}(\nu_1,\nu_2) \simeq (\tau_2(\nu_1) - \tau_2(\nu_2)) = [(1+b)\nu^o_{max}]^{1/\eta} \left[\frac{1}{\nu_1^{1/\eta}} - \frac{1}{\nu_2^{1/\eta}}\right] t_o \qquad (4.11)$$

We recall that the delay in the maximum intensity at frequencies below $\nu^*_{min}(1)$ is due to a different effect, that is the variation in the optical depth of the perturbation.

While the time intervals discussed above do not involve the amplitude of variability it is possible to introduce the "e-folding time scale" τ_e, defined as follows: $\tau_e(\nu,t) \equiv L(\nu,t)/(dL(\nu,t)/dt)$. For the sake of simplicity we consider here only case i) with the approximations discussed above and $\nu > \nu_{min}(1)$. In the two parts of the light curves, τ_1 and τ_2, τ_e is given respectively by

$$\tau_e(\nu,t) = \begin{cases} 1/(1+\xi t/t_o)\left\{(1+t/t_o)t/t_o + (1+t/t_o)^{(2-\xi)}x_2^\xi/a_s\xi\right\} t_o & t < \tau_1 \\ |\xi-1|^{-1}\left\{(1+t/t_o) + (1+t/t_o)^{(2-\xi)}x_2^\xi/ha_s\xi\right\} t_o & \tau_1 < t < \tau_2 \end{cases} \qquad (4.12)$$

Since $\xi < 2$, for $\tau_1 < t < \tau_2$, $\tau_e(\nu,t)$ is an increasing function of t (at fixed ν) and the shortest e-folding time scale is thus obtained at the beginning of this interval. For $t < \tau_1$, the same is true for $\xi < 1$ (for $\xi > 1$ the minimum of τ_e depends on ξ and ν).

In particular for $\nu > \nu^*_b$ we have

$$\tau_{min}(\nu) = \begin{cases} \left\{(\nu^o_{max}/\nu)^{\xi/\eta}/a_s\xi\right\} t_o & t < \tau_1 \ (\xi < 1) \\ |\xi-1|^{-1}\left\{(1+h) + (1+h)^{2-\xi}\left(\nu^o_{max}/\nu\right)^{\xi/\eta}/ha_s\xi\right\} t_o & \tau_1 < t < \tau_2 \end{cases} \qquad (4.12a)$$

From (4.12) we can see that also the e-folding time decreases with frequency, $x_2^\xi = (\nu^o_{max}/\nu)^{\xi/\eta}$. We recall that ξ/η gives the steepening of the stationary spectrum, $\Delta\alpha = \xi/\eta$ (see §3).

The contribution of the Inverse Compton emission may be important in the X-ray band: its temporal behaviour is compared in Fig. 5 with that of the synchrotron emission in the same band. Only two of the four cases are shown in the figure, i.e. (A,i) (constant thickness) and (B,ii) (increasing thickness). The parameter l now has a role analogous to ξ for the synchrotron emission (eq. (4.6)). Again, for $l < 1$, the amplitude reaches its maximum after τ_1 and decreases thereafter, while, for $l > 1$, the Compton flux is increasing for a time τ_2, after which the perturbation exits from the region of the jet considered here.

In the first case the Compton X–rays rise simultaneously with the synchrotron ones. In the second case, due to the fact that the region emitting X-rays through the Compton process is larger than that emitting X–rays through synchrotron, the maximum of the Compton flux is delayed with respect to the synchrotron one. We recall that the time behaviour of the Compton flux is largely independent of frequency, thus the light curves would be the same also in the hard X-ray band.

In §V we will introduce relativistic corrections for the observed amplitudes under various assumptions concerning the velocities of the stationary and perturbed fluid. Obviously the time scales should be corrected too. However the Doppler factor correction, apart from compressing or stretching the time scale, will not alter the general features that we have discussed, at least within the approximations adopted, of neglecting time delays across the jet and across the perturbation.

4.3 Normalized variability parameter

In §2 we defined an observational parameter $v(\nu)$ in order to quantify the "average" amplitude of the observed variations. Given the sampling of the available data, $v(\nu)$ refers to timescales from days to years.

The comparison with model predictions is not direct because of the necessity of choosing the instants of "observation" and of specifying a duty cycle to calculate the mean. Moreover our model is appropriate to discuss variations on time scales related to the evolution of the perturbation (hours to weeks). Additional variability may result from long term changes in the jet structure and, on short time scales, from random inhomogeneities in the radiating region. Tentatively, we will assume that the observed variability results uniquely from perturbations of the type described here and will compute $v(\nu)$ for N observations randomly chosen within a time interval

comprising the duration of one full event t_{max} plus a number M-1 of quiescent periods.

The results are reported in Tab. 3 for the 4 cases considered above and for values of b and k chosen so as to come close to the observed values. It can be seen from Tab. 3 that in all cases the model predicts too small amplitudes at low frequency for "single event" averages. However, introducing a duty cycle tends to smear out the high frequency amplitude more than the low frequency one so that a better agreement with observations can be obtained (in Tab. 3 the case for M=6 is reported). The necessary values of b and k are in the range 2-4, corresponding to values of $a_s \simeq 15 - 56$.

V. The case of a relativistic shock wave

The most plausible physical model for a perturbation of the kind discussed in the previous section is that of a relativistic shock wave. It is interesting that, using jump conditions with simple equations of state, it is possible to estimate the compression ratio across the shock as a function of the velocity of the upstream fluid in the frame of the shock u_1. The latter is determined by the velocity of the front β_s and of the stationary fluid β_1 in the frame of the observer. Furthermore, in the case of a shock wave, the velocity of the perturbed fluid, β_2, must be different from that of the stationary emitting fluid, β_1, which introduces different relativistic corrections for the stationary (upstream) and perturbed (downstream) emission. Thus not only the observed flux but also the amplitude of variability will depend on the stream velocities and on the viewing angle.

The relativistic jump conditions across a planar adiabatic shock are given by Königl (1980). In the particular case of upstream ultrarelativistic temperature ("adiabatic index" $\Gamma_1 = 4/3$), the solution of the jump equations is simply given by $u_1 u_2 = 1/3$, where u_1 and u_2 are the upstream and downstream velocities of the fluid in the frame of the shock. Thus, using the conservation of particle number $u_1 \gamma_1 n_1 = u_2 \gamma_2 n_2$, the shock strength $\Psi = n_2/n_1$ can be derived

$$\Psi = u_1 \gamma_1 \sqrt{9u_1^2 - 1} \tag{5.1}$$

Note that the compression ratio in the relativistic case can become arbitrarily large for increasing γ_1.

We will assume that the emitting relativistic electrons simply follow the compression of the fluid, so that the factor $(1+k)$ in §3 equals Ψ. This is clearly a crude approximation, which is motivated by the fact that the electron radiative lifetimes are rather short compared to the dynamical ones, making an adiabatic approximation for the electrons questionable. A direct estimate of the spectra produced by particle acceleration at the shock front would be extremely valuable (e.g. Peacock 1981, Schneider and Kirk 1989) but is clearly beyond the scope of the present paper.

As for the magnetic field, only the component parallel to the shock front is increased: so $1 \leq (1+b) \leq \Psi$, and we will assume an angle of 45^o between the field and the shock. We verified that for the relevant values of the magnetic field the magnetic energy density does not dominate that of the proton–electron plasma for an ultrarelativistic equation of state, so we will not consider magnetohydrodynamical jump equations.

With the above assumptions one can derive the enhancement of the synchrotron and Compton radiation in the frame of the shock as a function of u_1. The parameters a_s, a_c defined in the previous section for the synchrotron and Compton emission read:

$$a_s = u_1\gamma_1(9u_1^2-1)^{1/2}[(1+u_1^2\gamma_1^2(9u_1^2-1))/2]^{(1+\alpha)/2} \qquad (5.1a)$$

or

$$a_c = u_1^2\gamma_1^2(9u_1^2-1)[(1+u_1^2\gamma_1^2(9u_1^2-1))/2]^{(1+\alpha)/2} \qquad (5.1b)$$

The observed amplitude must include the relativistic corrections associated with the velocities of the shock itself β_s and of the upstream and downstream fluid velocities β_1 and β_2 in the observer frame. Using the expression given by Lind and Blandford (1985) for the spectral intensity observed from a shocked fluid in a thin source, with planar geometry, we obtain:

$$F_{obs}^{pert} = \delta(\beta_s)\delta(\beta_2)^{2+\alpha_o}F^{pert} \qquad (5.2)$$

where α_o is the spectral index of the emitted radiation, $\delta(\beta_s) = (1-\beta_s^2)^{1/2}/(1-\beta_s cos\theta)$ is the Doppler factor computed with the shock front velocity and $\delta(\beta_2)$ is the

Doppler factor for the post-shock fluid velocity in the observer frame. θ is the angle between the line of sight and the velocities, which are assumed parallel to the jet axis. In formula (5.2) it is assumed that the volume of the perturbed emission region is measured in the frame of the shock front. The relativistic correction factor for the flux observed from the stationary jet is $\delta_1^{2+\alpha_o}(\beta_1)$. It follows that the variability amplitude derived in the previous section (§4.1) transforms to

$$A_R(\nu,t) \simeq 1 + C_R\, a\, \frac{\int_{V^*(\nu)} \epsilon(\nu,x)\, dV}{\int_{V(\nu)} \epsilon(\nu,x)\, dV} \tag{5.3}$$

where a is given by eqs.(5.1 a,b) and

$$C_R = \frac{\delta(\beta_s)\, \delta(\beta_2)^{2+\alpha_o}}{\delta(\beta_1)^{2+\alpha_o}} \tag{5.3a}$$

The product of the intrinsic synchrotron enhancement a_s and the relativistic correction factor C_R characterizes the "strength" of the variability. In fact, at fixed frequency and time, $C_R a_s$ determines the amplitude. It has the same role as $(1+k)(1+b)^{1+\alpha_0}$ in the preceding section. We will compute this factor as a function of β_1 and θ, for various values of u_1.

Two cases must be distinguished. In the first one, the fluid enters the shock from the far side of the jet and exits on the nozzle side, in the second one the opposite situation occurs. Fig. 6 may serve as reference for the definition of the kinematics of the two cases.

The shock velocity in the observer frame β_s should be directed outwards in order to guarantee the properties discussed in §IV. This agrees with observations of superluminal motions, though it should be recalled that the variability we are modelling originates in a different portion of the jet and may not be strictly related to the radio knots. In the first case $\beta_s = (\beta_1 + u_1)/(1+\beta_1 u_1)$. Therefore β_s is always larger than u_1 and a high value of β_s does not require a high value of β_1. In the second case $\beta_s = (\beta_1 - u_1)/(1-\beta_1 u_1)$ so that $\beta_1 > u_1$ is required in order to advect the shock front outwards and a large value of β_s implies large β_1. Another important difference between the two configurations is that in the first case the velocity of the shocked fluid is larger than that of the stationary one ($\beta_2 > \beta_1$), while the opposite is true for the second case.

The computed value of the product $C_R a_s$ for the first configuration, is shown in Fig. 7 a,b for two values of u_1. From the discussion in the previous section (§4.3) values of $C_R a_s$ consistent with observations should be of the order of $10 - 10^2$ for a thickness $h \simeq 1$, while larger values are required for thinner perturbations.

We can see that the amplitude is larger for small viewing angles. For a modest value of the upstream fluid velocity, $u_1 = 0.7$ (Fig. 7a), the intrinsic strength of the shock is barely sufficient to produce the observed variability amplitude. For $u_1 = 0.9$ the appropriate range is met for viewing angles less than 50^o (Fig. 7b). The amplitude decreases for increasing β_1 and the dependence on the viewing angle is stronger for high β_1. Recall that $\beta_s > u_1$ and is larger for larger β_1.

The alternative kinematic situation, in which the shock propagates backward in the frame of the fluid, is illustrated in Fig. 8 a,b, for the same values of the shock compression, determined by u_1, as in the previous case. Now, due to the fact that the shocked fluid has smaller velocity than the stationary one in the observer frame, relativistic corrections work against variability, reducing the computed amplitude parameter to insufficient levels, except for the most extreme values of β_1. Furthermore, except for the highest values of β_1 the amplitude is larger for larger viewing angles. We consider this case rather implausible, at least for the high frequency emitting region, although it is a choice adopted in modelling intensity and polarization variability in the radio band (Hughes, Aller and Aller 1989 a,b, Jones 1988).

VI. Discussion

We have shown that a simple model perturbation of fixed amplitude, traveling at constant speed along a jet of the type envisaged by Ghisellini, Maraschi and Treves (1985) produces X-ray and UV variability with well defined spectral properties, i.e. with amplitude increasing with increasing frequency. This property follows naturally

from the structure of the underlying stationary jet and is in agreement with the observations presently available. The above statement is valid for frequencies above the "break" in the stationary spectrum, which is usually observed to occur between the infrared and UV bands. In a frequency range of about one decade below the "break" frequency, the variability amplitude is independent of frequency. At still lower frequencies the evolution is dominated by opacity effects in the outer regions of the jet and our model does not extend thus far.

Within these general properties, which are common to all the models considered here, the light curves may follow two different types of behaviour: if the emission of the stationary jet is weakly weighted towards the outer regions ($\xi < 1$) the light curve maxima at all frequencies are strictly simultaneous, while for a jet heavily dominated by the outer regions the maxima occur later at lower frequencies ($\nu > \nu_b$). Data of sufficient quality to test these properties are not available yet. A cross correlation analysis of variability at different frequencies within the EXOSAT energy range (0.3-6 keV) for PKS 2155-304 (Tagliaferri *et al.* 1990) did not show evidence of delays larger than few hundreds of seconds. However the analysis was limited to small amplitude variability and to a narrow frequency range.

It is interesting that a relativistic shock wave can easily produce compression ratios sufficient to explain the observed amplitudes. A discussion of the origin of such shocks is beyond the scope of this paper, however it is worth mentioning that the perturbations envisaged here should maintain individuality for a few decades in path length ($10^{14} - 10^{16} cm$). They may extend further out to generate the emission knots observed at radio wavelengths with VLBI, but the present model does not include these scales. Since we have assumed that the perturbation is adiabatic, with constant amplitude over a wide range of distances, the associated energy should be substantial. Relativistic effects clearly alleviate the energy requirements for objects seen at small angles.

If the shock velocity in the frame of the stationary fluid is in the same direction as the jet stream, relativistic corrections enhance the variability amplitude observed at small angles for a relatively wide parameter range, while, for oppositely directed shocks, relativistic corrections reduce the observed amplitude at small angles, except for extreme values of the bulk velocity. Thus the first alternative predicts that sources

viewed at small angles not only appear brighter, but also more variable, a point raised by Lind and Blandford (1985) in connection with the radio emission. Here only moderate values of the bulk velocity are required. The second alternative allows a similar conclusion but only if $\beta_1 > 0.98$.

In conclusion the model offers an interesting framework to interpret the observed hardening of the the X-ray spectra of BL Lac Objects. It predicts a definite correlation of X-ray and UV variability, which can be measured by future campaigns of coordinated observations. In this respect the joint operation of IUE and ROSAT offers a unique opportunity.

The model also predicts that the X-ray variability and its correlation with variability at lower frequency should be different for BL Lac sources with steep and hard X-ray spectra, which are expected to emit respectively via the synchrotron and Compton mechanisms.

Acknowledgments

Useful discussions with G. Ghisellini are gratefully acknowledged. We thank Dr. P. Hughes for a critical reading of the manuscript. A.C. acknowledges a grant from the A. Della Riccia Foundation. This work was supported in part by Ministero Universitá e Ricerca Scientifica e Tecnologica.

Appendix A

Simple analytic expressions for the total monochromatic luminosity are given in the text, on the assumption of a homogeneous perturbed region and neglecting the shift in the range of frequencies emitted by the perturbed region, with respect to the stationary one.

These approximations are critical mainly in the case *ii*), of a conical perturbed region with increasing thickness, because the frequency range can be quite different in different parts of the emitting volume. Here we give the correct expressions for the luminosities L^1 and L^2, appearing in eqs. (4.3), which were used in the numerical computation of the spectra and the light curves.

The volume elements for a parabolic slab (case *i*) and a conical (case *ii*) perturbed regions are given respectively by

$$dV_p = \pi R_o^3 x^{2\epsilon} dx \qquad dV_c = \pi R_o^3 \left\{ [x - (x^* - \Delta x^*)] \frac{x^{*\epsilon}}{\Delta x^*} \right\}^2 dx \tag{A.1}$$

Let us consider three volumes: the volume of the perturbed region

$$V^*(t) = \int_{x^* - \Delta x^*}^{x^*} dV_i \tag{A.2}$$

where with dV_i we indicate the appropriate volume element given in eq. (A.1); the volume $V(\nu)$ of the parabolic stationary jet emitting at the given frequency

$$V(\nu) = \int_{x_1(\nu)}^{x_2(\nu)} \pi R_o^3 x^{2\epsilon} dx \tag{A.3}$$

and finally the perturbed volume emitting at frequency ν

$$V^*(\nu, t) = \int_{x_1^{**}(\nu)}^{x_2^{**}(\nu)} dV_i \tag{A.4}$$

where

$$\begin{aligned} x_1^{**}(\nu, t) &= max[x^* - \Delta x^*, x_1^*(\nu)] \\ x_2^{**}(\nu, t) &= min[x^*, x_2^*(\nu)] \end{aligned} \tag{A.5}$$

and x_1, x_2 and x_1^*, x_2^* are obtained inverting eqs.(3.3a), (3.3b) and (4.1a) respectively (in the range [1,x_{max}]).

Thus for the synchrotron luminosity we have:

$$L^1(\nu,t) = \int_{x_1^{**}(\nu)}^{x_2^{**}(\nu)} 4\pi^2 R_o^3 \epsilon^* x^{2\epsilon} dx \qquad \text{case } i$$

or

$$L^1(\nu,t) = \int_{x_1^{**}(\nu)}^{x_2^{**}(\nu)} 4\pi^2 R_o^3 \epsilon^* \left\{ [x - (x^* - \Delta x^*)] \frac{x^{*\epsilon}}{\Delta x^*} \right\}^2 dx \qquad \text{case } ii \qquad (A.6)$$

and for $L^2(\nu,t)$

$$L^2(\nu,t) = L^{st}(\nu) - \int_{\hat{x}_1(\nu)}^{\hat{x}_2(\nu)} 4\pi^2 R_o^3 \epsilon x^{2\epsilon} dx \qquad \text{case } i$$

or

$$L^2(\nu,t) = L^{st}(\nu) - \int_{\hat{x}_1(\nu)}^{\hat{x}_2(\nu)} 4\pi^2 R_o^3 \epsilon \left\{ [x - (x^* - \Delta x^*)] \frac{x^{*\epsilon}}{\Delta x^*} \right\}^2 dx \qquad \text{case } ii \qquad (A.7)$$

where the last integral is extended to the perturbed part of $V(\nu)$ and the extremes are given by

$$\begin{aligned} \hat{x}_1(\nu,t) &= max[x^* - \Delta x^*, x_1(\nu)] \\ \hat{x}_2(\nu,t) &= min[x^*, x_2(\nu)] \end{aligned} \qquad (A.8)$$

Analogous expressions are used for Compton emission with the appropriate values of the integration limits.

Table 1. Specific Variability v

	N	5500 Å	2500Å	1500Å	0.2 keV	3 keV
1H 0414+009	4				0.05	0.26
Mrk 421	14		0.16	0.18	0.45	1.12
Mrk 180	3				0.37	0.73
1218+304	9				0.16	0.24
Mrk 501	9				0.05	0.26
PKS 2005-489	5				0.84	1.17
PKS 2155+304	9	0.26	0.27	0.37	0.43	0.65

N is the number of X–ray observations.

Table 2. Model parameters

	B_0	K_0	R_{max}	α_0	ϵ	ξ	η
a)	$\cdot 10^3$	$5\ 10^9$	10^{17}	0.75	0.4	0.49	0.98
b)	900	10^6	10^{16}	0.5	0.5	1.15	1.3

Model parameters for case a) and b). The model parameters are defined in the text, and are given in cgs units, R_{max} is the length of the jet. For both cases $\beta_p = 0.9$, $b = k = 4$ and $R_o = 10^{14}$.

Table 3. Computed $v(\nu)$

		5500-2500 Å	1500 Å	0.2 keV	3.0 keV
M=1	*a*) *i*)	0.016	0.017	0.12	0.95
	a) *ii*)	0.011	0.012	0.22	1.14
	b) *i*)	0.017	0.017	0.49	3.93
	b) *ii*)	0.15	0.15	0.82	3.38
M=6	*b*) *ii*)	0.20	0.20	0.70	1.54

The table reports the values of the variability parameter $v(\nu)$ for different jet parameters and characteristic of the perturbation (cases *a*, *b* and *i*, *ii*). In all these cases k=2 and b=2 were adopted for the intensity of the perturbation. The total number of "simulated observations" is always N=500, while M indicates the number of crossing periods of the perturbation through the whole jet, during which the "observations" are sampled.

References

Blandford, R.D., and Rees, M.J., 1978, in *Pittsburgh Conference on BL Lac Objects*, ed. A.N. Wolfe (Pittsburgh University Press), p. 328.

Bregman, J.N., *et al.* 1990, *Astrophys. J.*, **352**, 574.

Celotti, A., Maraschi, L., and Treves, A., 1989, in *BL Lac Objects*, eds. L. Maraschi, T. Maccacaro and M–H. Ulrich (Springer–Verlag), p. 332.

George, I.M., Warwick, R.S, and Bromage, G.E., 1988, *Mon.Not.R.astr.Soc.*, **232**, 793.

George, I.M., Warwick, R.S., and McHardy, I.M., 1988, *Mon.Not.R.astr.Soc.*, **235**, 787.

Ghisellini, G., and Maraschi, L., 1989, *Astrophys. J.*, **340**, 181.

Ghisellini, G., Maraschi, L., and Treves, A., 1985, *Astron. Astrophys.*, **146**, 204. (GMT)

Giommi, P., Barr, P., Garilli, B., Gioia, I.M., Maccacaro, T., Maccagni, D., and Schild, R.E., 1987, *Astrophys. J.*, **322**, 662.

Giommi, P., *et al.* , 1989, in *BL Lac Objects*, eds. L. Maraschi, T. Maccacaro and M–H. Ulrich (Springer–Verlag), p. 231.

Giommi, P., Barr, P., Garilli, B., Maccagni, D., and Pollock, A.M.T., 1990, *Astrophys. J.*, **356**, 432.

Hackney, R.L., Hackney, K.R., and Kondo, Y., 1982, in *Advances in UV Astronomy: Four Years of IUE* (NASA CP2238), p. 335.

Hughes, P.A., Aller, H.D., and Aller, M.F., 1989a, *Astrophys. J.*, **341**, 54.

Hughes, P.A., Aller, H.D., and Aller, M.F., 1989b, *Astrophys. J.*, **341**, 68.

Impey, C.D., and Neugebauer, G., 1988, *Astron. J.*, **95**, 307.

Jones, T.W., 1988, *Astrophys. J.*, **332**, 678.

Königl, A., 1980, *Phys. Fluids*, **23**, 1083.

Königl, A., 1989, in *BL Lac Objects*, eds. L. Maraschi, T. Maccacaro and M–H. Ulrich (Springer–Verlag), p. 321.

Lind, K.R., and Blandford, R.D., 1985, *Astrophys. J.*, **295**, 358.

Maccacaro, T., Gioia, I.M., Schild, R.E., Wolter, A., Morris, S.L., and Stocke, J.T.,

1989, in *BL Lac Objects*, eds. L. Maraschi, T. Maccacaro and M–H. Ulrich (Springer–Verlag), p. 222.

Maraschi, L., Tagliaferri, G., Tanzi, E.G. and Treves, A., 1986a, *Astrophys. J.*, **304**, 637.

Maraschi, L., Ghisellini, G., Tanzi, E.G., and Treves, A., 1986b, *Astrophys. J.*, **310**, 325.

Maraschi, L. and Maccagni, D., 1988, Mem.S.A.It., 59, 277.

Maraschi, L., Celotti, A., and Treves, A., 1989, in *Proc. 23th ESLAB Symp: "X-ray Astronomy"*, ESA SP–296, p. 825.

Marscher, A.P., 1980, *Astrophys. J.*, **235**, 386.

Marscher, A.P., and Gear, W.K., 1985, *Astrophys. J.*, **298**, 114.

O'Dell, S.L., 1988, *Astrophys. J.*, **327**, 60.

Peacock,J.A., 1981, *Mon.Not.R.astr.Soc.*, **196**, 135.

Schneider, P., and Kirk, J.G., 1989, *Astron. Astrophys.*, **217**, 344.

Stocke, J.T., *et al.* , 1985, *Astrophys. J.*, **298**, 619.

Tagliaferri, G., Stella, L., Maraschi, L., Treves, A., and Celotti, A., 1990, *Astrophys. J.*, submitted.

Treves, A., *et al.* , 1989, *Astrophys. J.*, **341**, 733.

Worrall, D.M., and Wilkes, B.J., 1990. *Astrophys. J.*, **360**, 396.

Figure Captions

Figure 1 a,b. Synchrotron (solid lines) and inverse Compton (dashed lines) spectra emitted by jet models *a*) and *b*) respectively: The continuous line without label refers to the stationary spectrum. The spectra emitted 1 hour, 1 day and 1 week (or 3 days) after the start of the perturbation at the jet nozzle are labelled accordingly. The perturbation is assumed to have a constant thickness (case *i*).

Figure 2 a,b. The same as Fig. 1 for a perturbation with growing thickness (case *ii*).

Figure 3 a,b. Synchrotron light curves at different frequencies are shown for model *a*) and *b*) respectively, for a perturbation of constant thickness (case *i*). The monochromatic luminosities are normalized to the stationary ones at the same frequency. Both scales are logarithmic.

Figure 4 a,b. Light curves as in Figs. 3, but the thickness of the perturbed region increases with time (case *ii*).

Figure 5. Synchrotron (solid lines) and inverse Compton (dashed lines) light curves at the same frequency, $\nu = 2\ 10^{17}\ Hz$, are compared. Labels denote jet model *a*), case *i*) and jet model *b*) case *ii*). The monochromatic luminosities are normalized to their stationary values. Both scales are logarithmic.

Figure 6. Schematic representations of the kinematic of a planar shock: (left) upstream fluid on the outer side of the jet, (right) upstream fluid on the inner side of the jet. The upper panels show the kinematic in the shock frame, while the lower ones refer to the frame of the observer. Note the different relation between β_1, β_2

and β_s.

Figure 7 a,b. The amplitude parameter $C_R\ a_s$computed with relativistic corrections for a planar shock (see text for precise definitions) is plotted as a function of the unperturbed fluid velocity β_1 for different values of the angle of view θ, for a case in which the upstream fluid enters the shock from the far side of the jet. The upstream velocities, determining the shock strength, are $u_1 = 0.7$ (panel a) and $u_1 = 0.9$ (panel b).The spectral index is $\alpha = 0.75$.

Figure 8 a,b. The same amplitude parameter as in Figs. 7 is computed for a "reverse" shock, in which the unperturbed fluid enters the shock from the "nozzle" side for the same values of u_1 and β_1.

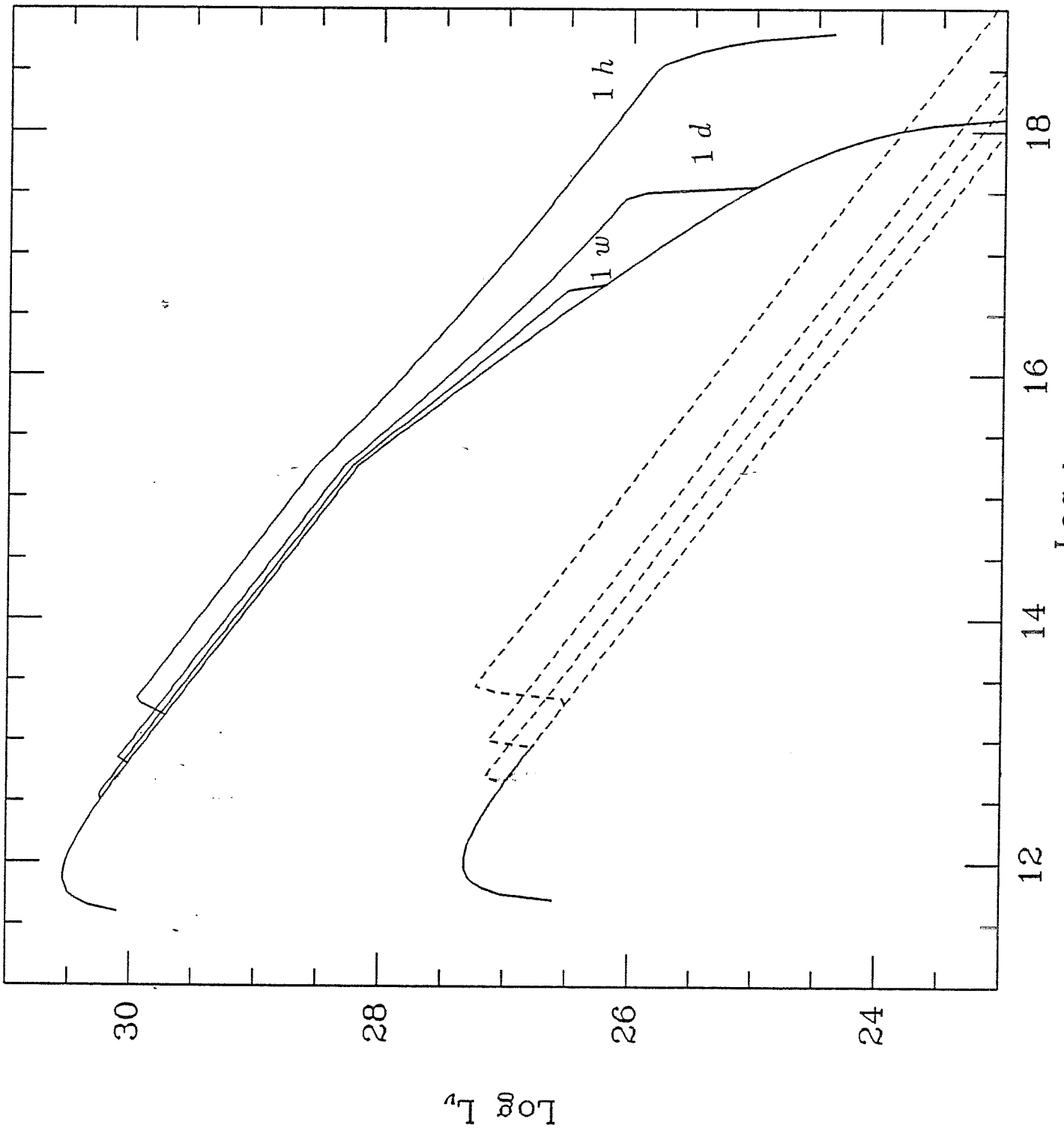

Fig. 1a

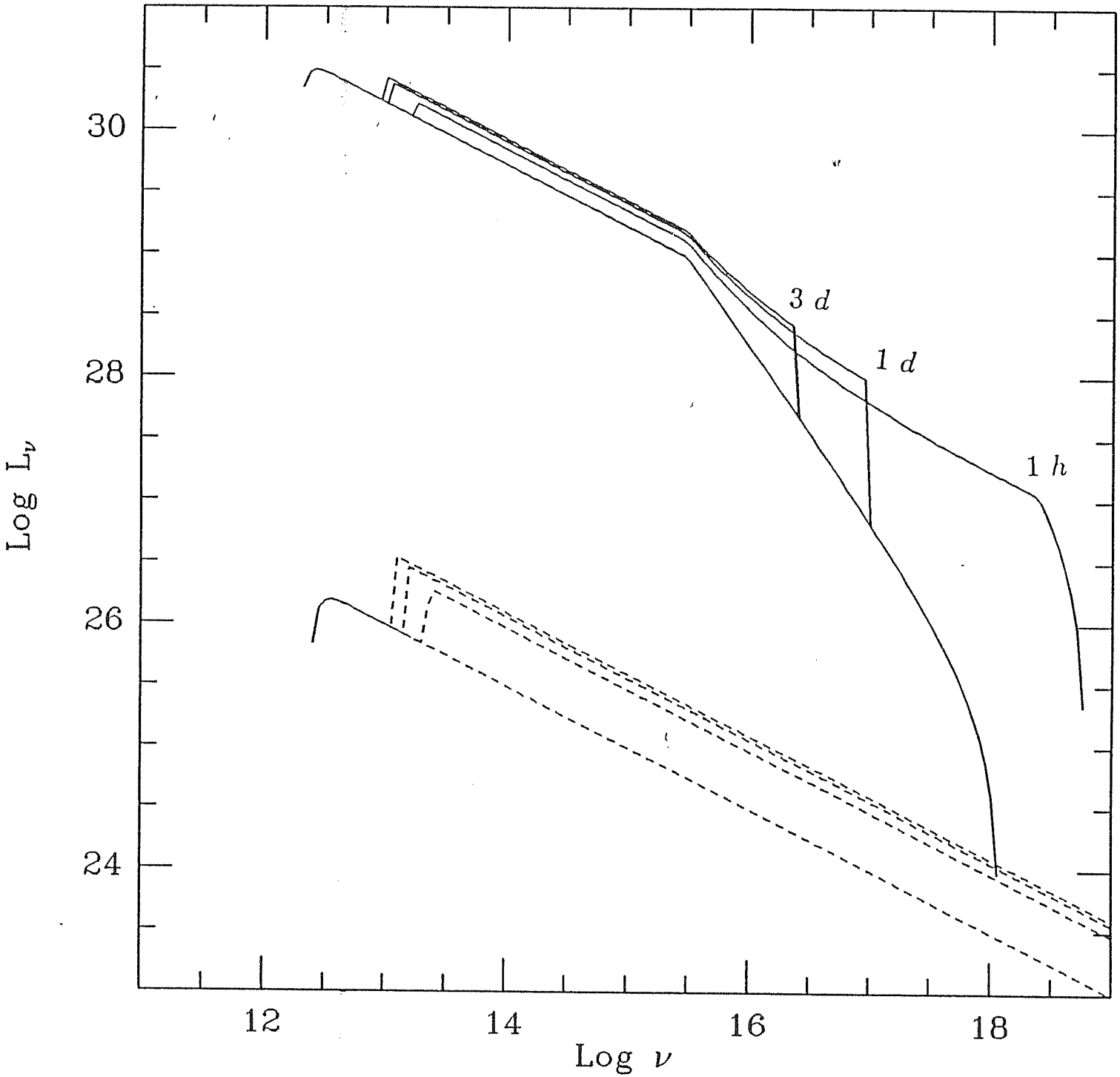

Fig. 1b

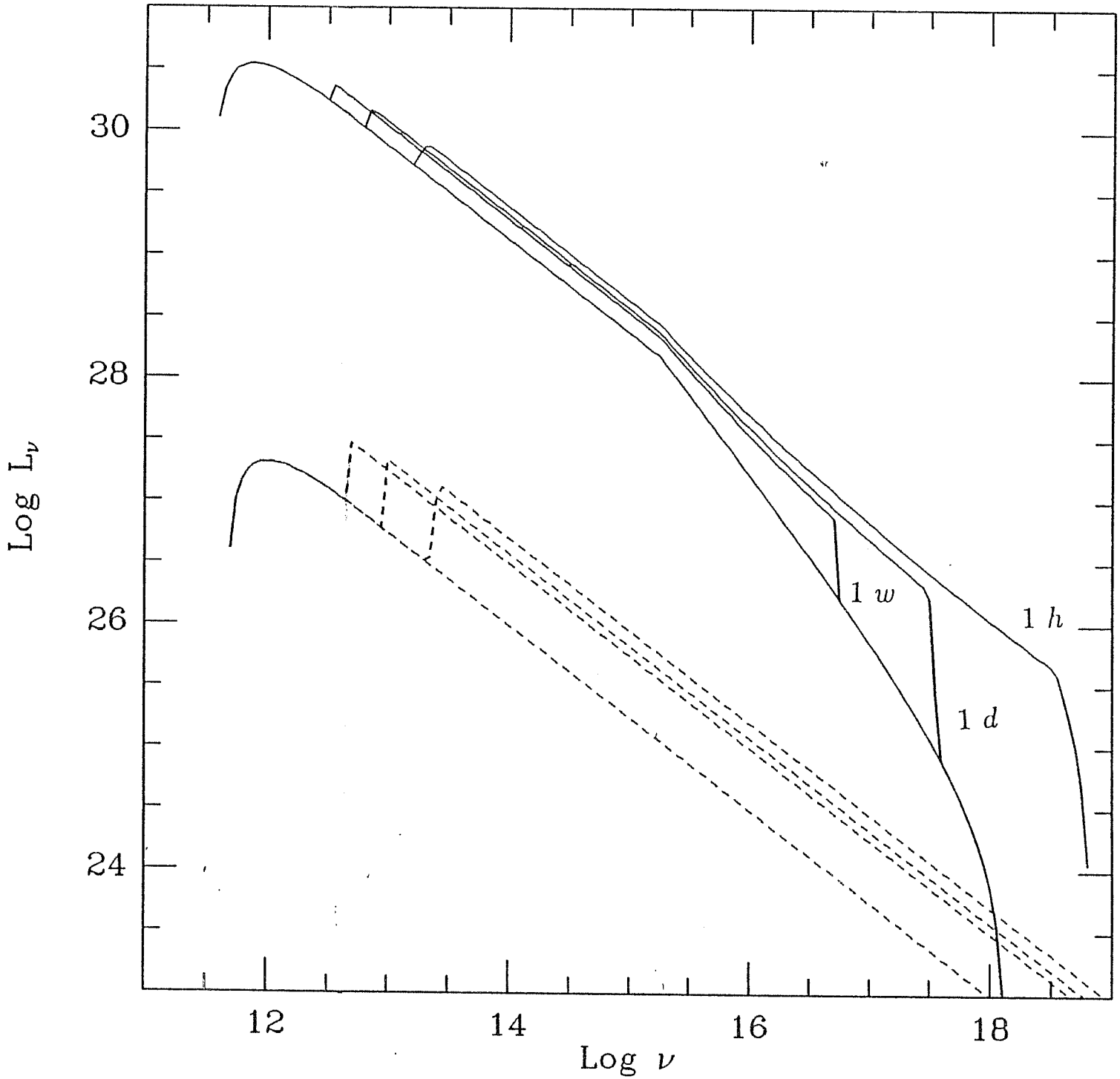
30
28
26
24
Log L_ν
12
14
16
18
Log ν
1 w
1 d
1 h

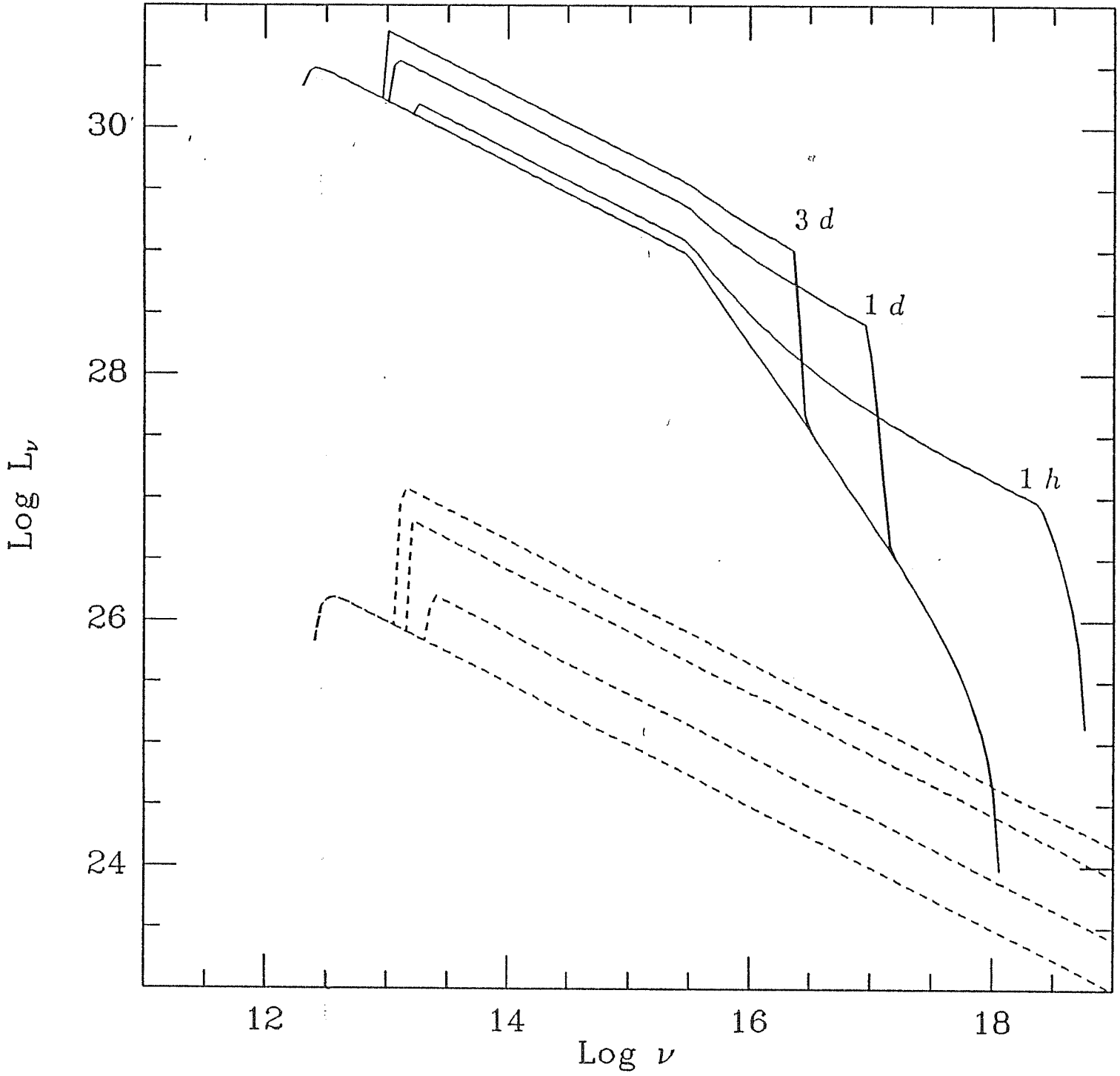

Fig. 2

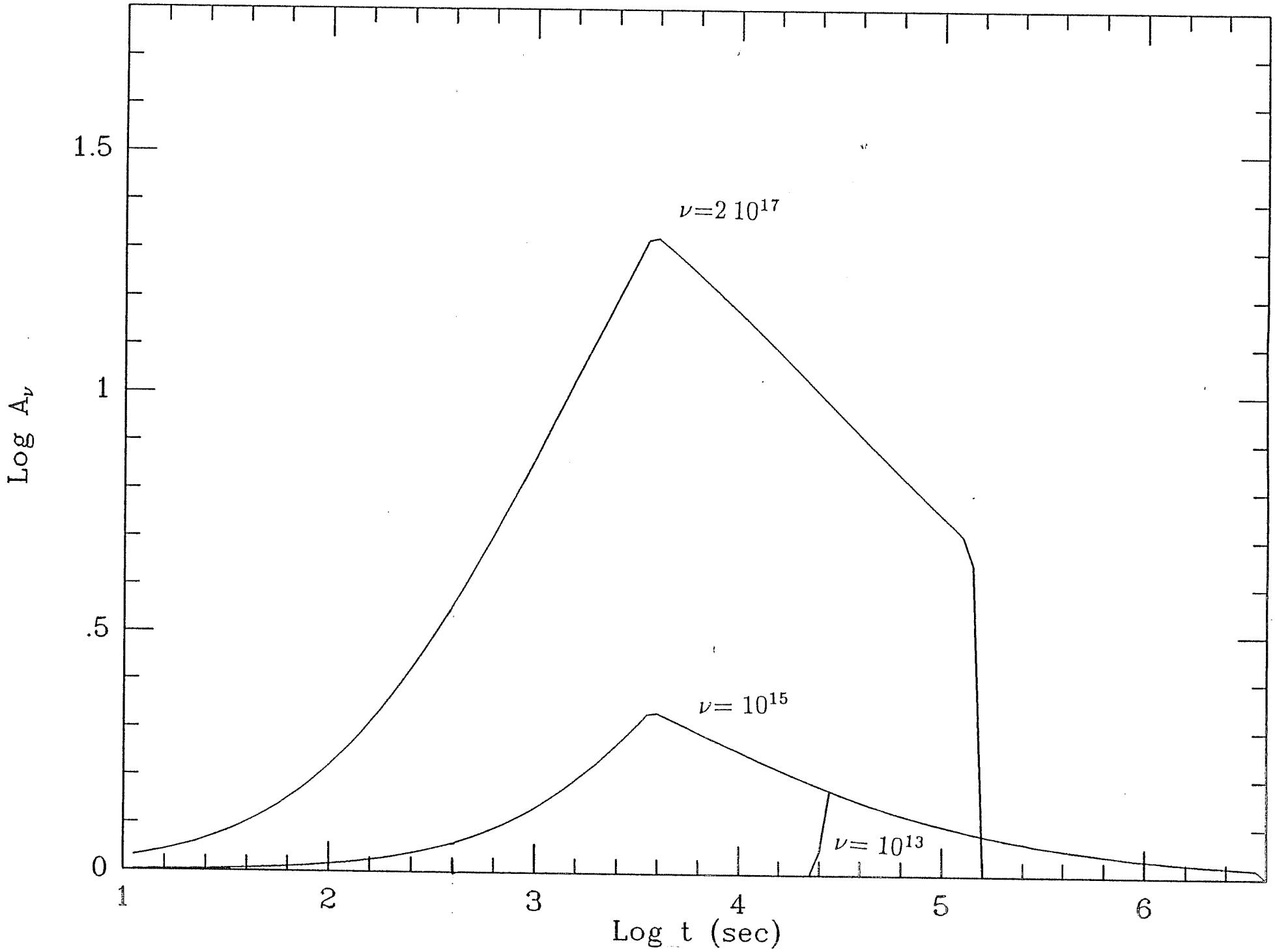
1.5
1
.5
0
Log A_ν
ν=2 10^{17}
ν= 10^{15}
ν= 10^{13}
1
2
3
4
5
6
Log t (sec)

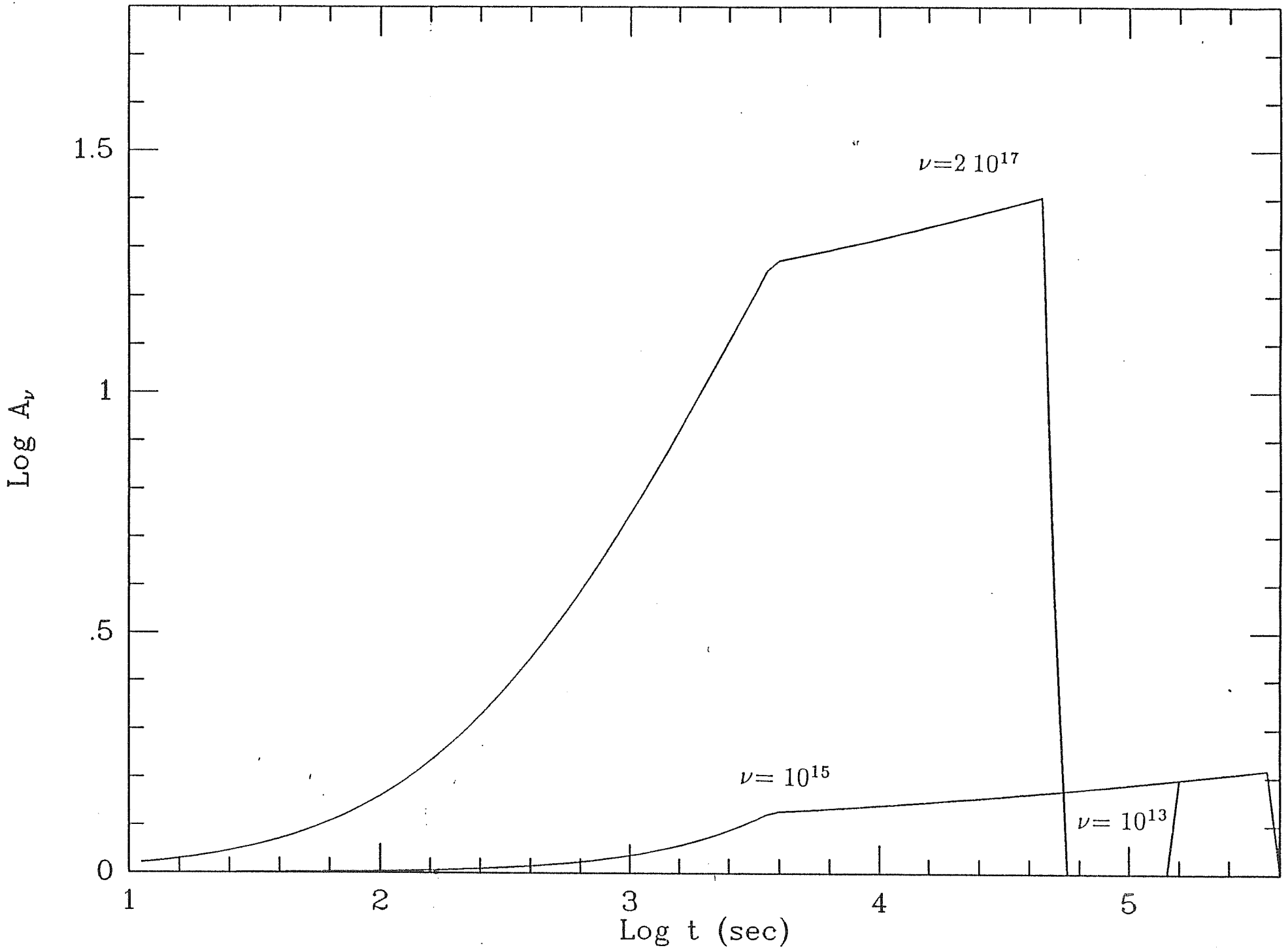
1.5
1
.5
0
Log A_ν
ν=2 10^{17}
ν= 10^{15}
ν= 10^{13}
1
2
3
4
5
Log t (sec)

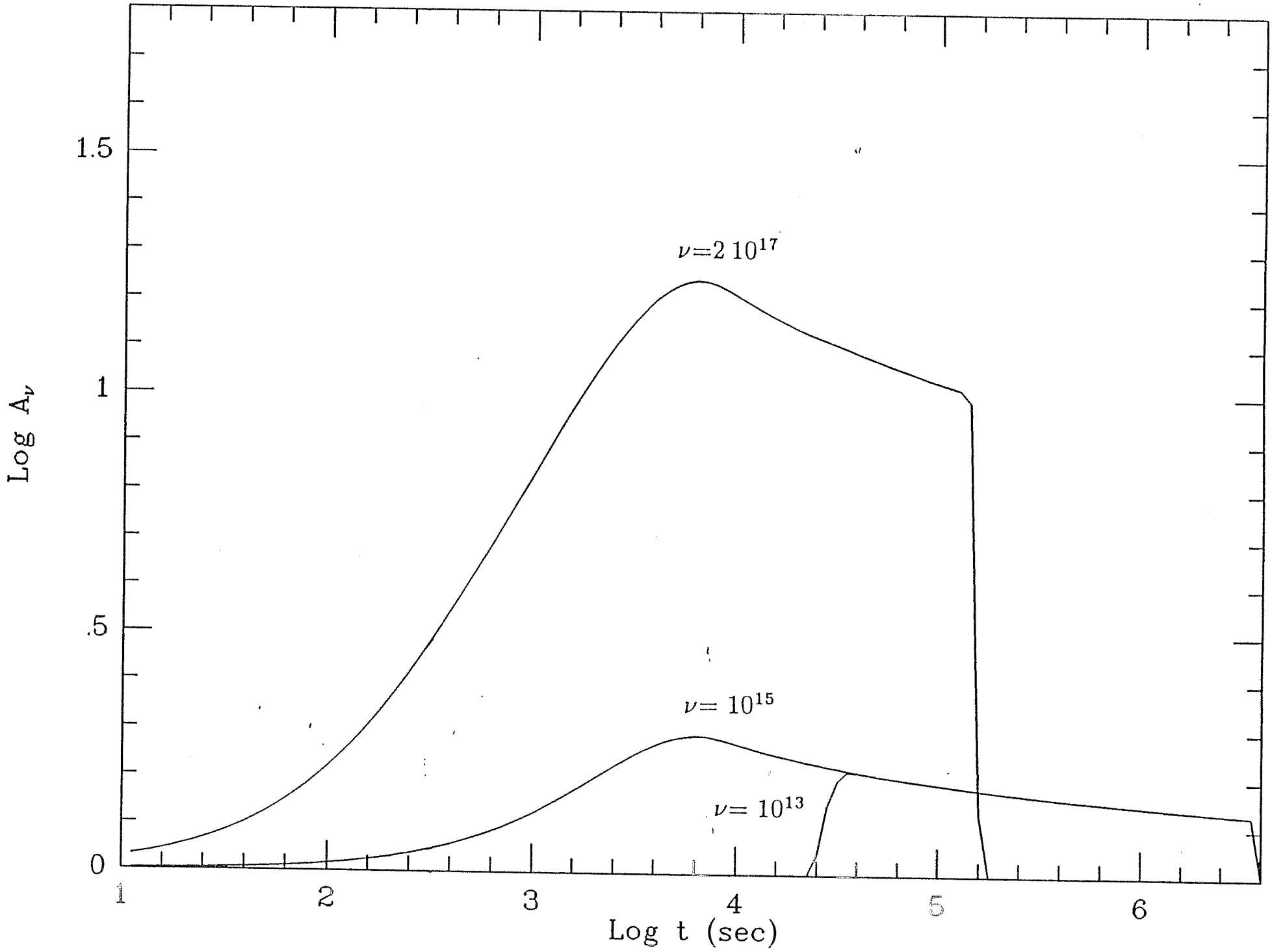
1.5
1
.5
0
Log A_ν
ν=2 10^{17}
ν= 10^{15}
ν= 10^{13}
1
2
3
4
5
6
Log t (sec)

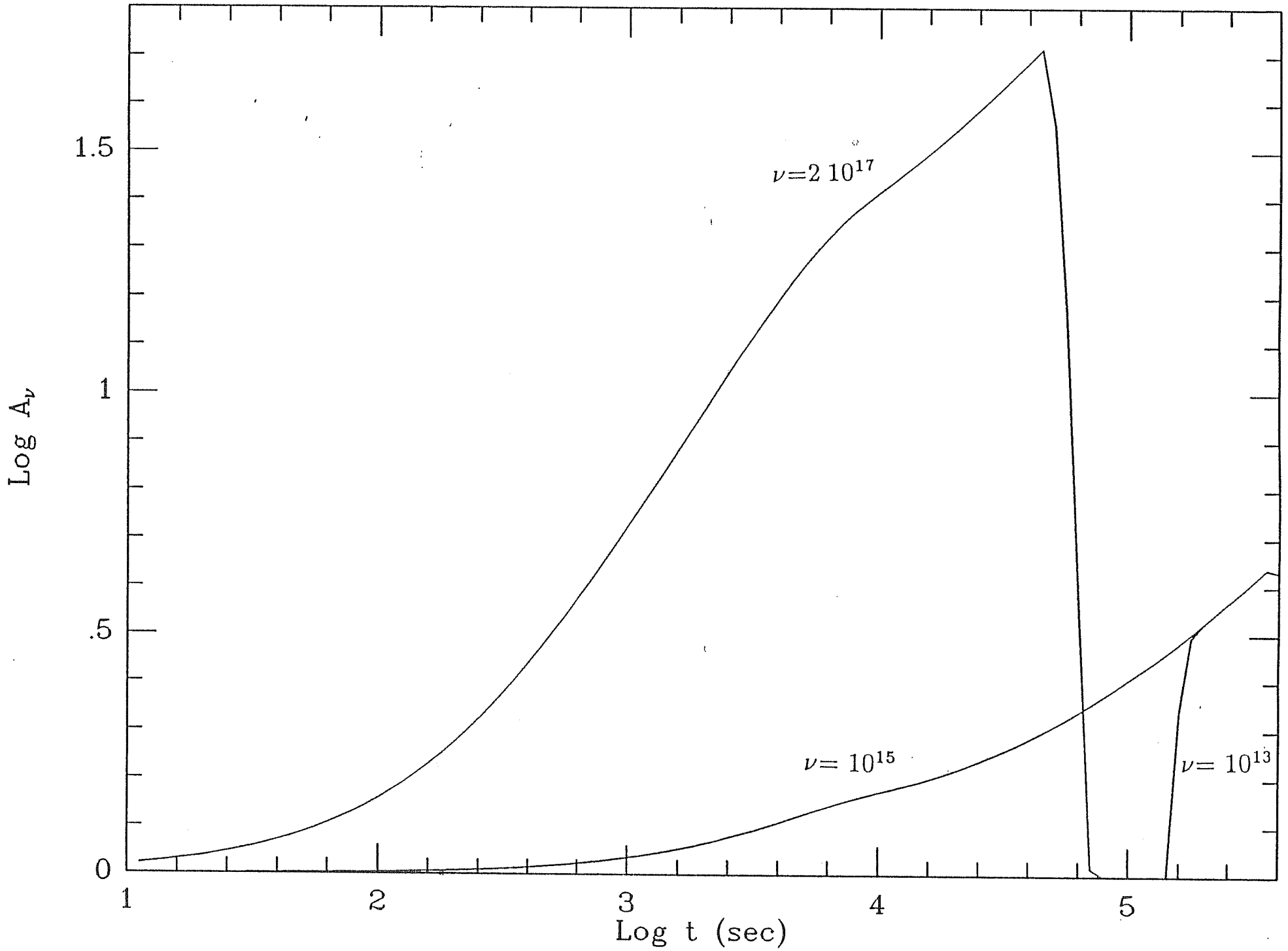
1.5
1
.5
0
Log A_ν
ν=2 10^{17}
ν= 10^{15}
ν= 10^{13}
1
2
3
4
5
Log t (sec)

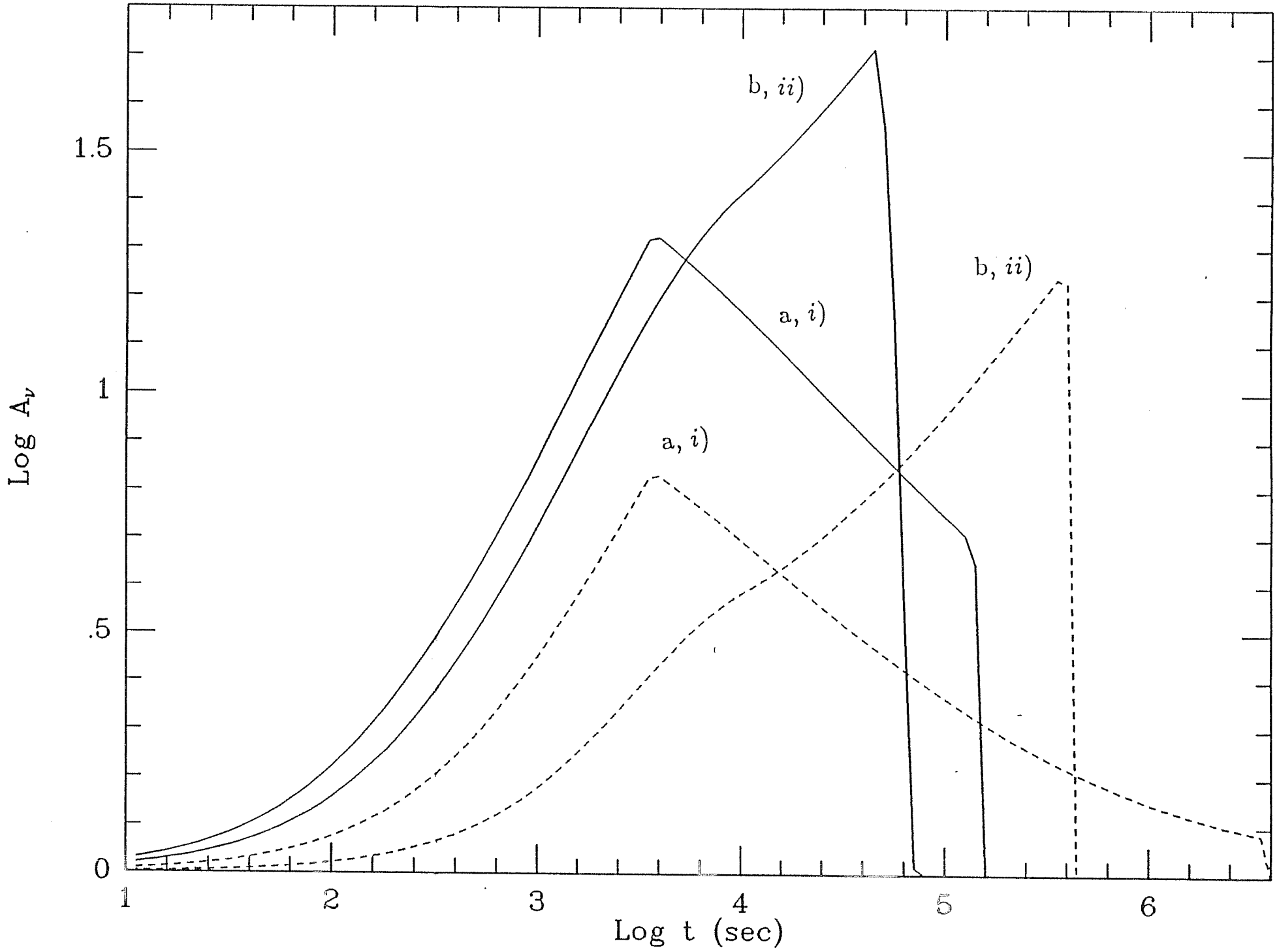

Fig. 5

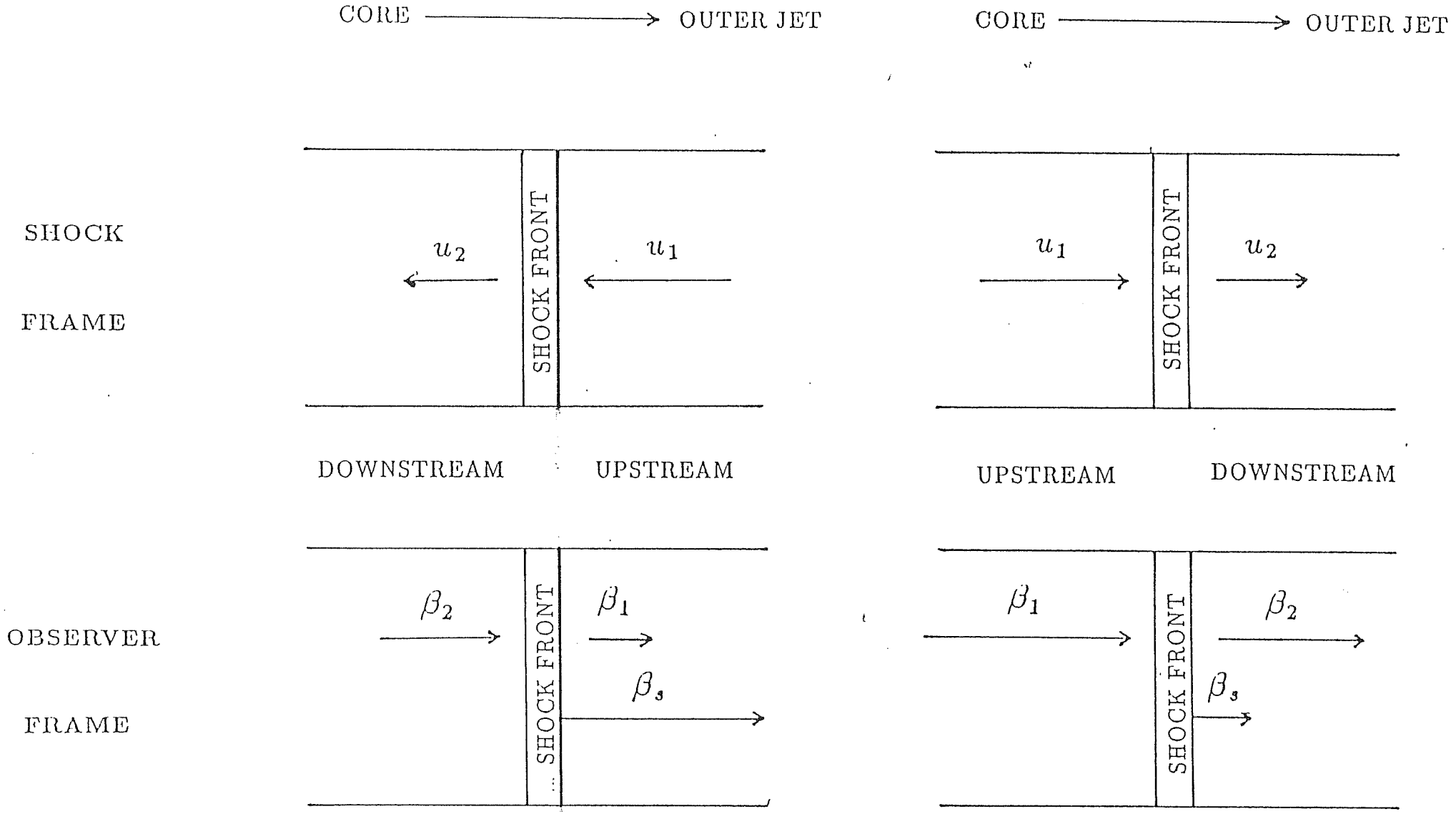
CORE
OUTER JET
CORE
OUTER JET
SHOCK
FRAME
SHOCK FRONT
u_2
u_1
u_1
u_2
DOWNSTREAM
UPSTREAM
UPSTREAM
DOWNSTREAM
OBSERVER
FRAME
SHOCK FRONT
β_2
β_1
β_s
β_1
β_2
β_s

Fig. 6

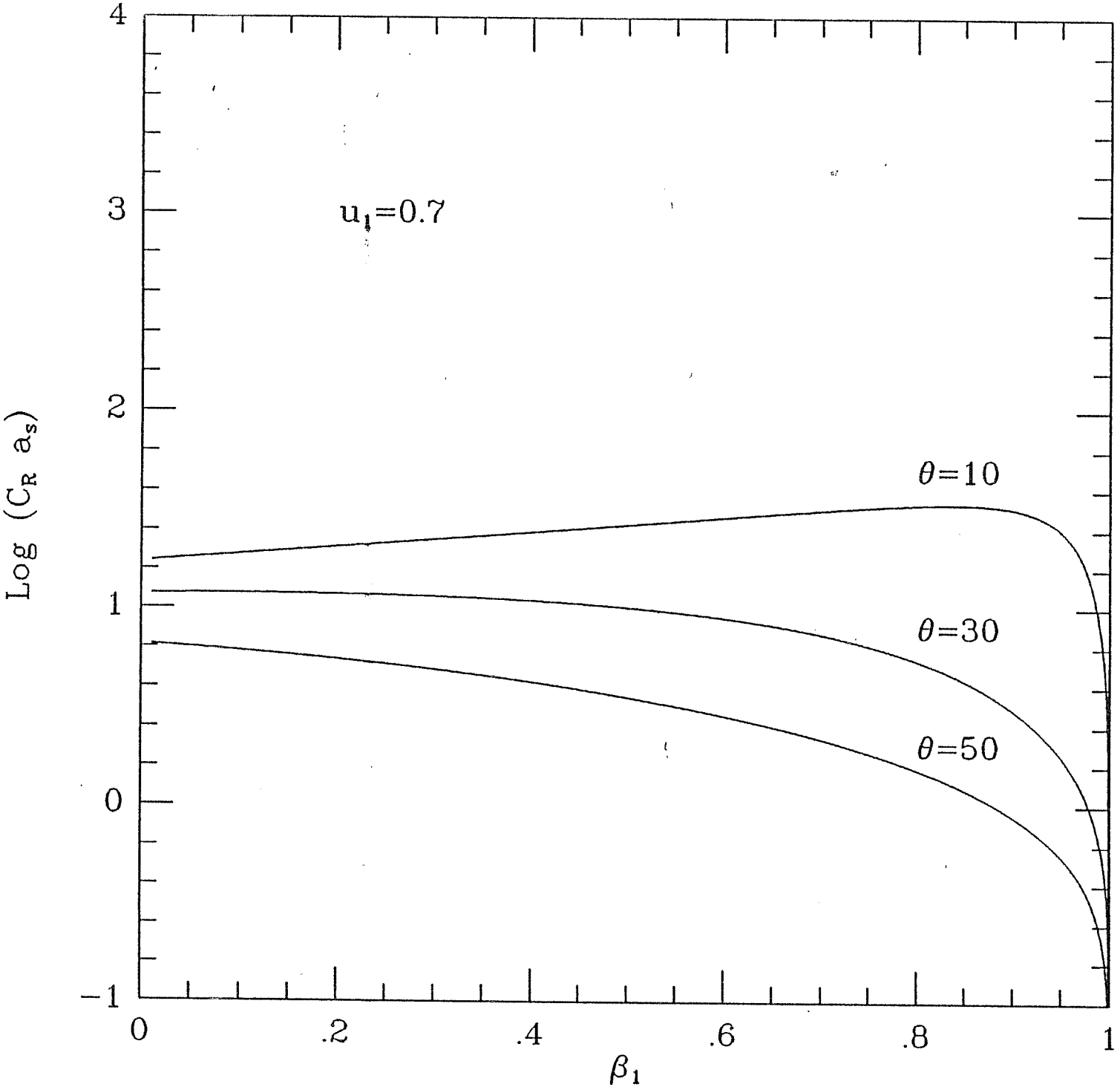

Fig. 7a

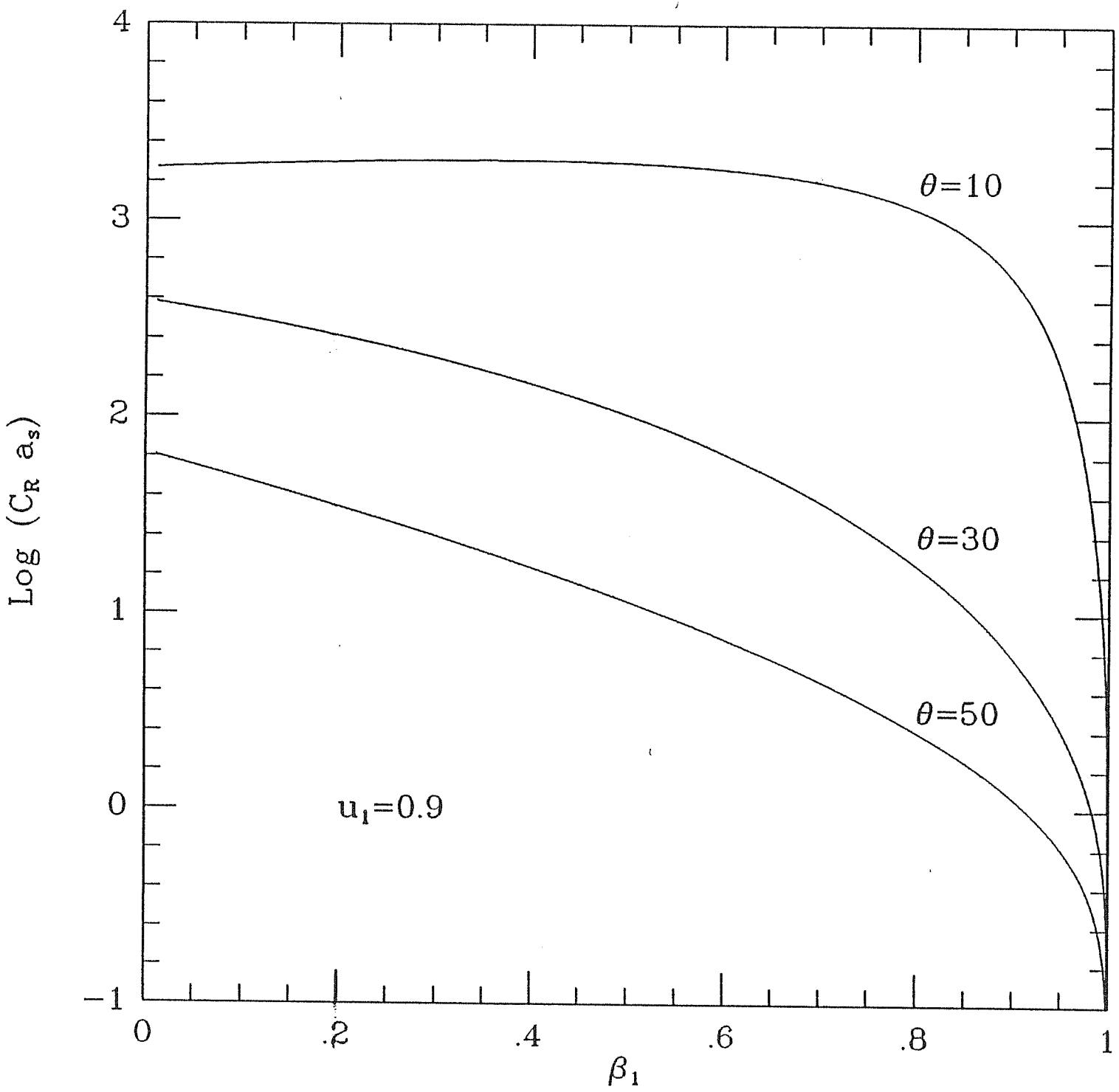

Fig. 7b

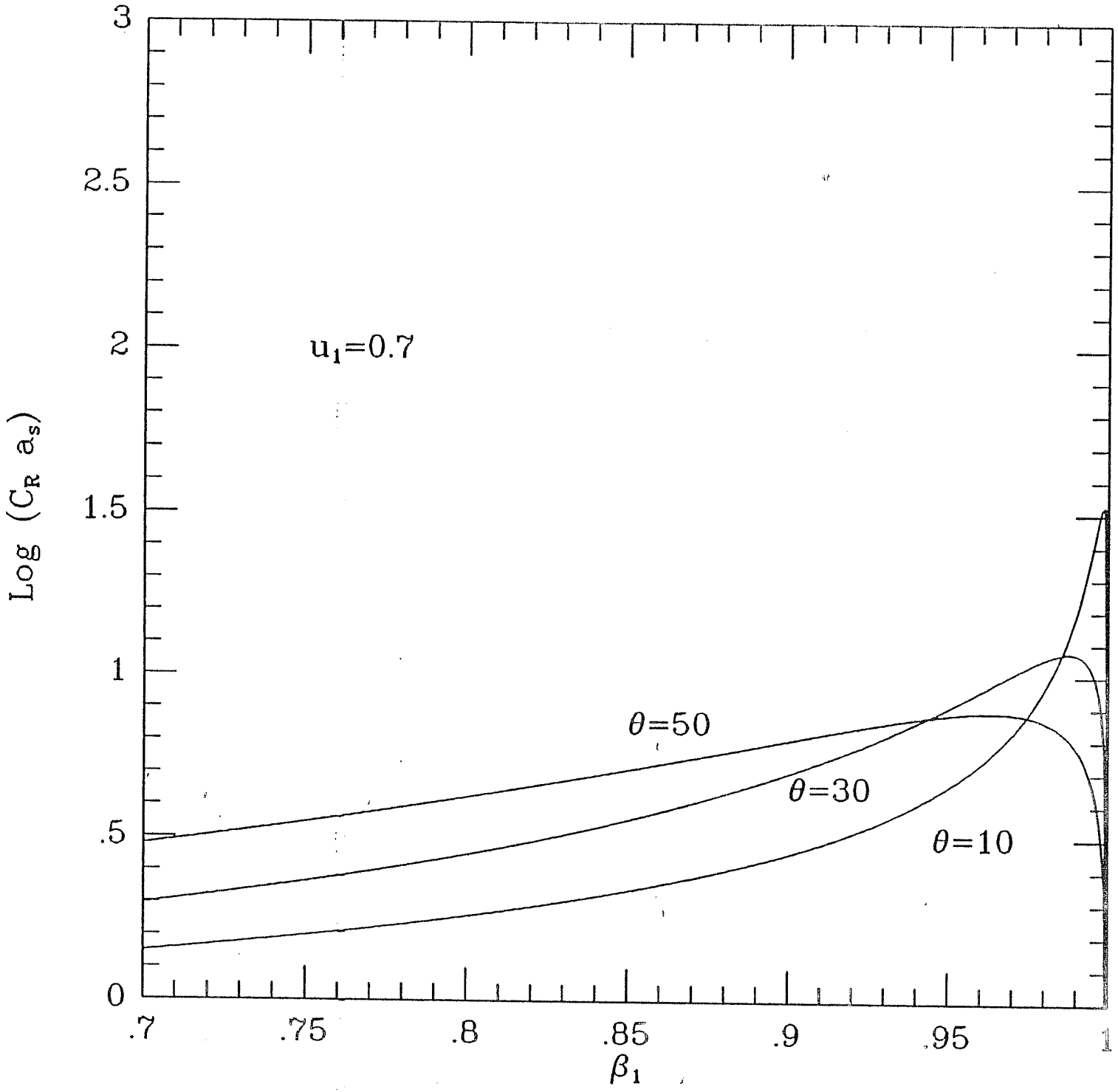
3
2.5
2
1.5
1
.5
0
Log (C_R a_s)
u_1=0.7
θ=50
θ=30
θ=10
.7
.75
.8
.85
.9
.95
1
β_1

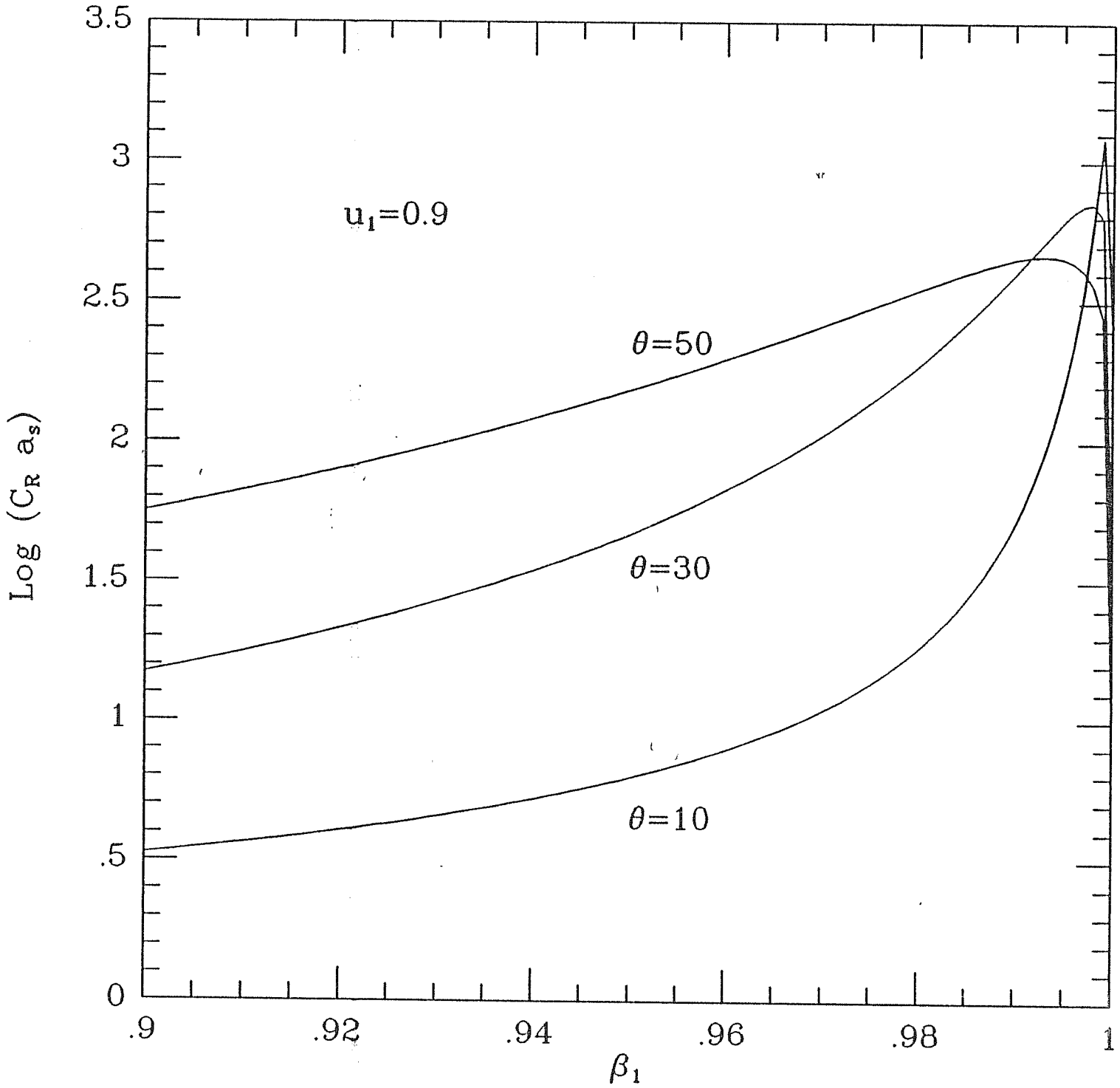
3.5
3
2.5
2
1.5
1
.5
0
.9
.92
.94
.96
.98
1
u_1=0.9
θ=50
θ=30
θ=10
Log (C_R a_s)
β_1

Fig. 81

Appendix B

X–ray variability of PKS 255–304

Short-term X-Ray Variability of the BL Lac Object PKS2155-304: Power Spectrum and Cross-Correlation Analysis

G. Tagliaferri[1], L. Stella[2,1,*], L. Maraschi[3],
A. Treves[3,4] and A. Celotti[4]

EXOSAT Preprint No. 130

[1] EXOSAT Observatory, Astrophysics Division, Space Science Department of ESA, ESTEC, Keplerlaan 1, 2200 AG Noordwijk, The Netherlands
[2] Osservatorio Astronomico di Brera, Via Brera 28, 20121 Milano, Italy
[3] Università di Milano, Dipartimento di Fisica, Via Celoria 16, 20133 Milano, Italy
[4] International School for Advanced Studies, Strada Costiera 11, 34014 Trieste, Italy
* Affiliated to I.C.R.A.

Accepted for publication in the Astrophysical Journal

Abstract

We present a detailed power spectrum and cross-correlation analysis of the X-ray light curves of the BL Lac object PKS 2155-304, obtained with EXOSAT. The power spectra show a marked *red noise*-type variability, with the power increasing steeply towards low frequency. The variability is more pronounced in the 1-6 keV band than in the 0.1-2 keV band. We show that the presence of data gaps (though limited to $< 20\%$ in the EXOSAT light curves) can flatten significantly the logarithmic slope of the power spectrum. A technique for bridging data gaps which reduces the power spectrum distortions is introduced. In this way an average power law slope of about -2.5 is obtained for the power spectrum from the 1-6 keV data. The average power spectrum of the light curves after the removal of a linear trend, as required in this case, is characterised by a slope of -1.9 ± 0.4 over the $10^{-4} - 3 \times 10^{-3}$ Hz frequency range. Longer observations and alternative power spectrum estimation techniques are required to further investigate the red noise properties of PKS 2155-304.

The 3-6 keV light curves are cross-correlated with the 0.1-2 keV and the 1-2 keV light curves, separately. We show that spurious time lags can be introduced by systematic uncertainties related to the swapping of the EXOSAT medium energy detectors and the switching on and off of the instruments. If these effects are taken into account no evidence of lags is found, with upper limits of a few hundred seconds. The short-term X-ray variability of PKS 2155-304 is compared with that of Seyfert galaxies and is briefly discussed within the framework of BL Lac emission models.

Subject headings: BL Lacertae objects - galaxies: individual - X-rays: sources.

1. Introduction

Short term (≤ 1000 s) X-ray variability provides a tool to investigate some of the basic properties of the "central engine" of active galactic nuclei (AGN); in particular it can be used to place constraints on emission mechanisms, the size of the emitting region and the efficiency of the mass/radiation conversion process (Fabian 1986 and references therein).

Long and relatively uninterrupted EXOSAT observations of Seyfert galaxies have revealed pronounced variability on all time scales longer than 200-300 seconds (e.g. Pounds and McHardy 1988; McHardy 1989). In most cases the power spectra are featureless and show little or no evidence for a characteristic variability timescales (see, however, the cases of NGC6814, Mittaz and Branduardi-Raymont 1989, and NGC4151, Fiore et al. 1989).

Here we apply power-spectrum and cross-correlation techniques to the EXOSAT light curves of the BL Lac object PKS 2155-304, which is the brightest of its class in X-rays. To our knowledge this is the first time that this type of analysis has been carried out for the X-ray light curves of a BL Lac object. In particular we explore the consequences of a number of systematic effects related to the uncertainties in the background subtraction of the EXOSAT ME detector, the presence of short duration data gaps and the lack of strict simultaneousness of the LE and ME light curves.

The paper is organized as follows: the light curves and power spectrum analysis are described in § 2; in § 3 we present the cross-correlation analysis; the significance of our results in the light of current models for BL Lac objects is discussed in § 4.

2. X-ray Light Curves and Power Spectrum Analysis

PKS 2155-304 was observed in the 0.1-10 keV band for a total of 80 hours at 9 epochs between 1983 and 1986 with the EXOSAT observatory (see White and Peacock 1988 for a description of the instruments). An extensive analysis of spectral data together with a presentation of the X-ray light curves can be found in Morini et al. (1987) and Treves et al. (1989) (see also Giommi et al. 1990). Here we perform a detailed analysis of the short-term variability using light curves from the low energy (LE) instrument of nominal energy range 0.05-2 keV (De Korte et al. 1981) and from the Argon chambers of the medium energy experiment (ME) (1-25 keV; Turner et al. 1981).

Table 1 gives the duration of the ME observations, the mean ME count rate in the 1-7.5 keV band, the number of array swaps (*i.e.* the interchange between the ME half detector pointing at the source and the half monitoring the background), and the duration and count rate in the CMA observation carried out with the 3000 Å Lexan filter. Table 1

reports also the *rms* fractional variability of the light curves with 300 s and 100 s resolution for the LE and the ME, respectively. It is apparent that the 1-7.5 keV light curves are characterised by a very strong variability (up to $\sim 50\%$ *rms*), whereas the low energy light curves (0.1-2 keV) are somewhat less variable.

During the three observations when the source was brightest, 1984 Nov 6 and 7 and 1985 Oct 24, the ME flux underwent variations by factors of about 3, 6 and 1.5 respectively, on time scales of a few hours (see Fig. 1). For these observations power spectra were calculated for the background subtracted 1-7.5 keV ME light curves with 10 s time resolution. The power spectrum of the 0.1-2 keV light curve from the LE (due to galactic absorption, a negligible signal is expected below 0.1 keV) was calculated only for the 1985 Oct 24 observation. During the 1984 Nov 6 and 7 observations more than one filter was used in front of the CMA, and, therefore, the LE light curves are divided in a number of short intervals (see Treves et al. 1989). The analysis was carried out with a direct Fourier transform algorithm for each observation in intervals of 1850 points, sampling a maximum duration of 18500 seconds. The long observation of 1985 Oct 24 contained three of these intervals in both the LE and ME. The mean count rate in each interval was subtracted.

We first carried out the analysis, as customary, by replacing the data gaps, mainly due to the swapping of the ME detector arrays, with zeroes. Despite the fact that the light curves contained only a small fraction of data gaps ($< 20\%$), this gap filling procedure was determined to affect strongly the derived spectral shape. For example the power spectrum of the November 7 observation calculated in this way showed a *red noise* component towards low frequencies which could be well approximated by a power law of slope ~ -1.3 (see Tagliaferri et al. 1989). However the power spectrum of the window function displayed also a power law-type of behaviour with a similar slope, therefore suggesting that the calculated *red noise* slope of the light curve power spectrum could be artificially increased by the high frequency power introduced by the window function. In the time domain this can be seen as follows: gaps replaced by zeroes introduce spurious spikes in the light curve, which, especially in the presence of long term trends, artificially increase the high frequency power in the power spectra.

To avoid these distortions we adopted another gap filling procedure which consisted

in replacing the data gaps with the moving average of the light curve calculated over a duration of 1 hr. By doing this data gaps are bridged in a smoother way which reduces the bias introduced by the window function. The power spectral slope obtained in this case for the November 7 observation is ~ -2. We determined that this slope is rather insensitive to the duration over which the moving average is calculated, as long as this duration is substantially shorter than the interval duration (such that the moving average follows the light curve behaviour on timescales of hours) and longer than the data gaps (such that data gaps are bridged with the moving average from a relatively high number of points and the statistical fluctuations are reduced).

The ME light curves and power spectra obtained in this way from individual observations are shown in Fig. 1. The power spectra were rebinned so as to appear nearly equispaced in a log-log diagram and normalised such that their integral, after subtraction of the counting statistics noise, gives the squared *rms* fractional variability. The error bars represent the standard deviation of the mean power in each frequency bin; this, in turn, is χ^2-distributed with 2N degrees of freedom (e.g. Jenkins and Watts 1969), where N=ML is the number of power estimates used to produce the average power in each frequency bin (from M power spectra and L independent Fourier frequencies). In all three spectra a strong *red noise* component is present which decreases with increasing frequencies. This component approaches the noise level at $\sim 10^{-3}$ Hz for the November 6, 1984 and October 24, 1985 observations, and at $\sim 10^{-2}$ Hz for the November 7, 1984 observation. In the power spectrum of the LE light curve of October 24 the *red noise* component is much less pronounced (reflecting the factor of ~ 3 smaller *rms* variability) and will not be further discussed.

In order to improve the signal to noise ratio and investigate the mean variability properties of the source, the ME power spectra from the three observations were averaged and the expected noise level subtracted. The results are reported in Fig. 2. Due to the logarithmic rebinnining in frequency, 2N varies from 10 for the 2 lowest frequency bins, to ~ 2000 close to the Nyquist frequency. Assuming that all these $\chi^2 - like$ distributions are well approximated by Gaussian distributions with the same average and variance, the power spectrum can be modelled by using a minimum χ^2 technique. A power law model

to the average noise-subtracted spectrum gives a reduced χ^2 of 0.9. The best fit *red noise* slope is about -2.5 ± 0.2 (68% confidence), in the interval $5 \times 10^{-5} - \sim 6 \times 10^{-3}$ Hz (see Fig. 2a). This value is somewhat lower than a value of -2, below which the removal of a linear trend is required to avoid "leakage" of power from low to high-frequencies and obtain a valid power spectrum estimate (cf. Deeter and Boynton 1982). Indeed, if a linear trend is subtracted from the light curves before the analysis, the corresponding average power spectrum (see Fig. 2b) shows considerably less power over a wide range of frequencies. In the absence of low frequency "leakage", instead, only the power estimates for frequencies $\leq 10^{-4} Hz$ should be affected by the linear trend removal. The red noise slope in the detrended power spectrum is -1.9 ± 0.4 (68% confidence) over the $10^{-4} - 3 \times 10^{-3}$ Hz. This slope is only poorly constrained, but still consistent with a value ≥ -2 for which standard Fourier techniques produce reliable results (Deeter 1982). Longer observations and analysis techniques involving alternative power spectrum estimators are required to investigate further the *red noise* properties of PKS 2155-304.

3. Cross-correlation analysis

The long and relatively continuous exposures and wide energy range (.05-10 keV) make the EXOSAT data very well suited to search for lags between the variability in the soft and hard X-ray bands by using cross-correlation function (CCF) analysis techniques. We first analysed the observations for which the 3000 Å Lexan filter was used uninterruptedly in front of the CMA (1985, Oct 24, Nov 2 and Nov 12; see Treves et al. 1989). The duration of these observations was about 15, 17 and 18 hours respectively. The CCF was calculated for both the LE (0.1-2 keV) and the 3-6 keV ME light curves, and the 1-2 keV and 3-6 keV ME light curves, over intervals covering the entire observation duration. The resulting CCFs are dominated by a broad peak (with a full width at half maximum of $\sim 2 \times 10^4$ s) indicating that correlated variability is present in the two considered energy bands. Moreover the position of this peak is not always consistent with zero delay, implying that variations in the soft energy band lagged those in the hard X-ray band by a few thousand seconds.

Due to systematic uncertainties in the background subtraction, the detector swap can introduce discontinuities in the ME light curves of up to ± 0.5 counts s^{-1} (Parmar and Izzo (1986); Parmar private communication). We tested the effect of these uncertainties by adding or subtracting a constant value of $0.2-0.3$ counts s^{-1} to one or more light curve intervals between array swaps. We found that by doing this the position of the broad peak in the CCF can in all cases be made consistent with zero. Another source of uncertainty is due to the fact that the LE light curves begin and end about 30 minutes after the ME light curve, as a result of the normal procedure of switching the instruments on and off. This was also found to affect the shape of the CCF. A safer approach consists in considering only the simultaneous parts of the two light curves and enlarging by a few minutes the gaps due to the array swaps (the ME data just before and after the gaps can be affected by the detector switching procedure). From the above analysis we found that lags in the range of $1-2\times 10^3$ s can be introduced by systematic uncertainties in the background subtraction across array swaps and by the lack of strict simultaneousness of the EXOSAT LE and ME light curves. We regard the lags derived with the above CCF analysis as spurious results.

In order to avoid systematic uncertainties and further constrain time lags, we calculated separate CCF for each of the $\sim 10^4$ s intervals defined by the array swaps. By doing this, the range of delays sampled by the CCF is reduced to $\leq 10^4$ s. On the other hand our previous results indicate that delays, if any, are in the range $1000-2000$ s, a value that is still sampled in the analysis described above. Owing to poor statistics the CCFs from the 1985 Nov 2 and Nov 12 observation calculated in this way did not produce useful information. During the October 24 observation the source signal was highest, only relatively weak trends were present and three array swaps were performed. The average of the four CCFs from individual intervals shows a peak centered around zero time lag (Fig. 3a). To derive quantitative information on possible delays between the variations in the LE and ME light curves, we fitted the average CCF with a constant plus a Gaussian function and determined the position of the Gaussian peak. Delays in the range from -770 to +220 s with respect to the hard X-ray light curves are included in the 90% confidence region. This analysis was repeated for the 1-2 keV and 3-6 keV ME bands: allowed delays range in this case from -100 to +500 s (Fig. 3b).

The data from the other two observations when the source was in a high state (November 6 and 7 1984, see Fig. 1) were analysed in the same way. For each observation the CCF of the 1-2 and 3-6 keV ME light curves was calculated over two $\sim 10^4$ s intervals, therefore avoiding the array swap. In order to exclude the effects of the steep trends present in these observations a linear trend was subtracted from the light curves. The resulting CCFs are shown in Fig. 4; the allowed range of the Gaussian centroids reported in Table 2 are consistent with those derived for the October 24 observation.

From the above analysis we can conclude that any delay between the soft and hard X-ray light curves of PKS2155-304 is less than 700-800 seconds.

4. Discussion

The present study emphasises that a number of systematic uncertainties have important consequences on the power spectrum and the cross-correlation estimates obtained from the EXOSAT lightcurves of PKS 2155-304. Our power spectrum analysis, based on Fourier techniques, suggests a power spectrum with a logaritmic slope of about -2. The fastest variability timescale inferred from the power spectra of Fig. 2 corresponds to $\sim 300 - 400$ s. However a more complete, longer and uninterrupted X-ray monitoring and alternative power spectrum analysis are necessary to further investigate the *red noise* properties of PKS2155-304. A review of recent results on the rapid variability of AGN in the X-ray band is given by McHardy (1989). For a number of Seyfert galaxies power spectra have been computed which can be described (in the $\sim 10^{-5} - 10^{-3}$ Hz range) by power laws of spectral indexes ranging from -1 to -2. By analogy with the case of PKS2155-304, we suspect that similar uncertainties might also affect simple power spectral studies of other AGN monitored with EXOSAT. A detailed comparison of the power spectral properties of PKS 2155-304 and Seyfert Galaxies seems therefore premature.

The cross-correlation analysis presented here shows no convincing evidence for any delay between the soft and hard X-ray short term variations of PKS2155-304; upper limits of several hundred seconds could be set. Lags of thousands of seconds of the ME with respect to the LE are suggested by Kaastra and Barr (1989) for NGC 5548 and by Pounds

and Turner (1987) for MCG 6-30-15. In view of the systematic effects discussed in Section 3, we caution that the above mentioned results should be regarded as preliminary.

Constraints on the emission mechanism can be set by the energy dependence of variability. In Seyfert galaxies, a widely adopted scheme attributes the soft (LE) X-rays to thermal emission from the inner region of a disk and the medium energy X-rays to Comptonization of softer photons in a hot corona (e.g. Kaastra and Barr 1989). In this case it is expected that disk instabilities of viscous, thermal or hydrodynamic origin (Abramowicz and Szuskiewicz, 1988, and references therein) can cause the soft X-ray flux to vary and induce variability of the hard X-ray flux. As a consequence the ME variations should lag the LE ones.

In PKS 2155-304 and in BL Lacs in general, one finds that the variability is larger in the ME band than in the LE, contrary to many Seyferts (*e.g.* Morini et al. 1986, George et al. 1988, Giommi et al. 1990, Treves et al. 1990 and references therein). This is consistent with the idea that in BL Lac objects with steep X-ray energy spectra, of which PKS 2155-304 can be taken as a prototype, the synchrotron mechanism is responsible for the emission, at least in X-rays. The highly relativistic radiating electrons should be accelerated near the nozzle of a relativistic jet (e.g. Ghisellini et al. 1985). The radiative time scales are extremely short, so the variability can be ascribed to variability in the relativistic electron injection process, perhaps driven by the propagation of a shock wave (Maraschi et al. 1989, Celotti et al. 1989, 1991). In this picture electrons diffuse from high to low energies so the amplitude of variability is expected to be larger at high energy and the hard variations are expected to be simultaneous or precede the soft ones. The results obtained from the present cross correlation analysis on PKS 2155-304 indicating the absence of lags larger than 700-800 s are consistent with this model. Future long observations will be of great importance to constrain possible lags between soft and hard X-ray variations on time scales of several hours.

References

Abramowicz, M.A., and Szuskiewicz, E., 1988, *Big Bang. Active Galactic Nuclei and Supernovae*, S.Hayakawa and K.Sato eds, Universal Academy Press, Tokyo

Celotti, A., Maraschi, L., Treves, A., 1989, *BL Lac Objects*, L.Maraschi, T.Maccacaro and M.-H.Ulrich eds, Springer-Verlag, Como, Italy, p. 332

Celotti, A., Maraschi, L., Treves, A., 1991, ApJ, in press

Deeter, J.E., 1983, ApJ, 281, 482

Deeter, J.E., and Boynton, P.E., 1982, ApJ, 261, 337.

DeKorte, P.A.J., et al., 1981, Space Sci. Rev., 30, 495

Fabian, A.C., 1986, *The Physic of Accretion onto Compact Objects*, K.O. Mason, M.G. Watson and N.E. White eds, Springer Verlag Berlin

Fiore, F., Massaro, E., Perola, G.C., and Piro, L., 1989, ApJ 347, 171

George, I.M., Warwick, R.S., and Bromage, G.E., 1988, MNRAS, 232, 793

Ghisellini, G., Maraschi, L., and Treves, A., 1985, A&A, 146, 204

Giommi, P., Barr, P., Garilli, B., Maccagni, D., and Pollock, A., 1990, ApJ, 356, 432

Jenkins, G.M., and Watts, D.G., 1969, *Spectral Analysis and its applications*, G.M. Jenkins and E. Parzen eds, Holden-Day series in Time Series Analysis

Kaastra, J.S., and Barr, P., 1989, A&A 226, 59

McHardy, I.M., 1989, *Two-Topics in X-Ray Astronomy*, ESA SP-296, p. 1111

Mittaz, J.P.D., and Branduardi-Raymont, G., 1989, MNRAS, 238, 1029

Maraschi L., Celotti, A., and Treves, A., 1989, *Two-Topics in X-Ray Astronomy*, ESA SP-296, p. 825

Morini, M., Chiappetti, L., Maccagni, D., Maraschi, L., Molteni, D., Tanzi E.G., Treves A., and Wolter, A., 1986, ApJ Lett., 306, L71

Parmar, A.N., and Izzo, C., 1986, *The EXOSAT Express*, no. 16, p. 21

Pounds, K.A., and Turner, T.J., 1987, *Variability of Galactic and Extragalactic X-ray sources*, A. Treves ed., Associazione per l'Avanzamento dell'Astronomia, Como, Italy, p. 1

Pounds, K.A., McHardy, I.M., 1988, *Physics of Neutron Stars and Black Holes*, Y. Tanaka

ed., Tokyo, Universal Academy Press Inc., p. 285

Press, W.H., 1978, Comments on Astrophysics, 7, 103

Tagliaferri, G., Stella, L., Maraschi, L., and Treves, A., 1989, *BL Lac Objects*, L. Maraschi, T. Maccacaro and M.-H. Ulrich eds, Springer-Verlag, Como, Italy, p. 314

Treves, A., Bonelli, G., Chiappetti, L., Falomo, R., Maraschi, L., Tagliaferri, G., and Tanzi, E.G., 1990, ApJ, in press

Treves A., Chiappetti L., Fabian A., Falomo, R., Maccagni, D., Maraschi, L., Morini, M., Tanzi, E.G., Tagliaferri, G., 1989, ApJ 341, 733

Turner, M.J.L., Smith, A., and Zimmermann, H.U., 1981, Space Sci. Rev., 30, 513

White, N.E., and Peacock, A., 1988, in "X–ray Astronomy with EXOSAT", N.E. White and R. Pallavicini eds, Mem.S.A.It., 59, 7

Figure Captions

Figure 1. Light curves (1-7.5 keV) and power spectra of three EXOSAT observations of PKS 2155-304. The power spectra of the same light curves after a linear trend removal are also shown. The error bars represent the standard deviation of the relevant χ^2 distribution of each power estimate (see text). The first two power estimates in the Nov 6 and 7 power spectra are obtained from a single Fourier frequency and a single interval; therefore, they are distributed like a χ^2 distribution with 2 degrees of freedom.

Figure 2. Upper panel: average power spectrum of the three ME light curves shown in Fig. 1. The expected noise level has been subtracted and the spectra are normalised in such a way that their integral gives the square of the *rms* variability. The power law fit described in the text is shown. Lower panel: the same power spectrum, after removal of a linear trend from the three ME light curves is shown. Upper limits are at 1σ above zero level.

Figure 3. Upper panel: CCF of the LE, 0.01-2.0 keV, and ME, 3-6 keV, light curves for 1985 October 24 observation. Lower panel: CCF of the 1-2 keV and 3-6 keV ME light curves for the same observation. In both cases a peak centered around zero time lag is present. Best fit models consisting of a constant plus Gaussian function are shown.

Figure 4. CCF of the 1-2 and 3-6 keV ME light curves from two different observations, after removal of a linear trend from the light curves.

Table 1 - Analysed observations

Date	No. of Array swaps	ME (1-7.5 keV) *counts* s^{-1}	Duration *s*	*rms* fractional variation (100s bins)	LE *counts* s^{-1}	duration *s*	*rms* fractional variation (300s bins)
1984 Nov 6	1	8.21 ± 0.05	17430	0.26 ± 0.02			
1984 Nov 7	1	11.25 ± 0.05	18040	0.47 ± 0.03			
1985 Oct 24	2	16.06 ± 0.04	54120	0.087 ± 0.003	3.72 ± 0.01	51480	0.031 ± 0.004
1985 Nov 2	3	5.52 ± 0.03	61680	0.067 ± 0.006	1.85 ± 0.01	60990	< 0.06 (3σ)
1985 Nov 12	5	2.90 ± 0.03	66380	0.14 ± 0.01	1.34 ± 0.01	63420	0.105 ± 0.008

Table 2

Cross correlation analysis: range of allowed time lags

Date	LE - ME (0.1-2)-(3-6) keV seconds	ME - ME (1-2)-(3-6) keV seconds
1985, October 24	-770 +220	-100 +500
1984, November 6		-350 +370[a]
1984, November 7		-10 +250[a]

a) detrended light curves

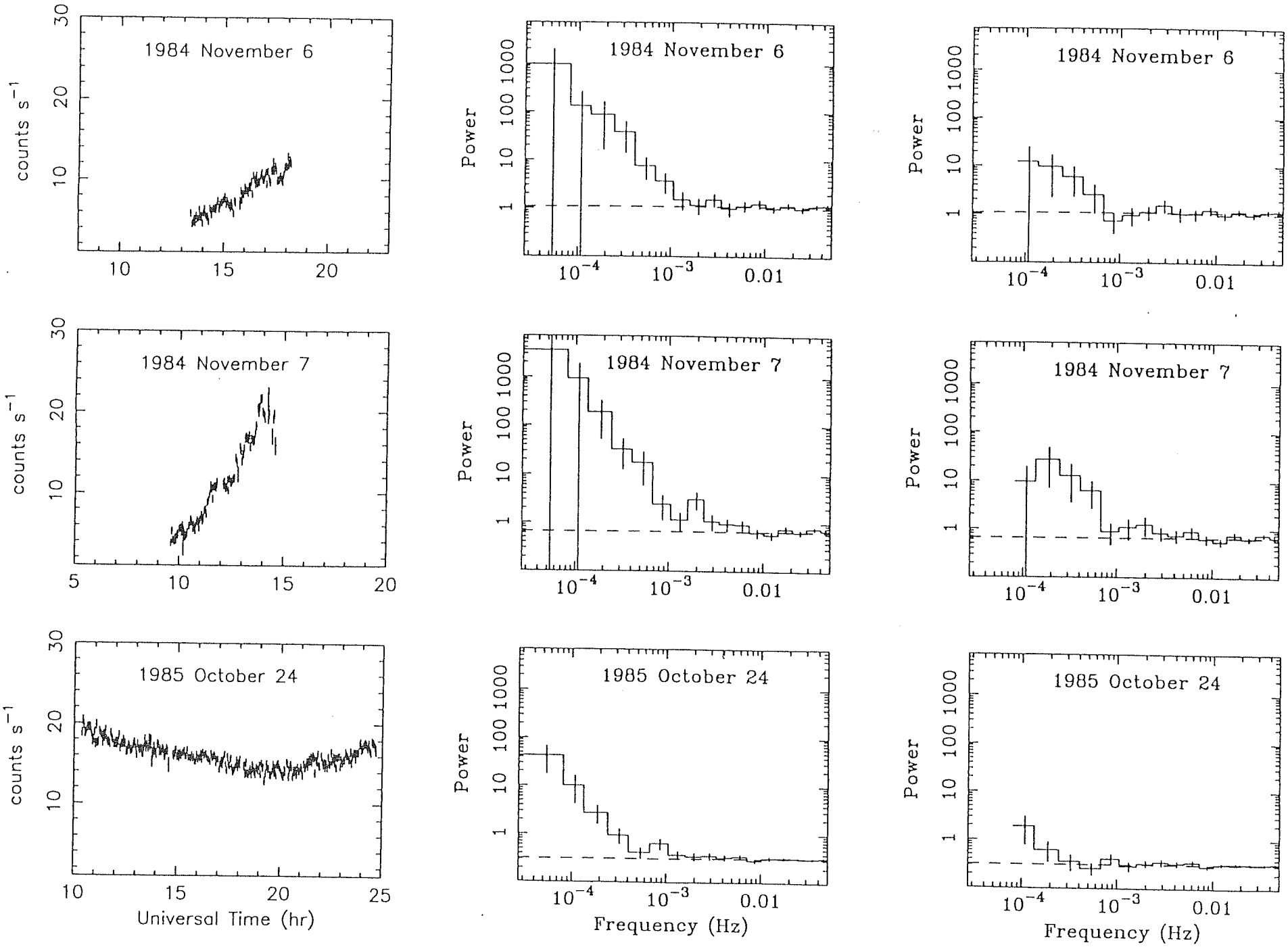
1984 November 6
counts s^{-1}
1984 November 6
Power
1984 November 6
Power
1984 November 7
counts s^{-1}
1984 November 7
Power
1984 November 7
Power
1985 October 24
counts s^{-1}
Universal Time (hr)
1985 October 24
Power
Frequency (Hz)
1985 October 24
Power
Frequency (Hz)

Fig 1

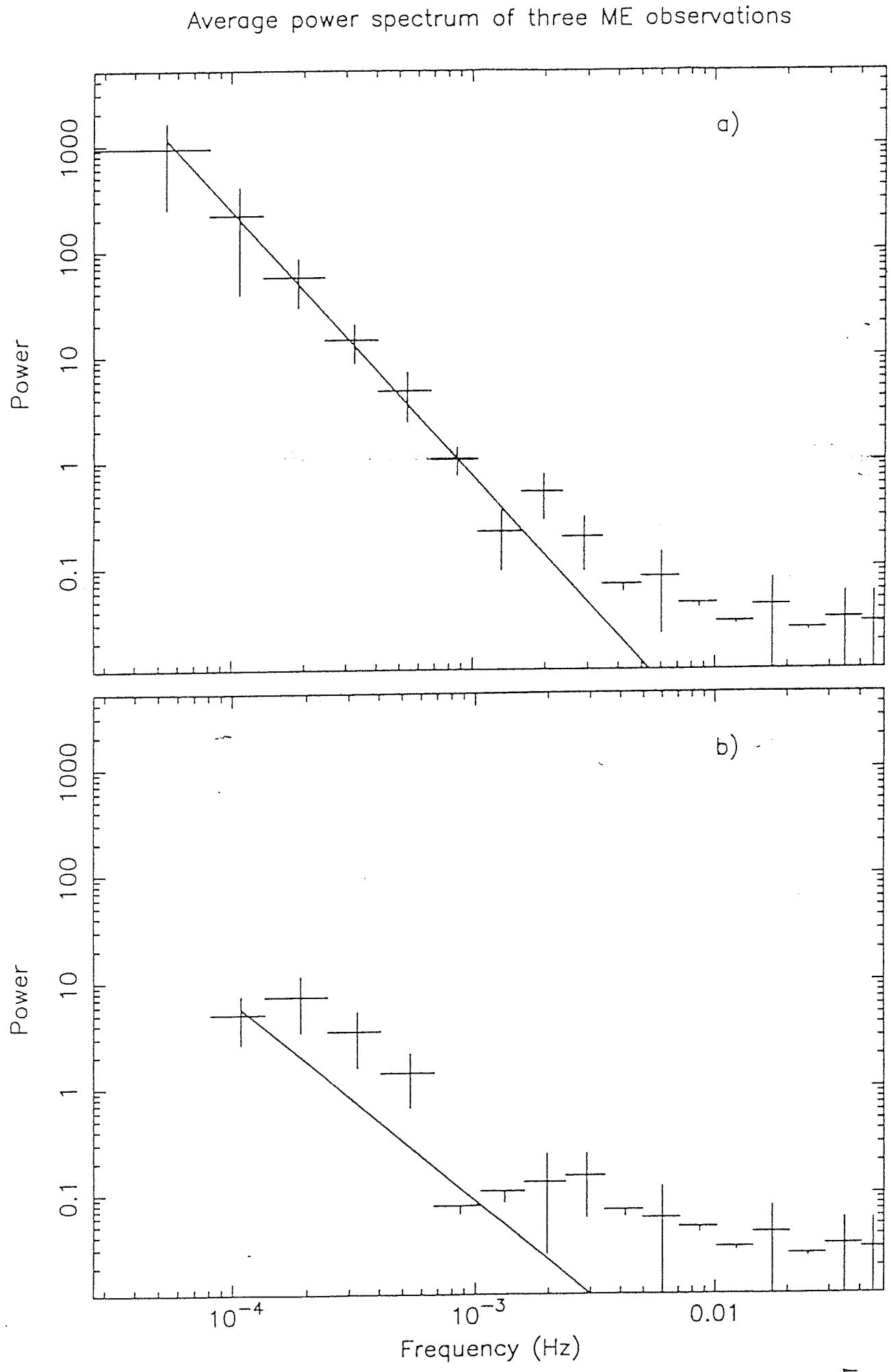
Average power spectrum of three ME observations
a)
b)
Power
Power
0.1
1
10
100
1000
10^{-4}
10^{-3}
0.01
Frequency (Hz)

Fig. 2

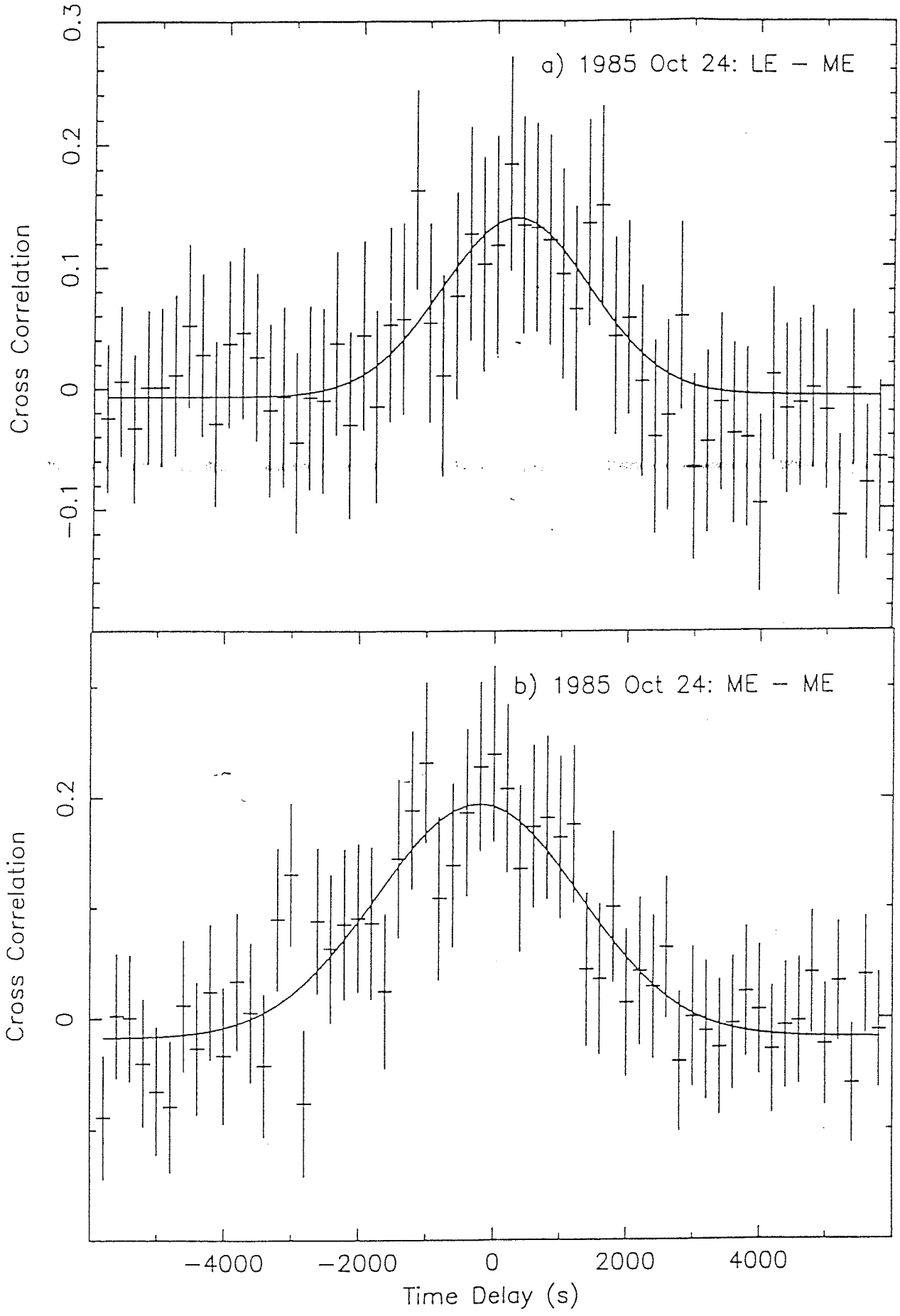
a) 1985 Oct 24: LE – ME
b) 1985 Oct 24: ME – ME
Cross Correlation
Cross Correlation
0.3
0.2
0.1
0
−0.1
0.2
0
−4000
−2000
0
2000
4000
Time Delay (s)

Fig. 3

Removed a linear trend from the light curves

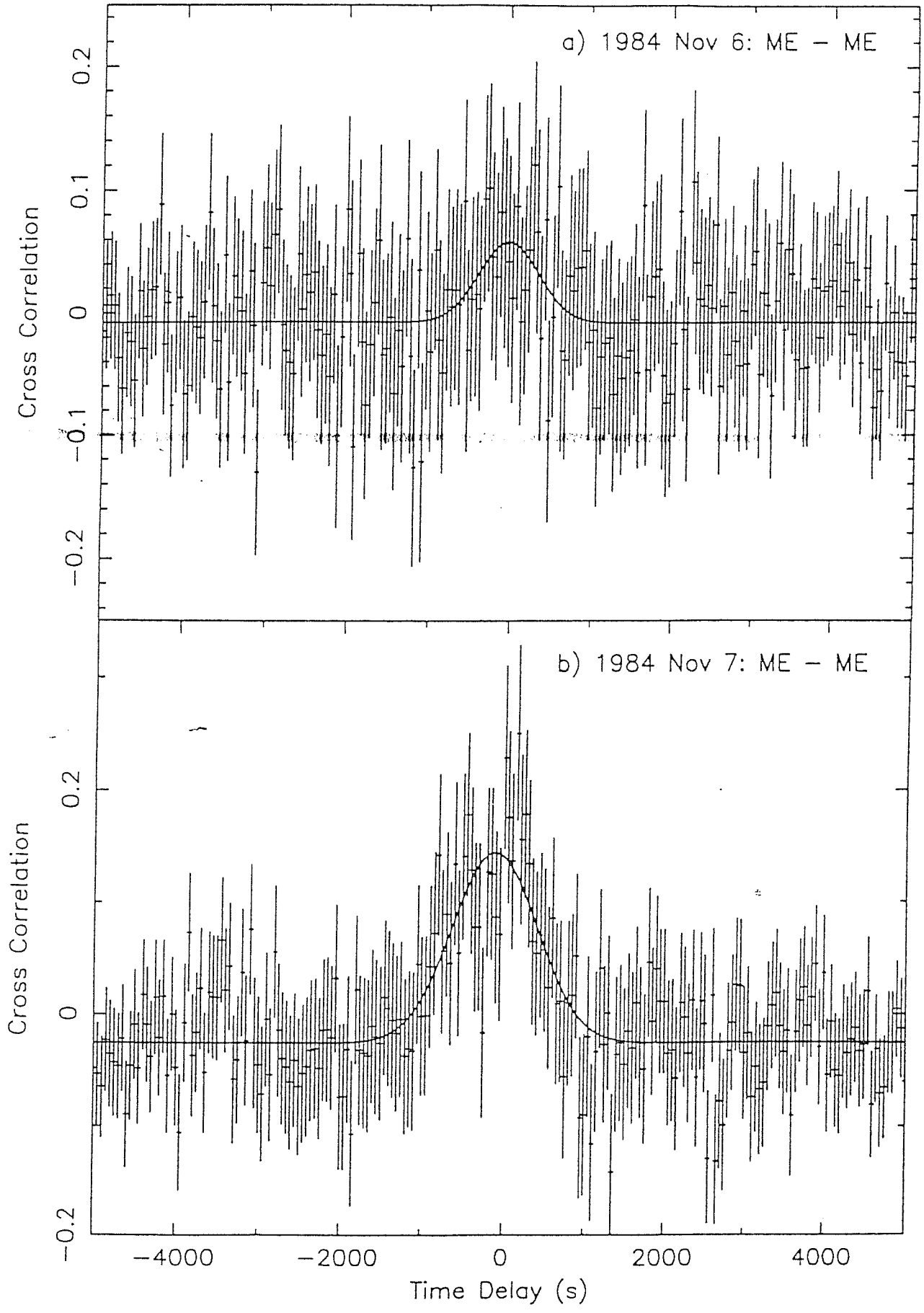

Fig. 4

Appendix C

Pair plasma jets

The Role for Electron-Positron Pairs in Fueling Parsec–scale Radio Jets

G.Ghisellini[1], A.Celotti[2,3], I.M.George[4] and A.C.Fabian[2]

[1] *Osservatorio Astronomico di Torino, Pino Torinese, Italy.*

[2] *Institute of Astronomy, Madingley Road, Cambridge CB3 OHA, U.K.*

[3] *International School for Advanced Studies, Trieste, Italy.*

[4] *HEASARC, Goddard Space Flight Center, Maryland MD20771, USA.*

To be submitted to *Mon. Not. R. Astron. Soc.*

Summary.

We try to answer to the question whether extragalactic jets are mainly constituted by an electron–proton plasma or by outflowing electron–positron pairs created in the inner regions of active galactic nuclei. We emphasize that, due to annihilation, there is a limit in the number flux of pairs that can reach the parsec–scale jet. This upper limit can be compared to the number flux of particles, calculated using the standard synchrotron theory, needed to produce the radiation we observe. Assuming a power law energy distribution for the emitting particles, our results critically depend on the lower energy cut–off of this distribution. We find that the emitting particles of the parsec–scale jet can be electron–positron pairs only if their minimum energy remains greater than approximately 50 MeV. Remarkably enough, the same low energy cut–off is found in the case of polarized jets constituted by electron–protons, to avoid Faraday depolarization. The need for an efficient acceleration mechanism inhibiting the cooling of the particles is therefore compelling.

1. Introduction

The development of Very Large Baseline Interferometry (VLBI) has led to the discovery that jets on parsec-scales are common in extragalactic compact sources (for review see Begelman, Blandford & Rees 1984). As first suggested by Rees (1971), these are thought to be the signature of plasma flowing from the central galaxy and supplying energy to the extended lobes. High resolution maps have shown that these structures are indeed constituted by discrete emitting blobs, which sometimes move with apparent superluminal velocities (see *e.g.* Porcas 1987).

In the simplest interpretation of superluminal motion, the emitting plasma moves at relativistic speeds at small angles to the line of sight. The emitted radiation is in this case beamed along the direction of motion, and this explains the observed high synchrotron brightness temperatures, without overproducing inverse Compton X–rays.

There is no consensus yet about the mechanism responsible for the bulk acceleration of the emitting plasma. One possibility is that the acceleration is provided by radiation pressure. However, acceleration of 'normal' (electron–proton) matter through electron scattering requires super–Eddington sources, while the more efficient mechanism of synchrotron absorption requires that a large fraction of the luminosity is emitted at low (radio–IR) frequencies (Ghisellini *et al.* 1990).

The acceleration problem could be much eased if the jets were formed by electron–positron pairs. Furthermore, $e^{\pm}$ pairs produce zero Faraday rotation and depolarization, and the strong upper limits on the density in polarized jets could be evaded.

The natural site of the production of $e^{\pm}$ pairs is the compact X and γ–ray region of the source, at few Schwarzschild radii from the putative massive black hole. In this region both the expected high temperature of the emitting plasma and the possible presence of non thermal particles make pair production an unescapable process (see reviews by Svensson 1986, 1990). The created pairs, if not confined or coupled (*e.g.* by a magnetic field) with the protons of the primary plasma, can form an outflowing wind driven by radiation pressure, the limiting luminosity being a factor $m_p/m_e = 1836$ lower than the Eddington value.

Quite model–independently, there is an *upper limit* to the number of pairs that can escape: the larger the density of the produced pairs, the larger their annihilation rate in the inner, acceleration region. Hence the $e^{\pm}$ density at a couple of source radii is very weakly dependent on the $e^{\pm}$ density at the base of the outflow.

It is interesting to ask if these pairs are a large fraction of the total mass of the matter flowing in the jet. The big uncertainty in answering this question is the knowledge of the particle density in the jet. If the jet is constituted mainly by 'normal' (electron–proton) matter, then a limit on the density can be derived for jets which are highly polarized, due to the lack of Faraday depolarization. But this limit is avoided if the jet is dominated by $e^{\pm}$ pairs, which do not produce any Faraday depolarization.

The density of the jet could be derived assuming that the outer lobes are powered by the kinetic energy flux transported by the jet, but this assumption is easily criticable, the transport possibly being in the form of a Poynting flux, the power of which is reconverted in internal energy only in the outer regions.

In this paper we estimate a *lower limit* to the particle density of the VLBI jets by calculating how many particles are necessary to produce the synchrotron radio emission we observe, including the effects of relativistic bulk motion. We then compare the *number* flux of the pairs escaping from the inner region with the one in the VLBI jet.

We assume that the outflow of pairs in the inner region occurs in a spherically isotropic manner for few source radii, and that after this isotropic wind region *all* the pairs are channeled into two jets.

Our results indicate that the synchrotron emitting particles in the VLBI jets can be $e^{\pm}$ pairs flowing from the inner region only if their energy distribution has a low energy cut–off of 20–50 MeV. This limit is remarkably similar to the one obtained in polarized sources in the case of electron–proton jets. Taken together, these two limits strongly argue for an efficient acceleration mechanism to operate, making the particle unable to cool below the cut–off energy.

In section 2 we calculate, following previous work by Phinney (1983), Guilbert & Stepney (1985) and Svensson (1986), the maximum number density of escaping pairs, assuming a steady $e^{\pm}$ pair dominated source. In section 3 we recall the standard

results of the synchrotron self–Compton theory necessary to derive the density of the emitting particles in the VLBI jets, including the effects of relativistic beaming. In section 4 we describe the two considered samples of sources: the first is a sample of blazars (BL Lac objects and Highly Polarized Quasars), while the second is a sample of radio sources listed in Pearson & Readhead (1988). We present our results in section 5 and discuss them in section 6.

We use $H_0 = 50$ Km/s/Mpc and $q_0 = 0.5$.

2. Dynamics of pairs

In recent years, there has been a growing realization of the importance of the $e^{\pm}$ pairs for the formation of the high energy spectrum of active galactic nuclei (see review by *e.g.* Svensson 1990 and references therein), but the aspects concerning the dynamics of pairs outflowing from a compact source has received comparatively less attention. However, a basic result, quite model independent, is apparent: there is a limit on the number of pairs escaping a compact source, due to the efficient annihilation they suffer at the base of the outflow. This limit could be evaded if the pairs were hot, since the annihilation cross section (similar to the Klein Nishina cross section), is a decreasing function of the temperature. But a large density of hot pairs results in a catastrophic Compton cooling, immediately lowering the temperature (or the mean energy) to subrelativistic values. Note also that even if a strong acceleration mechanism prevented pairs to cool (as synchrotron reabsorption, see Ghisellini, Guilbert & Svensson 1988), the resulting Comptonization would completely reprocess the emitted spectrum, driving it to have a Wien shape. In the following, therefore, we assume that the outflowing pairs are cold. Furthermore, we will assume a pure pair plasma wind, expanding with a velocity βc, corresponding to a Lorentz factor Γ_b. The density n'_+ is the density of positrons, assumed to be equal to the electron density, in the comoving (primed) frame. In this frame the annihilation rate of the (cold) pairs is

$$\dot{n}'_+ = \frac{3}{8} c \sigma_T {n'_+}^2 \tag{2.1}$$

where σ_T is the Thomson cross section.

We assume that pairs are created in a spherical source of radius R_0 characterized by a luminosity $L \gg (m_e/m_p)L_E$, where m_e and m_p are the electron and proton mass, and L_E is the Eddington luminosity. We assume that pairs are no longer created outside R_0, where they have a density $n'_+(R_0)$ and a scattering optical depth $\tau_0 \equiv 2\sigma_T R_0 n'_+(R_0) \gg 1$. With these assumptions, the pairs are driven by the radiation (whose energy density exceeds the energy density of pairs, see Section 2.1 for a particular model), and can be treated as a relativistic fluid. For radial distances R less than a few source radii, we assume that the pair wind is spherically symmetric, and that only at larger radii the wind is channeled into two jets.

The density of $e^{\pm}$ pairs in the wind decreases due to annihilation and adiabatic expansion, the former process being more important closer to R_0. The dynamics for such a steady outflow have been presented by Phinney (1983), Guilbert & Stepney (1985) and Svensson (1986). The density n'_+ can be found from the solution to the particle conservation equation

$$\frac{d}{dR}(R^2 c\beta\Gamma_b n'_+) = -R^2 \dot{n}'_+ \tag{2.2}$$

where R is the radial coordinate. As long as the particles and photons are able to interact they can be treated as an adiabatic fluid (photons cannot escape) whose dynamics is regulated by the conservation of the energy–momentum tensor, which gives the dependence of the bulk velocity βc on R. For $\beta \simeq 1$, $\Gamma_b \simeq \Gamma_{b,0} R/R_0$. Here we assume that $\Gamma_{b,0} = (3/2)^{1/2}$, corresponding to the relativistic sound speed. Solving eq. (2.2) for n'_+ we get (Guilbert & Stepney 1985)

$$n'_+ = \frac{n'_+(R_0)}{x^3 + \tau_0\, k(x^3 - 1)} \tag{2.3}$$

where $k = 1/(16\Gamma_{b,0})$ and $x = R/R_0$. The quantity $k\,\tau_0$ is the ratio of the annihilation to expansion terms as measured at R_0. For our assumptions $k \sim 0.05$, thus for $\tau_0 \ll 10$, annihilation is relatively unimportant with respect to expansion and $n'_+/n'_+(R_0)$ falls approximately as R^{-3}.

When n'_+ is low enough that the photons and particles cease to interact via Compton scattering, the photons are free to escape, and the outflow can no longer

be considered as a single fluid. This will occur at a 'trapping' radius R_{tr}. Here we define R_{tr} (as measured in the observer's frame) such that the number of scatterings *in the comoving frame* from that point to infinity is one:

$$N_{scatt} \equiv \int_{R'_{tr}}^{\infty} 2\, n'_{+}(R')\, \sigma_T\, dR' = \int_{R_{tr}}^{\infty} \frac{2\, n_{+}(R)}{\Gamma_b^2}\, \sigma_T\, dR = 1 \qquad (2.4)$$

In order to calculate R_{tr} it is necessary to find $n'_{+}(R)$ for $R > R_{tr}$. If annihilation is unimportant outside R_{tr}, then the number of particles is conserved, and if the velocity is constant then the density decreases as

$$n'_{+}(R) = n'_{+}(R_{tr}) \left(\frac{R_{tr}}{R}\right)^2, \qquad R > R_{tr} \qquad (2.5)$$

In order to determine the maximum radius at which annihilation is important, by analogy with R_{tr}, we define an annihilation radius, R_{an}, from which the optical depth for $e^{\pm}$ annihilation to infinity is equal to one. Now, the integral of equation (2.4) decreases with R_{tr} because n'_{+} decreases faster than R^{-2} (as for pure expansion with constant Γ_b). Since the annihilation cross-section ($\simeq 3\sigma_T/8$) is smaller than that for scattering, it follows that $R_{an} < R_{tr}$. Annihilation is therefore negligible at $R > R_{tr}$. For $R > R_{tr}$ we assume that particles freely stream, with constant Γ_b, until eventually they are channeled in the jets.

In Fig. 1 we show the number of scatterings (equation 2.4) as a function of R_{tr}, for different values of τ_0.

It can clearly be seen that $R_{tr} > R_{an}$ for all values of τ_0.

From equations (2.4) and (2.5) we get

$$x_{tr} = \frac{R_{tr}}{R_0} = \left[\frac{17}{1 + 1/(k\tau_0)}\right]^{1/3} \qquad (2.6a)$$

and

$$x_{an} = \frac{R_{an}}{R_0} = \left[\frac{7}{1 + 1/(k\tau_0)}\right]^{1/3} = \left(\frac{7}{17}\right)^{1/3} x_{tr} \qquad (2.6b)$$

Since $k \simeq 0.05$, for $1 < \tau_0 < 1000$ both R_{tr} and R_{an} are slightly dependent upon τ_0 (Fig. 2) and hence upon $n'_{+}(R_0)$. This is due to the fact that a higher initial $e^{\pm}$ pair density leads to a higher annihilation rate (see also Fig. 1). We stress that this implies that the density of the surviving pairs, (which we will compare with the

density of emitting particles in the observed radio jet) is almost independent of the pair production model one assumes.

We also note that since the particle density decreases so rapidly with R (for $\tau_0 = 10$, $R_{an} \simeq 1.33R_0$ and $R_{tr} \simeq 1.78R_0$), the fluid is unable to convert much of the internal energy contained in photons into bulk motion. Hence assuming no other accelerating mechanisms are operating, the maximum bulk Lorentz factor of the wind is $\Gamma_b \simeq 2.2$ (for $\tau_0 = 10$).

The density of positrons at R_{tr} can be calculated by means of equations (2.3) and (2.6b) which yield

$$n'_{tr} = \frac{\Gamma_{b,0}}{2\sigma_T R_0} \tag{2.7}$$

which corresponds to $\tau_{tr} = \Gamma_b(R_{tr})$.

We can now calculate the maximum number flux $\mathcal{F}_p = 4\pi R^2 \beta_b c \Gamma_b (2n'_+)$ of surviving particles, evaluating it at R_{tr} with $n'_+(R_{tr})$ given by equation (2.7) and setting $\Gamma_b(R_{tr}) = \Gamma_{b,0} x_{tr}$

$$\mathcal{F}_p(R_{tr}) = \mathcal{F}_{p,0} \frac{x_{tr}^3}{(1+k\tau_0)x_{tr}^3 - k\tau_0} = \frac{4\pi c}{\sigma_T} \Gamma_{b,0}^2 R_0 x_{tr}^3 \tag{2.8}$$

Since $n'_+(R_{tr})$ is independent of τ_0 (for fixed R_0), $\mathcal{F}_p$ depends on τ_0 only via R_{tr}, and changes by only an order of magnitude for $1 < \tau_0 < 1000$. This result is already contained (in a qualitative way) in Svensson (1986) in the form of the luminosity in rest mass of outflowing pairs.

We now assume that *all* the electrons and positrons able to escape within the $e^{\pm}$ pair wind are channeled along two jets. All the formulae derived so far assumed a spherically symmetric wind. We assume that the total number flux of pairs of this inner portion of the wind is conserved, even if the pairs, at a radius $R \sim$ a few R_0, are channeled into two jets. We assume, conservatively, that the jet formation mechanism is maximally efficient in channeling the pairs into two jets, and impose, in equation (5.2), conservation of the number flux, but allow for a further bulk acceleration of the plasma, as indicated by the required beaming of the radiation we observe and by the apparent velocities of superluminal sources. This additional acceleration of the plasma could occur *e.g.* at the base of the jet.

In section 5 the predicted number density of these particles is compared to that of emitting particles within the VLBI jet as deduced from SSC theory.

2.1 Pair production models

Even if the relevant density of the outflowing pairs is very weakly dependent on the initial density, it is interesting to ask what are the values of τ_0 expected in pair production models.

The assumption of a *steady* source allows the computation of the pair density through the pair balance equation: pair production must equal annihilation and escape.

Applying this equation, one can calculate the equilibrium pair density, or, equivalently, the fraction of the luminosity of the source which is converted into pair rest mass, *i.e.* the pair yield ξ.

In thermal, hot and steady plasmas, the pair yield is always small ($\xi < 10^{-3}$), and this translates in small values of the predicted τ_0 ($\tau_0 < 1$). In fact, in thermal models, the created pairs are assumed to have the same temperature of the particles of the high energy emission: at high (transrelativistic) temperatures, the annihilation rate is small, and can balance pair production only for small production rates. For lower temperatures, on the other hand, the pair production rate is small, and the density of pairs remains relatively small.

In non-thermal plasmas, the pairs (created through photon–photon collisions), join a thermal distribution at the Compton temperature, which is always subrelativistic. The annihilation rate is in this case given by equation (2.1), and can balance a much higher pair production rate than in the thermal case. As a consequence, up to 10 per cent of the luminosity can be converted into pair rest mass.

Defining the compactness ℓ as $\ell \equiv L\sigma_T/(R_0 m_e c^3)$, Svensson (1987) has shown that the pair optical depth τ_0 inside a non thermal source is

$$\tau_0 \simeq \left(\frac{4}{\pi}\xi\ell\right)^{1/2} \tag{2.9}$$

which is independent on the possible pair escape, as long as $\tau_0 > 1$. The pair yield ξ is a linear function of ℓ for $\ell < 30$, and saturates to a value ~ 0.1 for higher ℓ (Svensson 1987, Done, Ghisellini & Fabian 1990). Since the compactness depends on the ratio L/R_0, we can also express it in terms of the Eddington luminosity L_E and the Schwarzschild radius R_s: $\ell = (2\pi/3)(m_p/m_e)(3R_s/R_0)(L/L_E)$. Therefore, for $\ell > 30$ (or equivalently, for luminosities exceeding ~ 1 per cent of the Eddington value) the pair optical depth becomes:

$$\tau_0 \sim 20 \frac{L}{L_E} \frac{3R_s}{R_0} \tag{2.10}$$

This justifies the reference value $\tau_0 = 10$ we use.

Using equation (2.9), the ratio between the energy density in cool $e^{\pm}$ pairs to the radiation energy density can be expressed as $U_{pair}/U_{rad} \simeq 4\pi\tau_0/\ell = 8(\pi\xi/\ell)^{1/2} < 1$. This justifies our assumption of a radiation dominated fluid.

3. Synchrotron self–Compton models

The most common interpretation of the origin of flat and polarized radio spectra from compact sources involves incoherent synchrotron emission from a non-thermal distribution of relativistic electrons in a randomly oriented magnetic field. The flat spectrum is obtained as a superposition of spectra from a number of different components with different self–absorption frequencies (the 'Cosmic conspiracy'), or, almost equivalently, from an inhomogeneous jet. For each radio frequency the observed flux density is mainly produced by one particular component, the spectrum of which peaks at that frequency. This allows to identify the frequency of the VLBI observations as the self–absorption frequency of the observed component. On the other hand we are not allowed to make such an identification for the VLBI knots (at some distance from the core) which could be quasi–homogeneous components, whose spectrum peaks at a different frequency.

For sources in which the photon density is sufficiently high, electrons can also Compton scatter the synchrotron photons up to X–ray and γ-ray energies, as

described in the standard synchrotron self–Compton (SSC) models (*e.g.* Jones, O'Dell & Stein 1974a,b).

We assume that the synchrotron emitting particles have a differential energy distribution of the form $N'(\gamma) = N'_0 \gamma^{-(2\alpha+1)}$ for $\gamma_{min} \leq \gamma \leq \gamma_{max}$. The index of the optically thin synchrotron spectrum α is here considered in the range $0.5 \leq \alpha \leq 1$. The particle density, n'_{SSC}, is given by integrating $N'(\gamma)$ over all energies. This number therefore critically depends (for $\alpha > 0$), on the assumed low energy extreme of the distribution, where there are most of the particles.

The emitting particle distribution, the intensity of the magnetic field, B, and the dimension r_{VLBI} of the emission region (r_{VLBI} is the cross section radius of the jet), determine the emitted radio spectrum, the frequency ν_m where the spectrum peaks (directly related to the self–absorption frequency), and the predicted X–ray flux, F_x. Alternatively, from the observed (or assumed) quantities ν_m, F_m, F_x, D_L, α and θ_d, the electron density and the magnetic field can be uniquely determined. F_m is the radio flux at ν_m, D_L the luminosity distance, and θ_d the angular diameter of the source (in this case measured directly with VLBI).

As mentioned above, the most common interpretation of sources with flat radio spectra is that the emission at each frequency is dominated by a the component self–absorbing at that frequency. The dimension must therefore be computed at the same frequency. For a critical discussion of the 'observed' parameters see Marscher (1987).

In many cases, the estimated radiation densities imply a production of X–ray photons via the SSC process far in excess of that observed (the so–called Compton catastrophe). The widely accepted solution to this problem is that the inferred radiation density is overestimated due to relativistic motion of the emitting plasma close to the line-of-sight (Blandford & Rees 1978). This effect can be quantified by the Doppler factor $\delta = [\Gamma_b - (\Gamma_b^2 - 1)^{1/2} \cos\phi]$, where ϕ is the angle between the velocity of the emitting plasma and the line of sight. Such a hypothesis is well supported by other independent observations such as superluminal motions, one-sided jets, and rapid variability.

But *independently* of beaming, we can calculate a limit to the the particle density in the VLBI core by comparing the radio and the X-ray fluxes. The self–Compton

emission of the synchrotron component, in fact, has not to exceed the observed X–rays. Since the synchrotron and the self–Compton fluxes depend on the magnetic field and on the beaming factor in the same way, we have (using formulae given in Marscher 1987)

$$\tau_{VLBI} \equiv N_0' \sigma_T r_{VLBI} = t(\alpha) \frac{F_x \nu_x^\alpha}{F_m \nu_m^\alpha} \frac{1}{\ln(\nu_b/\nu_m)} \tag{3.1}$$

where the function $t(\alpha)$ is given in Table 1 for few values of α, and the fluxes have to be measured in the same units, as well as the frequencies. Note that τ_{VLBI} does not depend on redshift, which is instead necessary to calculate the size r_{VLBI}, and hence the particle density. Here we adopt a value of $\nu_b = 10^5$ GHz for the high energy cut-off in the synchrotron spectrum.

The limit derived in equation (3.1) corresponds to the particle optical depth of the VLBI component necessary to produce, via self–Compton emission, all the observed X–rays. If the VLBI component produced only a small fraction of the X–rays, the particle density would be proportionally lower. This in turn requires a larger magnetic field to produce the same synchrotron flux, and/or a larger enhancement factor produced by relativistic beaming. The former possibility is however constrained by the requirement that the VLBI component self–absorbs at the VLBI frequency. In fact the thick synchrotron flux ($\propto \theta_d^2 \nu^{5/2} B^{-1/2} \delta$) does not depend on the particle density, and can therefore be used to derive the value of the magnetic field. Taking into account simple radiation transfer effects, from the observed flux at the peak of the synchrotron spectrum we can derive the magnetic field

$$B = 10^{-5}\, b(\alpha)\, \theta_d^4\, \nu_m^5 F_m^{-2} \frac{\delta}{(1+z)} \quad \text{G} \tag{3.2}$$

where the angular diameter θ_d is in milliarcseconds, F_m and F_x are in Jy, ν_m in GHz. z is the redshift and the function $b(\alpha)$ is given in Table 1 for few values of α.

Substituting equations (3.1) and (3.2) into the expression for the thin synchrotron flux ($\propto \theta_d^2 B^{1+\alpha} \tau_{VLBI} \nu^{-\alpha} \delta^{3+\alpha}$), we derive the beaming factor δ

$$\delta = f(\alpha)\, F_m \left(\frac{\ln(\nu_b/\nu_m)}{F_x\, \theta_d^{6+4\alpha}\, \nu_x^\alpha\, \nu_m^{5+3\alpha}} \right)^{\frac{1}{2(2+\alpha)}} (1+z) \tag{3.3}$$

where F_x is in Jy, ν_x is in keV. The function $f(\alpha) \simeq 0.08\,\alpha + 0.14$ (Ghisellini 1987).

Few remarks are in order:

i) Equations (3.1)–(3.3) can be applied to sources *not* observed in the X–rays, but only in the optical, by substituting the corresponding X-ray flux and frequency with the corresponding optical ones. Indeed, we will do this for the sample of radio sources presented in Section 4.2, which are lacking X–ray data.

ii) The particle density we derive is an upper limit, since the radio component can produce much less X-rays than observed, therefore requiring a much lower τ_{VLBI}.

iii) On the other hand, the smaller τ_{VLBI}, the higher the beaming factor needed to produce the observed synchrotron (the B–field depends on τ_{VLBI} only through the beaming factor, eq. 3.2).

In the following, we take the derived upper limits on τ_{VLBI} as true values, and discuss the possibility of smaller values in section 5.

4. The samples

In order to check the hypothesis that parsec-scale jets consist of an $e^{\pm}$ dominated plasma, we consider here two samples of sources for which synchrotron emitting components have been detected at the VLBI scale.

4.1 THE BLAZAR SAMPLE

The first sample comprises 44 blazars (BL Lac objects and Highly Polarized Quasars [HPQs]). They present flat radio spectra, high linear polarization with a probably dominant non thermal emission, and strong variability. Relativistic beaming of the radio components is likely to be important for these sources, and in order to estimate the Doppler factor δ, we have compared the predicted and the observed X–ray flux, using the method outlined in the previous section. We have therefore selected a sample of blazars, observed in the X–ray band for which VLBI observations are available. We also consider, as a subsample, the sources for which superluminal motion has been detected (Porcas 1987).

In Table 2 we list our sample. It is essentially the list considered by Madau, Ghisellini & Persic (1987), to which we refer for references to the data, with the

addition of 3C 273 (Unwin *et al.* 1985), 0906 +430 and 1845 +797. For the latter two sources VLBI data are in Pearson & Readhead (1988) and the X–ray flux was derived from the Einstein archive.

Table 2 reports the source coordinates and common names, the redshift, the angular diameter measured from VLBI (when the major and minor axes a and b are given $\theta_d = \sqrt{ab}$ is adopted), the self–absorption frequency, the radio flux at ν_m, and the X–ray flux at 1 keV. Six new redshifts are taken from Impey & Tapia (1991) and Stickel *et al.* (1991). When the redshift is not measured a mean value of $z = 0.4$ is assumed (Ghisellini *et al.* 1986). Note that for some of the sources only an upper limit to the angular diameter is available.

4.2 THE 'PEARSON & READHEAD' SAMPLE

The second sample we use is extracted from the complete sample of radio sources, selected at 5 GHz with a radio flux exceeding 1.3 Jy, for which the VLBI size and the VLBI radio flux density has been measured. We excluded blazar sources already listed in Table 2. All the relevant informations are taken from Pearson & Readhead (1988), and are reported in Table 3, which has the same format as Table 2 for the objects for which an X-ray flux was found in the Einstein archive. For the source 1633+382 the X-ray flux is given in Worral *et al.* (1987). For the remaining objects, the X–ray flux is replaced by the optical magnitude in the V band. Also for these sources there are indications of relativistic motion (some are superluminal sources). For the fraction of the sources with no X–ray data, we have applied the same formalism of section 3 to derive the beaming factor δ, but now comparing the predicted and the observed *optical* fluxes. The derived Doppler factor should not critically depend on which flux is used, given the weak dependence of δ on the X or optical flux. We confirm the suggestion that part of these radio sources have to be beamed, to let the radio component not to overproduce, by self–Compton emission, the optical flux.

5. Results

5.1 PARTICLE DENSITY OF THE VLBI JET

Having derived the particle optical depth τ_{VLBI} by equation (3.1), we compute the particle density as

$$n'_{ssc} = \frac{\tau_{VLBI}}{2\alpha\sigma_T r_{VLBI}\gamma_{min}^{2\alpha}} \tag{5.1}$$

where $r_{VLBI} = (\theta_d/2)\, D_L\,/(1+z)^2$ is the linear cross sectional radius. No computation of the density has been made for sources with unknown redshift. The density n'_{SSC} has to be compared with the expected pair density, as derived in section 2.1, assuming that the number flux of $e^{\pm}$ pairs is conserved along the jet. We allow, however, for a change in velocity along the jet, since for some source the derived δ factor indicates that the plasma has been further accelerated (the typical value of $\Gamma_b(R_{tr}) \leq 2$). Therefore we set, for the VLBI component, $\Gamma_b(r_{VLBI}) = \delta$ for those sources with $\delta > 1$, and $\Gamma_b(r_{VLBI}) = \Gamma_b(R_{tr})$ for the remaining sources.

The particle number flux in the jet is

$$\mathcal{F}_p(r_{VLBI}) = \pi r_{VLBI}^2 \beta_b(r_{VLBI}) c \Gamma_b(r_{VLBI}) n'_{pair}(r_{VLBI}) \tag{5.2}$$

Conservation of number flux demands that equation (5.2) is equal to half (for two jet sources) the corresponding number flux of equation (2.8). Therefore the pair density $n'_{pair} = 2n'_{+}$, expected in the radio emitting component is

$$\begin{aligned} n'_{pair} &= 4\, n'_{+}(R_{tr}) \left(\frac{R_{tr}}{r_{VLBI}}\right)^2 \frac{\beta_b(R_{tr})\Gamma_b(R_{tr})}{\beta_b(r_{VLBI})\Gamma_b(r_{VLBI})} \\ &= \frac{2\Gamma_{b,0}}{\sigma_T R_0} \frac{\beta_b(R_{tr})\Gamma_b(R_{tr})}{\beta_b(r_{VLBI})\Gamma_b(r_{VLBI})} \left[\frac{17}{1+1/(k\tau_0)}\right]^{2/3} \left(\frac{R_0}{r_{VLBI}}\right)^2 \end{aligned} \tag{5.3}$$

In Fig. 3 we plot the values of n'_{pair} versus n'_{SSC} assuming $\alpha = 0.75$, $\tau_0 = 10$, $\gamma_{min} = 1$, and $R_0 = 10^{14}$ cm for the sources not known to be superluminal (Fig. 3a), and those known to be superluminal (Fig. 3b). For the latter sources it seems more reasonable to assume that the plasma in the jet is flowing with a velocity close to c. Different symbols distinguish BL Lac objects, HPQs, and the radio sources from the Pearson & Readhead sample. Furthermore, different symbols are used for resolved and unresolved sources. It is interesting to note that there seems to be no difference between BL Lac objects, HPQs, and radio sources. There also seems to be no obvious

difference between the resolved and unresolved sources, or between sources known to be superluminal and the remaining ones.

The main result from Fig. 3 is that all objects lie in the region of the plane such that $n'_{SSC} > n'_{pair}$, typically by two orders of magnitude in n'_{SSC} or in n'_{pair}. This can be seen more clearly in Fig. 4, which is the histogram of the ratio n'_{ssc}/n'_{pair} (the dashed area corresponds to the sources listed in Table 3).

5.2 CHANGING PARAMETERS

In order to check that our result is not an artifact of the assumed parameters, we have investigated its dependence on each of the following parameters:

i) R_0: for a fixed τ_0, it is clear from equation (5.3) that n'_{pair} depends linearly on R_0. To have n'_{pair} consistent with n'_{SSC} for all sources a size $R_0 \sim 10^{17}$ cm is then required. Such a source size is completely ruled out by the short variability time–scales observed for the X–ray flux. In addition, if one applies simple steady pair model, requiring $\tau_0 = 10$ and $R_0 = 10^{17}$ cm implies an X–ray luminosity in excess of 3×10^{48} erg/s (see equation 2.9).

ii) τ_0: for fixed R_0, n'_{pair} depends on τ_0 (eq. 5.3) only through R^2_{tr}, but as discussed in Section 2.1, R_{tr} varies only by a factor of $\simeq 2.5$ for $1 < \tau_0 < 1000$. Thus an increase of only a factor of six in n'_{pair} is expected even for extreme values of τ_0.

iii) α: the derived SSC particle density is dependent upon the assumed value of the spectral index α (equation 3.1). For flatter spectral indices, less (low energy) electrons are required in order to emit the observed spectrum, and hence n'_{SSC} is decreased. However, for $\alpha = 0.5$, less than 1/3 of the sources have a n'_{SSC} consistent with n'_{pair}. Note that, if α is estimated from the IR spectral index, Ghisellini *et al.* (1986) report an average value $\alpha_{IR} = 0.94$ for a sample of blazars, and $\alpha_{IR} = 1.25$ for a subsample of sources with strong emission lines.

iv) F_x, m_v: as discussed above, n'_{SSC} is proportional to the used X–ray or optical flux (equation 3.1). The derived density n'_{SSC} become consistent with n'_{pair} for the sources with the largest ratio n'_{SSC}/n'_{pair} if their VLBI component contributes only a factor 10^{-3}–10^{-4} of the total observed X–ray or optical fluxes. We think this is unlikely because:

a) We can calculate the beaming factor needed to lower the predicted X-ray or optical flux to the level required to have $n'_{SSC}/n'_{pair} = 1$. Taking into account that $n'_{pair} \propto 1/\Gamma_b(r_{VLBI}) \sim 1/\delta$ (see equation 5.3), we find that for some sources δ >30–50 is needed (examples are 1749+096, 0106+013, 0711+356, 0804+499, 0906+430). This exacerbates the acceleration problem. In addition, such high values of δ would contrast with the apparent velocities $\beta_{app}c$ measured in superluminal sources.

b) Detailed observation of the (arcsecond scale) jet in M87 (Biretta, Stern & Harris, 1991) from the radio through the X–rays have revealed that the knots in the jets have an overall spectrum similar to the one of the core, and only a factor of a few dimmer.

v) γ_{min}: this is the most critical parameter. If the emitting particles are not allowed (by some heating mechanisms) to completely cool down to $\gamma_{min} \simeq 1$, the number density of required particles can be drastically reduced. Since $n'_{SSC} \propto \gamma_{min}^{-2\alpha}$, a value of $\gamma_{min} \sim 100$ could make n'_{SSC} small enough to be consistent with n'_{pair} for all sources. Note that a value of $\sim$ 100 for γ_{min} is consistent with the values of γ one derives from $\gamma_m = [\nu_m/(\delta\nu_B)]^{1/2}$ which averages to 150-200 for the considered sources (here ν_B is the cyclotron frequency in the rest frame of the radio component).

6. Discussion

For a sample of blazars and radio sources, we have calculated the density of emitting particles in the radio emitting region using both standard SSC theory and $e^{\pm}$ pair–jet models.

In our study we neglected the possibility that pairs are created outside the central source. The interaction of ultrarelativistic protons with the ambient medium can lead to the formation of $e^{\pm}$ pairs, and this mechanism has been recently proposed by Giovanoni & Kazanas (1990) to explain the flatness of the radio spectrum of compact radio sources. We note that this mechanism needs a density of cold, target protons which is in excess of the limits derived by the polarization arguments, and therefore cannot be applied to sources having a polarized jet.

We find that the density of $e^{\pm}$ pairs able to reach the emission region is consistent with the densities deduced from SSC theory only for extreme choices of the parameters, and only if the $e^{\pm}$ pairs are not allowed to cool down to Lorentz factor $\gamma_{min} < 100$.

This result is strengthened by our assumption that all $e^{\pm}$ pairs escaping from the central source emit the observed SSC radiation. In fact a significant fraction of the escaping pairs could not reach the radio emission region, either as a result of isotropic escape (rather than being channeled in the jets), or as a result of interaction with the ambient medium.

Our result does not depend on the details of the pair production models for the compact source, even if we indeed assume that the $e^{\pm}$ pairs are produced in a compact region, and therefore that they undergo annihilation while escaping. In the framework of the best studied pair production models, the density of the $e^{\pm}$ we have assumed at the base of the outflow corresponds to extreme values of the compactness of the source. Therefore, if the X-ray source is less compact than we have implicitly assumed, our result is strengthened.

If the jet is dominated by 'normal' (electron–proton) plasma, observational limits on the degree of Faraday rotation and depolarization imply thermal electrons densities $n_e < 10^{-3}$ cm^{-3} (*e.g.* Walker *et al.* 1987). An $e^{\pm}$ pair dominated plasma avoids this requirement, and this is one of the main reasons leading to consider $e^{\pm}$ pair–dominated jets. Combining our findings with the above limits for the presence of thermal 'normal' matter, we can reach a firm conclusion. In fact our results indicate that a jet can be supplied by pairs from the central source only if all pairs have energies greater than 50 MeV at the VLBI scale, and do not cool below $\gamma_{min} \sim 100$. Remarkably enough, this value of γ_{min} is very similar to the one derived for an electron–proton plasma, from the depolarization argument (Wardle 1977, Jones & O'Dell 1977).

Therefore, independent on the nature of the emitting plasma, one can no longer evade the problem of an efficient acceleration mechanism operating in the jet, inhibiting the cooling of the emitting particles and able to maintain the majority of the electrons at relativistic energies.

We consider this as the main conclusion of our paper.

Speculating about the nature of this acceleration mechanism, we would like to suggest synchrotron reabsorption as one likely possibility (Ghisellini, Guilbert & Svensson 1988), that would be discussed in detail elsewhere (Ghisellini & Svensson, in preparation).

ACKNOWLEDGMENTS

We acknowledge the financial support of the SERC (IMG), Royal Society (ACF), A. Della Riccia Foundations and the italian MURST (AC).

REFERENCES

Begelman, M.C., Blandford, R.D. & Rees, M.J., 1984. *Rev. Mod. Phys.*, **56**, 255.

Biretta, J.A., Stern, C.P., & Harris, D.E., 1991. *Astron. J.*, **101**, 1632.

Blandford, R.D., & Rees, M.J., 1978. In *Pittsburgh Conference on BL Lac Objects*, ed. A.N. Wolfe (Pittsburgh University Press), p. 328.

Done, C., Ghisellini, G. & Fabian, A.C., 1990. *Mon. Not. R. astr. Soc.*, **245**, 1.

Ghisellini, G., 1987. *PhD Thesis*, SISSA, Trieste.

Ghisellini, G., Maraschi, L., Tanzi, E.G., & Treves, A., 1986. *Astrophys. J.*, **310**, 317.

Ghisellini, G., Guilbert, P.W., & Svensson, R., 1988. *Astrophys. J. Lett.*, **334**, L5.

Ghisellini, G., Bodo, G., Trussoni, E., & Rees, M.J., 1990. *Astrophys. J. Lett.*, **362**, L1.

Giovanoni, P.M., & Kazanas, D., 1990. *Nature*, **345**, 319.

Guilbert, P.W., & Stepney, S., 1985. *Mon. Not. R. astr. Soc.*, **212**, 523.

Impey, C.D., & Tapia, S., 1990. *Astrophys. J.*, **354**, 124.

Jones, T.W., O'Dell, S.L., & Stein, W.A., 1974a. *Astrophys. J.*, **188**, 353.

Jones, T.W., O'Dell, S.L., & Stein, W.A., 1974b. *Astrophys. J.*, **192**, 261.

Jones, T.W., & O'Dell, S.L., 1977. *Astr. Astrophys.*, **61**, 29.

Madau, P., Ghisellini, G., & Persic, M., 1987. *Mon. Not. R. astr. Soc.*, **224**, 257.

Marscher, A.P., 1987. In *Superluminal Radio Sources*, eds. Zensus, A. and Pearson, T.J. (Cambridge: Cambridge University Press), p. 280

Mutel, R.L., 1990, in *Parsec–Scale Radio Jets*, eds. Zensus, J.A., & Pearson, T.J. (Cambridge: Cambridge University Press), p. 98.

Pearson, T.J., & Readhead, A.C.S., 1988. *Astrophys. J.*, **328**, 114.

Phinney, E.S., 1983. *Ph. D. Thesis*, University of Cambridge.

Porcas, R.W., 1987. In *Superluminal Radio Sources*, eds. Zensus, A. and Pearson, T. (Cambridge: Cambridge University Press), p. 12

Rees, M.J., 1971. *Nature*, **229**, 312.

Stickel, M., Padovani, P., Urry, C.M., Fried, J.W. & Kühr, H., 1991. *Astrophys. J.*, in press.

Svensson, R., 1986. In *Radiation-Hydrodynamics in Stars and Compact Objects*, IAU Coll. No. 89, eds. Mihalas, D. & Winkler, K.-H.A. (Springer-Verlag, Berlin), p. 325.

Svensson, R., 1987. *Mon. Not. R. astr. Soc.*, **227**, 403.

Svensson, R., 1990. In *Physical Processes in Hot Cosmic Plasmas*, eds. W. Brinkmann *et al.* (Kluwer Academic Publishers, The Netherlands), p. 357.

Unwin, S.C., Cohen, M.H., Pearson, T.J., Seielstad, C.A., Walker, R.C, Simon, R.S., & Linfield, R.P., 1985. *Astrophys. J.*, **289**, 109.

Walker, R.C., Benson, J.M., & Unwin, S.C., 1987. *Astrophys. J.*, **316**, 546.

Wardle, J.F.C., 1977. *Nature*, **269**, 563.

Worral, D.M., Giommi, P., Tananbaum, H., & Zamorani G., 1987. *Astrophys. J.*, **313**,, 596.

Figure Captions

Fig.1. The number of Compton scatterings, N_{scatt} from R to infinity as a function of R/R_0 (from eq. 2.5). The assumed parameters are $R_0 = 10^{14}$ cm, $\Gamma_{b,0} = \sqrt{3/2}$. Separate curves are shown for several values of τ_0. The dashed lines at $N_{scatt} = 1$ and 8/3 are the values appropriate to our definitions of R_{tr} and R_{an} respectively (see text). It is clear that $R_{tr} > R_{an}$ for all values of τ_0 considered. It can be seen that the higher annihilation rate for higher τ_0 gives rise to similar values of R_{tr} and R_{an} over a large range of τ_0.

Fig. 2. The fiducial 'trapping' (R_{tr}/R_0) and annihilation (R_{an}/R_0) radii as a function of τ_0. Note the slight dependence of both radii on τ_0, although the ratio $R_{tr}/R_{an} \simeq 1.34$ is independent of τ_0. $R_0 = 10^{14}$ cm.

Fig. 3. The derived particle density from the $e^{\pm}$ pair-jet model (n'_{pair}) against that from SSC theory (n'_{SSC}) for our sample of sources, for $R_0 = 10^{14}$ cm, $\tau_0 = 10$, $\alpha = 0.75$ (see text). The dashed line represents $n'_{pair} = n'_{SSC}$. Filled symbols distinguish those sources with measured VLBI diameter, θ_d, from those with only an upper limit (open). Objects for which superluminal motion has not been reported in Porcas (1987) are shown in (a), superluminal sources are shown in (b).

Fig. 4. Histogram of the logarithm of the ratio n'_{SSC}/n'_{pair}. The dashed part of the histogram refers to the radio sources listed in Table 3, for which n'_{SSC} and the beaming factor δ have been estimated requiring that the emitting particles do not overproduce the optical flux, by self–Compton emission.

Table 1. Costants function of α

α	0.25	0.5	0.75	1.0
$t(\alpha)$	1.33	0.56	0.29	0.16
$b(\alpha)$	1.8	3.2	3.6	3.8

Table 2.

Source	z	θ_d	ν_m	F_m	F_x	δ	n'_{SSC}	n'_{pair}
		$m.a.s$	GHz	Jy	Jy		cm^{-3}	cm^{-3}
0048–097	.....	0.40	5.0	0.71	6.6E-8	3.24	.....	.....
0106+013	2.107	<0.40	5.0	2.30	2.2E-7	18.9	3.3E+2	5.8E+0
0212+735^{sl}	2.370[1]	0.60	5.0	1.50	2.3E-7	6.79	3.6E+2	7.6E+0
0219+428	0.444	1.50	5.0	0.20	1.6-7	0.093	8.7E+2	5.1E+0
0235+164^{sl}	0.940[2]	0.50	5.0	1.75	1.7E-7	6.53	2.5E+2	9.8E+0
0306+102	.....	0.50	5.0	0.73	1.1E-7	2.13	.....	.....
0316+041	0.018	0.30	22.0	1.20	1.8E-5	0.32	4.2E+5	2.3E+4
0336–019	0.852	<1.00	5.0	2.10	4.7E-8	3.04	3.0E+1	5.4E+0
0420–014	0.915	<0.70	5.0	1.50	5.2E-7	2.60	6.5E+2	1.3E+1
0454+844	.....	0.55	5.0	1.30	5.0E-8	3.71	.....	.....
0521–365	0.055	1.80	5.0	0.86	6.8E-7	0.17	3.3E+3	7.6E+1
0716+714	.....	0.35	5.0	0.50	2.2E-7	2.30	.....	.....
0735+178^{sl}	0.424	<0.30	5.0	1.29	3.2E-7	7.27	1.4E+3	4.0E+1
0754+100	.....	0.60	5.0	0.53	1.7E-7	1.06	.....	.....
0818–128	.....	0.80	5.0	0.47	7.0E-8	0.69	.....	.....
0829+046	.....	0.90	5.0	0.26	1.9E-7	0.26	.....	.....
0851+202^{sl}	0.306	0.30	5.0	2.30	1.7E-6	8.77	4.9E+3	4.7E+1
0906+430^{sl}	0.670	0.10	5.0	0.88	1.0E-7	43.3	1.6E+3	4.3E+1
1101+384	0.030	<0.30	5.0	0.24	1.4E-5	0.49	2.6E+6	8.5E+3
1147+245	.....	0.90	5.0	0.39	8.0E-8	0.46	.....	.....
1215+303	.....	0.70	5.0	0.33	8.5E-7	0.38	.....	.....
1219+285	0.102	0.50	5.0	0.13	4.2E-7	0.23	2.8E+4	3.4E+2
1226+023[3],^{sl}	0.158	0.80	10.7	10.0	1.6E-5	1.5	6.4E+3	1.3E+2
1253–055^{sl}	0.538	0.30	5.0	0.90	1.4E-6	4.19	7.8E+3	5.7E+1
1308+326	0.996	0.50	5.0	1.97	3.0E-7	6.82	3.9E+2	9.3E+0
1400+162	0.244	1.40	5.0	0.08	1.0E-7	0.039	2.0E+3	1.1E+1
1538+149	0.605[2]	0.60	5.0	0.56	1.5E-7	1.31	6.4E+2	4.2E+1

1641+399^{sl}	0.595	0.30	22.	6.90	6.6E-7	5.26	1.8E+2	4.2E+1
1652+398	0.034	<0.50	5.0	0.40	1.7E-7	0.80	1.0E+4	2.4E+3
1727+502	0.055	1.20	5.0	0.04	2.1E-6	0.012	3.3E+5	1.7E+2
1749+096	0.322[2]	0.20	5.0	1.43	3.5E-7	14.3	2.4E+3	6.1E+1
1803+784^{sl}	0.684[2]	0.40	5.0	1.80	1.6E-7	8.49	3.1E+2	1.3E+1
1807+698	0.051	1.40	5.0	1.21	6.0E-7	0.36	2.9E+3	1.4E+2
1845+797^{sl}	0.057	0.50	5.0	0.31	1.1E-6	0.45	5.1E+4	9.3E+2
2007+776^{sl}	0.342[2]	0.40	5.0	1.17	1.1E-7	4.71	4.4E+2	4.3E+1
2200+420^{sl}	0.069	0.35	5.0	1.60	8.2E-7	4.43	9.0E+3	6.6E+2
2201+044	0.028	0.70	5.0	0.16	2.1E-7	0.18	2.7E+4	1.8E+3
2223−052^{sl}	1.404	0.40	10.7	2.20	1.1E-6	3.77	9.8E+2	2.6E+1
2230+114^{sl}	1.037	<0.50	5.0	0.54	3.4E-7	1.87	1.6E+3	3.3E+1
2234+282	0.795	<0.50	5.0	1.21	5.0E-8	5.22	1.1E+2	1.3E+1
2251+158^{sl}	0.859	<0.30	5.0	0.90	5.6E-7	5.98	2.7E+3	3.1E+1
2254+074	0.190[2]	1.00	5.0	0.14	1.0E-7	0.11	1.9E+3	3.2E+1
2335+031	.....	1.70	5.0	0.03	2.3E-8	0.016	.....	.....
2345−167	0.600	<0.40	5.0	2.50	1.8E-7	11.0	2.6E+2	1.1E+1

^{sl} Superluminal source [from Porcas (1987) and Mutel (1990)]

[1] from Impey & Tapia (1990); [2] from Stickel *et al.* (1991); [3] from Unwin *et al.* (1985)

Table 3.

Source	z	θ_d	ν_m	F_m	F_x	δ	n'_{SSC}	n'_{pair}
		$m.a.s$	GHz	Jy	Jy		cm^{-3}	cm^{-3}
0836+710	2.170	0.34	5.0	1.04	1.5e-6	8.1	5.6E+3	1.9E+1
0923+392^{sl}	0.699	1.13	5.0	4.71	3.5E-7	3.5	9.1E+1	4.0E+0
1633+382	1.814	0.57	5.0	0.43	8.0E-8	2.2	4.3E+2	2.4E+1
1739+522	1.375	0.37	5.0	0.89	1.0E-7	7.3	3.9E+2	1.5E+1
1928+738^{sl}	0.302	0.49	5.0	2.11	3.4E-7	4.8	6.5E+2	3.2E+1
Source	z	θ_d	ν_m	F_m	m_v	δ	n'_{SSC}	n'_{pair}
		$m.a.s$	GHz	Jy			cm^{-3}	cm^{-3}
0016+731	1.781	0.46	5.0	1.58	18.0	5.97	4.4E+3	1.3E+2
0108+388	.....	0.85	5.0	0.56	22.0	0.76	.....	.....
0133+476	0.859	1.13	5.0	1.60	19.0	1.10	7.1E+2	1.2E+1
0710+439	0.518	0.96	5.0	0.63	20.7	0.61	5.2E+2	1.1E+1
0711+356	1.620	0.11	5.0	0.27	17.0	8.38	2.7E+5	1.6E+2
0804+499	1.430	0.23	5.0	1.34	17.5	12.7	1.6E+4	2.3E+1
0850+581^{sl}	1.322	0.48	5.0	0.94	18.0	2.71	6.9E+3	2.4E+1
0859+470	1.462	1.40	5.0	1.15	18.7	0.70	1.0E+3	3.6E+0
1624+416	2.550	0.33	5.0	0.43	22.0	7.01	6.2E+2	2.6E+1
1954+513	1.220	1.06	5.0	0.85	18.5	0.71	2.2E+3	6.2E+0
2021+614	0.227	0.60	5.0	1.01	19.5	1.40	2.4E+3	1.1E+2
2351+456	2.000	0.69	5.0	0.32	20.6	1.05	1.3E+3	3.4E+1
2352+495	0.237	0.82	5.0	0.73	19.0	0.57	3.8E+3	3.5E+1

^{sl} Superluminal source [from Porcas (1987) and Mutel (1990)]

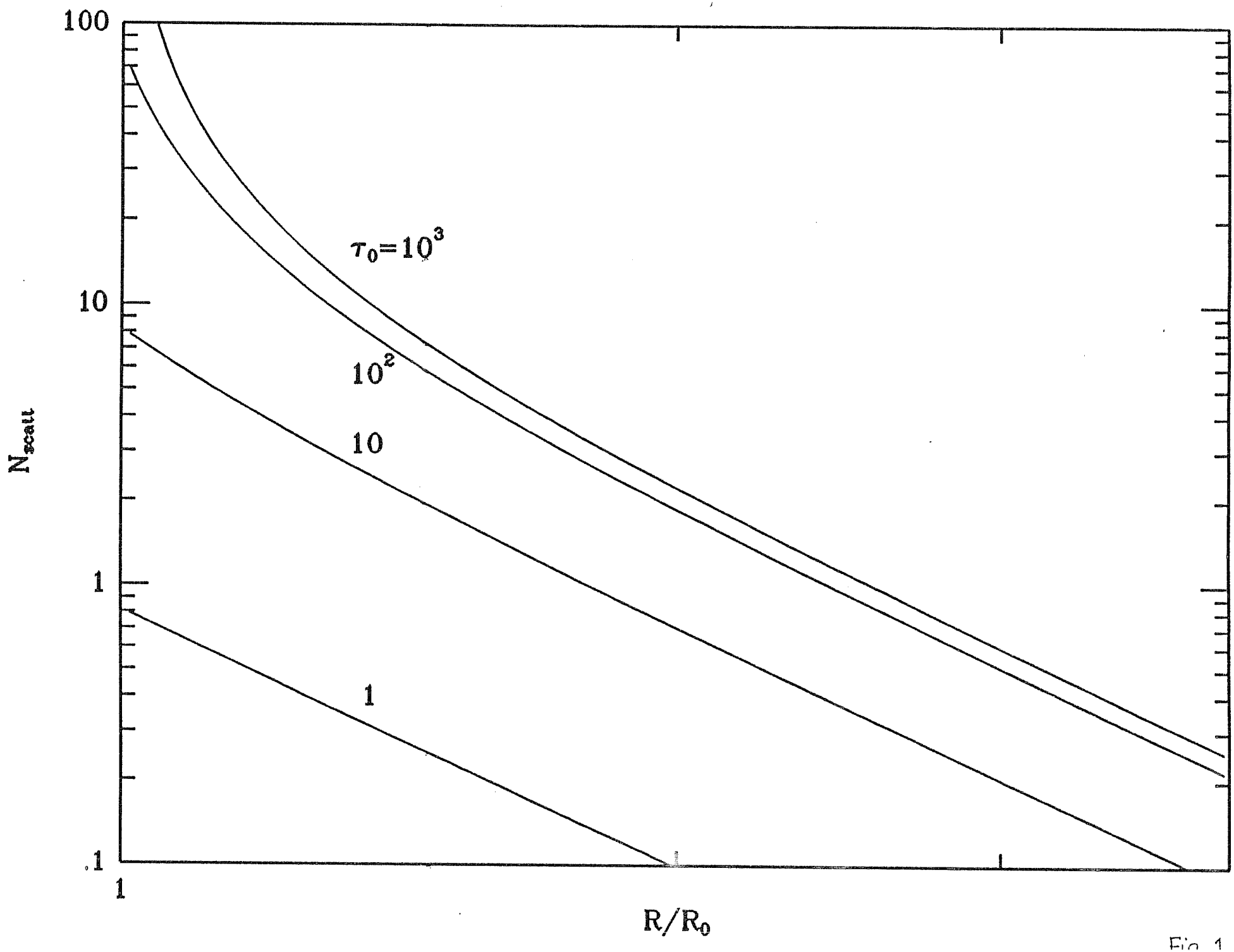

Fig. 1

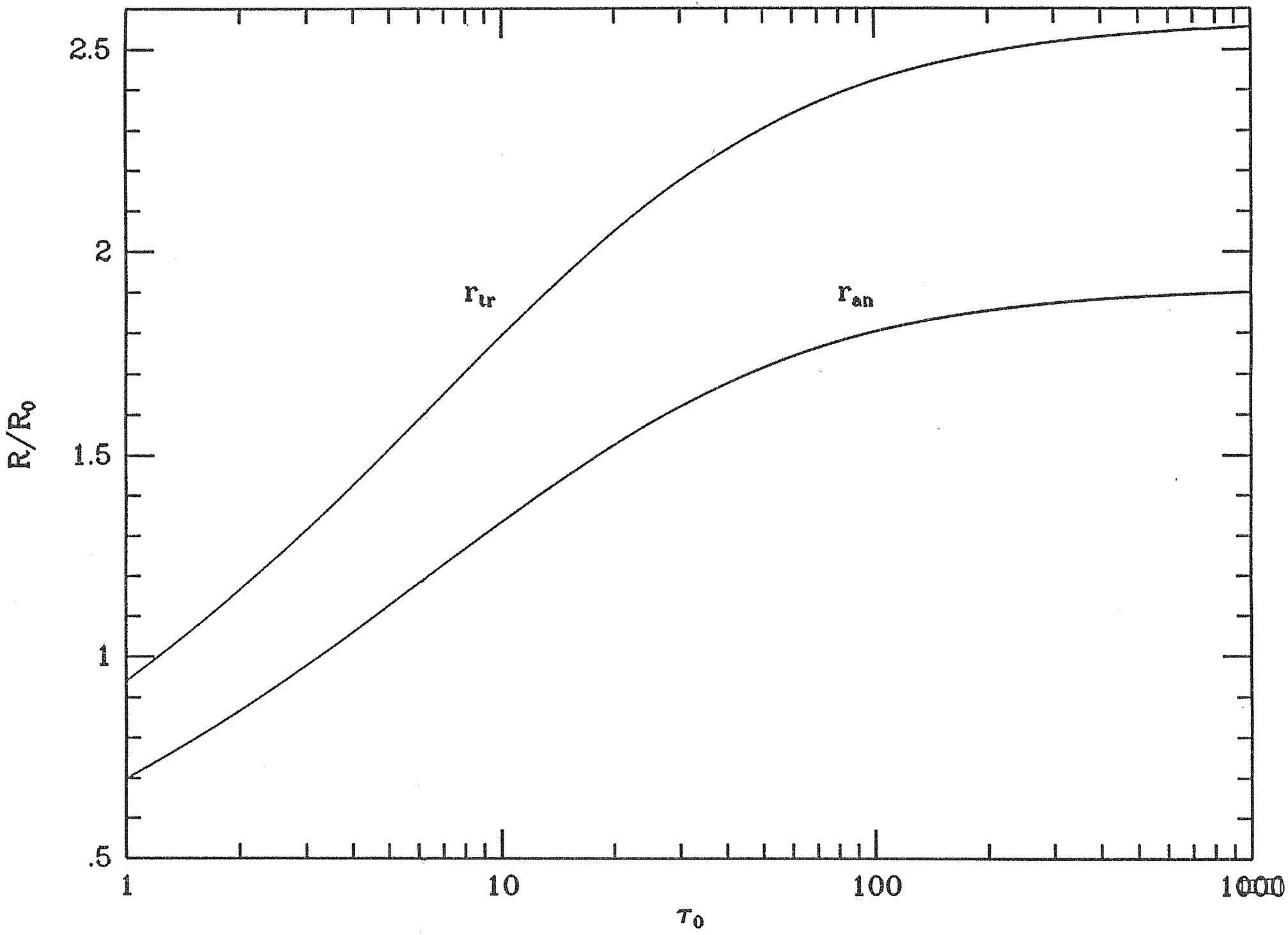

Fig. 2

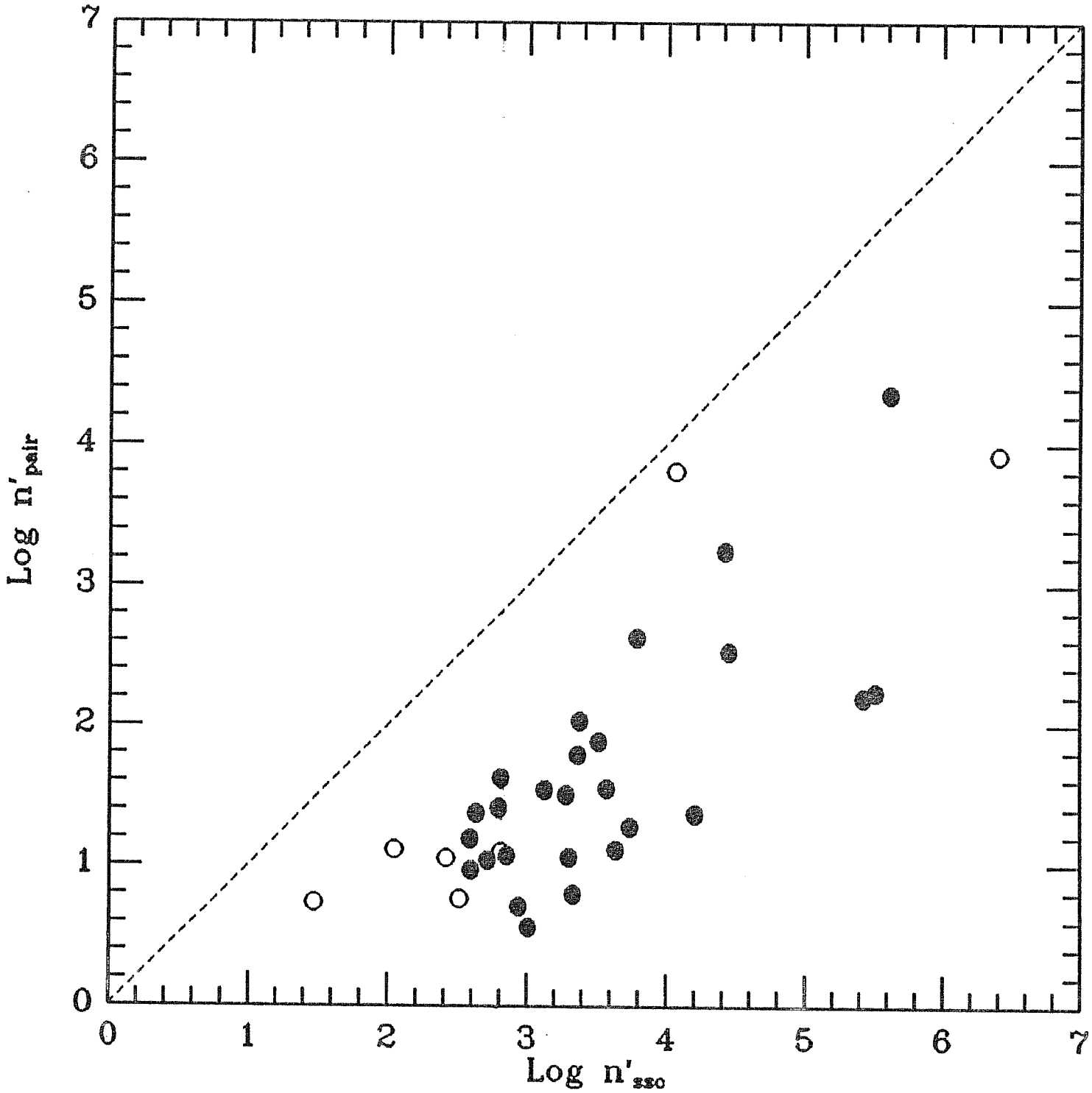

Fig. 3a

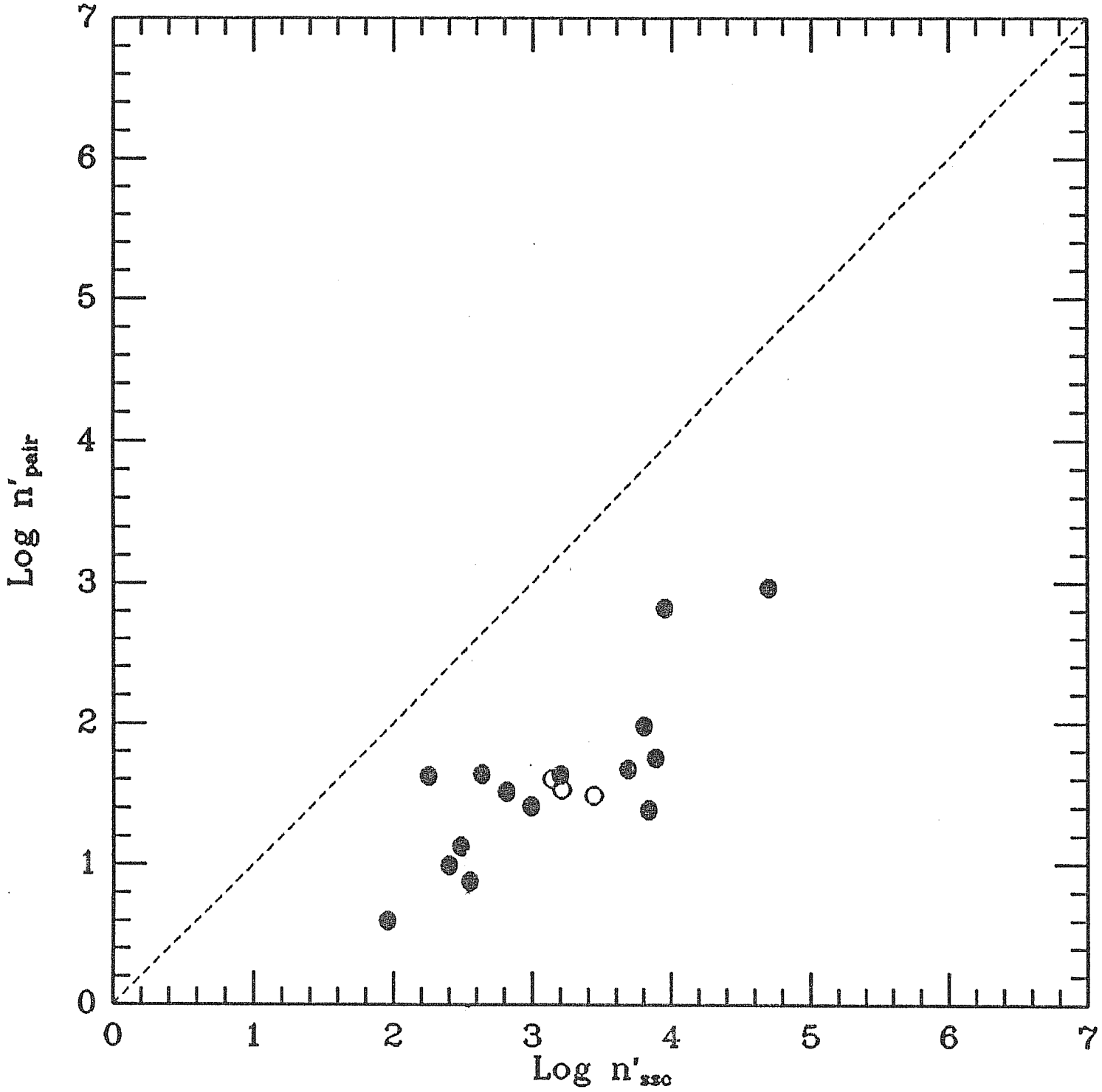

Fig. 3b

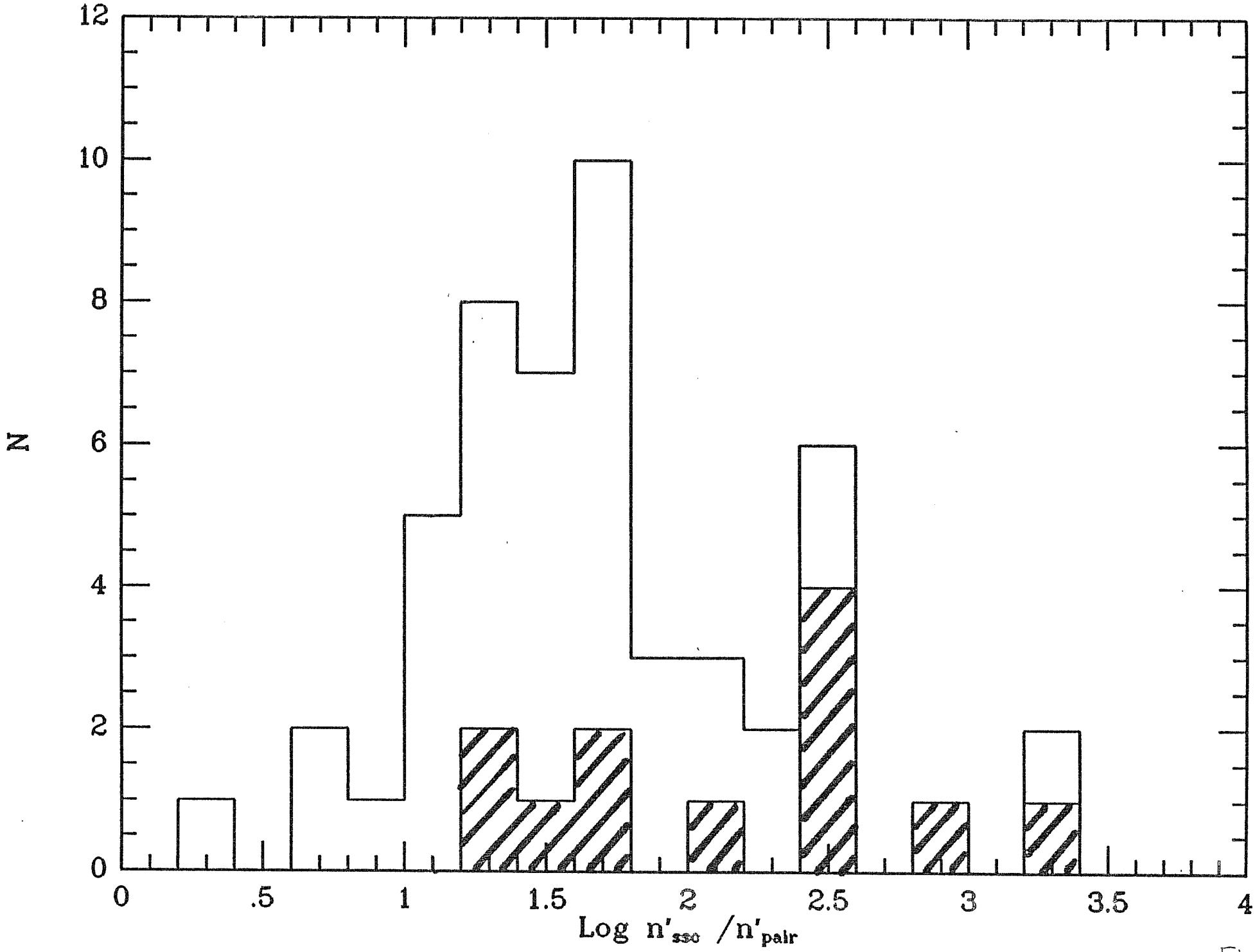

Fig. 1

Appendix D

Magnetic field in the inner region of AGN

On the magnetic energy density in the X-ray emission region of Active Galactic Nuclei

A. Celotti[1,2], G. Ghisellini[3] and A.C. Fabian[1]

[1] *Institute of Astronomy, Madingley Road, Cambridge CB3 0HA*

[2] *International School for Advanced Studies, Trieste, Italy*

[3] *Osservatorio Astronomico di Torino, Pino Torinese, Italy*

Mon. Not. R. Astron. Soc., in press

SUMMARY

We estimate upper limits on the magnetic energy density in the compact X–ray emission region of the Seyfert galaxies NGC 4051 and NGC 6814 and the quasars 3C273, 3C279 and H1821+643 using synchrotron self-Compton theory. The size of the emission region is obtained from the X-ray variability timescale and the electron density from the assumption that the X–ray emission in AGN is due to non–thermal Comptonization of soft 'blue bump' photons. The competition between synchrotron self–Compton emission and direct Comptonization then enables us to estimate the relative importance of the magnetic and radiation fields. Equipartition between magnetic and X-ray energy density is at best only marginally possible and in several cases is strongly ruled out. This poses serious problems for many theories for the acceleration and radiation of particles in the X-ray emission region. We discuss several alternative pictures that do allow equipartition to occur. The most promising model, suggested by the work of Rees, paradoxically requires the magnetic field to be strong. It then confines many small, dense, clouds in the region which cause the optical and UV photosphere to lie beyond the X-ray emission region. The primary radiation is then synchrotron self–Compton emission.

1 INTRODUCTION

Recent observations of Active Galactic Nuclei (AGN), made at increased spectral resolution and in new wavebands (such as the near IR, millimeter and soft X-ray bands), indicate that several different emission processes contribute to the overall spectrum, including both primary and reprocessed radiation (*e.g.* Bregman 1990). The EUV region (the 'EUV' or 'big blue' bump) appears to carry much of the bolometric luminosity in many AGN. This emission is probably due to quasi-blackbody radiation from an accretion disc.

Variability observations have become a powerful test of models of continuum production, particularly for the conditions in the innermost parts of AGN. Resolution on short timescales has allowed upper limits on the dimensions of the X-ray emitting regions to be estimated, in some cases giving results as small as 10^{12}–10^{13} cm (Lawrence *et al.* 1987, Matsuoka *et al.* 1990; Kunieda *et al.* 1990). Simultaneous variability observations in different spectral bands put strong constraints on the spatial distribution of the emitting regions and indicate whether the same radiative process dominates at different frequencies (*e.g.* Done *et al.* 1990b).

There is no certainty about the nature of the X–ray emission mechanism, but it is often assumed that the X–rays are Compton–scattered photons of an EUV-soft X bump from a non–thermal distribution of relativistic electrons. In particular, the recent simultaneous optical and X–ray observations of NGC 4051 argue strongly for relativistic Comptonization as the radiation mechanism for the X–rays (Done *et al.* 1990b). In this source, the steadiness of the infrared to UV flux, during rapid X–ray flux variations, means that any variable optical component lies below an extrapolation of the X–ray continuum. This apparently rules out synchrotron and synchrotron self–Compton emission (SSC) as candidates for the X–ray emission, since they predict a variable optical component on or above such an extrapolation. Whilst Comptonization by a thermal distribution of non-relativistic electrons cannot be ruled out so easily, it does require finely-tuned values of the Thomson depth and temperature to be maintained throughout rapid variability. For the sources studied here we therefore assume that the X-rays are produced by a population of relativistic electrons which inverse Compton–scatter EUV photons.

In this paper, we use spectral and variability information to constrain the

synchrotron and self-Compton emission that can be produced in the X-ray emitting region, as predicted by standard SSC theory (Jones, O'Dell & Stein 1974a, b). Most theories of accretion predict that magnetic fields are amplified in the flow and many theories of the acceleration of electrons in AGN require strong magnetic fields. Consequently, it is generally supposed that synchrotron self–Compton radiation is also an important energy loss process in the central engine.

Assuming that the X-rays are due to Comptonization of the EUV photons and using variability timescales to estimate the dimension of the emission region, we derive the density of the relativistic electrons necessary to produce the observed X–ray flux. If a magnetic field is present, these electrons also produce infrared to X-ray radiation through SSC emission. By requiring that this radiation does not exceed the observed flux, we derive upper limits on the intensity of the magnetic field. The method parallels that commonly used to estimate magnetic field strengths in extended radio sources, where the size of the region is deduced from the angular size. In that case the electron density is obtained from the observed synchrotron radiation and the X–ray emission (or lack of it) produced from inverse Compton scattering of the microwave background gives a measurement (or lower limit) to the magnetic field in the emission region. Another method assumes that the peak in the synchrotron spectrum is due to synchrotron self-absorption.

We have applied this method to two Seyfert galaxies, NGC 4051 and NGC 6814, and three quasars 3C273, 3C279 and H1821+643 and find, under our assumptions, that their X–ray emission regions cannot be magnetically dominated in the sense that equipartition between the magnetic and radiation energy densities can be reached only for extreme values of the parameters. One of the strongest limits is found for NGC 6814 for which equipartition can be reached only if the dimension R is at least a factor 10^3 smaller than that inferred from variability constraints. This makes the region implausibly small.

Our results pose problems for those models invoking magnetic fields to accelerate particles to high energies. If the magnetic energy density is not dominant then it is difficult to understand how magnetic fields can accelerate particles to create radiation which has a higher energy density. The magnetic energy cannot, of course, be replenished (or changed) faster than the radiation escapes from the emission region.

We have therefore carried out an inspection of our assumptions in order to see whether some modification allows equipartition magnetic fields to occur. Paradoxically, we find that the magnetic field itself provides an interesting and plausible solution. A very strong magnetic field can support dense clouds which free-free absorb the optical and UV radiation, without significantly affecting the direct X-ray radiation, and so obviate our optical and UV spectral constraints. The X-rays are then best explained as SSC emission.

In Section 2 we describe our procedure. The sample and the properties of the individual sources are given in Section 3. The results are presented in Section 4 and discussed in Section 5.

2 CONSTRAINTS ON THE MAGNETIC FIELD

Consider a homogeneous spherical region with a size R, estimated from the X–ray variability timescale t_{var}, filled with electrons with a power–law energy distribution $N(\gamma) = K\gamma^{-p}$ [cm^{-3}], for Lorentz factors $\gamma < \gamma_{max}$, and soft photons with a blackbody spectrum. The density is calculated considering the maximum temperature blackbody, from the same volume, whose emission does not exceed the observed UV or soft X–ray (at 0.2 keV) fluxes. The assumption of a 'maximum blackbody' sets the highest possible limit on the derived magnetic field.

We define a characteristic optical depth for electron scattering, $\tau = \sigma_T RK$ (σ_T is the Thomson cross section). Assuming that the X–ray emission is due to Compton scattering of the soft photons by the relativistic electrons, we can estimate τ by dividing the extrapolated X-ray flux density by the blackbody flux density, at the frequency where the blackbody peaks (Ghisellini 1987). Setting $R = c\,t_{var}/(1+z)$ we then derive the normalization K of the electron distribution, whose slope p is fixed by the observed X-ray spectral index through $p = 2\alpha_x + 1$ [$F(\nu) \propto \nu^{-\alpha_x}$].

If a magnetic field is present in the emission region, electrons emit synchrotron, first–order, second–order and higher order self–Compton radiation, as predicted by standard SSC theory. The corresponding luminosities depend on the magnetic field intensity B, the density of the emitting electrons K and the dimensions R of the region (see Appendix A).

Having derived R and K, the only remaining unknown physical quantity,

which determines the synchrotron and self–Compton intensities, is the strength of the magnetic field. We can consequently impose a limit on it by requiring that the predicted SSC flux does not exceed the observed flux at any observed frequency. This limit depends on the assumed energy extent of the distribution of the emitting electrons, the maximum Lorentz factor γ_{max} of which determines which process (synchrotron or self–Compton) dominates at a given frequency. Synchrotron radiation dominates at a given frequency ν if $\nu < (4/3)\nu_B\gamma_{max}^2$, where ν_B is the cyclotron frequency, so requiring $B > 268\,\nu_{GHz}/\gamma_{max}^2$ G, where ν_{GHz} is the observed frequency measured in GHz. If the B–field is lower, the flux at ν is not due to synchrotron emission. It is mainly due to first–order Compton scattering if $\nu < (16/9)\nu_B\gamma_{max}^4$, or to higher–order Compton scattering otherwise.

For each pair of values of B and γ_{max}, the SSC spectrum is completely determined and can be compared with the observed data: the values of the two parameters which predict a flux exceeding the observed one are not allowed. In this way we define a forbidden area in the $B - \gamma_{max}$ plane.

Since the observed X-ray flux is produced by Compton scattering, we require that the electron population has a minimum $\gamma_{max} \sim (\nu_x/\nu_{bb})^{1/2}$, where ν_x is the maximum observed X-ray frequency, and ν_{bb} is the frequency where the assumed maximum blackbody peaks. We also considered third–order Compton emission, but, because it gives weaker limits on the magnetic field in the range of parameters considered, it is neglected in the following discussion.

For low values of γ_{max} the synchrotron flux can be completely self absorbed. The relation between the magnetic field and the Lorentz factor γ_t of electrons emitting mainly at the synchrotron self–absorption frequency is (see, *e.g.* Ghisellini 1989)

$$\gamma_t = c_t \left[\frac{RK}{B}\right]^{1/(4+p)} \tag{1}$$

where the value of the constant c_t is given in Appendix A.

In the self–absorbed regime (*i.e.* for $\gamma_{max} < \gamma_t$), the synchrotron flux $\propto B^{-1/2}$: for a fixed γ_{max} an increased magnetic field results in a decreased flux and a (linearly) increased maximum–emitted frequency $\nu_{s,max}$. Therefore in this regime we can derive a lower or upper limit on the magnetic field, depending on the value of the observed frequency used for the comparison between the predicted and the observed flux.

Moreover if $\gamma_{max} < \gamma_t$ the inverse Compton fluxes must be calculated using the self–absorbed synchrotron radiation energy density.

A complete description of the formulae used is given in Appendix A, together with the frequency ranges appropriate for synchrotron and self–Compton fluxes.

3 THE SAMPLE

We have applied the above method to five sources which belong to two classes of AGN: two Seyfert galaxies, NGC 4051 and NGC 6814, the radio loud quasar 3C273, the Optically–Violent–Variable (OVV) quasar 3C279 and the radio quiet quasar H1821+643. Basically, we selected sources with well–defined X–ray variability timescales and with evidence for 'blue bump' component.

For each source, except NGC 4051 for which simultaneous optical and X–ray data are available, we use the lowest IR-UV fluxes obtained from different instruments. The maximum temperature EUV blackbodies consistent with the size of the X–ray region and the spectral data are computed; the soft X–ray flux is constrained by extrapolating the best–fitting power–law of the harder X-ray flux down to 0.2 keV. (Increasing this energy also increases the blackbody temperature, leading to stronger results). In Table 1 we list the redshifts, the blackbody temperatures T_{bb} and the dimension R, estimated from X–ray variability. We also give the minimum γ_{max} needed to emit the maximum X–ray frequency at which the source has been observed, by upscattering of the blackbody photons of frequency ν_{bb}: it is indicated by $\gamma_{min} \equiv (3\nu_x/4\nu_{bb})^{1/2}$.

We assume $H_0 = 100$ km s^{-1} Mpc^{-1}, $q_0 = 0$.

3.1 NGC 4051

Done *et al.* (1990b) present results on correlated variability in the Seyfert galaxy, NGC 4051 (z=0.0023). This source has previously shown rapid, large amplitude, variability in the X–ray down to time-scale of 100s (Lawrence *et al.* 1987, Matsuoka *et al.* 1990) and up to 20–30 per cent in the optical band (Lyutyi 1977, Penston *et al.* 1974). As a conservative value for estimating the X–ray dimension we use $t_{var} = 300$ s.

NGC 4051 has been observed simultaneously in the X-ray band (2–20 keV) by the GINGA satellite, in the B band from a series of CCD images and in the IR band

with the UKIRT. A spectrum in the UV band from IUE, even if not simultaneous, gives information on the overall spectral distribution and shows that the optical–UV spectrum is not badly contaminated by the thermal radiation of an accretion disc.

We show in Fig. 1a the overall energy distribution, after subtraction of the stellar contribution and the dereddening in the optical and IR band made by Done *et al.* (1990b). The high luminosity state for the X-ray flux, corrected for galactic absorption, is best-fitted by the power law $F(\nu) = 2.74 \times 10^{-15}\nu^{-0.79}$ erg s^{-1} cm^{-2} Hz^{-1}. The source has been observed down to 0.2 keV by EXOSAT (Lawrence *et al.* 1985). The data between 10 and 83 μm are IRAS data, taken from Ward *et al.* (1987): due to the lack of IR variability these can be considered as a good indication of the spectral distribution at low frequencies.

The analysis of Done *et al.* (1990b) shows no short timescale correlation between the IR-optical and X-ray fluxes. A greater than 50 per cent increase in the X–ray flux produced corresponding upper limits of 4 per cent and 1 per cent for the nuclear variability in the IR (K band) and optical (B band) over the same interval, after removing the effects of atmospheric variations in the optical light curve.

The lack of correlated variability allowed Done *et al.* (1990b) to exclude the possibility that the optical and X-ray fluxes are produced as primary radiation by the same population of electrons, as is the case in the standard SSC model. This led to the conclusion that they should be produced in different spatial regions or that the optical emitting region is one order of magnitude bigger than the X-ray one. (The possibility of a varying inverse Compton flux with a stationary synchrotron emission proposed by Ghisellini *et al.* (1989) requires, unlike NGC 4051, a synchrotron–dominated source).

Our strongest limits on the magnetic field in this source are obtained by requiring that the variations produced at IR and optical frequencies during a 50 per cent variation in X-ray flux do not exceed the observed ones (4 per cent of the total flux in the IR and 1 cent of the total flux in the optical).

3.2 NGC 6814

The recent results on X-ray variability from GINGA observations (Kunieda *et al.* 1990) confirm earlier HEAO-1 results (Tennant *et al.* 1981) and indicate a maximum size smaller than $R \sim 1.5 \times 10^{12}$ cm. This need not be the size of the central engine, but is just the size of the X-ray emission region which may occupy

only a small fraction of the volume of the central engine. The X–ray emission may be a transient phenomenon which moves around in the central engine (*e.g.* flares above the accretion disc).

We consider the overall spectrum shown in Fig. 1b. The IR-optical data are from McAlary *et al.*(1983) and McAlary *et al.*(1988), the J,H,K,L band fluxes are obtained by subtracting the stellar contribution. The UV data are averages of two short (SWP10680L and SWP10693L) and one long (LWR8961R) wavelength spectra from *IUE*. We use the X–ray state reported by Tennant *et al.*(1981) (best–fitting power–law spectrum $F(\nu) = 5.9 \times 10^{-17}\,\nu^{-0.67}$ erg cm^{-2} s^{-1} Hz^{-1}) from HEAO 1 observations.

The source has also been observed in the soft X–rays with EXOSAT (Mittaz & Branduardi–Raymont 1989) and up to 120 keV by HEAO 1 (Rothschild *et al.* 1983).

3.3 3C273

A variation of the X–ray (2–10 keV) flux by a factor 2 in $t_{var} = 0.5$ day for the quasar 3C273 (z=0.158) has been reported by Marshall *et al.*(1981). The overall spectrum for 3C273, shown in Fig. 1c, has been obtained from the data of Courvoisier *et al.*(1987), Robson *et al.*(1986), Clegg *et al.*(1983), Landau *et al.*(1983) and Aller *et al.*(1985). The UV datum at $\lambda_{obs} = 916$Å is from Reichert *et al.*(1988). The X-ray power law ($F(\nu) = 5.2 \times 10^{-19}\,\nu^{-0.54}$ erg cm^{-2} s^{-1} Hz^{-1}) refers to the EXOSAT observation reported by Turner *et al.*(1990).

The observed γ–ray flux (Bassani *et al.* 1985) is below the extrapolation of the X–ray spectrum. Therefore we conservatively assume that the X–ray spectrum extends to an energy of 1 MeV.

3.4 3C279

We also consider a blazar, the OVV source 3C279 ($z = 0.538$). The dimension of the X–ray region is deduced from the variability timescale of 45 min reported by Makino *et al.*(1989) for a 20 per cent X–ray flux variation. We therefore assume that $t_{var} = 225$ min.

The spectrum, shown in Fig. 1d, has been constructed from the data of Makino *et al.*(1990), Brown *et al.*(1989), Landau *et al.*(1986). The X–ray data are from Makino *et al.*(1990), who report a best–fitting power–law spectrum, $F(\nu) = 9.75 \times 10^{-19}\,\nu^{-0.58}$ erg cm^{-2} s^{-1} Hz^{-1} from a GINGA observation.

3.5 H1821+643

H1821+643 ($z = 0.297$) is a radio–quiet quasar for which an X–ray variation of a factor 2 in 10 days is reported by Snyder & Wood (1984).

The spectral data, in Fig. 1e, are from Kolman *et al.* (1990). The X–ray power law ($F(\nu) = 6.18 \times 10^{-19}\, \nu^{-0.6}$ erg cm^{-2} s^{-1} Hz^{-1}) is a fit of *Einstein Observatory* data (0.1–3.5 keV), and is consistent both with EXOSAT and GINGA results at higher energies (Warwick, Barstow & Yaqoob 1989, Kii *et al.* 1991).

4 RESULTS

The $B - \gamma_{max}$ constraints obtained for each object are shown in Figs. 2a,b,c,d,e. As explained in Section 2, the comparison of the predicted SSC flux with the flux observed at any given frequency defines an allowed region in the B–γ_{max} plane. Curved lines are defined by the synchrotron ($\nu \propto B\gamma_{max}^2$), first– ($\nu \propto B\gamma_{max}^4$), or second– ($\nu \propto B\gamma_{max}^6$) order self–Compton relations between B and the minimum γ_{max} needed to emit a given frequency. In general, limits derived by the synchrotron flux refer to the largest values of γ_{max}. As an illustration in Fig. 1c, we show the computed SSC spectrum for $B = 200$ G and $\gamma_{max} = 120$.

In Fig. 2b the (dash-dot) line defining the self absorption value γ_t is shown as a function of the magnetic field (equations 1 and A1). On the left side of this line the synchrotron radiation is completely self absorbed, and the self–Compton flux is calculated using the energy density of the self–absorbed synchrotron radiation (see equations A2–A4). Continuous vertical lines refer to the minimum γ_{max} needed to produce, through scattering of blackbody photons, the maximum X–ray frequency at which the object has been observed, indicated in Table 1 as $\gamma_{min} = (3\nu_x/4\nu_{bb})^{1/2}$, where ν_{bb} is the peak frequency of the blackbody. Only the right–hand side (higher γ_{max}) region of the parameter space is allowed. It is clear that stronger limits on the magnetic field can be obtained if hard X–ray or γ–ray observations (*e.g.* from the *Gamma Ray Observatory*, GRO) increase this minimum value of the maximum Lorentz factor of the electrons. The dashed vertical line (labelled $\gamma_{1\ MeV}$) refers to the value of γ_{max} needed to produce radiation at 1 MeV, which is the threshold energy for electron–positron pair production through photon–photon collisions. The lines labelled B_{eq} indicate the values of the magnetic field in equipartition with the

radiation energy density. This is obtained by integrating the X–ray flux up to the frequency $(4/3)\nu_{bb}\gamma_{max}^2$. This value can strongly underestimate the radiation energy density since it neglects the contribution from the (unobserved) EUV radiation field. Future observations in the UV from the Hubble Space Telescope will give tighter limits on the UV photon density.

For three of the sources we find that equipartition is not possible in the relevant range of γ_{max}. For 3C279 and H1821+643 it is reached only if γ_{max} is within a factor two of the minimum value, on the assumption that the spectrum of these sources extends no more than 20 keV. Increasing γ_{max} increases both B_{eq}/B and the radiation energy density.

For a more detailed description of our results, consider the source NGC 6814, for which strong limits are found (see Figs. 1b and 2b). From the observed spectrum the strongest limits on B appear to be due to the long wavelength data of the UV spectrum. For high values of γ_{max} (> 700) these frequencies can be emitted as optically–thin synchrotron and the implied upper limit on B, evident in Fig. 2b as a horizontal line, is $B \simeq 600\,\mathrm{G}$. For lower values of γ_{max} the first–order Compton emission dominates at this frequency. The constraints derived on B depend on γ_{max}, due to the logarithmic term in the Compton emission (see Appendix A). On the left–hand side of the line γ_t the flux is self–absorbed and the limits are imposed by the optically–thick synchrotron or Comptonized self–absorbed fluxes.

In Table 1 we also list the estimated radiation energy density U_x, computed for the minimum value of the Lorentz factor γ_{min}, the energy density of the relativistic electrons U_e and the value of the maximum allowed magnetic energy density implied by our limits, again estimated at γ_{min}. It is shown that, except for NGC 4051, the particle energy density of the emitting electrons is a small fraction of the photon density, and can be comparable with the magnetic one.

4.1 Parameters

The calculated ratio of magnetic to radiation energy density depends on our assumptions. In the following, we discuss how our results change as some of the assumed parameters are varied.

i) The first point concerns the determination of the soft photon energy density,

which fixes the value of the electron density K. It is estimated by assuming a maximum temperature blackbody, T_{bb}, neglecting any dilution factor which is relevant if the blackbody and X–ray emission regions do not coincide. Both these assumptions tend to overestimate the photon density and, consequently, underestimate the electron density. Relaxing these assumptions therefore results in tighter limits on B.

ii) A second critical parameter is the dimension R of the source. Since variability timescales yield only an upper limit on R, it may be smaller than our adopted value. To produce the same optically–thin synchrotron flux we must have $R^2 \tau B^{1+\alpha} = \text{const}$, while the X-ray energy density $U_x \propto R^{-2}$. In changing R we must also consider the possible changes in the temperature and flux of the assumed blackbody. In general, if R decreases, then higher values of T_{bb} are allowed, until eventually the observed flux becomes inconsistent with a further temperature change. To illustrate this, consider the simpler case of a constant T_{bb}. Here the scattering optical depth τ is constant, and equipartition is possible for R_{eq} given by

$$R_{eq} = R(U_B/U_x)^{(1+\alpha)/(2-2\alpha)} \tag{2}$$

where U_B and U_x are calculated with the initial R.

If T_{bb} increases so that the soft photon flux increases (corresponding to a more powerful blackbody), then we need fewer electrons to produce the X-ray flux, and so τ decreases. In this case equipartition is reached for a dimension larger than that indicated by equation (2). On the other hand, when the blackbody is limited by the low energy X-ray flux, a decrease in R corresponds to an higher T_{bb}, but also to a larger τ. In this case equipartition is possible with a size smaller than that estimated by equation (2).

To estimate the effects of decreasing R, we calculate for each new size the maximum temperature blackbody and the new limits on the magnetic field, until the minimum possible scattering optical depth, τ_{min}, is reached. If equipartition is not allowed even using the size corresponding to τ_{min}, we decrease R further, but now keeping $\tau = \text{const} = \tau_{min}$. We then use equation (2) to estimate R_{eq}, where R, U_B and U_x are the values found for $\tau = \tau_{min}$. As a particular example of this, consider the source NGC 6814. In this case a decrease in R implies an increase

of τ, therefore we use equation (2) to estimate the maximum size needed to reach equipartition. Assuming the minimum ratio $B_{eq}/B \simeq 4$ from Fig. 2b (just for γ_{min}), equipartition can be reached for dimensions of the emitting region at least 10^3 times smaller than that deduced from the variability timescale ($R \simeq 1.5 \times 10^{12}$ cm). For 3C273, a minimum value of τ is reached for $R \simeq 5 \times 10^{14}$ cm. Using this dimension we find $B_{eq}/B \simeq 8$. To obtain equipartition we again require a dimension a factor 10^3 smaller than that estimated from variability.

iii) The results are also affected by the lack of simultaneous X-ray and optical–UV data. Therefore we have also calculated the limits imposed by lower flux X–ray states. For NGC 6814, from the EXOSAT observation (Mittaz & Branduardi–Raymont 1989) with a best–fitting power–law spectrum $F(\nu) = 1.3 \times 10^{-20}\,\nu^{-0.51}$ erg cm^{-2} s^{-1} Hz^{-1}, we find a minimum ratio of $B_{eq}/B \simeq 2$. Decreasing R, from equation (2) we find that R_{eq} must still be at least a factor 8 smaller than that implied by the variability constraints. Weaker limits for the magnetic field in 3C273 can be obtained by considering both the low X–ray state and assuming a dimension corresponding to the minimum possible τ, for which $B_{eq}/B \simeq 2.5$. We have also considered the possibility that the size of the X–ray emission region in 3C273 is much larger that the 0.5 light days assumed on the basis of the observation of Marshall *et al.* (1981). No later observation of 3C273 shows such rapid variability, the observed two–folding timescale being 20 days or more (Turner *et al.* 1990). Taking $t_{var} = 19$ days, we still find similar strong results.

iv) There is increasing evidence that the typical observed 2–10 keV X–ray spectrum, at least for Seyfert galaxies, can be explained by a combination of a direct power–law spectrum with $\alpha_x \simeq 0.9$ and its reflection from a cold disc (*e.g.* George & Fabian 1991). The value of the spectral index can in turn be explained naturally as due to pair reprocessing, consistent with the high value of compactness (Zdziarski *et al.* 1990). For this reason we have computed the limits on the magnetic field assuming an intrinsic X-ray spectral index $\alpha_x = 0.9$, keeping the total number of X-ray photons in the range 2–6 keV constant. We find no significant variations of the allowed region of the $B - \gamma_{max}$ space.

For the other sources the results are similar, but less extreme. For each object we have considered the different observed X–ray states. For each state we calculate

the limits on B for the value of R such that τ is minimized. Equipartition can be reached in some cases, with an absolute maximum $B/B_{eq} \simeq 7$, but only over a restricted range of γ_{max}. For the quasars, it is not clear that the variability is persistent and involves the whole X–ray spectrum. For example, the variability of H1821+643 may be dominated by a soft component. Nevertheless, as we have seen for 3C273, increasing the variability timescale by a factor of 10 does not qualitatively change our result.

We conclude that equipartition can be obtained in some sources only for very restricted values for γ_{max}. It requires a small (sometimes extreme) value of the radius.

In Appendix B we describe a qualitative but simpler way to estimate the ratio of the magnetic and radiation energy densities.

4.2 Effects of beaming

For two of the sources considered here, namely 3C273 and 3C279, there is some evidence that relativistic beaming (due to bulk relativistic motion towards the observer) can be important. Both are superluminal radio sources, and 3C279 showed a very fast increase of the X–ray flux, corresponding to $\Delta L/\Delta t > 2 \times 10^{42}$ erg s^{-2} (Makino *et al.* 1989). The importance of relativistic beaming is measured by the Doppler factor $\delta = (\Gamma - \sqrt{\Gamma^2 - 1}\cos\theta)^{-1}$, where Γ is the bulk Lorentz factor of the plasma moving at an angle θ with the line of sight. For 3C279 Makino *et al.* (1989) estimated $\delta \geq 1.6$. We have therefore included the possibility that the X–ray flux is beamed, by taking into account the following: 1) the comoving size of the emitting region, larger than what variability indicates: $R = c\ t_{var}\ \delta/(1+z)$; 2) the maximum temperature blackbody (assumed unbeamed) corresponding to this size; 3) the optical depth τ of the emitting plasma, as measured in the comoving frame; 4) the predicted monochromatic fluxes, enhanced by the factor $\delta^{3+\alpha}$ (see Appendix A); 5) the equipartition magnetic field, scaling as δ^{-3}.

We then found, for 3C279, the value of δ for which the magnetic and the radiation energy densities are in equipartition, assuming the spectrum extends up to a (rest frame) energy of 1 MeV. We found $\delta \simeq 3$.

For 3C273 the evidence of beamed X–ray emission is weaker than for 3C279,

even if beaming can be very important for the radio flux. Indeed, the presence of a fluorescent iron line argues *against* strong beaming effects. If the source of X–rays moves away from a disk in a direction normal to its surface, the absorbed luminosity by photoelectric effect by cold matter in the disk scales approximately as $\Gamma^{-3-\alpha}$. On the other hand the observer sees an enhanced (by $\delta^{3+\alpha}$) direct monochromatic flux. The equivalent width of the line therefore scales as $(\delta\Gamma)^{-3-\alpha}$. Comparing the typical equivalent width of the iron line observed in Seyfert galaxies ($\sim$ 150 eV) with the one observed in 3C273 ($\sim$ 50 eV, Turner *et al.* 1990), and assuming $\theta \sim 10°$, we derive $\delta = 1.3$. The limits on the magnetic field, calculated assuming this value of δ, remain unchanged.

5 DISCUSSION

We have shown that equipartition magnetic fields are excluded from the X-ray emission regions of several AGN under the assumption that the X-rays are due to inverse–Compton scattering of EUV photons by relativistic electrons. The AGN we have considered sample the full range of active galaxies from low luminosity Seyfert galaxies to highly luminous quasars.

The result is surprising and possibly of great significance when it is considered that many models for the inner regions of AGN invoke strong magnetic fields. In the following, we therefore examine the robustness of the result by reconsidering our assumptions and offering some alternative models.

Direct production of synchrotron and self–Compton radiation by a single population of electrons is apparently ruled out by the variability constraints in NGC 4051. There are no obvious reasons to suppose that the other sources, at least Seyfert galaxies and quasars which show uncoordinated variability behaviour, are different.

Thermal Comptonization is an alternative picture for the X–ray emission. However this requires "ad hoc" values of electron temperature and Thomson optical depth in highly variable sources in order to produce a narrow range of observed X–ray spectral indexes; it also requires an appropriate value for the dilution factor q, in order that the soft photon peak is just on the extrapolation of the X–ray power law. Moreover a rapid energy–exchange mechanism is needed in order to maintain a thermal distribution and to transfer energy from the ions to the electrons.

Our limits on synchrotron self–Compton emission rely on the X-ray emission region being directly visible in the optical and UV bands. This would not be the case if the X–ray emission region is blanketed in sufficient cold gas that free–free absorption occurs throughout the optical and UV wavebands. The main problem with a diffuse absorbing blanket is that it would have to be so dense and thick that the X-rays would also be absorbed (at the least by photoelectric absorption). An acceptable solution is obtained if the absorbing gas is distributed in small dense clouds with a large covering fraction and a total column density $N < 10^{21} N_{21}$ cm^{-2}, with $N_{21} < 1$ in order that phtoelectric absorption of soft X-rays is not observed. The pressure of the clouds is then so high that they would rapidly disperse at the internal sound speed if not confined. A scenario in which very dense cold clouds can survive close to the central engine in AGN has been suggested by Rees (1987). This mainly dealt with the Broad–Line Region, at much larger radii than the X–ray emission region. The intracloud pressure is proposed there to be due to a strong magnetic field, maintained either by the accretion flow or by a relativistic wind. It was also suggested that much stronger magnetic fields may be present at smaller radii and that they support a population of very dense clouds. Free–free absorption can therefore allow the strong, equipartition magnetic field, apparently ruled out by our above results, to support a blanket of dense, cold clouds which hide its radiation signature.

In all our sources, the intensity of the X–ray spectrum itself, if due to Comptonization of EUV photons, rules out equipartition magnetic fields. Since we cannot argue that the X-rays are also absorbed, we must fall back on SSC emission as the source of the X–ray emission. In order that this can apply, the energy density of the EUV bump in the X–ray emission region must be less than the energy density of the synchrotron radiation. This can easily be achieved by using a small dilution factor, meaning that the quasi-blackbody component of the EUV bump is emitted by a much larger region than the X–ray emission. In the above, we have assumed a maximum dilution factor of unity.

The lack of correlated optical and X–ray variability in NGC 4051 is now explained as due to free–free absorption of the direct optical SSC radiation from the X–ray emission region. Future searches for ultraviolet variability, *e.g.* using the High Speed

Photometer on the Hubble Space Telescope, should be very important in improving the constraints on small dense clouds.

To be more specific about the properties of the cold clouds, let us assume that the flux at frequency $10^{15}\nu_{15}$ Hz is absorbed by clouds of temperature $10^5 T_5$ K and size ℓ such that the column density $n\ell < 10^{21} N_{21}\,\mathrm{cm}^{-2}$. As mentioned already, $N_{21} < 1$ in order that soft X-ray absorption is not observed (soft X–ray observations will define this limit more precisely). We expect that the cloud temperature, found by balancing heating and cooling by bremsstrahlung, is close to $T_5 \sim 1 - 2$. The density, n, must then exceed

$$n_{min} \simeq 2 \times 10^{18} \frac{T_5^{1/2} \nu_{15}^3}{N_{21}}\ \mathrm{cm}^{-3}\,.$$

This means that $\ell < 450 N_{21} T_5^{-1/2} \nu_{15}^{-3}$ cm and the thermal pressure $P > 6 \times 10^7 T_5^{3/2} \nu_{15}^3 N_{21}^{-1}$ erg cm^{-3}. This pressure is consistent with the equipartition magnetic field required by the X-ray variability. The X-ray emission region then consists of an equipartition magnetic field with unit covering fraction provided by many ($> 10^{20}$ if their distance is $\sim 10^{14}$ cm) small dense clouds at the temperature of the EUV bump.

The dense clouds will reprocess and reradiate most of the SSC power from wavebands longer than the UV. Although the power involved may be high, it probably does not dominate the EUV bump since the region also contains other relatively cold gas with a column density of at least $10^{24}\,\mathrm{cm}^{-2}$. This is required in order to explain the strength of the fluorescent iron line commonly observed in these active galaxies (see George & Fabian 1991 and references therein). This gas is presumably in the form of an accretion disc and its thermal emission is primarily responsible for the EUV bump.

The picture for the X–ray emission region which is suggested by our results thus consists of relativistic electrons, accelerated above an accretion disc, producing SSC radiation on an equipartition–strength magnetic field. The SSC emission is absorbed at UV and lower frequencies by surrounding dense clouds, pressure–confined by the strong magnetic field. There may, of course, be clouds of lower density at larger radii which further redistribute the flux. We shall consider the model in more detail* elsewhere.

* Including the effects of cooled electron-positron pairs produced in the X-ray

We assume that beaming of the radiation, and strong anisotropy of the radiation field, are ruled out for the objects where the iron fluorescence lines have been detected. We have calculated a limit for the importance of beaming in 3C273, where the equivalent width of the fluorescent iron line is 50eV (Turner *et al.* 1990). For 3C279, where the iron line has not been detected (an upper limit of 60eV is reported by Makino *et al.* 1989), beaming can be important and we estimated a Doppler factor $\delta \simeq 3$ to have equipartition between magnetic and radiation energy densities.

Finally, it is possible that the electron injection spectrum is steep, and/or has a low value of $\gamma_{max} \lesssim 30$, so that multiple Compton scattering dominates over synchrotron emission (Ghisellini 1989). This process, like thermal Comptonization, requires fine tuning. However, there may be feedback, such as the pair loading discussed by Done *et al.* (1990a), which selects only favoured values of the spectral parameters.

In conclusion, the overall spectrum and X-ray variability have enabled us to obtain strong limits on the magnetic field density in the X–ray emission regions of a sample of AGN. The magnetic field cannot be in equipartition with the radiation field, as expected, if at the same time the emission region is transparent at optical and UV wavelengths. If it is not transparent, then an equipartition field is allowed. The opacity in the region is plausibly due to free–free absorption in dense, cold gas clouds, pressure–confined by the strong magnetic field. The primary radiation process is then SSC.

---

emission region by photon-photon collisions (see Zdziarski *et al.* 1991 and references therein). They also give free-free absorption in the IR and may even dominate into the optical if they can cool to a sufficiently low temperature before annihilating. Pairs do not of course give significant photoelectric absorption in the X-ray band

APPENDIX A

Here we show explicitly the expressions used for the monochromatic SSC intensities $I(\nu)$ in different frequency ranges. The expressions assume that the sources are not beamed. In the end of this appendix we generalize them to the case of beaming.

Consider a homogeneous spherical region with dimension R, with a random magnetic field of intensity B, and an isotropic distribution of relativistic electrons $N(\gamma)\,d\gamma = K\,\gamma^{-p}\,d\gamma$, for $1 < \gamma < \gamma_{max}$. The observed flux is compared to $F(\nu) = \pi(R/d_L)^2\,I(\nu)$ where d_L is the luminosity distance (Weinberg 1972).

We indicate with 's', '1C', '2C' quantities which refer to synchrotron, first– or second–order Compton, respectively, with "thin" and "thick" the transparent or self–absorbed regime (in the case of Compton emission it means that the scattered radiation energy density is calculated from self–absorbed synchrotron emission). The Lorentz factor, γ_t, of the electrons emitting mainly at the synchrotron self–absorption frequency ν_t, is given by (see *e.g.* Ghisellini 1989)

$$\gamma_t = \left[\frac{9\pi\sqrt{3\pi}}{64}\left(\frac{3}{2}\right)^p g(p)\frac{eKR}{B}\right]^{1/(p+4)} \qquad (A1)$$

and $\nu_t = 4\gamma_t^2\,\nu_B/3$ where $\nu_B = eB/2\pi mc$ is the cyclotron frequency. The constant c_t defined in equation (1) is therefore given by $c_t(p) = \left[(9\pi\sqrt{3\pi}/64)(3/2)^p g(p) e\right]^{1/(p+4)}$.

In different frequency ranges a different emitting regime is dominant. For $\nu < \nu_t$

$$I_{s,thick}(\nu) = \frac{2mf(p)}{\sqrt{3}}\frac{\nu^{5/2}}{\nu_B^{1/2}}. \qquad (A2)$$

If $\gamma_{max} < \gamma_t$ and for $\nu_{s,max} < \nu < \nu_{1C,max}$, the inverse Compton fluxes are calculated from the synchrotron self–absorbed photon density and are given by

$$I_{1C,thick}(\nu) = \frac{2mf(p)}{\sqrt{3}}\left[\frac{\tau\,(4/3)^\alpha}{2}\right]\nu^{-\alpha}\frac{\nu_{s,max}^{5/2+\alpha}}{5/2+\alpha}\frac{1}{\nu_B^{1/2}}. \qquad (A3)$$

If $\gamma_{max} < \gamma_t$ and for $\nu_{1C,max} < \nu < \nu_{2C,max}$ we have

$$I_{2C,thick}(\nu) = \left[\frac{\tau\,(4/3)^\alpha}{2}\right] I_{1C,thick}(\nu)\ln\Lambda_{2,thick}. \qquad (A4)$$

If $\gamma_{max} > \gamma_t$ thin synchrotron emission is possible between $\nu_t < \nu < \nu_{s,max}$, with an intensity given by

$$I_{s,thin}(\nu) = c_1(\alpha) RK B^{1+\alpha}\nu^{-\alpha}. \qquad (A5)$$

For $\nu_t < \nu_{s,max} < \nu < \nu_{1C,max}$,

$$I_{1C,thin}(\nu) = \left[\frac{\tau\,(4/3)^{\alpha}}{2}\right] I_{s,thin}(\nu) \ln \Lambda_{1,thin}. \qquad (A6)$$

If $\gamma_t < \gamma_{max}$ and for $\nu_{1C,max} < \nu < \nu_{2C,max}$,

$$I_{2C,thin}(\nu) = \left[\frac{\tau\,(4/3)^{\alpha}}{2}\right] I_{1C,thin}(\nu) \ln \Lambda_{2,thin}. \qquad (A7)$$

In the above equations, $\alpha = (p-1)/2$, $\tau = \sigma_T\, R\, K$, σ_T is the Thomson cross section, m and e the mass and electric charge of electron and

$$f(p) = \frac{\Gamma\left(\frac{3p-1}{12}\right)\Gamma\left(\frac{3p+19}{12}\right)\Gamma\left(\frac{p+5}{4}\right)\Gamma\left(\frac{p+8}{4}\right)}{(p+1)\Gamma\left(\frac{3p+2}{12}\right)\Gamma\left(\frac{3p+22}{12}\right)\Gamma\left(\frac{p+7}{4}\right)\Gamma\left(\frac{p+6}{4}\right)}, \qquad (A8)$$

$$c_1(\alpha) = \frac{\sqrt{\pi}e^2}{4c}\left(\frac{e}{2\pi mc}\right)^{1+\alpha} A(p) 3^{p/2}, \qquad (A9)$$

$$A(p) = \frac{\Gamma\left(\frac{p+5}{4}\right)\Gamma\left(\frac{3p-1}{12}\right)\Gamma\left(\frac{3p+19}{12}\right)}{(p+1)\Gamma\left(\frac{p+7}{4}\right)}, \qquad (A10)$$

$$g(p) = \frac{\Gamma\left(\frac{3p+22}{12}\right)\Gamma\left(\frac{3p+2}{12}\right)\Gamma\left(\frac{p+6}{4}\right)}{\Gamma\left(\frac{p+8}{4}\right)}. \qquad (A11)$$

As reference values, for $\alpha = 0.5$, $f(2) \simeq 0.5$, $A(2) \simeq 0.597$ and $g(2) \simeq 1.213$.

The maximum frequency emitted by synchrotron radiation is $\nu_{s,max} = 4/3\,\nu_B\,\gamma_{max}^2$. To calculate the Λ terms in the Compton expressions we use an approximation to the exact Klein–Nishina cross section, setting the scattering cross–section equal to zero for

$$\gamma\nu/\nu_{KN} > 3/4, \qquad (A12)$$

where

$$\nu_{KN} \equiv mc^2/h = 1.236 \times 10^{20}\,\mathrm{Hz}. \qquad (A13)$$

With this approximation the maximum frequency of the first ($\nu_{1C,max}$) and second order ($\nu_{2C,max}$) Compton spectra are

$$\nu_{1C,max} = \min\left[\frac{4}{3}\gamma_{max}^2\nu_{s,max}\,;\,\frac{3}{4}\nu_{KN}\gamma_{max}\right], \qquad (A14)$$

$$\nu_{2C,max} = \min\left[\frac{4}{3}\gamma_{max}^2\nu_{1C,max}\,;\,\frac{3}{4}\nu_{KN}\gamma_{max}\right]. \qquad (A15)$$

The Λ terms are, at a given (scattered) frequency ν,

$$\Lambda_{1,thin} = \frac{\min\left[\nu_{s,max};\, 3\nu_{KN}/4;\, 3\nu_{KN}^2/(4\nu)\right]}{\max\left[\nu_t;\, 3\nu/(4\gamma_{max}^2)\right]}, \qquad (A16)$$

$$\Lambda_{2,thin} = \frac{\min\left[\nu_{1C,max};\, 3\nu_{KN}/4;\, 3\nu_{KN}^2/(4\nu)\right]}{\max\left[\nu_t;\, 3\nu/(4\gamma_{max}^2)\right]}, \qquad (A17)$$

$$\Lambda_{2,thick} = \frac{\min\left[\nu_{1C,max};\, 3\nu_{KN}/4;\, 3\nu_{KN}^2/(4\nu)\right]}{\max\left[\nu_{s,max};\, 3\nu/(4\gamma_{max}^2)\right]}. \qquad (A18)$$

Neglecting the spectral curvature of the first–order spectrum produced by the logarithmic term when calculating the second–order Compton from thin synchrotron, we use

$$\ln\Lambda_{1,thin}\,\ln\Lambda_{2,thin} = 2\ln(\gamma_{max}/\gamma_t)\ln\Lambda_{2,thin} \qquad (A19)$$

with $\Lambda_{2,thin}$ given as above.

The formulae given above can be generalized to include the effect of beaming. Define $\delta = [\Gamma - \sqrt{\Gamma^2-1}\cos\theta]^{-1}$, where Γ is the bulk Lorentz factor of the emitting plasma moving at an angle θ with the line of sight. In the observer frame $I_*(\nu_{obs}) = I(\nu_{obs})\ \delta^{3+\alpha}$ ($\alpha = -5/2$ for self–absorbed synchrotron), where $I(\nu_{obs})$ is given by the above formulae. The size R is estimated as $R = c\ t_{var}\ \delta/(1+z)$. For a given observed frequency ν_{obs} we calculate $\nu = \nu_{obs}\ (1+z)/\delta$ and select the radiation process dominant at ν. We then compare the observed flux with $F_*(\nu_{obs}) = \pi(R/d_L)^2\, I_*(\nu_{obs})$.

APPENDIX B

Here we describe a qualitative but simpler way to estimate the limits on the magnetic field in terms of radiation and magnetic energy densities.

A simple estimate of the synchrotron (U_s) and first–order self–Compton (U_{1C}) radiation energy densities is given by

$$U_{s(1C)} \simeq \frac{3R}{4c}\int N(\gamma)\dot{\gamma}_{s(1C)} m_e c^2 d\gamma \qquad (B1)$$

where $3R/(4c)$ is the mean light travel–time across a spherical thin source, $\dot{\gamma} m_e c^2$ is the energy–loss rate of the emitting electrons, $\dot{\gamma}_s m_e c^2 = (4/3)U_B\gamma^2\sigma_T c$ and

$\dot{\gamma}_{1C} m_e c^2 = (4/3) U_s \gamma^2 \sigma_T c$ for synchrotron and self–Compton emission, U_B is the magnetic energy density and σ_T is the Thomson cross section.

Let us define

$$y \equiv \tau < \gamma^2 > \qquad (B2)$$

with

$$< \gamma^2 >= \frac{\int N(\gamma) \gamma^2 d\gamma}{\int N(\gamma) d\gamma}$$

and $\tau = R\sigma_T \int N(\gamma) d\gamma \sim R\sigma_T K$. Note that $< \gamma^2 >= \gamma_{max}$ if $p = 2$, corresponding to an X-ray spectral index $\alpha = 0.5$, and if the minimum Lorentz factor of the electron distribution is ~ 1. With the above definitions we have

$$U_s = y\, U_B \quad , \quad U_{1C} = y\, U_s. \qquad (B3)$$

These relations are valid as long as Compton losses are in the Thomson regime.

The X–ray energy density U_x from the upscattering of soft 'blue bump' photons with energy density qU_{bump} is given by

$$U_x = qy\, U_{bump}. \qquad (B4)$$

$q \leq 1$ is a dilution factor, smaller than unity if the soft photons are produced in a region different to, or larger than, the X–ray one. We assume q=1. For $q < 1$, the lower photon energy density in the X–ray region requires a larger electron density in order to produce the observed X–ray flux which in turn implies tighter limits on the magnetic field.

First, to be consistent with our assumptions, we require the contribution from SSC emission to the X–ray flux to be negligible compared to the first–order Compton scattered 'blue bump' radiation.

Now consider the X–ray flux up to a given frequency ν_x. Synchrotron radiation contributes at ν_x if $\nu_{s,max} = (4/3)\gamma^2_{max} \nu_B > \nu_x$. In this case, the synchrotron emission does not exceed the observed X-ray flux if $U_s < U_x$, or, equivalently, if $U_B < qU_{bump}$. For frequencies $\nu_{s,max} < \nu_x < \nu_{max,1C} = (16/9)\gamma^4_{max} \nu_B$ the first–order Compton scattering contributes to the X-ray flux. In this case SSC radiation does not overproduce X-rays if $U_s < q\, U_{bump}$. If $\nu_{max,1C} < \nu_x$, it is the second–order Compton scattering that contributes in X-rays, and we require

$U_{1C} < q\,U_{bump}$. These inequalities can be written, using equations (B3) and (B4), as

$$\frac{U_B}{U_{bump}} < q \qquad \text{or} \qquad \frac{U_B}{U_x} < \frac{1}{y}, \qquad \nu_x < \nu_{s,max}$$

$$\frac{U_B}{U_{bump}} < \frac{q}{y} \qquad \text{or} \qquad \frac{U_B}{U_x} < \frac{1}{y^2}, \qquad \nu_{s,max} < \nu_x < \nu_{1C,max}$$

$$\frac{U_B}{U_{bump}} < \frac{q}{y^2} \qquad \text{or} \qquad \frac{U_B}{U_x} < \frac{1}{y^3}, \qquad \nu_x > \nu_{1C,max} \qquad (B5)$$

where the second relations give a direct comparison of U_B with the X–ray energy density.

A second limit can be imposed by requiring that the computed SSC flux does not exceed the observed one at a frequency ν. For example, consider the limit imposed by synchrotron and the first–order Compton spectrum. The requirements $U_s < U_{obs}$ and $U_{1C} < U_{obs}$, using again relations (B3) and (B4), imply

$$\frac{U_B}{U_x} < \frac{U_{obs}}{qy^2 U_{bump}}, \qquad \nu < \nu_{s,max} \qquad (B6)$$

$$\frac{U_B}{U_x} < \frac{U_{obs}}{qy^3 U_{bump}}, \qquad \nu_{s,max} < \nu < \nu_{1C,max} \qquad (B7)$$

As examples, we compare these estimates with the limits found for NGC 6814 and 3C273. For the case of NGC 6814, if $\gamma_{max} \simeq 100$ then the UV emission can be produced by first–order Compton scattering of the synchrotron radiation. Rough estimates from equation (B4) give $y \simeq 1.7$ and $U_{obs}/U_{bump} \simeq 10^{-2}$ and using equation (B7) we find $U_B/U_x < 2 \times 10^{-3}$, which correspond to $B_{eq}/B > 22$. For $\gamma_{max} \simeq 2000$, UV radiation can be emitted by the synchrotron process. With $y \simeq 10$ and using equation (B5), we have $U_B/U_x < 10^{-4}$, *i.e.* $B_{eq}/B > 100$. Both limits are in good agreement with the ones shown in Fig. 2b.

From the spectrum of 3C273 reported in Fig. 1c is possible to see that the strongest limits on B are imposed by the X–ray flux. With $\gamma_{max} \simeq \gamma_{1MeV}$ it is possible to estimate $y \simeq 8$, and using equation (B6), a limit of $B_{eq}/B > 23$ is obtained, in agreement with the limits shown in Fig. 2c.

ACKNOWLEDGMENTS

We thank Martin Rees for helpful discussions. AC and ACF thank the Angelo Della Riccia Foundations and the Royal Society for financial support, respectively.

Table 1

Source	z	R (cm)	T_{bb} (K)	γ_{min}	U_x	U_e	U_B
NGC 4051	0.0023	9.0×10^{12}	3.6×10^4	42	5.9×10^4	1.1×10^5	2.5×10^4
NGC 6814	0.0053	1.5×10^{12}	2.4×10^4	39	6.4×10^7	3.1×10^5	4.8×10^6
3C273	0.158	1.1×10^{15}	8.5×10^4	205	2.1×10^6	2.2×10^2	2.5×10^3
3C279	0.538	2.6×10^{14}	3.1×10^5	18	2.8×10^7	4.2×10^2	$> 4 \times 10^8$
H1821+64	0.297	2.0×10^{16}	1.6×10^4	71.7	2.4×10^5	3.1	1.8×10^3

Rest frame parameters for each source (assuming no beaming, *i.e.* $\delta = 1$). z is the redshift, R the dimension of the X–ray emitting region estimated from the variability timescale. T_{bb}(K) is the temperature of the maximum blackbody, emitted in a region of dimension R and consistent with the data. $\gamma_{min} = (3\nu_x/4\nu_{bb})^{1/2}$ indicates the minimum value of the Lorentz factor needed to emit the highest observed frequency by scattering EUV photons. U_x (erg cm^{-3}) is the radiation energy density estimated integrating the X–ray spectrum up to the maximum observed frequency; U_e the energy density in the relativistic electrons and U_B is the estimated upper limit to the magnetic energy density, corresponding again to the minimum Lorentz factor γ_{min}.

Figure captions

Fig. 1a Overall spectral distribution for the Seyfert galaxy NGC 4051. The composite spectrum is obtained from the simultaneous IR, optical (B band) and X–ray data reported in Done *et al.* (1990b). The best-fitting GINGA X–ray power–law spectrum is $F(\nu) = 2.74 \times 10^{-15} \nu^{-0.79}\,\mathrm{erg\,cm^{-2}\,s^{-1}\,Hz^{-1}}$ (extrapolated as described in the text), after correction for galactic absorption. The two low–flux points in the IR and optical bands correspond to the maximum nuclear contribution allowed to vary simultaneously with the X-rays (Done *et al.* 1990b). The UV points are from *IUE* spectra (SWP33531 and LWP13231). The dashed line is the maximum temperature ($T_{bb} \simeq 3.6 \times 10^4$ K in the observer frame) EUV blackbody consistent with the data. The emission region of the blackbody is assumed to be coincident with the X–ray one. The data between 10 and 83 μm are IRAS data, taken from Ward *et al.* (1987).

Fig. 1b Spectrum of the Seyfert galaxy NGC 6814. The IR-optical data are from McAlary *et al.* (1983) and McAlary *et al.* (1988): the J,H,K,L band fluxes are obtained after subtracting the stellar contribution. The UV data are averages of two short (SWP10680L and SWP10693L) and one long (LWR8961R) wavelength *IUE* spectra. We use the X–ray state reported by Tennant *et al.* (1981) (best-fitting power–law $F(\nu) = 5.9 \times 10^{-17} \nu^{-0.67}\,\mathrm{erg\,cm^{-2}\,s^{-1}\,Hz^{-1}}$) from HEAO 1 observations. The maximum luminosity blackbody has a temperature $T_{bb} \simeq 2.4 \times 10^4$ K (observer frame).

Fig. 1c The overall spectrum for 3C273 is obtained with data from Courvoisier *et al.* (1987), Robson *et al.* (1986), Clegg *et al.* (1983), Landau *et al.* (1983), Aller *et al.* (1985). The UV datum at $\lambda_{obs} = 916$Å is from Reichert *et al.* (1988). The reported blackbody has a temperature of $T_{bb} \simeq 7.3 \times 10^4$ K (observer frame). The X-ray power–law ($F(\nu) = 5.2 \times 10^{-19}\ \nu^{-0.54}\,\mathrm{erg\,cm^{-2}\,s^{-1}\,Hz^{-1}}$) refers to the EXOSAT observation reported by Turner *et al.* (1990). The dash-dot line shows an SSC spectrum, computed for $B = 200$ G and $\gamma_{max} = 120$.

Fig. 1d The spectrum of 3C279 constructed from the data of Makino *et al.* (1990), Brown *et al.* (1989), Landau *et al.* (1986). The maximum temperature of the reported blackbody is $T_{bb} \simeq 2 \times 10^5$ K (observer's frame). The X–ray data are from Makino *et al.* (1990) who reports a best–fitting power–law $F(\nu) = 9.75 \times 10^{-19}\, \nu^{-0.58}\, \mathrm{erg\,cm^{-2}\,s^{-1}\,Hz^{-1}}$ from a GINGA observation.

Fig. 1e The data for the source H1821+643 are from Kolman *et al.* (1990). The blackbody has a temperature of $T_{bb} \simeq 1.2 \times 10^4$ K (observer's frame). The X–ray power–law ($F(\nu) = 6.18 \times 10^{-19}\, \nu^{-0.6}\, \mathrm{erg\,cm^{-2}\,s^{-1}\,Hz^{-1}}$) is a fit to *Einstein Observatory* data (0.1–3.5 keV) and is consistent both with EXOSAT and GINGA results at higher energies.

Fig. 2a The figure shows the maximum allowed magnetic field versus the maximum Lorentz factor of the electron distribution for NGC 4051. The region on the right side of the oblique line (indicated by crosses) is the region not allowed by the overall spectrum of the source. The vertical continuous line represents the minimum value of the Lorentz factor needed to produce the observed X–ray frequency by scattering the soft 'blue bump' photons; the permitted region therefore extends to the right of this line. The dashed vertical line represents the value of γ_{max} required to emit a reference frequency of 1 MeV. The line labelled B_{eq} shows the magnetic field in equipartition with the radiation energy density (which depends on the extension of the X–ray spectrum).

Fig. 2b As Fig. 2a but for the source NGC 6814. The dash-dot line shows the dependence of the Lorentz factor γ_t of the electrons, mainly emitting at the synchrotron self–absorption frequency, as a function of B. The limits on the magnetic field are imposed by the self–absorbed fluxes on the left–hand side of this line.

Fig. 2c As Fig. 2a but for 3C273. The source has been observed in γ–rays, but below the extrapolation of the X–ray spectrum; we assume that the X–ray power law

extends up to 1 MeV.

Fig. 2d As Fig. 2a but for the source 3C279.

Fig. 2e As Fig. 2a but for the source H1821+643.

REFERENCES

Aller, H.D., Aller, M.F., Latimer, G.E. & Hodge, P.E., 1985. *Astrophys. J. Suppl.*, **59**, 513.

Bassani, L., Dean, A.J., Di Cocco, G. & Perotti, F., 1985. In *Active Galactic Nuclei*, ed. J. Dyson (Manchester University Press), p. 252.

Bregman, J.N., 1990. *Astron. Astrophys. Rev.*, **2**, 125.

Brown, L.M.J. *et al.*, 1989. *Astrophys. J.*, **340**, 129.

Clegg, P.E. *et al.*, 1983. *Astrophys. J.*, **273**, 58.

Courvoisier, T.J.–L., *et al.*, 1987. *Astron. Astrophys.*, **176**, 197.

Done, C., Ghisellini, G. & Fabian, A.C., 1990a. *Mon. Not. R. astr. Soc.*, **245**, 1.

Done, C., Ward, M.J., Fabian, A.C., Kunieda, H., Tsuruta, S., Lawrence, A., Smith, M.G. & Wamsteker, W., 1990b. *Mon. Not. R. astr. Soc.*, **243**, 713.

George, I.M. & Fabian, A.C. 1991, *Mon. Not. R. astr. Soc.*, **249**,, 352.

Ghisellini, G., 1987. *Ph. D. Thesis*, SISSA, Trieste.

Ghisellini, G., 1989. *Mon. Not. R. astr. Soc.*, **236**, 341.

Ghisellini, G., George, I.M., & Done, C., 1989. *Mon. Not. R. astr. Soc.*, **241**, 43P.

Jones, T.W., O'Dell, S.L., & Stein, W.A., 1974a. *Astrophys. J.*, **188**, 353.

Jones, T.W., O'Dell, S.L., & Stein, W.A., 1974b. *Astrophys. J.*, **192**, 261.

Kii, T. *et al.* 1991. *Astrophys. J.*, **367**, 455.

Kolman, M., Halpern, J.P., Shrader, C.R. & Filippenko, A., 1990, preprint.

Kunieda, H., Turner, T.J., Awaki, H., Kojama, K., Mushotzky, R. & Tsusaka, Y., 1990. *Nature*, **345**, 786.

Landau, R., Jones, T.W., Epstein, E.E., Neugebauer, G., Soifer, B.T., Werner, M.W., Puschell, J.J. & Balonek, T.J., 1983. *Astrophys. J.*, **268**, 68.

Landau, R. *et al.*, 1986. *Astrophys. J.*, **308**, 78.

Lawrence, A., Watson, M.G., Pounds, K.A. & Elvis, M., 1985. *Mon. Not. R. astr. Soc.*, **217**, 685.

Lawrence, A., Pounds, K.A., Watson, M.G. & Elvis, M.S., 1987. *Nature*, **325**, 694.

Lyutyi, V.M., 1977. *Sov. Astr.*, **21** 655.

Makino, F. *et al.*, 1989. *Astrophys. J. Lett.*, **347**, L9.

Makino, F., *et al.*, 1990. Contribution to the Conference: *Variability of Active Galactic Nuclei*, Atlanta, Georgia, in press.

Marshall, N., Warwick, R.S. & Pounds, K.A., 1981. *Mon. Not. R. astr. Soc.,* **194**, 987.

Matsuoka, M., Yamauchi, M., Piro, L. & Murakami, T., 1990. *Astrophys. J.,* **361**, 440.

McAlary, C.W., McLaren, R.A., McGonegal, R.J. & Maza, J., 1983. *Astrophys. J. Suppl.,* **52**, 341.

McAlary, C.W. & Rieke, G.H., 1988. *Astrophys. J.,* **333**, 1.

Mittaz, J.P.D. & Branduardi–Raymont, G., 1989. *Mon. Not. R. astr. Soc.,* **238**, 1029.

Penston, M.V., Penston, M.J., Selmes, R.A., Becklin, E.E. & Neugebauer, G., 1974. *Mon. Not. R. astr. Soc.,* **169**, 357.

Rees, M.J., 1987. *Mon. Not. R. astr. Soc.,* **228**, 47P.

Reichert, G.A., Polidan, R.S., Wu, C.-C. & Carone, T.E., 1988. *Astrophys. J.,* **325**, 671.

Robson, E.I., Gear, W.K., Brown, L.M.J., Courvoisier, T. L.-J., Smith, M.G., Griffin, M.J. & Blecha, A., 1986. *Nature,* **323**, 134.

Rothschild, R.E., Mushotzky, R.F., Baity, W.A., Gruber, D.E., Matteson, J.L. & Peterson, L.E., 1983. *Astrophys. J.,* **269**, 423.

Snyder, W.A. & Wood, K.S., 1984. In *X-ray and UV Emission from Active Galactic Nuclei*, MPE Report 184, ed. W. Brinkman and J. Trümper (Garching), p. 114.

Tennant, A.F., Mushotzky, R.F., Boldt, E.A. & Swank, J.H., 1981. *Astrophys. J.,* **251**, 15.

Turner, M.J.L. *et al.* 1990. *Mon. Not. R. astr. Soc.,* **244**, 310.

Ward, M., Elvis, M., Fabbiano, G., Carleton, N.P., Willner, S.P. & Lawrence, A., 1987. *Astrophys. J.,* **315**, 74.

Warwick, R.S., Barstow, M.A. & Yaqoob, T. 1989. *Mon. Not. R. astr. Soc.,* **238**, 917.

Weinberg, S., 1972. *Gravitation and Cosmology* (John Wiley & Sons).

Zdziarski, A., Ghisellini, G., George, I.M., Svensson, R., Fabian, A.C. & Done, C., 1990. *Astrophys. J. Lett.,* **363**, L1.

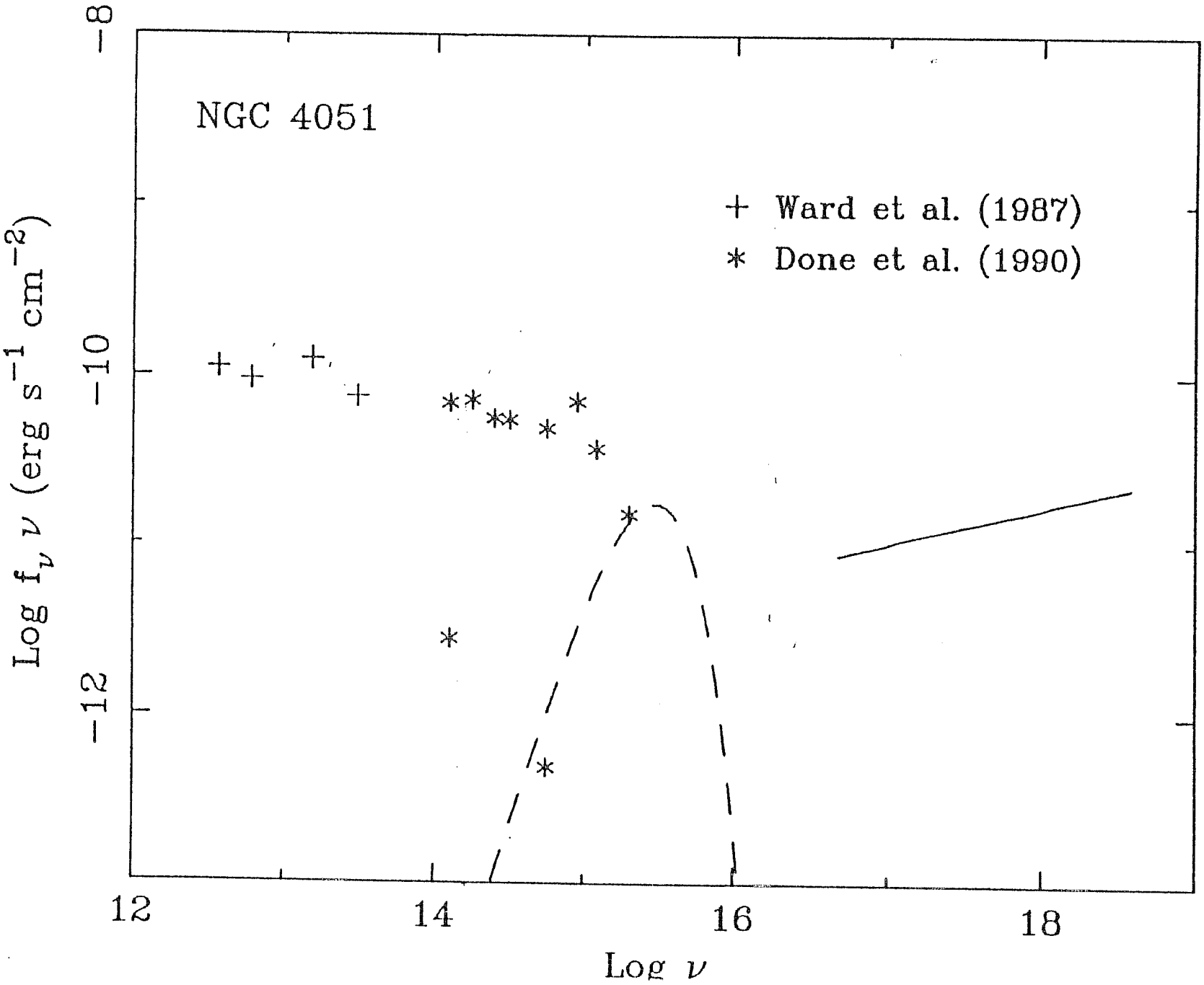
NGC 4051
+ Ward et al. (1987)
* Done et al. (1990)
Log $f_\nu \nu$ (erg s^{-1} cm^{-2})
−8
−10
−12
12
14
16
18
Log ν

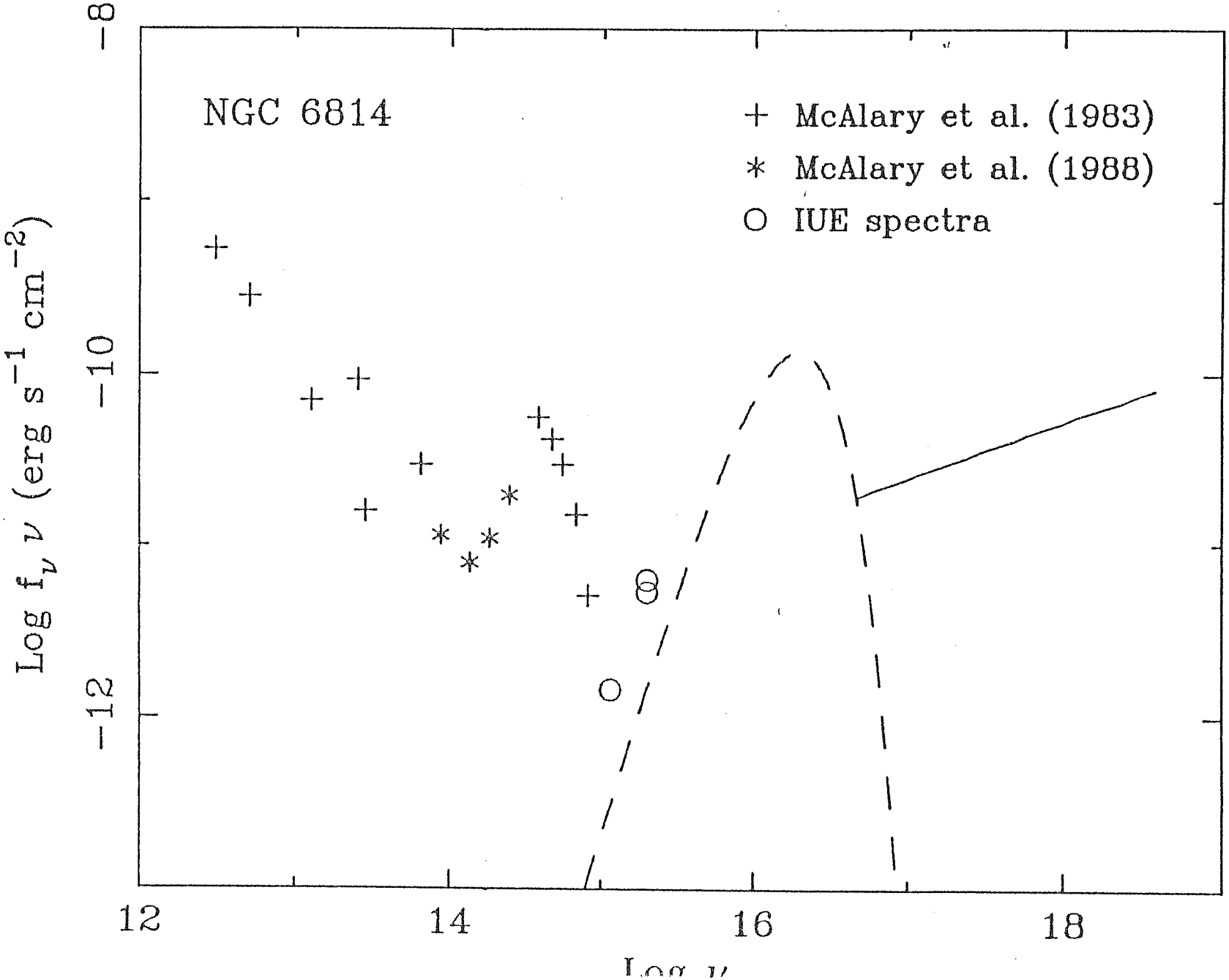
NGC 6814
+ McAlary et al. (1983)
* McAlary et al. (1988)
O IUE spectra
Log f_ν ν (erg s^{-1} cm^{-2})
−8
−10
−12
12
14
16
18
Log ν

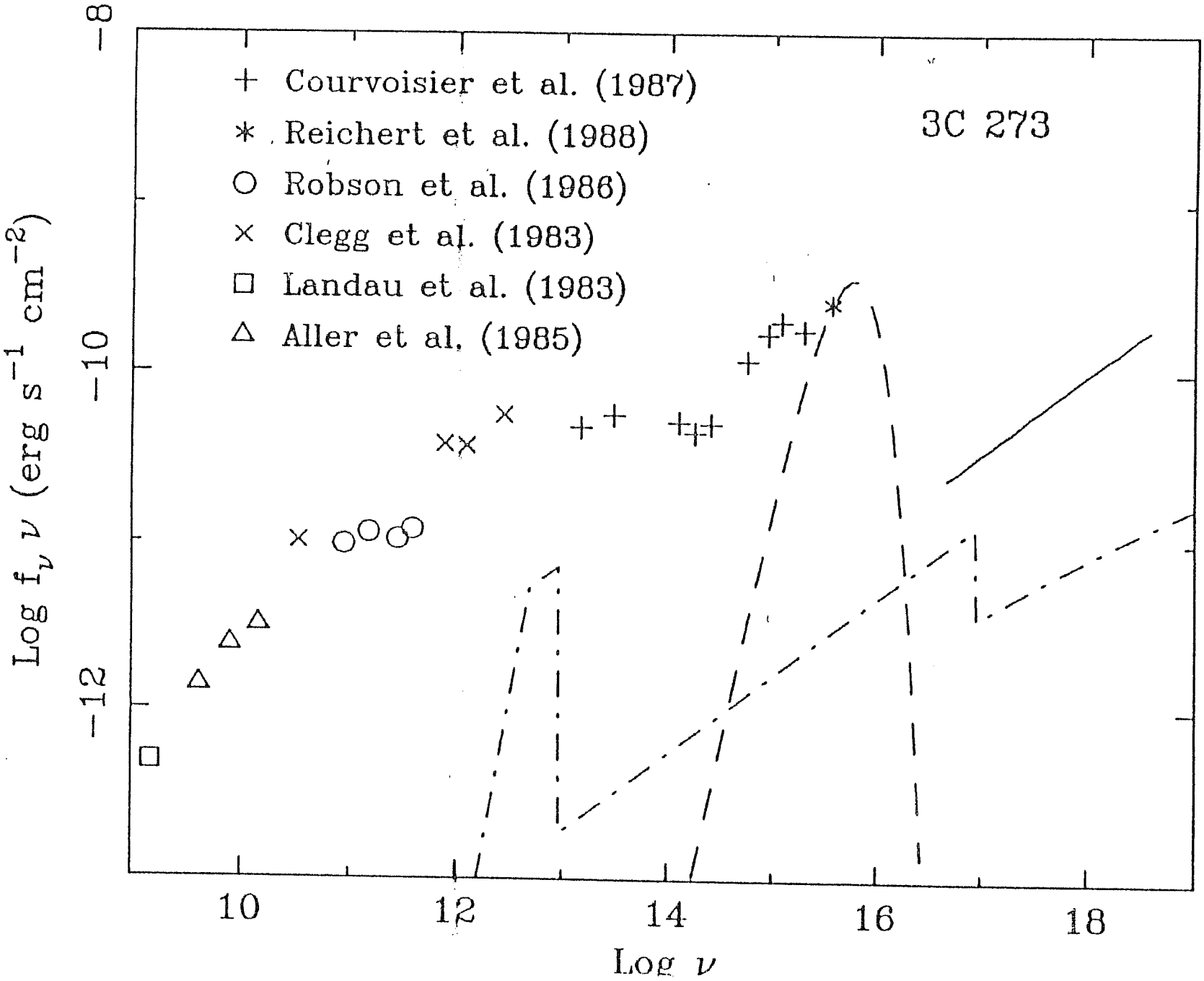
+ Courvoisier et al. (1987)
* Reichert et al. (1988)
○ Robson et al. (1986)
× Clegg et al. (1983)
□ Landau et al. (1983)
△ Aller et al. (1985)
3C 273
Log f_ν ν (erg s^{-1} cm^{-2})
−8
−10
−12
10
12
14
16
18
Log ν

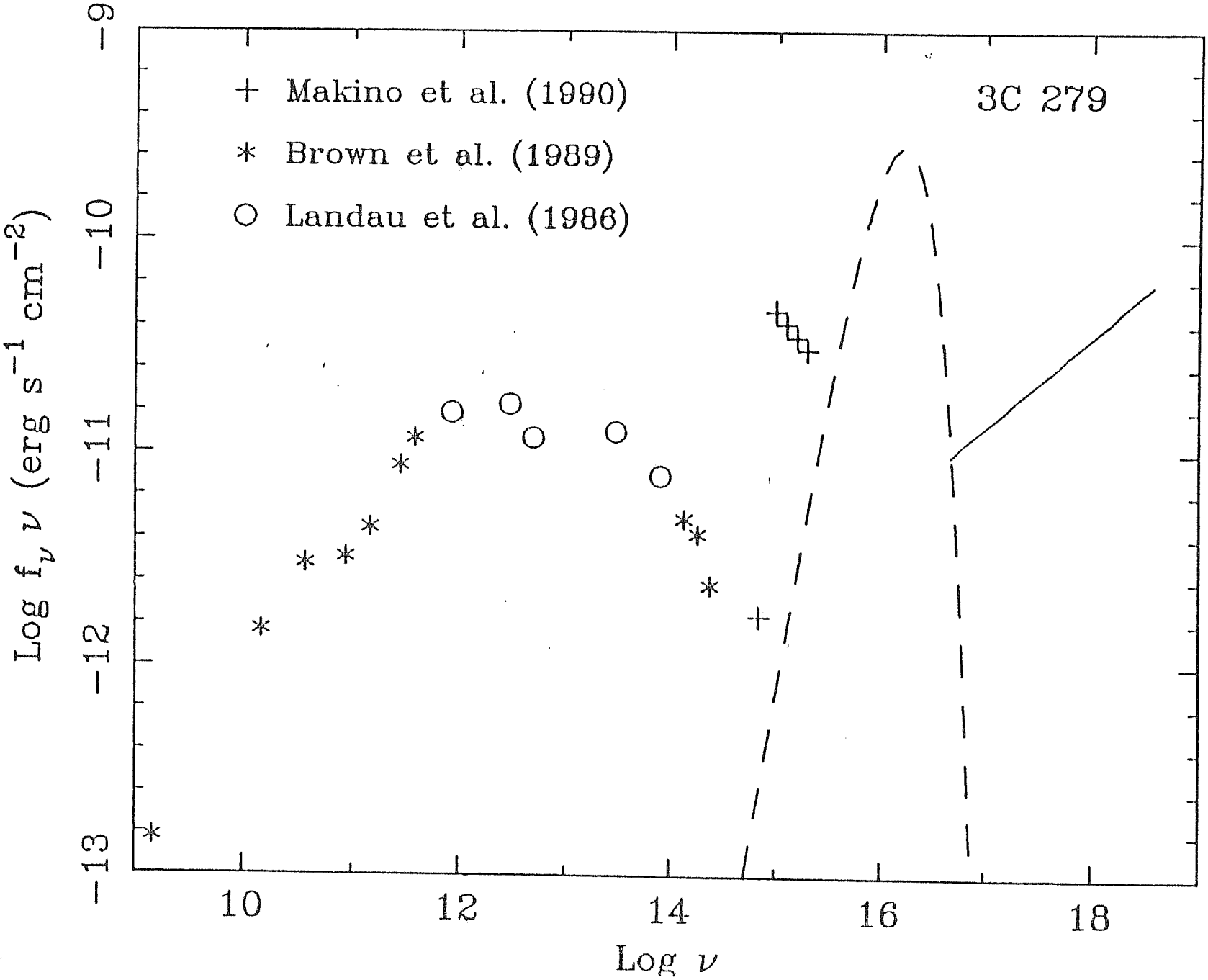
+ Makino et al. (1990)
* Brown et al. (1989)
O Landau et al. (1986)
3C 279
Log $f_\nu \nu$ (erg s^{-1} cm^{-2})
−9
−10
−11
−12
−13
10
12
14
16
18
Log ν

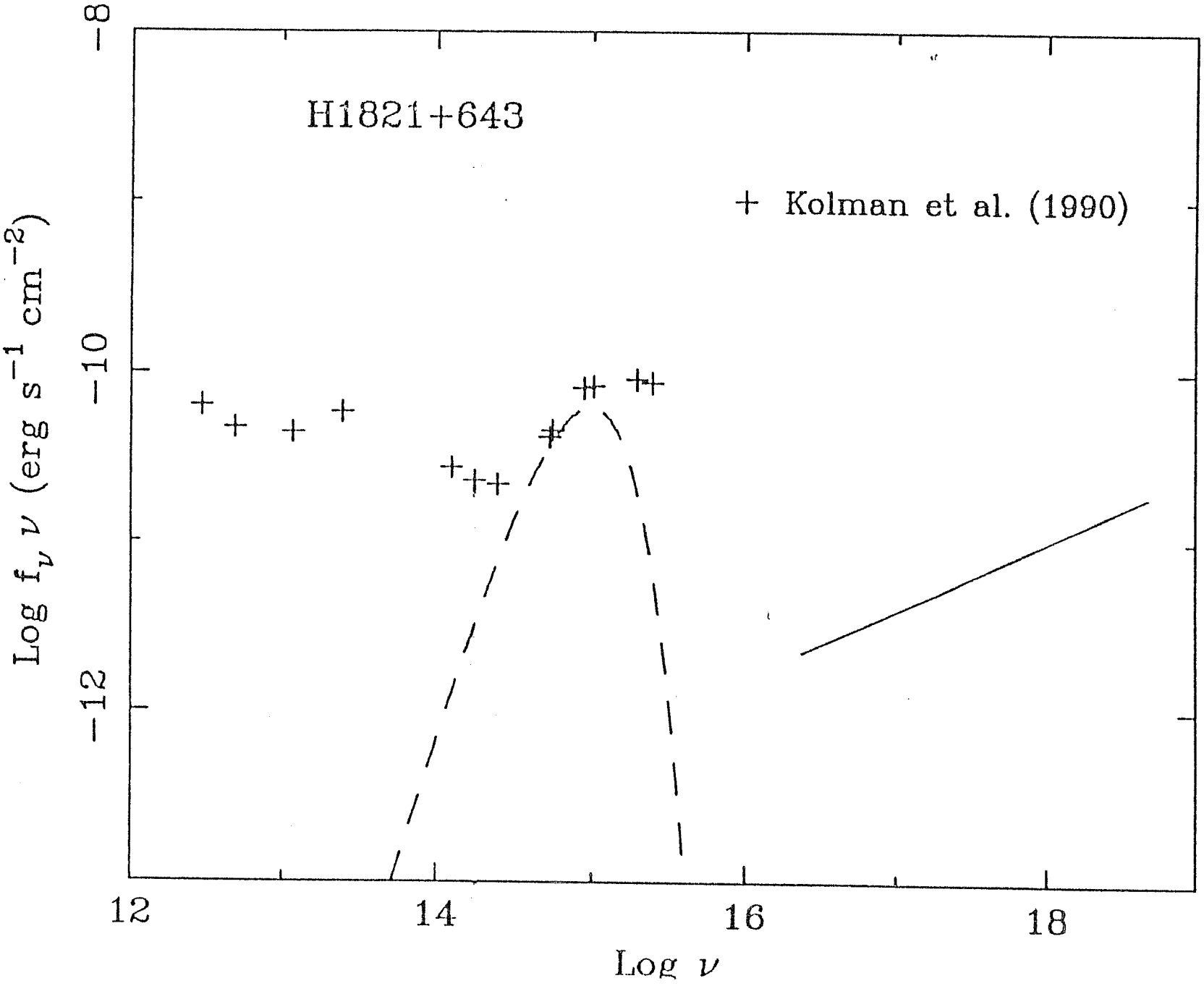
H1821+643
+ Kolman et al. (1990)
Log $f_\nu \nu$ (erg s^{-1} cm^{-2})
Log ν
−8
−10
−12
12
14
16
18

Fig. 1

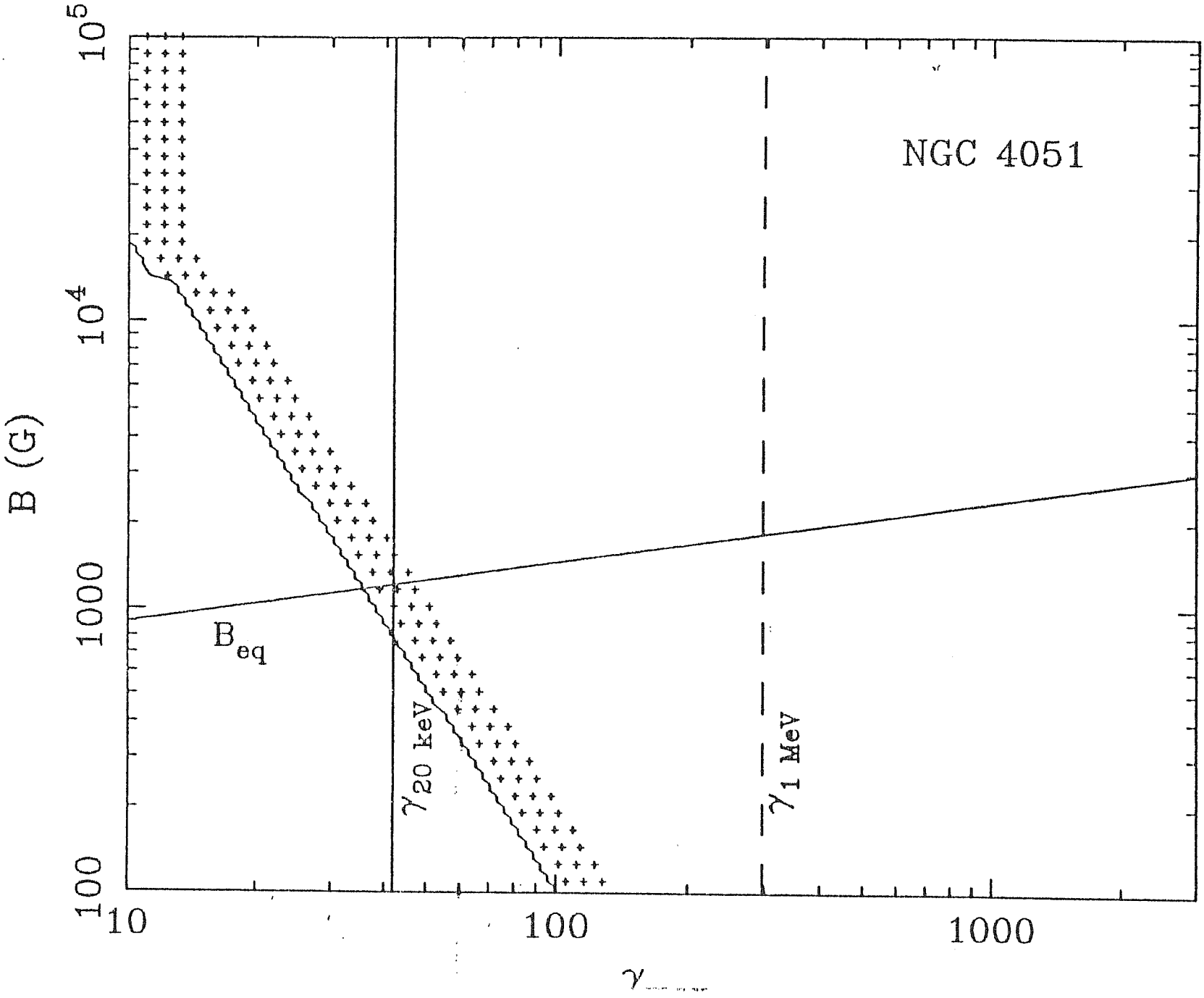
NGC 4051
B (G)
10^5
10^4
1000
100
10
100
1000
B_{eq}
$\gamma_{20\ keV}$
$\gamma_{1\ MeV}$
γ

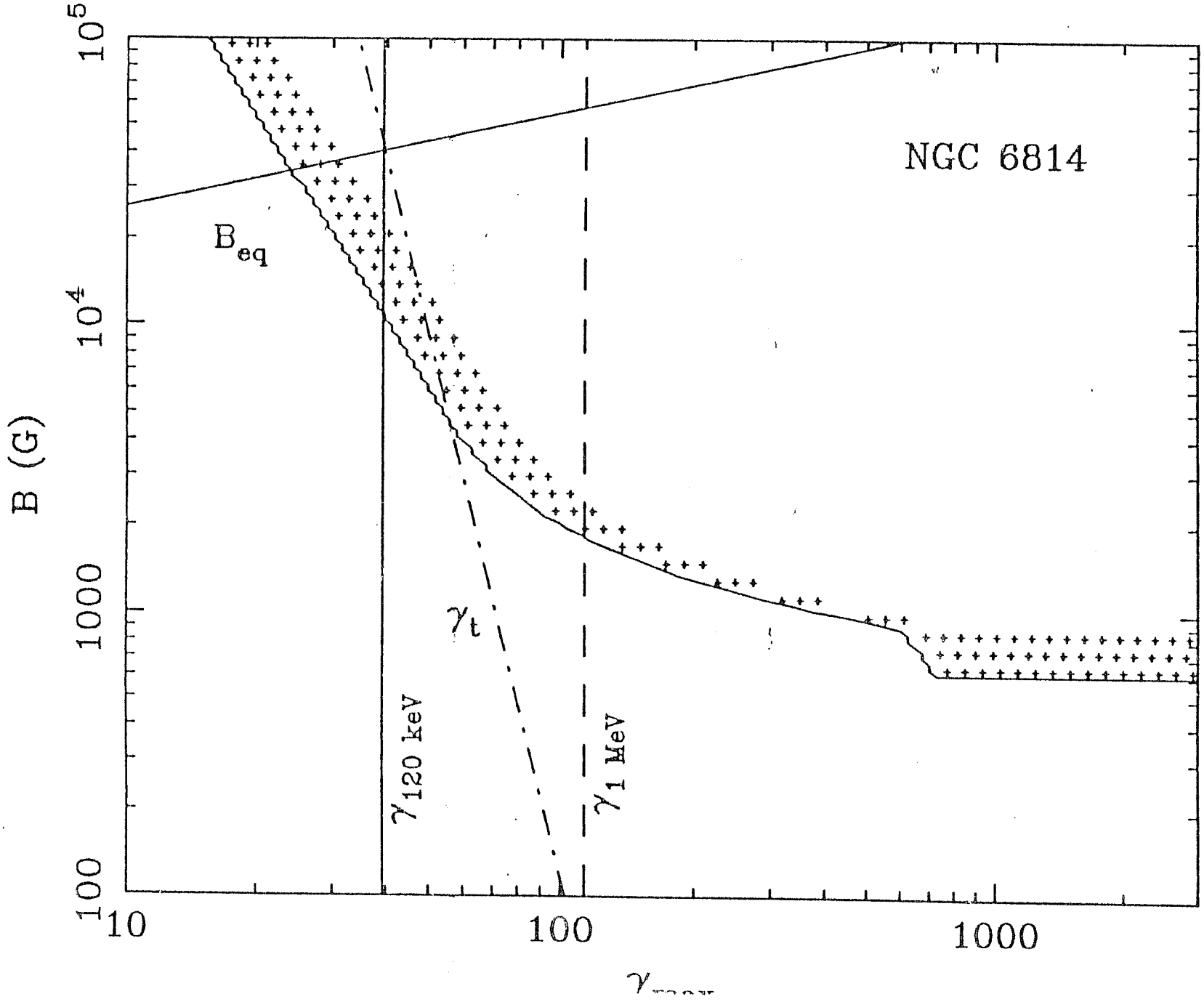
NGC 6814
B_{eq}
γ_t
$\gamma_{120\ keV}$
$\gamma_{1\ MeV}$
B (G)
10^5
10^4
1000
100
10
100
1000
γ_{max}

3C 273
γ_1 MeV
B_{eq}
B (G)
10^5
10^4
1000
100
10
100
1000

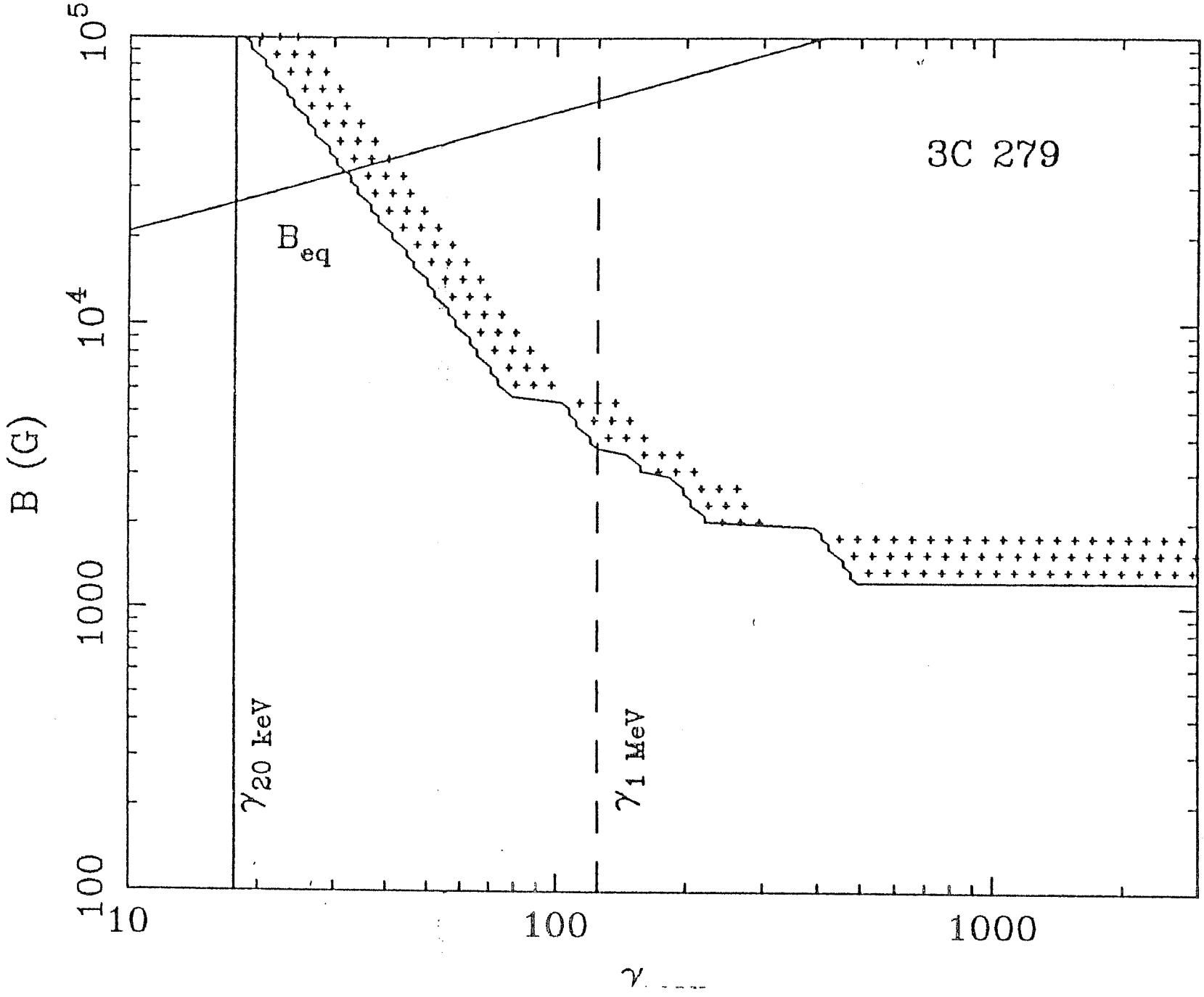
3C 279
B_{eq}
$\gamma_{20\ keV}$
$\gamma_{1\ MeV}$
B (G)
γ
10^5
10^4
1000
100
10
100
1000

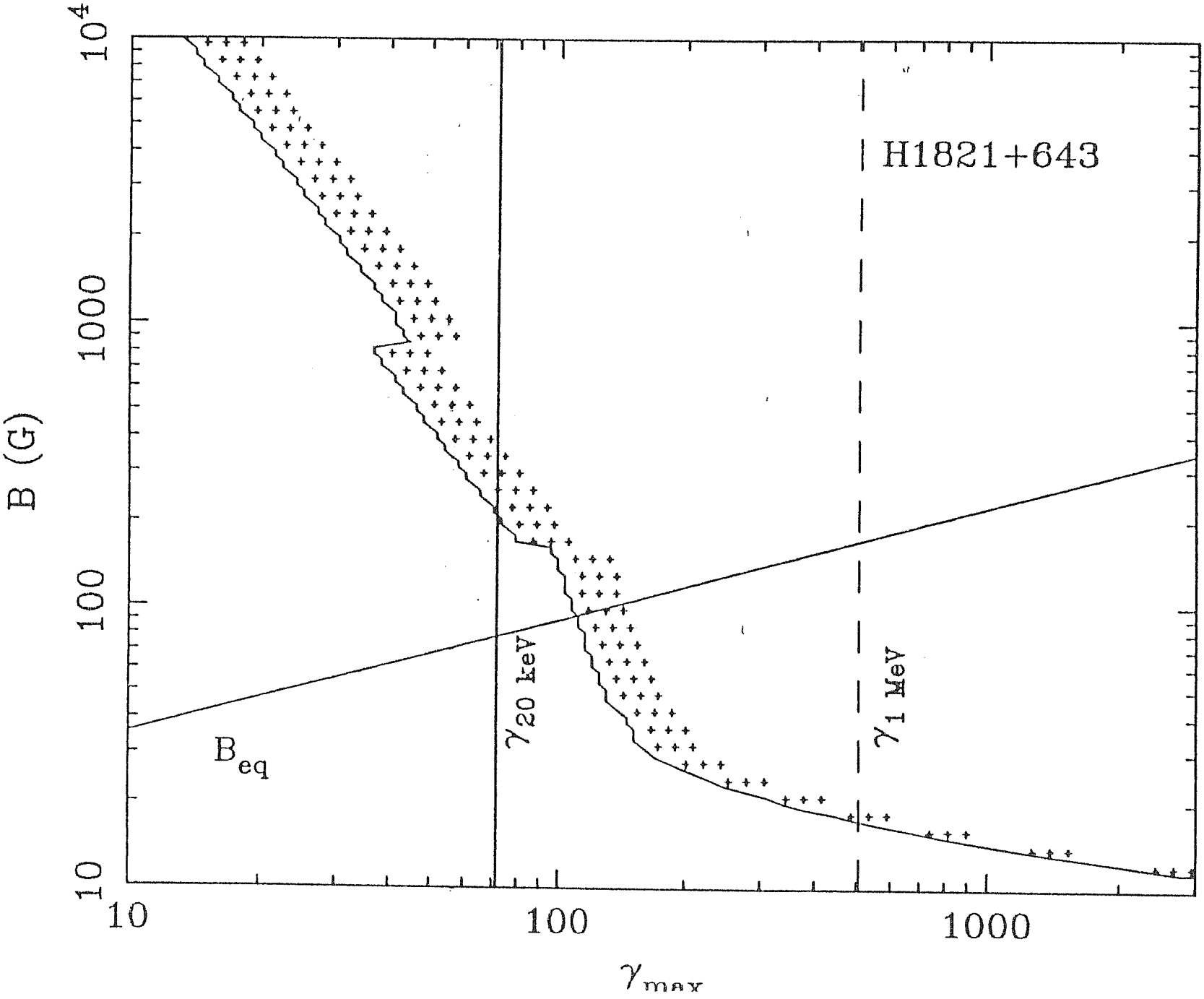
H1821+643
B (G)
10^4
1000
100
10
10
100
1000
γ_{max}
B_{eq}
$\gamma_{20\ keV}$
$\gamma_{1\ MeV}$

References

Abraham, R.G., McHardy, I.M., & Crawford, C.S., 1991. *Mon. Not. R. astr. Soc.*, in press.

Abramowicz, M.A., Ellis, G.F.R. & Lanza, A., 1990. *Astrophys. J.*, **361**, 470.

Abramowicz, M.A., Bao, G., Lanza, A. & Zhang, X.–H., 1989. In *Proc. 23th ESLAB Symp: "X-ray Astronomy"*, ESA SP–296, p. 871.

Aller, H.D., Aller, M.F., Latimer, G.E. & Hodge, P.E., 1985. *Astrophys. J. Suppl.*, **59**, 513.

Antonucci, R.J. & Barvainis, R., 1988. *Astrophys. J. Lett.*, **332**, L13.

Antonucci, R.J. & Ulvestad, J.S., 1985. *Astrophys. J.*, **294**, 158.

Arnaud, K.A., Branduardi–Raymont, G., Culhane, J.L., Fabian, A.C., Hazard, C., McGlynn, T.A., Shafer, R.A., Tennant, A.F. & Ward M.J., 1985. *Mon. Not. R. astr. Soc.*, **217**, 105.

Baath, L.B., 1991. *Astron. Astrophys.*, **241**, L1.

Baity, W.A., Mushotzky, R.F., Worral, D.M., Rothschild, R.E., Tennant, A.F. & Primini, F.A., 1984. *Astrophys. J.*, **244**, 429.

Balonek, T.J., 1982. *Astrophys. J. Lett.*, **240**, L3.

Barbieri, C., Vio, R., Cappellaro, E. & Turatto, M., 1990. *Astrophys. J.*, **359**, 63.

Barr, P., Giommi, P., Pollock, A., Tagliaferri, G., Maccagni, D. & Garilli, B., 1989. In *"BL Lac Objects"*, eds. L. Maraschi, T. Maccacaro and M–H. Ulrich (Springer–Verlag), p. 290.

Barthel, P.D., 1989. *Astrophys. J.*, **336**, 606.

Barthel, P.D., 1991. In *"The Physics of Active Galactic Nuclei"*, Proc. Conf. Heidelberg, June 1990, in press.

Barvainis, R., 1987. *Astrophys. J.*, **320**, 537.

Barvainis, R., 1990. *Astrophys. J.*, **353**, 419.

Bassani, L., Dean, A.J., Di Cocco, G. & Perotti, F., 1985. In *"Active Galactic Nuclei"*, ed. J. Dyson (Manchester University Press), p. 252.

Bassani, L., Butler, R.C., Di Cocco, G., Della Ventura, A., Perotti, F., Villa, G., Baker, R.E., Dean, A.J. & Lee, T.J., 1986. *Astrophys. J.*, **311**, 623.

Becker, P.A. & Begelman, M.C., 1990. *Astrophys. J.*, **364**, 203.

Begelman, M.C., 1990. In *"Variability of Active Galactic Nuclei"*, Proc. Conf. Atlanta, May 1990, eds. H.R. Miller & P.W. Wiita, in press.

Begelman, M.C., Blandford, R.D. & Rees, M.J., 1984. *Rev. of Mod. Phys.*, **56**, 255.

Begelman, M.C., Rees, M.J. & Blandford, R.D., 1979. *Nature*, **279**, 770.

Begelman, M.C., Sarazin, C.L., Hatchett, S.P., McKee, C.F. & Arons, J., 1980. *Astrophys. J.*, **238**, 722.

Benford, G., 1979. *Mon. Not. R. astr. Soc.*, **183**, 29.

Biermann, P.L. & Strittmatter, P.A., 1987. *Astrophys. J.*, **322**, 643.

Bignami, G.F., Fichtel, C.E., Hartman, R.C. & Thompson, D.J., 1979. *Astrophys. J.*, **232**, 649.

Biretta, J.A. & Cohen, M.H., 1987. In *"Superluminal Radio Sources"*, eds. A. Zensus & T. Pearson (Cambridge: Cambridge University Press), p. 40.

Biretta, J.A., Stern, C.P. & Harris, D.E., 1991. *Astron. J.*, **101**, 1632.

Blandford, R.D., 1990. In *"Active Galactic Nuclei"*, Lecture Notes 1990, SAAS–FEE Advanced Course 20, eds. T.J.–L. Courvoisier & M. Mayor (Berlin: Springer–Verlag).

Blandford, R.D. & Eichler, D., 1987. *Phys. Reports*, **154** 1.

Blandford, R.D. & Königl, A., 1979. *Astrophys. J.*, **232**, 34.

Blandford, R.D. & McKee, C.F., 1976. *Phys. Fluids*, **19**, 1130.

Blandford, R.D. & Rees, M.J., 1974. *Mon. Not. R. astr. Soc.*, **169**, 395.

Blandford, R.D. & Rees, M.J., 1978. In *"Pittsburgh Conference on BL Lac Objects"*, ed. A.N. Wolfe (Pittsburgh University Press), p. 328.

Blandford, R.D., McKee, C.F. & Rees, M.J., 1977. *Nature*, **267**, 211.

Bodo, G., Ferrari, A., Massaglia, S. & Tsinganos, K., 1985. *Astron. Astrophys.*, **149**, 246.

Boyd, T.J.M. & Sanderson, J.J., 1969. *"Plasma Dynamics"* (New York: Barnes and Noble).

Branduardi–Raymont, G., 1989. In *"Active galactic Nuclei"*, Proc. IAU Symp. No. 124, eds. D.E. Osterbrock & J.S. Miller (Reidel, Dordrecht), p. 177.

Bregman, J.N., 1990. *Astron. Astrophys. Rev.*, **2**, 125.

Bregman, J.N. & Hufnagel, B.R., 1989. In *"BL Lac Objects"*, eds. L. Maraschi, T. Maccacaro & M–H. Ulrich (Springer–Verlag), p. 159.

Bregman, J.N., *et al.*, 1984. *Astrophys. J.*, **276**, 454.

Bregman, J.N., *et al.*, 1986. *Astrophys. J.*, **301**, 708.

Bregman, J.N., *et al.* 1990, *Astrophys. J.*, **352**, 574.

Bregman, J.N., Maraschi L. & Urry, M., 1987. In *"Exploring the Universe with I.U.E."*, ed. Y. Kondo (Dordrecht: D. Reidel), p. 685.

Brodie, J., Bowyer, S. & Tennant, A., 1987. *Astrophys. J.*, **318**, 175.

Browne, I.W.A., 1987. In *"Superluminal Radio Sources"*, eds. A. Zensus & and T. Pearson (Cambridge: Cambridge University Press), p. 129.

Browne, I.W.A., 1989. In *"BL Lac Objects"*, eds. L. Maraschi, T. Maccacaro & M–H. Ulrich (Springer–Verlag), p. 401.

Brunner, H., Worral, D.M, Wilkes, B.J. & Elvis, M., 1990. In *Proc. 23th ESLAB Symp: "X-ray Astronomy"*, ESA SP–296, p. 905.

Butcher, H.R., van Bruegel, W. & Miley, G.K., 1980. *Astrophys. J.*, **235**, 749.

Canizares, C. & Kruper, J., 1984. *Astrophys. J. Lett.*, **278**, L99.

Carleton, N.P., Elvis, M., Fabbiano, G., Willner, S.P., Lawrence, A. & Ward, M., 1987. *Astrophys. J.*, **18**, 595.

Cawthorne, T.V. & Wardle, J.F.C., 1988. *Astrophys. J.*, **332**, 696.

Cawthorne, T.V., Scheuer, A.G., Morison, I. & Muxlow, T.W.B., 1986. *Mon. Not. R. astr. Soc.*, **219**, 883.

Cavaliere, A. & Morrison, P., 1980. *Astrophys. J. Lett.*, **238**, L64.

Cavaliere, A., Giallongo, G. & Vagnetti, F., 1986. *Astron. Astrophys.*, **156**, 33.

Cavallo, G. & Rees, M.J., 1978. *Mon. Not. R. astr. Soc.*, **183**, 359.
Celotti, A., 1989. Thesis, University of Milano.
Celotti, A., Ghisellini, G. & Fabian, A.C., 1991a. *Mon. Not. R. astr. Soc.*, in press.
Celotti, A., Ghisellini, G. & Fabian, A.C., 1991b. In *"The Physics of Active Galactic Nuclei"*, Proc. Conf. Heidelberg, June 1990, in press.
Celotti, A., Maraschi, L. & Treves, A., 1989. In *"BL Lac Objects"*, eds. L. Maraschi, T. Maccacaro & M–H. Ulrich (Springer–Verlag), p. 332.
Celotti, A., Maraschi, L. & Treves, A., 1991. *Astrophys. J.*, **377**, 403.
Celotti, A., Rees, M.J. & Fabian, A.C., 1991. To be submitted to *Mon. Not. R. astr. Soc.*
Chini, R., Kreysa, E. & Biermann, P.L., 1989. *Astron. Astrophys.*, **219**, 87.
Clavel, J., Wamstaker, W. & Glass, I.S., 1989. *Astrophys. J.*, **337**, 236.
Clavel, J. *et al.* 1990. *Mon. Not. R. astr. Soc.*, **246**, 668.
Cobb, W.K., Wardle, J.F.C. & Roberts, D.H., 1988. In *"The Impact of VLBI on Astrophysics and Geophysics"*, Proc. IAU Coll. N. 129, eds. M.J. Reid & J.M. Moran (Dordrecht: Kluwer), p. 153.
Cohen, R.D., 1986. In *"Highlights of Modern Astrophysics"*, eds. S.L. Shapiro & S.A. Teukolsky (New York: Wiley), p. 299.
Cohen, R.D., 1990. In *"Parsec–Scale Radio Jets"*, eds. J.A. Zensus & T.J. Pearson (Cambridge Univ. Press), p. 317.
Cohen, R.D., Smith, H.E., Junkkarinen, V.T. & Burbridge, E.M., 1987. *Astrophys. J.*, **318**, 577.
Collin–Souffrin, S., 1991. *Astron. Astrophys.*, in press.
Courvoisier, T.J.–L., 1991. Preprint.
Courvoisier, T.J.–L. *et al.* 1990. *Astron. Astrophys.*, **234**, 73.
Courvoisier, T.J.–L. & Clavel, J., 1990. In *"Structure and Emission Properties of Accretion Disks"*, Proc. IAU Coll. 129, Paris 1990, eds. C. Bertout *et al.* (Edition Frontieres).
Daly, R.A. & Marscher, A.P., 1988. *Astrophys. J.*, **334**, 539.
Davidson, K. & Netzer, H., 1979. *Rev. Mod. Phys.*, **51**, 715.
de Kool, M. & Begelman, M.C., 1989. *Astrophys. J.*, **345**, 135.
Dent, W.A., 1965. *Science*, **148**, 1458.
Done, C. & Fabian, A.C., 1989. *Mon. Not. R. astr. Soc.*, **240**, 81.
Done, C., Ghisellini, G. & Fabian, A.C., 1990. *Mon. Not. R. astr. Soc.*, **245**, 1.
Done, C., Ward, M.J., Fabian, A.C., Kunieda, H., Tsuruta, S., Lawrence, A., Smith, M.G. & Wamsteker, W., 1990. *Mon. Not. R. astr. Soc.*, **243**, 713.
Edelson, R.A. & Malkan, M.A., 1986. *Astrophys. J.*, **308**, 59.
Edelson, R.A. & Malkan, M.A., 1987. *Astrophys. J.*, **323**, 516.
Edelson, R.A., Saken, J.M., Pike, G.F., Urry, C.M., George, I.M., Warwick, R.S., Miller, H.R., Carini, M.T. & Webb, J.R., 1991. *Astrophys. J. Lett.*, **372**, L9.
Elvis, M., Wilkes, B.J. & McDowell, J.C., 1990. In *"Extreme Ultraviolet Astronomy"*, eds. R.F. Malina & S. Bowyer (New York: Pergamon).
Fabbiano, G., Miller, L., Trinchieri, G., Longair, M. & Elvis, M., 1984. *Astrophys. J.*, **277**, 115.
Fabian, A.C., 1979. *Proc. R. Soc. Lond. A.*, **366**, 449.

Fabian, A.C., 1986. In *"The Physics of Accretion onto Compact Objects"*, eds. Mason, K.O., Watson, M.G. & White, N.E. (Springer–Verlag), p. 229.

Fabian, A.C., 1988. In *"Supermassive Black Holes"*, ed. M. Kafatos (Cambridge: Cambridge University Press), p. 234.

Fabian, A.C., 1989. In *Proc. 23th ESLAB Symp: "X-ray Astronomy"*, ESA SP–296, p. 1097.

Fabian, A.C. & Rees, M.J., 1979. *Mon. Not. R. astr. Soc.*, **187**, 13P.

Fabian, A.C., Rees, M.J., Stella. L. & White, N.E., 1988. *Mon. Not. R. astr. Soc.*, **238**, 729.

Fanaroff, B.L. & Riley, J.M., 1974. *Mon. Not. R. astr. Soc.*, **167**, 31P.

Feigelson, E.D., 1982. In *"Extragalactic Radio Sources", I.A.U Symp. No. 97*, eds. D. Heeschen & C.M. Wade, p. 107.

Feigelson, E.D., Bradt, H., McClintock, J., Remillard, R., Urry, C.M., Tapia, S., Geldzahler, B., Johnston, K., Romanishin, W., Wehinger, P.A., Wyckoff, S., Madejski, G., Schwartz, D.A, Thorstensen, J. & Schaefer, B.E., 1986. *Astrophys. J.*, **302**, 337.

Ferland, G.J. & Persson, S.E., 1989. *Astrophys. J.*, **347**, 656.

Ferland, G.J. & Rees, M.J., 1988. *Astrophys. J.*, **332**, 141.

Ferland, G.J., Korista, K.T., & Peterson, B.M., 1990. *Astrophys. J. Lett.*, **363**, L21.

Fiore, F. & Massaro, E., 1989. In *Proc. 23th ESLAB Symp: "X-ray Astronomy"*, ESA SP–296, p. 935.

Fiore, F., Massaro, E., Perola, G.C. & Piro, L., 1989. *Astrophys. J.*, **347**, 171.

Fugmann, W., 1988. *Astron. Astrophys.*, **205**, 86.

Gabuzda, D.C., Wardle, J.F.C. & Roberts, D.H., 1989. *Astrophys. J. Lett.*, **336**, L59.

George, I.M. & Fabian, A.C., 1991. *Mon. Not. R. astr. Soc.*, **249**, 352.

George, I.M., Warwick, R.S & Bromage, G.E., 1988. *Mon. Not. R. astr. Soc.*, **232**, 793.

Ghisellini, G., 1987. *Ph. D. Thesis*, ISAS, Trieste.

Ghisellini, G., 1989. *Mon. Not. R. astr. Soc.*, **236**, 341.

Ghisellini, G. & Maraschi, L., 1989. *Astrophys. J.*, **340**, 181.

Ghisellini, G. & Svensson, R., 1991. *Mon. Not. R. astr. Soc.*, in press.

Ghisellini, G., George, I.M. & Done, C., 1989. *Mon. Not. R. astr. Soc.*, **241**, 43P.

Ghisellini, G., Guilbert, P.W. & Svensson, R., 1988. *Astrophys. J. Lett.*, **334**, L5.

Ghisellini, G., Maraschi, L. & Treves, A., 1985. *Astron. Astrophys.*, **146**, 204.

Ghisellini, G., Bodo, G., Trussoni, E. & Rees, M.J., 1990. *Astrophys. J. Lett.*, **362**, L1.

Ghisellini, G., Celotti, A., George, I.M. & Fabian, A.C., 1991. To be submitted to *Mon. Not. R. astr. Soc.*.

Ghisellini, G., Maraschi, L., Tanzi, E. & Treves, A., 1986. *Astrophys. J.*, **310**, 317.

Giommi, P., Barr, P., Garilli, B., Maccagni, D. & Pollock, A.M.T., 1990. *Astrophys. J.*, **356**, 432.

Giommi, P. *et al.*, 1989. In *"BL Lac Objects"*, eds. L. Maraschi, T. Maccacaro & M–H. Ulrich (Springer–Verlag), p. 231.

Giommi, P. *et al.* 1991. Preprint.

Giovanoni, P.M. & Kazanas, D., 1990. *Nature,* **345**, 319.
Grindlay, J.E, Band, D., Seward, F., Leahy, D., Weisskopf, M.C. & Marshall, F.E., 1984. *Astrophys. J.,* **277**, 286.
Guilbert, P.W. & Rees, M.J., 1988. *Mon. Not. R. astr. Soc.,* **233**, 475.
Guilbert, P.W., Fabian, A.C., & McCray, R., 1983. *Astrophys. J.,* **266**, 466.
Guilbert, P.W., Fabian, A.C., & Rees, M.J., 1983. *Mon. Not. R. astr. Soc.,* **205**, 593.
Guilbert, P.W., Fabian, A.C., & Ross, R.R., 1982. *Mon. Not. R. astr. Soc.,* **199**,, 763.
Guilbert, P.W., Fabian, A.C., & Stepney, S., 1982. *Mon. Not. R. astr. Soc.,* **199**, 19P.
Haardt, F. & Maraschi, L., 1991. *Astrophys. J. Lett.,* in press.
Heckman, T., 1991. In *"Massive Stars in Starbursts"*, Proc. of the ST ScI Symp., May 1990, eds. N. Walborn & C. Leitherer.
Holt, S.S., Mushotzky, R.F., Becker, R.H., Boldt, E.A., Serlemitsos, P.J., Szymkowiak, A.E. & White, N.E., 1980. *Astrophys. J. Lett.,* **241**, L13.
Hughes, P.A., Aller, H.D. & Aller, M.F., 1985. *Astrophys. J.,* **298**, 301.
Hughes, P.A., Aller, H.D. & Aller, M.F., 1989a. *Astrophys. J.,* **341**, 54.
Hughes, P.A., Aller, H.D. & Aller, M.F., 1989b. *Astrophys. J.,* **341**, 68.
Impey, C.D., 1987. In *"Superluminal Radio Sources"* eds. A. Zensus & T. Pearson (Cambridge: Cambridge University Press), p. 233.
Impey, C.D. & Neugebauer, G., 1988. *Astron. J.,* **95**, 307.
Impey, C.D. & Tapia, S., 1990. *Astrophys. J.,* **354**, 124.
Inoue, H., 1989. In *Proc. 23^{th} ESLAB Symp: "X-ray Astronomy"*, ESA SP–296, p. 783.
Jones, T.W., 1988. *Astrophys. J.,* **332**, 678.
Jones, T.W. & O'Dell, S.L., 1977. *Astron. Astrophys.,* **61**, 291.
Jones, T.W. & Stein, W.A., 1990. *Astrophys. J.,* **349**, 443.
Jones, T.W., O'Dell, S.L. & Stein, W.A., 1974a. *Astrophys. J.,* **188**, 353.
Jones, T.W., O'Dell, S.L. & Stein, W.A., 1974b. *Astrophys. J.,* **192**, 261.
Kaastra, J.S. & Barr, P., 1989. *Astron. Astrophys.,* **226**, 59.
Kazanas, D., 1989. *Astrophys. J.,* **347**, 74.
Königl, A., 1981. *Astrophys. J.,* **243**, 700.
Königl, A., 1989. In *"BL Lac Objects"*, eds. L. Maraschi, T. Maccacaro and M–H. Ulrich (Springer–Verlag), p. 321.
Koratan, A.P. & Gaskell, C.M., 1991. *Astrophys. J. Lett.,* **370**, L61.
Krichbaum, T.P. *et al.* 1990. *Astron. Astrophys.,* **237**, 3.
Krolik, J.H. & Begelman, M.C., 1988. *Astrophys. J.,* **329**, 702.
Krolik, J.H. & Vrtilek, J.M., 1984. *Astrophys. J.,* **279**, 521.
Krolik, J.H., McKee, C.F. & Tarter, C.B., 1981. *Astrophys. J.,* **249**, 422.
Krolik, J.H., Kallmann, T.R., Fabian, A.C. & Rees, M.J., 1985. *Astrophys. J.,* **295**, 104.
Kundt, W., 1987. In *"Astrophysical Jets and Their Engines"*, ed. W. Kundt (Dordrecht: Reidel), p. 1.
Kundt, W. & Gopal–Krishna, 1980. *Nature,* **288**, 149.

Kunieda, H., Turner, T.J., Awaki, H., Koyama, K., Mushotzky, R. & Tsusaka, Y., 1990. *Nature,* **345**, 786.

Laing, R.A., 1988. *Nature,* **331**, 149.

Lamb, R.C., Ling, J.C., Mahoney, W.A., Riegler, A., Wheaton, W.A. & Jacobson, A.S., 1983. *Nature,* **305**, 37.

Landau, L.D. & Lifshitz, E.M., 1959. *"Fluids Mechanics"* (Oxford: Pergamon).

Landau, R. *et al.*, 1986. *Astrophys. J.,* **308**, 78.

Laor, A. & Netzer, H., 1989. *Mon. Not. R. astr. Soc.,* **238**, 897.

Laor, A. & Netzer, H. & Piran, T., 1990. *Mon. Not. R. astr. Soc.,* **242**, 560.

Lawrence, A., 1987. *Pub. Astron. Soc. Pacific,* **99**, 309.

Lawrence, A., Pounds, K.A., Watson, M.G. & Elvis, M.S., 1985. *Mon. Not. R. astr. Soc.,* **217**, 685.

Lawrence, A., Pounds, K.A., Watson, M.G. & Elvis, M.S., 1987. *Nature,* **325**, 692.

Lightman, A.P. & White, T.R., 1988. *Astrophys. J.,* **335**, 57.

Lightman, A.P. & Zdziarki, A., 1987. *Astrophys. J.,* **319**, 643.

Lightman, A.P., Zdziarski, A.A. & Rees, M.J., 1987. *Astrophys. J. Lett.,* **315**, L113.

Lind, K.R. & Blandford, R.D., 1985, *Astrophys. J.,* **295**, 358.

Longair, M.S. & Ryle, S.M., 1979. *Mon. Not. R. astr. Soc.,* **188**, 625.

Maccacaro, T., Gioia, I.M., Schild, R.E., Wolter, A., Morris, S.L. & Stocke, J.T., 1989. In *"BL Lac Objects"*, eds. L. Maraschi, T. Maccacaro & M–H. Ulrich (Springer–Verlag), p. 222.

Maccagni, D., Garilli, B., Barr, P., Giommi, P. & Pollock, A., 1989. In *"BL Lac Objects"*, eds. L. Maraschi, T. Maccacaro & M–H. Ulrich (Springer–Verlag), p. 281.

Madau, P., Ghisellini, G. & Persic, M., 1987. *Mon. Not. R. astr. Soc.,* **224**, 257.

Madejski, G. & Schwartz, D., 1989. In *"BL Lac Objects"*, eds. L. Maraschi, T. Maccacaro & M–H. Ulrich (Springer–Verlag), p. 267.

Madejski, G., Mushotzky, R.F., Weaver, K.A., Arnaud, K.A. & Urry, C.M., 1991. *Astrophys. J.,* in press.

Makino, F., 1989. In *Proc. 23th ESLAB Symp: "X-ray Astronomy"*, ESA SP–296, p. 803.

Makino, F. *et al.*, 1987. *Astrophys. J.,* **313**, 662.

Makino, F., *et al.*, 1988. In *"Physics of Neutron Stars and Black Holes"* ed. Y. Tanaka (Univ. Acad. Press, Tokyo).

Makino, F., Kii, T., Hayashida, K., Inoue, H., Tanaka, Y., Ohashi, T., Makishima, K., Awaki, H., Koyama, K., Turner, M.J.L. & Williams, O.R., 1989. *Astrophys. J. Lett.,* **347**, L9.

Makishima, K., 1986. *"The Physics of Accretion onto Compact Objects"*, eds. K.O. Mason, M.G. Watson & N.E. White (Springer–Verlag), p. 249.

Malkan, M.A., 1983. *Astrophys. J.,* **268**, 582.

Maraschi, L., 1991. In *"Variability in Blazar"*, Proc. Conf. Turku, Jan 1991, in press.

Maraschi, L. & Maccagni, D., 1988. *Mem. Soc. Astron. It.,* **59**, 277.

Maraschi, L., Celotti, A. & Ghisellini, G., 1991. In *"The Physics of Active Galactic Nuclei"*, Proc. Conf. Heidelberg, June 1991, in press.

Maraschi, L., Celotti, A. & Treves, A., 1989. In *Proc. 23th ESLAB Symp: "X-ray Astronomy"*, ESA SP–296, p. 825.

Maraschi, L., Perola, G.C. & Treves, A., 1980. *Astrophys. J.*, **241**, 910.

Maraschi, L., Ghisellini, G., Tanzi, E.G. & Treves, A., 1986, *Astrophys. J.*, **310**, 325.

Maraschi, L., Tanzi, E., Tarenghi, M. & Treves, A., 1983. *Astron. Astrophys.*, **125**, 117.

Maraschi, L., Chiappetti, L., Falomo, R., Garilli, B., Malkan, M., Tagliaferri, G., Tanzi, E.G. & Treves, A., 1991. *Astrophys. J.*, **368**, 138.

Margon, B., 1984. *Ann. Rev. Astron. Astroph.*, **22**, 507.

Marscher, A.P., 1977. *Astrophys. J.*, **216**, 244.

Marscher, A.P., 1980. *Astrophys. J.*, **235**, 386.

Marscher, A.P., 1987. In *"Superluminal Radio Sources"*, eds. A. Zensus & T. Pearson (Cambridge: Cambridge University Press), p. 280.

Marscher, A.P. & Gear, W.K., 1985. *Astrophys. J.*, **298**, 114.

Masnou, J.–L., Wilkes, B.J., Elvis, M., McDowell, J.C. & Arnaud K.A., 1991. *Astron. Astrophys.*, in press..

Mathews , W.G. & Ferland, G.J., 1987. *Astrophys. J.*, **323**, 456.

Matsuoka, M., Takano, S. & Makishima, K., 1986. *Mon. Not. R. astr. Soc.*, **222**, 605.

Matsuoka, M., Piro, L., Yamauchi, M. & Murakami, T., 1990. *Astrophys. J.*, **361**, 440.

McAlary, C.W. & Rieke, G.H., 1988. *Astrophys. J.*, **333**, 1.

McHardy, I.M., 1988. In *Mem. Soc. Astr. It.*, **59**, 239.

McHardy, I., 1989. In *"BL Lac Objects"*, eds. L. Maraschi, T. Maccacaro & M.H. Ulrich (Springer-Verlag: Berlin), p. 189.

Mead, A.R.G., Ballard, K.R., Brand, P.W.J.L., Hough, J.H., Brindle, C. & Bailey, J.A., 1990. *Astron. Astrophys. Suppl.*, **83**, 183.

Meisenheimer, K. & Heavens, A.F., 1986. *Nature*, **323**, 419.

Melia, F. & Königl, A., 1989. In *"BL Lac Objects"*, eds. L. Maraschi, T. Maccacaro & M.H. Ulrich (Springer-Verlag: Berlin), p. 372.

Miley, G.K., 1980. *Ann. Rev. Astr. Astroph.*, **18**, 165.

Milgrom, M., 1979. *Astron. Astrophys.*, **78**, L17.

Miller, J.S. 1989. In *"BL Lac Objects"*, eds. L. Maraschi, T. Maccacaro & M.H. Ulrich (Springer-Verlag: Berlin), p. 395.

Mittaz, J.P.D. & Branduardi–Raymont, G., 1989. *Mon. Not. R. astr. Soc.*, **238**, 1029.

Moffet, A.T., Gubbay, J. Robertson, D.S & Legg, A.J., 1972. *"External Galaxies and Quasi–Stellar Objects", I.A.U. Symp. No. 44*, ed. D.S. Evans (Dordrecht: Reidel), p. 228.

Molendi, S., Maraschi, L. & Stella, L., 1991. *Mon. Not. R. astr. Soc.*, in press.

Moore, R.L. & Stockman, H.S., 1981. *Astrophys. J.*, **235**, 717.

Moore, R.L. & Stockman, H.S., 1984. *Astrophys. J.*, **279**, 465.

Moore, R.L. *et al.*, 1982. *Astrophys. J.*, **260**, 415.

Morganti, R., Robinson, A., Fosbury, R.A.E., di Serego Alighieri, S., Tadhunter, C.N. & Malin, D., 1991. *Mon. Not. R. astr. Soc.*, in press.

Morini, M., Anselmo, F. & Molteni, D., 1989. *Astrophys. J.*, **347**, 750.

Morini, M., Chiappetti, L., Maccagni, D., Maraschi, L., Molteni, D., Tanzi, E.G., Treves, A. & Wolter, A., 1986. *Astrophys. J. Lett.*, **306**, L71.

Morris, S.L., Stocke, J.T., Gioia, I.M., Schild, R.E., Wolter, A., Maccacaro, T. & Della Ceca, R., 1991. *Astrophys. J.*, in press..

Mushotzky, R.F., Marshall, F.E., Boldt, E.A., Holt, S.S. & Serlesmitsos, P.J., 1980. *Astrophys. J.*, **235**, 377.

Mutel, R.L., 1990. In *"Parsec-Scale Radio Jets"*, eds. J.A. Zensus & T.J. Pearson (Cambridge Univ. Press), p. 98.

Mutel, R.L., Phillips, R.B., Su, B. & Bucciferro, R.R, 1990. *Astrophys. J.*, **352**, 81.

Nandra, K., Pounds, K.A., Stewart, G.C., Fabian, A. & Rees, M.J., 1989. *Mon. Not. R. astr. Soc.*, **236**, 39P.

Nandra, K., Pounds, K.A., Stewart, G.C., George, I.M., Hayashida, K., Makino, F. & Ohashi, T., 1991. *Mon. Not. R. astr. Soc.*, **248**, 760.

Netzer, H., 1990. In *"Active Galactic Nuclei"*, Lecture Notes 1990, SAAS–FEE Advanced Course 20, eds. T.J.–L. Courvoisier & M. Mayor (Berlin: Springer–Verlag).

Neugebauer, G., Green, R.F., Matthews, K., Schmidt, M., Soifer, B.T. & Bennet, J., 1987. *Astrophys. J. Suppl.*, **63**, 615.

Norman, M.L., Smarr, L., Wilson, J.R. & Smith, M.D., 1981. *Astrophys. J. Lett.*, **247**, 52.

O'Dell, S.L., 1988. *Astrophys. J.*, **327**, 60.

O'Dell, S.L., Dennison, B., Broderick, J.J., Altschuler, D.R., Condon, J.J., Payne, H.E., Mitchell, K.J., Aller, H.D., Aller, M.F. & Hodge, P.E., 1988. *Astrophys. J.*, **326**, 668.

Ohashi, T., 1989. In *"BL Lac Objects"*, eds. L. Maraschi, T. Maccacaro & M.H. Ulrich (Springer-Verlag: Berlin), p. 296.

Oke, J.B. 1967. *Astrophys. J.*, **147**, 901.

Orr, M.J.L. & Browne, W.A., 1983. *Mon. Not. R. astr. Soc.*, **200**, 1067.

Ostriker, J.P. & Vietri, M., 1985. *Nature*, **318**, 446.

Padovani, P. & Rafanelli, P., 1988. *Astron. Astrophys.*, **205**, 53.

Padovani, P. & Urry, C.M., 1990. *Astrophys. J.*, **356**, 75.

Padovani, P. & Urry, C.M., 1991a. *Astrophys. J.*, **368**, 373.

Padovani, P. & Urry, C.M., 1991b. In *"The Physics of Active Galactic Nuclei"*, Proc. Conf. Heidelberg, June 1990, in press.

Padovani, P., Burg, R.I. & Edelson, R.A., 1990. *Astrophys. J.*, **353**, 438.

Pan, H.–C., Stewart, G.C. & Pounds, K.A., 1990. *Mon. Not. R. astr. Soc.*, **242**, 177.

Pauliny–Toth, I.I.K., 1987. In *"Superluminal Radio Sources"*, eds. A. Zensus & T. Pearson (Cambridge: Cambridge University Press), p. 55.

Peacock, J.A., 1987. In *"Astrophysical Jets and Their Engines"*, ed. W. Kundt (Dordrecht: Reidel), p. 185.

Peréz–Fournon, I., Colina, L., Gonzáles–Serrano, J.I. & Biermann, P.L., 1988. *Astrophys. J. Lett.*, **329**, L81.

Perley, R.A., Bridle, A.H. & Willis, A.G., 1984. *Astrophys. J. Suppl.*, **54**, 292.

Perola, G.C., Piro, L., Altamore, A., Fiore, F., Boksenberg, A., Penston, M.V., Snijders, M.A.J., Bromage, G., Clavel, J., Elvius, A., & Ulrich, M.H., 1986. *Astrophys. J.*, **306**, 508.

Phillips, R.B. & Mutel, R.L., 1988. *In "The Impact of VLBI on Astronomy and Geophysics", I.A.U. Symp. No. 129*, eds. M.J. Reid & J.M. Moran (Dordrecht: Kluwer), p.103.

Phinney, E.S., 1987. *"Superluminal Radio Sources"* (Cambridge: Cambridge University Press), p. 301.

Phinney, E.S., 1989. In *"Theory of Accretion Discs"*, NATO ASI Series C, vol. 290, ed. F. Meyer *et al.* (Kluwer), p. 457.

Piro, L., Yamauchi, M. & Matsuoka, M., 1990. *Astrophys. J. Lett.*, **360**, L35.

Pogge, R.W.I., 1988. *Astrophys. J.*, **332**, 702.

Pollock, A., Brand, P.W.J.L., Bregman, J.N. & Robson, E.I., 1985. *Spa. Sci. Rev.*, **40**, 607.

Pomphrey, R.B., 1976. *Astron. J.*, **81**, 489.

Porcas, R.W., 1987. In *Superluminal Radio Sources*, eds. Zensus, A. and Pearson, T. (Cambridge: Cambridge University Press), p. 12.

Pounds, K.A., & McHardy, I.M., 1988. In *"Physics of Neutron Stars and Black Holes"*, ed. Y. Tanaka (Univ. Acad. Press, Tokyo), p. 285.

Pounds, K.A, Nandra, K., Stewart, G.C., George, I.M. & Fabian, A.C., 1990. *Nature*, **344**, 132.

Pringle, J.E., 1981. *Ann. Rev. Astr. Astroph.*, **19**, 137.

Quirrenbach, A., Witzel, A., Kian, S.J., Kricjbaum, T., Hummel, C.A. & Alberdi, A., 1989. *Astron. Astrophys.*, **226**, L1.

Rees, M.J., 1966. *Nature*, **211**, 468.

Rees, M.J., 1971. *Nature*, **229**, 510.

Rees, M.J., 1981. In *"Origin of Cosmic Rays"*, Proc. IAU Symp. No. 94 , eds. G. Setti, G. Spada & W. Wolfendale (Dordrecht: Reidel), p. 139.

Rees, M.J., 1981. In *"Plasma Astrophysics"*, Proc. Workshop Varenna, (ESA SP–161), p. 267.

Rees, M.J., 1982. In *"Extragalactic Radio Sources"*, Proc. IAU Symp. No. 97, eds. D.S. Heeschen & C.M. Wade (Dordrecht: Reidel), p. 211.

Rees, M.J., 1984. In *"VLBI and Compact Radio Sources"*, Proc. IAU Symp. No. 110, eds. R. Fanti *et al.* (Dordrecht: Reidel), p. 207.

Rees, M.J., 1984. *Ann. Rev. Astr. Astroph.*, **22**, 471.

Rees, M.J., 1987. *Mon. Not. R. astr. Soc.*, **228**, 47P.

Rees, M.J., Netzer, H. & Ferland, G.J., 1989. *Astrophys. J.*, **347**, 640.

Reichert, G.A., Mushotzky, R. & Holt, S.S., 1986. *Astrophys. J.*, **303**, 87.

Remillard, R.A., Grossan, B., Bradt, H.V., Ohashi, T., Hayashida, K., Makino, F. & Tanaka, Y., 1991. Submitted to *Nature*.

Reynolds, S.P., 1982. *Astrophys. J.*, **256**, 13.

Roberts, D.H., Gabudza, D.C. & Wardle, J.F.C., 1987. *Astrophys. J.*, **323**, 536.

Roberts, D.H. *et al.*, 1990. In *"Parsec–Scale Radio Jets"*, eds. J.A. Zensus & T.J. Pearson (Cambridge Univ. Press), p. 110.

Rothschild, R.E., Mushotzky, R.F., Baity, W.A., Gruber, D.E., Matteson, J.L. & Peterson, L.E., 1983. *Astrophys. J.*, **269**, 423.

Rudnik, L. & Edgar, B.K., 1984. *Astrophys. J.*, **279**, 74.

Rybicki, G. & Lightman, A., 1979. *"Radiative Processes in Astrophysics"* (Wiley–Interscience Publ.).

Sanders, D.B., Phinney, E.S., Neugebauer, G., Soifer, G.T. & Mattews, K., 1989. *Astrophys. J.*, **347**, 29.

Sanders, R., 1983. *Astrophys. J.*, **266**, 73.

Scheuer, P.A.G. & Readhead, A.C.S., 1979. *Nature*, **277**, 182.

Schield, G.A., 1978. *Nature*, **272**, 706.

Schwartz, D.A., Brissenden, R.J.V., Tuohy, I.R, Feigelson, E.D., Hertz, P.L. & Remillard, R.A., 1989. In *"BL Lac Objects"*, eds. L. Maraschi, T. Maccacaro & M.H. Ulrich (Springer-Verlag: Berlin), p. 209.

Shakura, N.I. & Sunyaev, R.A., 1973. *Astron. Astrophys.*, **24**, 337.

Shapiro, P.R., Milgrom, M. & Rees, M.J., 1986. *Astrophys. J. Suppl.*, **60**, 393.

Shapiro, S.L. & Teukolsky, S.A., 1983. *" Blach Holes, White Dwarfs and Neutron Stars"*, (John Wiley & Sons).

Shapiro, S.L., Lightman, A.P. & Eardley, D.M., 1976. *Astrophys. J.*, **204**, 187.

Sitko, M.L., Schmidt, G.D. & Stein, W.A., 1985. *Astrophys. J. Suppl.*, **59**, 323.

Smith, P.S., Elston, R., Berriman, G., Allen, R.G. & Balonek, T.J., 1988. *Astrophys. J. Lett.*, **326**, L39.

Stepney, S., 1983. *Mon. Not. R. astr. Soc.*, **202**, 467.

Stickel, M., Padovani, P., Urry, C.M., Fried, J.W. & Kühr, H., 1991. *Astrophys. J.*, **374**, 431.

Stocke, J.T., Liebert, J., Schmidt, G., gioia, I., Maccacaro, T., Schield, R., Maccagni, D. & Arp, H., 1985. *Astrophys. J.*, **298**, 619.

Sun, W.–H. & Malkan, M.A., 1989. *Astrophys. J.*, **346**, 68.

Svensson, R., 1982. *Astrophys. J.*, **258**, 335.

Svensson, R., 1986. In *"Radiation-Hydrodynamics in Stars and Compact Objects"*, Proc. IAU Coll. No. 89, eds. Mihalas, D. & Winkler, K.-H.A. (Springer-Verlag, Berlin), p. 325.

Svensson, R., 1987. *Mon. Not. R. astr. Soc.*, **227**, 403.

Svensson, R., 1990. In *"Physical Processes in Hot Cosmic Plasmas"*, eds. W. Brinkmann *et al.* (Kluwer Academic Publishers, The Netherlands), p. 357.

Tadhunter, C.N. & Tsvetanov, Z., 1989. *Nature*, **341**, 422.

Tagliaferri, G., Stella, L., Maraschi, L., Treves, A. & Celotti, A., 1991. *Astrophys. J.*, in press.

Tanzi, E.G., Barr, P., Bouchet, P., Chiappetti, L., Cristiani, S., Falomo, R., Giommi, P., Maraschi, L. & Treves, A., 1986. *Astrophys. J. Lett.*, **311**, L13.

Treves, A. & Girardi, E., 1990. In *"Variability of Active Galaxies"*, eds. .J. Duschl, S.J. Wagner & M. Camezind (Springer–Verlag), p. 175.

Treves, A., Maraschi, L. & Abramowicz, M., 1989. In *Advanced Series in Astrophysics and Cosmology. Vol. 5. "Accretion"* (World Scientific).

Treves, A., Perola, C. & Stella, L., 1991. *"Iron Line Diagnostic in X–ray Sources"*, Proc. Conf. Varenna, October 1990, in press.

Treves, A., Bonelli, G., Chiappetti, L., Falomo, R., Maraschi, L., Tagliaferri, G. & E.G. Tanzi, E.G., 1990. *Astrophys. J.,* **359**, 98.

Treves, A., Morini, M., Chiappetti, L., Fabian, A., Falomo, R., Maccagni, D., Maraschi, L. Tanzi, E.G. & Tagliaferri, G., 1989, *Astrophys. J.,* **341**, 733.

Tucker, W.H., 1975. *"Radiation Processes in Astrophysics"* (Cambridge, USA: MIT Press).

Turner, T.J. & Pounds, K.A., 1989. *Mon. Not. R. astr. Soc.,* **240**, 833.

Ulrich, M–H., 1989. In *"BL Lac Objects"*, eds. L. Maraschi, T. Maccacaro & M–H. Ulrich (Springer–Verlag), p. 45.

Ulrich, M.–H., 1990. In *"Structure and Emission Properties of Accretion Disks"*, Proc. IAU Coll. 129, Paris 1990, eds. C. Bertout *et al.* (Edition Frontieres).

Urry, M., 1984. *Ph. D. Thesis*, University of Maryland.

Urry, M., 1986. In *"The Physics of Accretion onto Compact Objects"*, eds. K.O. Mason, M.G. Watson & N.E. White (Springer–Verlag), p. 357.

Urry, M.C. & Mushotzky, R.F., 1982. *Astrophys. J.,* **253**, 38.

Urry, C.M. & Padovani, P., 1990. In *"Variability of Active Galactic Nuclei"*, Proc. Conf., Atlanta, May 1990, in press.

Urry, C.M. & Padovani, P., 1991. *Astrophys. J.,* **371**, 60.

Urry, C.M. & Shafer, R.A., 1984. *Astrophys. J.,* **280**, 569.

Urry, C.M., Padovani, P. & Stickel, M., 1991. *Astrophys. J.,* in press..

Urry, C.M., Maraschi, L. & Phinney, S.E., 1990. *Comm. Ap.*, in press.

Valtaoja, E., Lehto, H., Teerikorpi, P., Korhonen, T., Valtonen, M., Terasranta, H., Salonen, E., Urpo, S., Tiuri, M., Piirola, V. & Saslaw, W.C., 1985. *Nature,* **314**, 148.

Valtaoja, E., Lainela, M. & Teräsranta, H., 1989. In *"BL Lac Objects"*, eds. L. Maraschi, T. Maccacaro & M.H. Ulrich (Springer-Verlag: Berlin), p. 39.

van der Laan, H., 1966. *Nature,* **211**, 1131.

Visvanathan, N., 1973. *Astrophys. J.,* **179**, 1.

Visvanathan, N. & Elliot, J.L., 1976. *Astrophys. J.,* **179**, 721.

Walker, R.C., Benson, J.M. & Unwin, S.C., 1987. *Astrophys. J.,* **316**, 546.

Wandel, A. & Mushotzky, R.F., 1986. *Astrophys. J. Lett.,* **306**, L61.

Wandel, A. & Urry, C.M., 1989. In *"BL Lac Objects"*, eds. L. Maraschi, T. Maccacaro & M.H. Ulrich (Springer-Verlag: Berlin), p. 388.

Wardle, J.F.C. & Roberts, D.H., 1988. In *"The Impact of VLBI on Astrophysics and Geophysics"*, Proc. IAU Coll. N. 129, eds. M.J. Reid & J.M. Moran (Dordrecht: Kluwer), p. 143.

Wardle, J.F.C., Moore, R.L. & Angel, J.R.P., 1984. *Astrophys. J.,* **279**, 93.

Wardle, J.F.C., Roberts, D.H., Brown, L.F., Kollgaard, R.I. & Gabuzda, D.C., 1990. In *"Parsec–Scale Radio Jets"*, eds. J.A. Zensus & T.J. Pearson (Cambridge Univ. Press), p. 20.

Warwick, R.S., Yaqoob, T., Pounds, K.A., Matsouka, M. & Yamauchi, M., 1989. *Publ. astr. Soc. Japan*, **41**, 721.

Watson, M.G., Stewart, G.C., Brinkmann, W. & King, A.R., 1986. *Mon. Not. R. astr. Soc.,* **222**, 261.

Wehrle, A.E. & Cohen, M., 1989. *Astrophys. J. Lett.,* **346**, L69.

Weinberg, S., 1972. *"Gravitation and Cosmology"* (New York: Wiley & Son).
Whittle, M., Pedlar, A., Meurs, E.J.A., Unger, S.W., Axon, D.J. & Ward, M.J., 1987. *Astrophys. J.*, **326**, 125.
White, N.E., Fabian, A.C. & Mushotzky, R.F., 1984. *Astron. Astrophys.*, **133**, L9.
Wilkes, B.J. & Elvis, M., 1987. *Astrophys. J.*, **323**, 243.
Wills, B.J., Netzer, H. & Wills, D., 1985. *Astrophys. J.*, **288**, 94.
Woltjer, L., 1989. In *"BL Lac Objects"*, eds. L. Maraschi, T. Maccacaro & M–H. Ulrich (Springer–Verlag), p. 460.
Woltjer, L., 1990. In *"Active Galactic Nuclei"*, Lecture Notes 1990, SAAS–FEE Advanced Course 20, eds. T.J.–L. Courvoisier & M. Mayor (Berlin: Springer–Verlag).
Worral, D.M. & Wilkes, B.J., 1990. *Astrophys. J.*, **360**, 396.
Yaqoob, T. & Warwick, R.S., 1989. In *Proc. 23th ESLAB Symp: "X-ray Astronomy"*, ESA SP–296, p. 1089.
Yaqoob, T. & Warwick, R.S., 1991. *Mon. Not. R. astr. Soc.*, **248**, 153.
Zdziarski, A. & Coppi, P.S., 1991. *Astrophys. J.*, **376**, 480.
Zdziarski, A., Ghisellini, G., George, I.M., Svensson, R., Fabian, A.C. & Done, C., 1990. *Astrophys. J. Lett.*, **363**, L1.
Zensus, T., 1989. In *"BL Lac Objects"*, eds. L. Maraschi, T. Maccacaro & M.H. Ulrich (Springer-Verlag: Berlin), p. 3.
Zensus, T. & Pearson, T., 1987. *"Superluminal Radio Sources"* (Cambridge: Cambridge University Press).
Zwitter, T., Calvani, M., Bodo, G. & Massaglia, S., 1989. *Fund. of Cosmic Phys.*, **13**, 309.